



HAL
open science

Asymmetric copolymers: neither block nor random

Bárbara Isabel Farias Mancilla

► **To cite this version:**

Bárbara Isabel Farias Mancilla. Asymmetric copolymers: neither block nor random. Polymers. Université Paul Sabatier - Toulouse III, 2020. English. NNT : 2020TOU30288 . tel-03324610

HAL Id: tel-03324610

<https://theses.hal.science/tel-03324610>

Submitted on 23 Aug 2021

HAL is a multi-disciplinary open access archive for the deposit and dissemination of scientific research documents, whether they are published or not. The documents may come from teaching and research institutions in France or abroad, or from public or private research centers.

L'archive ouverte pluridisciplinaire **HAL**, est destinée au dépôt et à la diffusion de documents scientifiques de niveau recherche, publiés ou non, émanant des établissements d'enseignement et de recherche français ou étrangers, des laboratoires publics ou privés.

Université Fédérale



Toulouse Midi-Pyrénées

THÈSE

En vue de l'obtention du DOCTORAT DE L'UNIVERSITÉ DE TOULOUSE

Délivré par l'Université Toulouse III - Paul Sabatier

Présentée et soutenue par
Bárbara Isabel FARIAS MANCILLA

Le 24 Novembre 2020

**Asymmetric copolymers: Neither block nor
random**

École doctorale : **SDM - SCIENCES DE LA MATIERE - Toulouse**

Spécialité : **Chimie Macromoléculaire et Supramoléculaire**

Unité de recherche :

**IMRCP - Laboratoire des Interactions Moléculaires et
Réactivité Chimique et Photochimique**

Thèse dirigée par

Dr. Simon HARRISSON et Pr. Mathias DESTARAC

Jury

Dr. Mona SEMSARILAR, Rapportrice

Pr. Debora BERTI, Rapportrice

Dr. Eric MANOURY, Examineur

Dr. Maud SAVE, Examinatrice

Dr. Barbara LONETTI, Invité

Dr. Carlos GUERRERO SANCHEZ, Invité

Pr. Mathias DESTARAC, Directeur de thèse

Dr. Simon HARRISSON, Co-directeur de thèse

ACKNOWLEDGMENTS

I would like to start by thanking my supervisor Dr. Simon Harrisson, who accepted me as Ph. D. student. He was always very patient, and had the knowledge and wisdom to guide me during my formation as researcher within these three years. Despite the adversity and hard moments, he always was there supporting me. Also, a special acknowledgment to Dr. Carlos Guerrero Sanchez, because of him I found the opportunity to develop my Ph.D. in this exciting project. I also acknowledge Pr. Mathias Destarac for all the support and advices that I received from him, and also because when I needed help he was on my side.

I would like to thank Dr. Barbara Lonetti for all her help, advices and friendship during the development of my Ph.D. research. I learned so much from her, she showed me a new world with neutron scattering. We spent very good time in the beam time in Grenoble and Garching. It was awesome!

I acknowledge also to Dr. Olivier Colombani for our great collaboration in my last article as Ph.D. student.

I acknowledge all the members of the team P3R (Dr. Olivier Coutelier, Dr. Stephane Mazières, Dr. Marc Guerre, Marvin, Mingxi, Sasha, Alexis, Maksym) for the support, laughs and good moments we spent. I will miss summer and Christmas lunch. I really hope to cross ways again with all of you.

I want to specially thank my very dear friends Clemence and Hai Yen, for all the time we shared between science, laughs, coffee, tea and cakes. I will always keep in my memories all these fantastic moments together and I will terribly miss you. Hopefully we can see each other again, may be in a congress or just to chat with tea or coffee, as we used to.

I specially acknowledge all the help and friendship from Lucie. Even when there were desperate moments for me, trying to find some material or reagent at the very last minute, she always had the chance to help me. I will not forget how she helped me to get the envelopes to send my thesis manuscript to the reporters. (Which takes me to thank to LHFA laboratory) Lucie had always a smile and nice words for all the persons crossing her way, I think that is why I thank her the most.

I acknowledge all the persons at the IMRCP laboratory, with whom I shared good moments at lunch or coffee time and also helped me when I needed. I can only remember good things about all of you!

I thank to my friends in Mexico who never stopped being close to me, despite the over 13 000 km of distance.

I want to acknowledge very much to my brothers: Rurik, Benjamin and Omar; my sisters in law Lizbeth and Amanda and of course to my nieces and nephews: Andreiev, Benjamin, Enid, Farid, Valentina and Jose. You are the best in my life, I love you forever, thank you for never stop believing in me and cheering me up.

And the most important acknowledgment and dedication is for my beloved parents Isabel Mancilla Martinez y Jose Farias Sanchez. They are no longer physically in this earth, they transcended to another level. I am hoping that wherever you are right now, you are so happy and proud. Thank you for all your love and your teachings, thank you for making me who I am now. I know you are still with me and most importantly you will always be alive in my heart.

To the beloved memory of

Isabel Mancilla Martínez

and

José Farías Sánchez

TABLE OF CONTENT

ABBREVIATIONS	IX
INTRODUCTION	1
CHAPTER 1. BIBLIOGRAPHY	9
1 Synthesis of asymmetric copolymers.....	17
1.1 Spontaneous synthesis	18
1.2 Stepwise synthesis	19
1.3 Forced synthesis.....	20
1.4 Concurrent polymerization	21
2 Stimuli-responsive polymers	22
2.1 pH-responsive polymers	22
2.1.1 <i>pH-responsive polymers with acidic groups</i>	22
2.1.2 <i>pH-responsive polymers with basic groups</i>	24
2.2 Self-assembly in solution	25
<i>pH-responsiveness of PAA amphiphilic block copolymers</i>	26
2.3 Thermoresponsive polymers	28
<i>Polymers with LCST behavior</i>	29
2.4 PNIPAM LCST modification with hydrophobic end-groups.....	31
2.5 PNIPAM LCST modification with hydrophilic or hydrophobic comonomers	33
3 Properties of asymmetric copolymers	34
3.1 Critical micelle concentration and cloud point	35
3.2 Self-assembly of gradient copolymers	38
<i>The reel-in effect</i>	40
3.3 Microphase separation and thermal properties in bulk	43
4 CONCLUSIONS	47
LITERATURE	48
CHAPTER 2. P(AA-MBA) ASYMMETRIC COPOLYMERS: A PH RESPONSIVE SYSTEM	55
1 Study of properties in bulk: Microphase separation of copolymers	64
2 Study of properties in solution: Degree of ionization	67
2.1 Ionization behavior of weak polyacids (polyelectrolytes).....	67

2.2	Study of degree of ionization	69
2.2.1	<i>Potentiometric titration reproducibility</i>	71
2.2.2	<i>Effect of the composition profile on the ionization behavior</i>	72
2.2.3	<i>Effect of AA content on the ionization behavior</i>	74
3	CONCLUSIONS	84
4	MATERIALS AND METHODS.....	85
4.1	Materials	85
4.2	Size Exclusion Chromatography (SEC).....	85
4.3	¹ H NMR	86
4.4	Differential scanning calorimetry.....	86
4.5	Synthesis of P(tBA- <i>n</i> BA) block copolymers (IK).....	86
4.6	Synthesis of P(tBA- <i>n</i> BA) linear gradient copolymers (IK, BF).....	87
4.7	Synthesis of P(tBA- <i>n</i> BA) diblock copolymers (JZ).....	87
4.8	Synthesis of P(tBA- <i>n</i> BA) triblock copolymers (JZ)	88
4.9	Synthesis of P(tBA- <i>n</i> BA) block copolymers (BF).....	89
4.10	Synthesis of the different statistical S _x % copolymers	89
4.11	Acidolysis of S ₁₆ %, S ₃₀ %, S ₇₀ %, S ₈₄ % and PAA	90
4.12	Potentiometric titration experiments.....	91
4.12.1	<i>Preparation of polymer solutions</i>	91
4.12.2	<i>Titration experiments</i>	91
4.13	Gaussian model.....	92
4.14	Koper and Borkovec's model	93
	LITERATURE	94
CHAPTER 3. P(AA-<i>n</i>BA) ASYMMETRIC COPOLYMERS: SELF-ASSEMBLY BEHAVIOR ..97		
1	DLS analysis.....	103
1.1	Self-assembly analysis by DLS in buffer solutions	103
1.2	Self-assembly analysis by DLS by potentiometric titration	106
2	Self-assembly analysis by cryo-TEM.....	109
3	SANS Analysis.....	112
3.1	Self-assembly analysis by small angle neutron scattering	112
4	CONCLUSIONS	125
5	MATERIALS AND METHODS.....	127

5.1	Dynamic Light Scattering (DLS)	127
5.1.1	<i>DLS study of polymer solutions prepared by direct dissolution in buffers</i>	127
5.1.2	<i>DLS pH Titration Study</i>	127
5.2	Cryogenic Transmission Electron Microscopy (Cryo-TEM)	128
5.3	Small-Angle Neutron Scattering.....	128
CHAPTER 4. P(DMA-NIPAM) COPOLYMERS: A THERMORESPONSIVE SYSTEM.....		131
1	Synthesis of poly(DMA_{50%}-<i>grad</i>-NIPAM_{50%}) copolymers.....	137
2	Dynamic light scattering experiments	142
2.1	Comparison by molar mass.....	148
3	SANS as a function of temperature.....	149
3.1	Parameters obtained from Guinier region and forward scattering.....	156
4	¹H NMR as a function of temperature.....	161
5	CONCLUSIONS	169
6	MATERIALS AND METHODS.....	171
6.1	Proton Nuclear Magnetic Resonance (¹ H NMR)	171
6.2	Size exclusion chromatography (SEC)	171
6.3	Dynamic Light Scattering (DLS)	171
6.4	Small Angle Neutron Scattering.....	172
6.5	Synthesis of copolymers	172
6.5.1	<i>Synthesis of block copolymers poly(DMA_{50%}-<i>b</i>-NIPAM_{50%})</i>	<i>172</i>
6.5.2	<i>Synthesis of diblock copolymers poly(DMA_{84%}-<i>S</i>-NIPAM_{16%})_{50%}-<i>b</i>-poly(DMA_{16%}-<i>S</i>-NIPAM_{84%})_{50%}.....</i>	<i>173</i>
6.5.3	<i>Synthesis of triblock copolymers poly(DMA_{21%}-<i>b</i>-poly(DMA_{50%}-<i>S</i>-NIPAM_{50%})_{58%}-<i>b</i>-poly(NIPAM)_{21%}</i>	<i>174</i>
6.5.4	<i>Synthesis of gradient copolymers poly(DMA_{50%}-<i>grad</i>-NIPAM_{50%}).....</i>	<i>175</i>
6.5.5	<i>Synthesis of statistical copolymers poly(DMA_{50%}-<i>stat</i>-NIPAM_{50%}).....</i>	<i>176</i>
LITERATURE		177
GENERAL CONCLUSIONS		179
APPENDIX 1: SCATTERING TECHNIQUES FOR POLYMER ANALYSIS.....		182
DYNAMIC LIGHT SCATTERING		182
SMALL ANGLE NEUTRON SCATTERING.....		183

APPENDIX 2. HYDRODYNAMIC DIAMETERS AND PDI FOR P(AA-NBA) COPOLYMERS AT DIFFERENT PH	185
SELF-ASSEMBLY ANALYSIS BY DLS IN BUFFER SOLUTIONS	185
SELF-ASSEMBLY ANALYSIS BY DLS BY POTENTIOMETRIC TITRATION	186
APPENDIX 3. P(DMA-NIPAM) COPOLYMERS SCATTERING DATA FROM DLS AND SANS	189
HYDRODYNAMIC DIAMETERS AND PDI FROM 25 TO 70 °C OBTAINED BY DLS	189
PARAMETERS OBTAINED FROM THE ANALYSIS AND FITTING OF SANS CURVES	191
<i>ABSTRACT</i>	199

ABBREVIATIONS

AA	Acrylic acid
ACHN	1,1'-Azobis(cyclohexanecarbonitrile)
AIBN	Azobisisobutyronitrile
ATRP	Atom transfer radical polymerization
CMC	Critical micelle concentration
cryo-TEM	Cryogenic transmission electron microscopy
D_n	Hydrodynamic diameter
DLS	Dynamic light scattering
DMA	Dimethylacrylamide
DMF	Dimethylformamide
DSC	Differential scanning calorimetry
HCl	Hydrochloric acid
¹H NMR	Proton nuclear magnetic resonance
LCST	Lower critical solution temperature
M_n	Number average molecular weight
M_w	Weight average molecular weight
NaCl	Sodium chloride
N_{agg}	Aggregation number
NaOH	Sodium hydroxide
nBA	<i>n</i> -butyl acrylate
NIPAM	<i>N</i> -isopropylacrylamide
NMP	Nitroxide mediated polymerization
PAA	Poly(acrylic acid)
PDMA	Poly(dimethylacrylamide)

PnBA	Poly(<i>n</i> -butyl acrylate)
PNIPAM	Poly(<i>N</i> -isopropylacrylamide)
RAFT	Reversible addition fragmentation chain transfer
RDRP	Reversible deactivation radical polymerization
R_g	Radius of gyration
R_h	Hydrodynamic radius
SANS	Small angle neutron scattering
SEC	Size exclusion chromatography
<i>t</i>BA	<i>t</i> -butyl acrylate
T_{cp}	Cloud point temperature
TFA	Trifluoroacetic acid
T_g	Glass transition temperature
THF	Tetrahydrofuran
UCST	Upper critical solution temperature

INTRODUCTION

Les copolymères sont des polymères qui contiennent au moins deux types différents d'unités répétitives. Il existe de nombreuses façons de disposer ces unités le long de la chaîne du copolymère. Un premier modèle correspond aux copolymères à blocs, fabriqués à partir de chaînes de polymères de compositions chimiques différentes qui sont jointes de manière covalente. Un deuxième modèle correspond aux copolymères statistiques dont les monomères sont mélangés au hasard. Entre ces structures, on peut définir des copolymères asymétriques, comme des copolymères dans lesquels les différents types de monomères ne sont ni complètement séparés, comme dans un copolymère à blocs, ni mélangés de façon homogène, comme dans un statistique. Ces copolymères comprennent des copolymères à gradient, dans lesquels la composition du copolymère varie progressivement au long de la chaîne. Par conséquent, les propriétés des copolymères asymétriques devraient être intermédiaires par rapport à celles des copolymères à bloc et des copolymères statistiques.

Les copolymères asymétriques peuvent avoir différents profils de composition. Par exemple, des gradients linéaires, des gradients spontanés, des gradients effilés, des gradients par étapes, des gradients à blocs, entre autres. Celles-ci sont nommées en fonction de la variation de la composition instantanée du copolymère en fonction de la conversion du monomère lors de la synthèse du polymère. Grâce à cette diversité de structures, il est possible d'obtenir une grande variété de propriétés.

Dans ce travail, notre objectif est d'aborder la question de comment le profil de composition affecte les propriétés d'un copolymère asymétrique. Faut-il recourir à une synthèse élaborée comme par exemple une synthèse multi-étape ? Ou une simple synthèse suffirait-elle pour obtenir une structure asymétrique similaire à l'un des profils de composition mentionnés ci-dessus ?

Afin de répondre à ces questions, dans cette thèse, différentes structures de copolymères ont été étudiées. Ce sont des copolymères à blocs composés de deux blocs homopolymères, des copolymères statistiques, des copolymères asymétriques dibloc (composés par deux blocs statistiques de compositions différentes), les copolymères asymétriques tribloc (composés d'un bloc d'homopolymère A, un deuxième bloc qui est un copolymère statistique à 50% de monomère A et un troisième bloc d'homopolymère B) et des copolymères à gradient linéaire. Les copolymères à blocs ont été obtenus par une simple extension de chaîne d'un homopolymère, le copolymère statistique a été obtenu par copolymérisation de deux monomères, les copolymères

asymétriques dibloc et tribloc ont été obtenus par addition séquentielle de monomères et le copolymère à gradient linéaire a été obtenu par synthèse forcée. La composition globale de tous les polymères est de 50% (de chaque monomère) et deux poids moléculaires ciblés ont été choisis (10 et 20 kg mol⁻¹).

Deux systèmes de copolymères différents ont été choisis pour étudier leurs propriétés en fonction des différentes distributions en monomères. Le premier système est le poly (acide acrylique-acrylate de *n*-butyle) (P (AA-*n*BA)), un copolymère amphiphile qui réagit au pH en raison de la présence d'unités AA. Le deuxième groupe de copolymères est le poly (diméthylacrylamide-*N*-isopropylacrylamide), un copolymère doublement hydrophile qui adopte un caractère amphiphile lorsque la température augmente et que les segments riches en NIPAM deviennent hydrophobes.

La thèse est divisée en quatre chapitres :

Le chapitre 1 comprend une étude bibliographique décrivant des copolymères asymétriques et de leurs propriétés. Au début du chapitre, le concept de copolymère asymétrique est défini, ainsi que les différences et similitudes qu'ils ont avec les copolymères à blocs et statistiques. Ensuite, les voies de synthèse pour obtenir des copolymères asymétriques sont décrites, notamment les synthèses spontanée, forcée, par étapes et en catalyse tandem. Dans la synthèse spontanée, l'exigence est que les monomères possèdent des rapports de réactivité différents, tandis que dans la synthèse forcée, les monomères peuvent avoir des rapports de réactivité différents ou similaires, puisque le profil de composition est contrôlé par la vitesse d'addition du monomère. Puisque dans cette thèse des polymères sensibles au pH et à la température sont à l'étude, une section sur les polymères sensibles aux stimuli est incluse, qui décrit les caractéristiques les plus importantes des polymères sensibles au pH et à la température. Enfin une section présentant les propriétés des copolymères asymétriques est présentée. Les propriétés en solution telles que la concentration micellaire critique et la température du point de trouble, sont des conséquences du comportement d'auto-assemblage. Il est également décrit comment ces propriétés sont affectées par un changement de profil passant de copolymères à blocs à copolymères à gradient. A la fin de cette section, la séparation microphasique) en masse de copolymères asymétriques est également discutée, elle est principalement étudiée par des méthodes calorimétriques.

Le chapitre 2 se concentre sur l'étude des propriétés physiques des copolymères AA-*n*BA en masse et en solution. Dans la première section, leurs propriétés en masse sont analysées par calorimétrie différentielle à balayage, qui révèle que les copolymères à

blocs ont deux T_g bien définies et séparées en raison de la séparation de microphasique, tandis que les copolymères statistiques affichent une T_g simple et étroite. D'autre part, les copolymères à gradient ont présenté également une T_g unique mais large, tandis que les structures diblocs ont présenté deux T_g similaires au copolymère à blocs, mais dans avec des pics plus larges. Enfin, les copolymères triblocs présentent une T_g principale large, très similaire à celle du copolymère à gradient. Les similitudes de propriétés thermiques des copolymères asymétriques s'expliquent par la faible ségrégation microphasique inhérente à leur structure. La deuxième section du chapitre examine le comportement d'ionisation des différentes structures des copolymères P(AA-*n*BA) en effectuant des titrages potentiométriques. Une brève introduction aux polyélectrolytes faibles est également incluse. La section suivante contient l'analyse de reproductibilité, qui a été réalisée pour garantir l'exactitude des résultats obtenus à partir des titrages potentiométriques. Dans la partie suivante, un ensemble de copolymères statistiques a été analysé afin d'étudier le comportement d'ionisation en fonction de différents taux d'AA. Ensuite, l'effet du profil de composition a été étudié en comparant les comportements d'ionisation des copolymères statistiques, à blocs et gradient. Cette étude a montré que la distribution d'AA au sein de la chaîne affecte fortement le comportement d'ionisation, par exemple le copolymère à bloc a présenté les unités d'AA les plus acides des trois structures. Enfin, les courbes de titrage (expérimentales et simulées) des copolymères asymétriques et à blocs ont été comparées afin d'observer si le dibloc ou le tribloc mime efficacement le comportement d'ionisation du copolymère à gradient.

Le chapitre 3 explore le comportement d'auto-assemblage en fonction du pH des copolymères P(AA-*n*BA). La première section décrit les auto-assemblages étudiés par DLS qui ont été effectués par deux voies : 1) les copolymères ont été directement dissous dans des solutions tampons à différents pH et 2) les copolymères ont été dissous dans une solution aqueuse à un pH basique et après le pH a été modifié par titrage potentiométrique. Les deux types d'études sont cohérents, puisque les deux montrent l'état figé des agrégats formés par le copolymère à blocs, alors que les copolymères asymétriques présentent un comportement dynamique. La deuxième partie consiste en des expériences de cryo-TEM à différents pH pour des échantillons sélectionnés. Les observations de DLS ont été confirmées. Les copolymères à blocs sont restés sous forme de micelles sphériques de la même taille dans toute la gamme de pH étudiée, tandis que pour les structures asymétriques, des changements de morphologie et de taille ont été observés en modifiant le pH. La dernière section de ce chapitre comprend les résultats obtenus à partir d'expériences SANS. D'abord, le

traitement des données du copolymère dibloc asymétrique ($M_n = 10 \text{ kg mol}^{-1}$) est décrit, ensuite le reste des polymères sont comparés. Etant donné que le copolymère bloc présente un comportement figé, très différent des copolymères asymétriques, il est discuté séparément. Toutes les observations de SANS sont en accord avec les observations de DLS et cryo-TEM.

Le chapitre 4 se concentre sur les copolymères thermosensibles DMA-NIPAM. La première section comprend la discussion expérimentale pour la synthèse de copolymères à gradient DMA-NIPAM. La deuxième section traite de l'analyse DLS en fonction de la température, et il a été observé que les copolymères statistiques présentent un point de trouble à 60°C et par contre les copolymères à blocs et asymétriques, ne présentent aucune température de point de trouble. Cependant, les copolymères à bloc et asymétriques présentent des transitions en ce qui concerne la taille de leurs agrégats en fonction de la température. La section suivante présente les résultats obtenus à partir de SANS en fonction de la température, dans lesquels il a été possible d'extraire des informations de la région de Guinier et de la diffusion vers l'avant, tel que le rayon de giration et le nombre d'agrégation des assemblages de polymères. Des caractéristiques similaires ont été observées entre les copolymères à blocs de masse molaire plus faible et les copolymères asymétriques de masse molaire plus élevée. En effet, la courte longueur de chaîne des copolymères à blocs entraîne un effet de la présence de DMA à proximité des unités NIPAM. Enfin, une section avec des expériences de ^1H RMN en fonction de la température est incluse. Les résultats sont en accord avec ceux obtenus en DLS et SANS, montrant des caractéristiques similaires entre le copolymère à bloc de faible masse molaire et les copolymères asymétriques de masse molaire supérieure.

INTRODUCTION

Copolymers are polymers that contain two or more different types of repeating units. There are many ways to arrange these units along the copolymer chain. At one extreme are the block copolymers, made from polymer chains of different chemical composition that are covalently joined together. On the other extreme are statistical copolymers whose monomers are randomly mixed. In between these structures we can define asymmetric copolymers, as copolymers in which the different types of monomer are neither completely separated, as in a block copolymer, nor homogeneously mixed, as in a gradient. These copolymers include gradient copolymers, in which the copolymer composition gradually varies along the chain. It is expected that the properties of asymmetric copolymers are also in between those of block and statistical copolymers.

Asymmetric copolymers can have different composition profiles. For instance, linear gradients, spontaneous gradients, tapered gradients, stepwise gradients, block gradients among others. These are named according to how the instantaneous copolymer composition varies as a function of monomer conversion during the polymer synthesis. Thanks to this diversity in structures it is possible to obtain a wide variety of properties.

In this work we aim to address the question of how the different composition profiles affect the properties of an asymmetric copolymer. Is it necessary to appeal to a complicated synthesis? Or would it be sufficient with a simple synthesis to obtain an asymmetric structure which resembles one of the previously mentioned composition profiles?

In order to answer these questions, in this thesis different copolymer structures have been studied. These are: block copolymers consisting of two homopolymer blocks, statistical copolymers, asymmetric diblock copolymers (composed of two statistical blocks with different composition), asymmetric triblock copolymers (composed of one block of homopolymer A, a second block which is a statistical copolymer of 50% monomer A and a third block of homopolymer B) and linear gradient copolymers. The block copolymers were obtained by simple chain extension of a homopolymer, the statistical copolymer was obtained by copolymerizing two monomers, the asymmetric diblock and triblock copolymers were obtained by sequential addition of monomers and the linear gradient copolymer was obtained by a forced synthesis. The overall composition for all the polymers is 50% and two targeted molecular weights were chosen (10 and 20 kg mol⁻¹).

Two different copolymer systems were chosen to study their properties as a function of the different monomer distribution. The first system is poly(acrylic acid-*n*-butyl acrylate) (P(AA-*n*BA)), an amphiphilic copolymer that is pH-responsive due to the presence of AA units. The second group of polymers is poly(dimethylacrylamide-*N*-isopropylacrylamide), a double hydrophilic copolymer that adopts an amphiphilic character as the temperature increases and the NIPAM-rich segments become hydrophobic.

The manuscript is divided onto four chapters:

Chapter 1 comprises a bibliographic investigation of asymmetric copolymers and their properties. At the beginning of the chapter, the concept of an asymmetric copolymer is defined, and also the differences and similarities that they have with block and statistical copolymers are explained. After, the synthetic routes to obtain asymmetric copolymers are described, which comprise the spontaneous, forced, stepwise and tandem catalysis synthesis. In the spontaneous synthesis the requirement is that the monomers possess different reactivity ratios while in the forced synthesis the monomers can either have different or similar reactivity ratios, since the composition profile is controlled by the monomer addition rate. Since in this thesis pH and thermo responsive polymers are under study, a section on stimuli responsive polymers is included, which describes the most important characteristics of pH and thermosensitive polymers. Finally, a section with the properties of asymmetric copolymers is presented. The properties in solution such as critical micelle concentration and cloud point temperature are a consequence of the self-assembly behavior and it is described how these properties are affected by changes in the composition profile from block to gradient copolymers. At the end of this section, the microphase separation in bulk of asymmetric copolymers is also discussed, which has been mainly studied by calorimetric methods.

Chapter 2 focuses on the study of the physical properties of P(AA-*n*BA) copolymers in bulk and in solution. In the first section their properties in bulk are analyzed by differential scanning calorimetry, which reveals that block copolymers have two well defined and separated T_g s due to microphase separation, while the statistical copolymer displayed one single and narrow T_g . On the other hand, gradient copolymers also displayed one single but broad T_g , while the diblock structures exhibited two T_g s similar to block copolymer, but in this case they were broader. Finally, the triblock copolymer displayed one main and broad T_g very similar to that of the gradient copolymer. The similarities in thermal properties of asymmetric copolymers are explained by the the weak microphase segregation inherent to their structure. The second section of the chapter examines the ionization behavior of the different structures of P(AA-*n*BA) copolymers by performing

potentiometric titrations. A short introduction to weak polyelectrolytes is also included. The following section contains the reproducibility analysis, which was performed to ensure the accuracy of the results obtained from the potentiometric titrations. In the next part, a set of statistical copolymers were analyzed in order to study their ionization behavior as a function of different AA composition. After, the effect of the composition profile was studied by comparing the ionization behaviors of statistical, block and gradient copolymers. This study showed that the AA distribution within the chain strongly affects the ionization behavior, for instance the block copolymer displayed the most acidic AA units of the three structures. Finally, the titration curves (experimental and simulated) of the asymmetric and block copolymers were compared in order to observe whether the diblock or triblock effectively mimicked the ionization behavior of the gradient copolymer.

Chapter 3 explores the self-assembly behavior as a function of pH of the P(AA-*n*BA) copolymers. The first section describes the self-assembly studied by DLS, which were carried out by two routes: 1) by directly dissolving the copolymers in buffer solutions at different pHs, and 2) by dissolving the copolymers in aqueous solution at basic pH and after the pH was modified by potentiometric titration. Both types of experiments were consistent, since they showed the frozen state of the aggregates formed by the block copolymer and by contrast the dynamic behavior of asymmetric copolymers was exhibited. The second part consists of cryo-TEM experiments at different pH for selected samples, and the observations from DLS were confirmed. The block copolymers remained as spherical micelles with the same size through all the pH range under study, while for the asymmetric structures, changes in morphology and size were observed by modifying the pH. The final section of this chapter includes the results obtained from SANS experiments. It is first described the data treatment of the asymmetric diblock copolymer ($M_n = 10 \text{ kg mol}^{-1}$), and after the rest of the polymers are discussed together. Since the block copolymer exhibited frozen behavior, very different from the asymmetric copolymers, it is discussed separately. All the observations from SANS were in agreement with the observations from DLS and cryo-TEM.

Chapter 4 focuses on thermally responsive P(DMA-NIPAM) copolymers. The first section comprises the experimental discussion for the synthesis of P(DMA-NIPAM) gradient copolymers. The second section deals with the DLS analysis as a function of temperature, and it was observed that the statistical copolymers displayed a cloud point at 60 °C and by contrast block and asymmetric copolymers, did not exhibit any cloud point temperature. However, block and asymmetric copolymers did display transitions in regard to the size of their aggregates as function of temperature. The following section

presents the results obtained from SANS as a function of temperature, in which it was possible to extract information from the Guinier region and forward scattering, such as the radius of gyration and aggregation number of the polymer assemblies. Similar characteristics were observed between lower molar mass block copolymers and higher molar mass asymmetric copolymers, which were attributed to the short length scale of the block copolymers in which the chain is short enough so that the NIPAM units are strongly affected by the presence of DMA. Finally, a section with ^1H NMR experiments as a function of temperature is included, and the results were in agreement with those of DLS and SANS, showing similar features between the low molar mass block copolymer and higher molar mass asymmetric copolymers.

CHAPTER 1.

BIBLIOGRAPHY

CHAPITRE 1. BIBLIOGRAPHIE

Les copolymères sont des polymères qui contiennent au moins deux types de monomères. Ces monomères peuvent être répartis de plusieurs manières le long de la chaîne du polymère. Les structures les plus connues sont les copolymères à bloc et statistiques. Dans les copolymères à blocs, les monomères sont très bien séparés, formant différents blocs d'homopolymère A et d'homopolymère B. Par contre, dans les copolymères statistiques, les monomères sont statistiquement répartis le long de la chaîne. La manière dont les unités monomères sont réparties au long de la chaîne polymère affecte directement les propriétés du polymère. Alors que les propriétés des polymères statistiques sont une moyenne de celles de leurs homopolymères, les copolymères à bloc combinent les propriétés des segments d'homopolymères. Ainsi, un copolymère statistique de monomères hydrophobes et hydrophiles peut être modérément soluble dans l'eau, tandis que le copolymère à bloc correspondant est amphiphile.

Entre les structures à blocs et statistiques, on peut trouver des copolymères asymétriques¹, qui sont des macromolécules dont la composition évolue progressivement au long de la chaîne polymérique. Parmi ces structures, il existe des copolymères à gradient, dans lesquels au moins une section de la chaîne a une composition qui varie continuellement. Il existe différents types de copolymères à gradient, comprenant des gradients linéaires^{2,3}, des gradients hyperboliques⁴, des gradients par étapes^{5,6}, des gradients exponentiels⁷, des gradients spontanés⁸, des blocs effilés⁹ et des quasi-blocs¹⁰.

Ceux-ci sont nommées en fonction de la variation de la composition instantanée du copolymère en fonction de la conversion du monomère pendant la synthèse du polymère. On suppose que la composition instantanée dans le milieu réactionnel impacte directement la variation de composition du copolymère tout au long de sa chaîne, car la longueur de la chaîne est proportionnelle à la conversion dans une polymérisation vivante ou contrôlée. Cependant, cette hypothèse ne prend pas en compte la structure discrète des chaînes individuelles et la variation de la séquence des monomères d'une chaîne à l'autre. En conséquence, le profil de composition en fonction de la longueur de chaîne de toute chaîne individuelle peut s'écarter largement de la composition idéalisée en fonction du profil de conversion de la polymérisation globale. La similitude entre ces structures est une distribution asymétrique des unités de monomères le long de la chaîne polymère.

étapes. Certaines structures asymétriques ainsi que des structures à blocs et statistiques sont présentées dans la Figure 1.2.

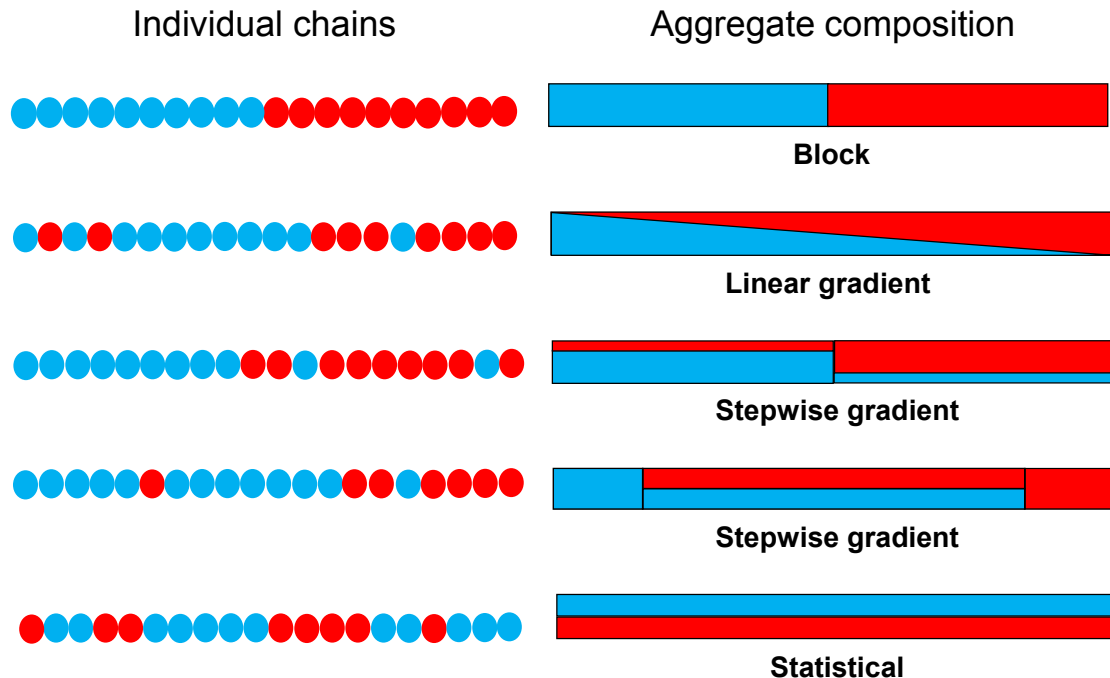


Figure 1.2. Différentes structures de copolymères : bloc, gradient linéaire asymétrique, gradient asymétrique par étapes et statistiques.

SYNTHÈSE DES COPOLYMÈRES ASYMÉTRIQUES

Il existe différentes voies de synthèse pour l'obtention de copolymères asymétriques. Il est possible de réaliser la synthèse en une seule étape ou via une synthèse multi-étapes. Bien que cette dernière implique un contrôle amélioré du profil de copolymère final, il existe des événements indésirables tels que des réactions secondaires, qui peuvent conduire à une déviation du profil de composition souhaité.

La préparation de copolymères asymétriques doit être effectuée par des techniques de polymérisation vivantes ou contrôlées telles que la polymérisation radicalaire par désactivation réversible (RDRP)¹¹⁻¹⁴, dans laquelle presque toutes les chaînes sont initiées au début de la réaction et restent actives au moins par intermittence pendant toute la réaction. Les copolymères asymétriques ne peuvent pas être préparés par des techniques de polymérisation radicalaire conventionnelles car la durée de vie de la chaîne dans ces synthèses est très courte par rapport au temps total de réaction.¹³ Par conséquent, tout changement de composition au cours de la polymérisation, que ce soit

en raison de la consommation préférentielle d'un monomère ou l'addition de monomère à la réaction ne se reflète pas dans le profil de composition des chaînes individuelles, mais se manifeste par des différences de composition entre les chaînes de polymères. Cela produit un mélange de copolymère statistique de compositions différentes plutôt qu'un copolymère asymétrique.¹⁵

CHAPTER 1. BIBLIOGRAPHY

Copolymers are polymers that contain two or more types of monomer. These monomers may be distributed in many different ways along the polymer chain. The best known structures are block and statistical copolymers. In block copolymers, the monomers are very well separated, forming different blocks of homopolymer A and homopolymer B. On the other hand, in statistical copolymers the monomers are statistically distributed along the chain. The way in which monomeric units are distributed along the polymer chain directly affects the properties of the polymer. Roughly speaking, while the properties of statistical polymers are an average of those of their homopolymers, block copolymers combine the properties of the homopolymer segments. Thus, a statistical copolymer of hydrophobic and hydrophilic monomers may be moderately water-soluble, while the corresponding block copolymer is amphiphilic.

Between block and statistical structures one can find asymmetric copolymers,¹ which are macromolecules whose composition gradually changes along the polymeric chain. Among these structures exist gradient copolymers, in which at least one section of the chain has a continually varying composition. There are various types of gradient copolymers, including linear gradients^{2,3}, hyperbolic gradients⁴, stepwise gradients^{5,6}, exponential gradients⁷, spontaneous gradients⁸, tapered blocks⁹ and quasi-blocks¹⁰. These are named according to how the instantaneous copolymer composition varies as a function of monomer conversion during the polymer synthesis. This is assumed to transfer to the variation of copolymer composition with chain length, as chain length is proportional to conversion in a living or controlled polymerization. However, this assumption masks the discrete structure of individual chains and variation in monomer sequence from one chain to another. As a result, the composition vs chain length profile of any individual chain may deviate widely from the idealized composition vs conversion profile of the overall polymerization. The similarity among these structures is an asymmetric distribution of the monomeric units along the polymer chain.

As depicted in Figure 1.1, block copolymers contain two segments of clearly different composition, with a well-defined transition between the segments. Statistical copolymers, whose composition is independent of chain length, possess neither a well-defined transition between segments nor two segments with measurably different composition. Meanwhile, the asymmetric structures contain segments that are enriched or impoverished in one monomer, but because of the randomness inherent in the structure, there is no clear transition between the segments.

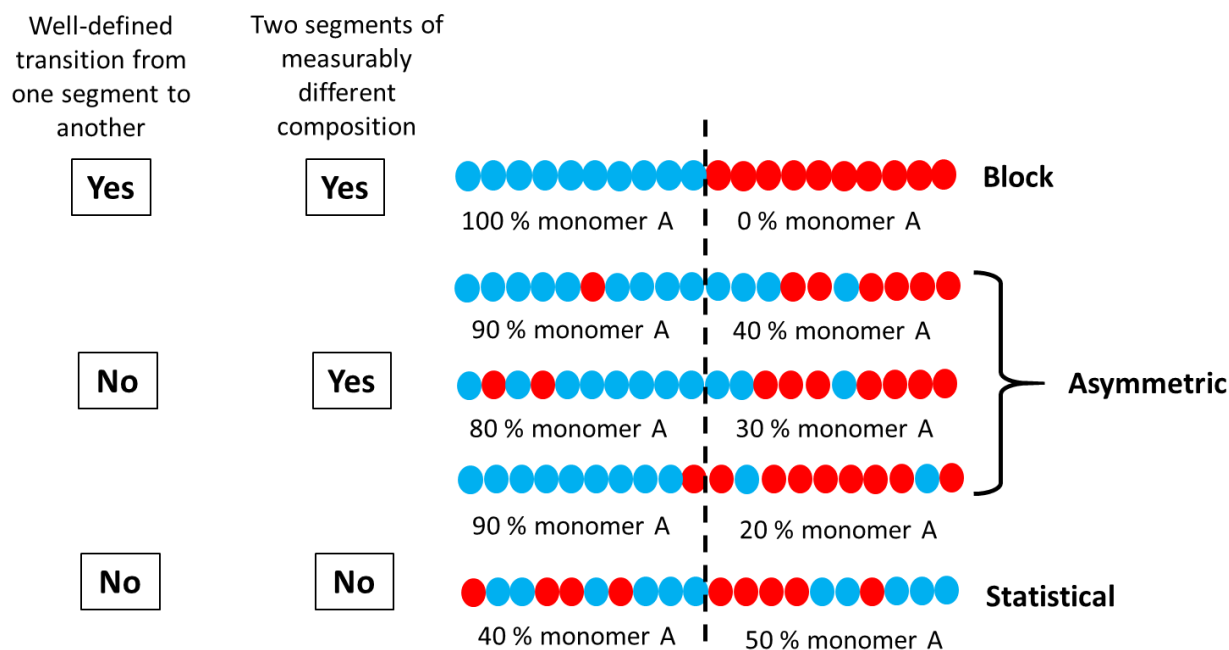


Figure 1.1. Differences between block, asymmetric and statistical copolymer chains. The dashed line divides each polymer chain into two segments with equal amount of monomer units, which helps to better visualize the differences between segments in the chain.

Then, in order to classify a copolymer as asymmetric, it should have the following characteristics¹:

1. the majority of the chains should contain at least two segments of measurably different composition.
2. the chains should not have a well-defined transition from one segment to another, as in the case of block copolymers.

This definition encompasses various architectures with different aggregate composition profiles but which are difficult to distinguish at the level of individual chains, including gradient and stepwise gradient copolymers. Some asymmetric structures as well as block and statistical structures are presented in Figure 1.2.

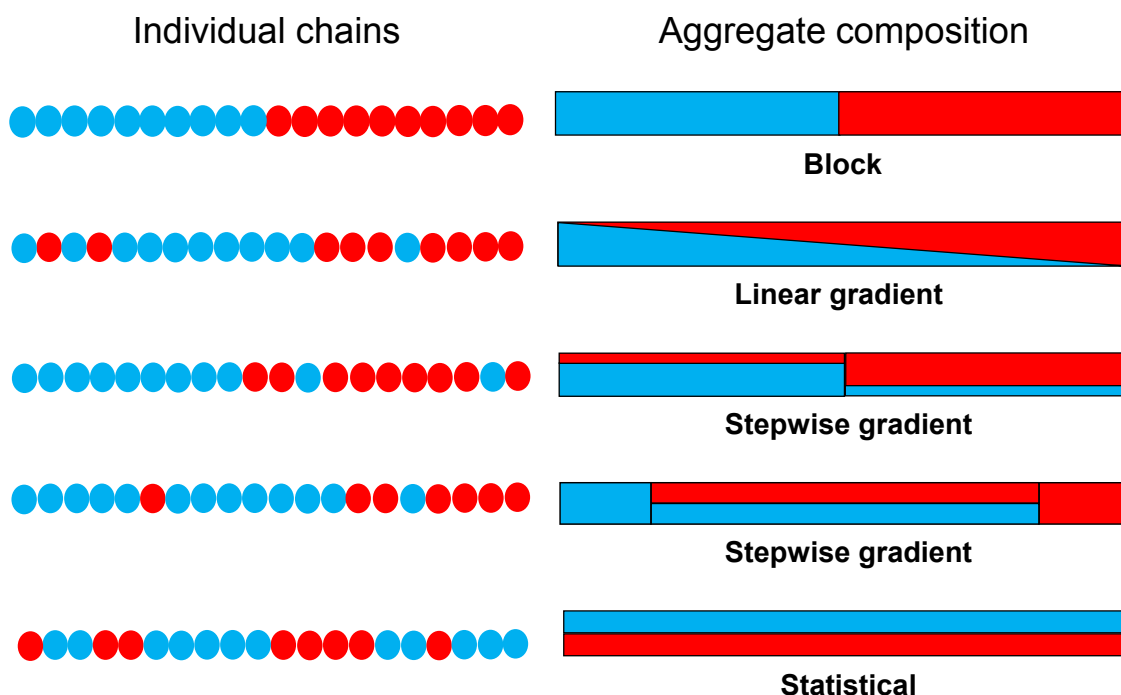


Figure 1.2. Different structures of copolymers: block, asymmetric linear gradient, asymmetric stepwise gradient and statistical copolymers.

1 SYNTHESIS OF ASYMMETRIC COPOLYMERS

There are various synthetic routes to asymmetric copolymers. It is possible to carry out the synthesis in one-pot medium or via a multi-step synthesis. Although the latter implies enhanced control over the final copolymer profile, there are undesired events such as side reactions, which would lead to a deflection from the desired composition profile.

The preparation of asymmetric copolymers needs to be performed by living or controlled polymerization techniques such as reversible deactivation radical polymerization (RDRP)^{11–14}, in which nearly all chains are initiated at the beginning of the reaction, and remain at least intermittently active for most of the reaction. Asymmetric copolymers cannot be prepared by conventional radical polymerization techniques as the chain lifetime in these syntheses is very short compared to the total reaction time.¹³ Hence, any change in the composition through the polymerization, whether as a result of preferential consumption of one monomer or addition of monomer to the reaction, is not reflected in the composition profile of individual chains, but instead is manifested as differences in composition between polymer chains. This produces a blend of statistical copolymer of different compositions rather than an asymmetric copolymer.¹⁵

Different synthetic routes have been used to obtain asymmetric copolymers, such as anionic¹⁶ and cationic^{17–22} polymerization, catalyzed copolymerizations of olefins²³ and epoxides²⁴, ring opening metathesis polymerization (ROMP)^{25–29} and RDRP techniques (atom transfer radical polymerization (ATRP)^{30–35}, nitroxide mediated polymerization (NMP)^{36–43}, organometallic-mediated radical polymerization (OMRP)⁴⁴ and reversible addition fragmentation chain transfer polymerization (RAFT)^{45–51})

The most common techniques to synthesize asymmetric copolymers, are depicted in Figure 1.3 and described in the next section.

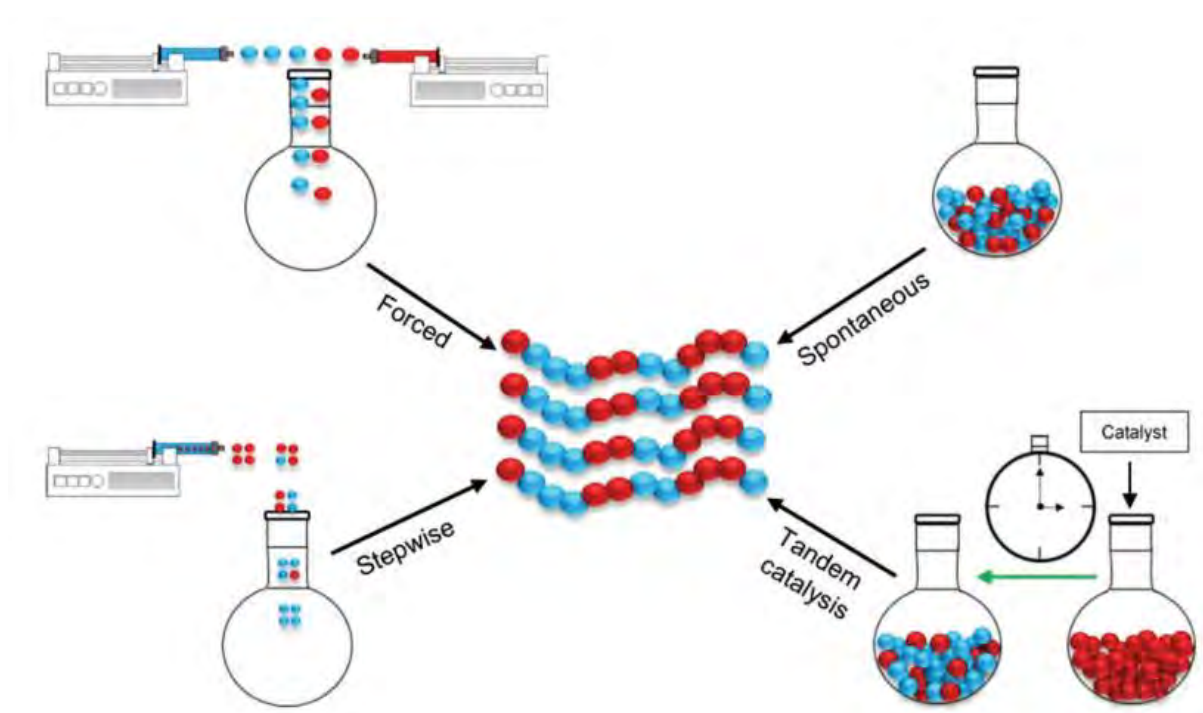


Figure 1.3. Principal synthesis routes to obtain asymmetric copolymers: Forced synthesis, spontaneous synthesis, stepwise synthesis and tandem catalyst synthesis.

1.1 Spontaneous synthesis

This is the simplest method to obtain an asymmetric copolymer, since it only requires that the monomers possess different reactivity ratios. In this way, one monomer will react faster and the other one will be slowly incorporated in the polymer chain. In this case the polymer composition will be defined by the initial monomer feed. Diverse techniques have been used to obtain spontaneous gradients. Among them one can find catalyzed transfer polycondensation⁵², catalyzed copolymerization of olefins⁵³ and epoxides⁵⁴, and diverse CLRP such as ATRP^{30–34}, NMP^{36,37,40}, OMRP⁴⁴ and RAFT^{45–47,49,50}.

However, in general, the final result of this technique is the obtaining of block-like structures, in which an initial segment of nearly constant composition is followed by a final segment of homopolymer, or shallow gradients with little change in composition along the chain. Another disadvantage is that when the more reactive monomer is consumed, the reaction often stops. If both monomers have similar reactivity ratios, it is not possible to obtain a strong gradient structure.⁸ When two monomers with very different reactivity ratios are polymerized together, strong gradients can be obtained but this difference in reactivity also makes it difficult to control the reaction. In order to avoid this drawback, MADIX polymerization (macromolecular design by interchange of xanthates) has been used to perform the polymerization of less activated monomers and also of more activated monomers under acceptable levels of control.^{45,46}

1.2 Stepwise synthesis

This method can be defined as a series of sequential copolymerizations at different monomer composition. In this way, by adding more blocks, a continuous composition profile can be approached as closely as desired. Different methods have been used to obtain stepwise gradient copolymers, for example ATRP, NMP, RAFT, and anionic living polymerization.

An example of stepwise synthesis is the many-shot polymerization of styrene and n-butyl acrylate to obtain linear and v-shaped gradient copolymers of high molar mass.⁵⁵ This synthesis was performed by RAFT emulsion polymerization (Figure 1.4).

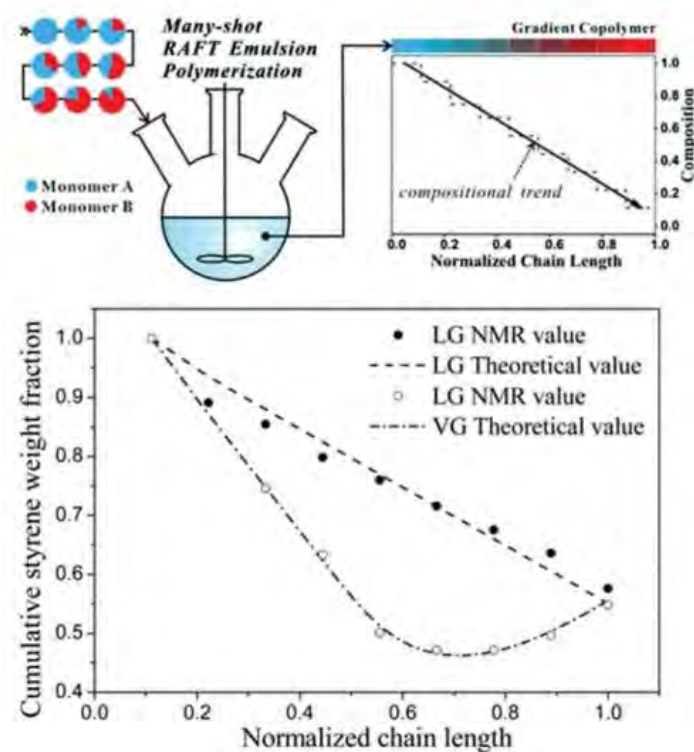


Figure 1.4. Many shot emulsion polymerization method for preparation of linear and V-shaped gradient copolymers. Reproduced from Guo et al. (2014) published in *Polymer Chemistry*.⁵⁵

1.3 Forced synthesis

Forced synthesis involves adding monomer continuously to the reaction vessel (Figure 1.5) in order to control the monomer composition throughout the reaction. This requires more control over the set up and preparation of the polymerization. The use of an addition pump is required in order to control at least one of the monomer feed rates. This method involves more complicated engineering and control in comparison to spontaneous or stepwise techniques. Nevertheless, the prize to gain here is the control over the composition profile of the polymer chains and a continuous variation in the monomer distribution. In a forced synthesis, asymmetric copolymers can be obtained from a greater variety of monomers than in a spontaneous synthesis and the composition profile can be varied, even with the same monomer pairs. This technique is the simplest to apply to monomers with similar reactivity but it also can be used with monomers of different reactivity. On the other hand, this method also presents drawbacks, including poor reproducibility, lower polymerization rate, broader molar mass distribution and higher fraction of dead chains.³

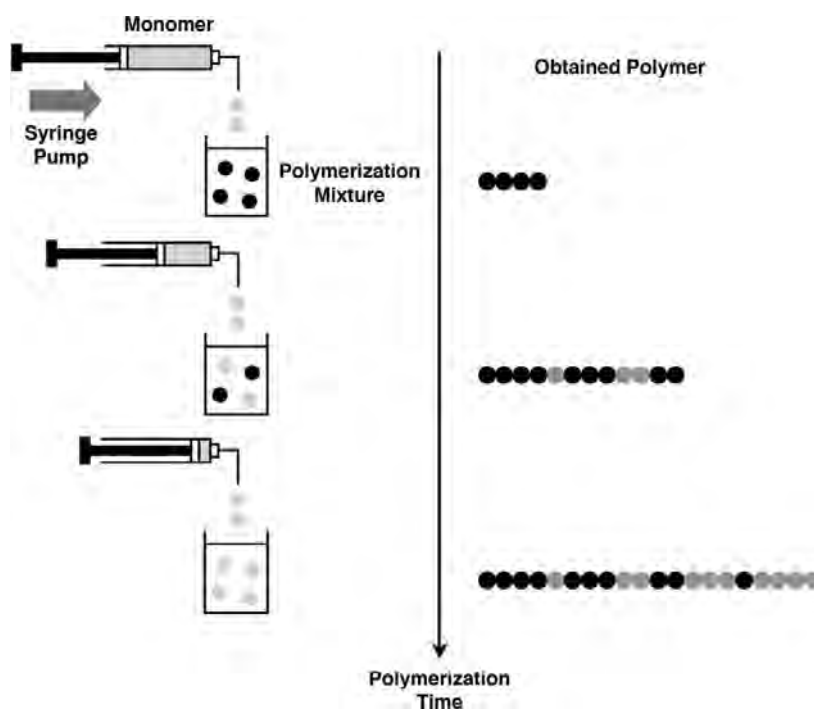


Figure 1.5. Example of forced synthesis to obtain a gradient copolymer. Reproduced from Seno et al. (2008) published in *Journal of Polymer Science part A: Polymer chemistry*.⁵⁶

1.4 Concurrent polymerization

A more sophisticated form to obtain asymmetric copolymers is the tandem catalyst polymerization (Figure 1.6), in which the monomer is simultaneously polymerized and converted into a different monomer. This technique was first established by Terishima, Sawamoto and coworkers in which they obtained linear gradient copolymers from monomers with similar reactivity, in one-pot approach. This procedure involves selective transesterification only on the monomer and not on the polymer chain. Thus the pendant groups in the polymeric species must be inert to the transesterification reaction.^{57–59}

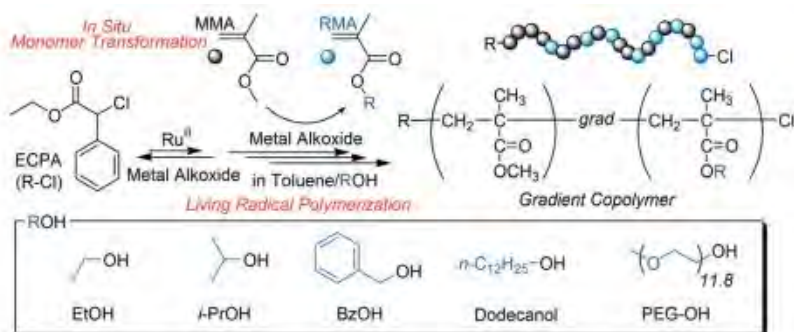


Figure 1.6. Concurrent tandem catalysis of Ru-catalyzed RDRP and metal alkoxide-catalyzed transesterification. Reproduced from Nakatani et al. (2009) published in *Journal of American Chemical Society*.⁵⁷

2 STIMULI-RESPONSIVE POLYMERS

Stimuli-responsive polymers or smart polymers are macromolecules which undergo phase transitions in response to subtle changes in the environmental conditions. Stimuli can be classified as physical (temperature^{60–67}, light⁶⁸, magnetic field.⁶⁹), chemical (pH^{8,39,70–73}, solvent composition,⁷⁴ CO₂⁴⁵, redox⁷⁵) or biological (glucose⁷⁶, enzymes). Physical stimuli generally modify chain dynamics. Chemical stimuli modulate molecular interactions whether between polymer and solvent molecules or between polymer chains. Biological stimuli involve enzymatic reactions or recognition of molecules. Stimuli-responsive polymers are able to react to one or more stimuli. One of the important characteristics of stimuli-responsive polymers is that they have the ability to return to their original state upon application of a counter-stimulus.

The most studied stimuli-responsive copolymers are pH and thermo-responsive copolymers, because of their potential applications in drug delivery systems.^{19,70}

2.1 pH-responsive polymers

Polymers that are pH-sensitive experience changes in solubility or undergo morphological transitions in response to changes in pH. pH-responsive polymers are polyelectrolytes bearing weak acidic or basic units which are protonated or deprotonated by modifying the pH of the solution. Polymers with acidic groups (such as carboxylic acids, sulfonic acids and phosphonic acids) or basic groups (such as pyridines and tertiary amines) are said to be pH-responsive because when these groups are ionized, there is a change in morphology.

Individual acidic or basic groups of pH-responsive polymers can be ionized similarly to those of a monoacid or a monobase. As the polymer becomes more highly charged, further ionization becomes more difficult because of the electrostatic effects produced by adjacent ionized groups. As a result, the effective acid dissociation constant (pKa) of a polyacid depends on numerous factors including polymer concentration, ionic strength and degree of ionization. Chain conformation, solubility and volume of pH-responsive copolymers can be designed by controlling the charges along the polymer chain.^{5,77}

2.1.1 pH-responsive polymers with acidic groups

Weak polyacids accept protons at low pH and release protons at neutral and high pH. They are classified according to their functional groups.

Polyacids bearing carboxylic acid groups are the most widely studied. The ionization of the carboxylic acid group directly affects its hydrophilicity and the chain conformation. The carboxylic acid groups lose protons at high pH producing more negatively charged groups in the polymer chain. Figure 1.7 shows the structures of polyacrylic acid (PAA) chains when they are protonated and deprotonated. The dissociation constant (pK_a) of the acid determines the pH at which the acid is ionized. In addition to the degree of ionization, for polyacids, pK_a depends on the structure, composition and molar mass of the polymer. Polyacrylic acid (PAA)^{8,36,39} and polymethacrylic acid (PMAA)⁷⁸ are the most frequently reported polyacids, because they can be easily obtained by various polymerization techniques. In some investigations acrylate monomers have been polymerized with other monomers via RDRP techniques and a further selective acidolysis on the acrylate monomer was performed to obtain polymers with carboxylic groups^{79–81}. Figure 1.8 shows some monomer structures with weak acidic groups, used to obtain pH-responsive polymers.

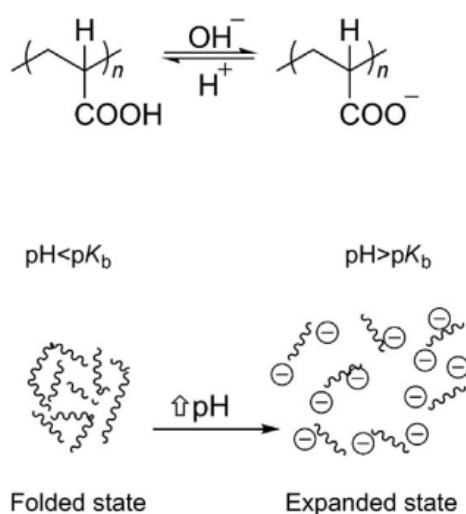


Figure 1.7. Structures and states depending on the ionization of the ionic chain groups of poly(acrylic acid). Reproduced from Garcia-Fernandez et al. (2019) published in Smart Polymers and their Applications.⁷⁷

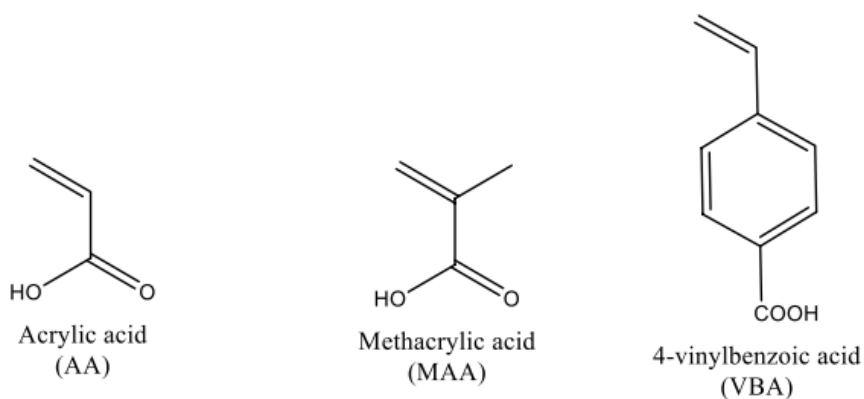


Figure 1.8. Monomers with acidic groups for the synthesis of pH-responsive polymers.

Other polyacids such as sulfonic, phosphonic and boronic acids, have been investigated. The most widely used sulfonic polyacids are poly(2-acrylamido-2-methylpropane sulfonic acid)⁸² and poly(4-styrene sulfonic acid). Sulfonic polyacids are preferred for the preparation of hydrogels⁸³. Due to their high degree of ionization, sulfonic polyacids exhibit a gradual transition over a broad pH range. The phosphonic acids (poly(vinylphosphonic acid)) have been applied for the synthesis of hydrogels which are swollen under basic pH conditions.⁸⁴ Polymers bearing boronic acid groups (poly(aminophenylboronic acid ethyl methacrylate)) in their structures are used as self-healing gels and glucose sensors.⁷⁶

2.1.2 pH-responsive polymers with basic groups

Weak polybases, which have amine pendant groups, accept protons at low pH and form a positively charged polymer chain. They undergo ionization/deionization transitions at pH around 7-11. The most studied polybases are methacrylates, methacrylamides and vinylic polymers containing tertiary amines^{85,86}, but other polybases with nitrogen-containing groups have also been reported, such as pyrrolidone⁸⁷, pyridine⁸⁸ and imidazole.⁸⁹ Figure 9 depicts some monomer structures with basic groups used to synthesize pH-responsive polymers.

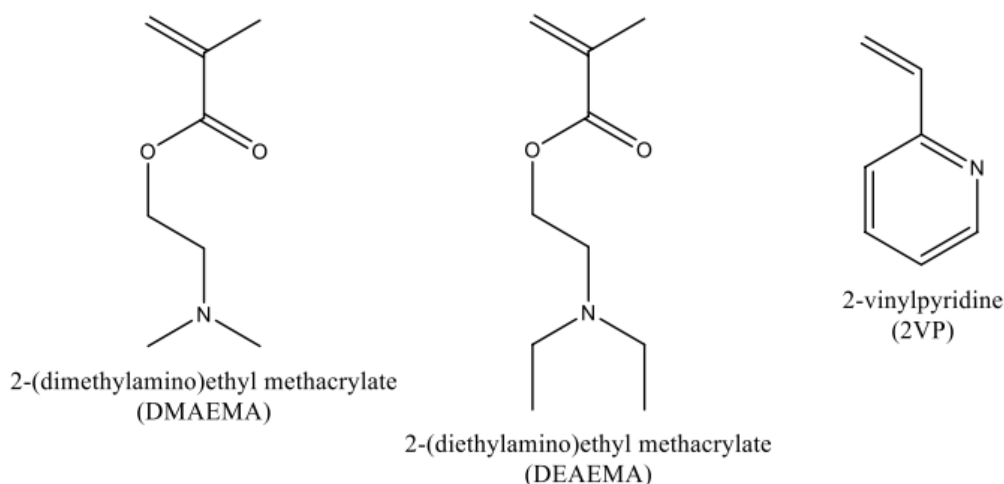


Figure 1.9. Monomers with basic groups for the synthesis of pH-responsive polymers.

2.2 Self-assembly in solution

When an amphiphilic copolymer is dissolved in a selective solvent, it forms aggregates because of the association of the solvophobic block. This process leads to morphologies like spheres, vesicles, rods or sheets.⁹⁰ The different self-assembled morphologies of amphiphilic copolymers (Figure 1.10), are produced by the inherent molecular curvature which influences the packing of the copolymer chains. Determined self-assembled morphologies can be targeted according to the packing parameter, which is defined as:

$$p = \frac{v}{a_0 l_c}$$

Where v represents the volume of the hydrophobic chains, a_0 is the optimal area of the hydrophilic head group and l_c is the length of the hydrophobic tail. It has been established that the formation of spherical micelles are favored when $p \leq 1/3$, cylindrical micelles are formed with $1/3 \leq p \leq 1/2$ and vesicles with $1/2 \leq p \leq 1$.⁹¹

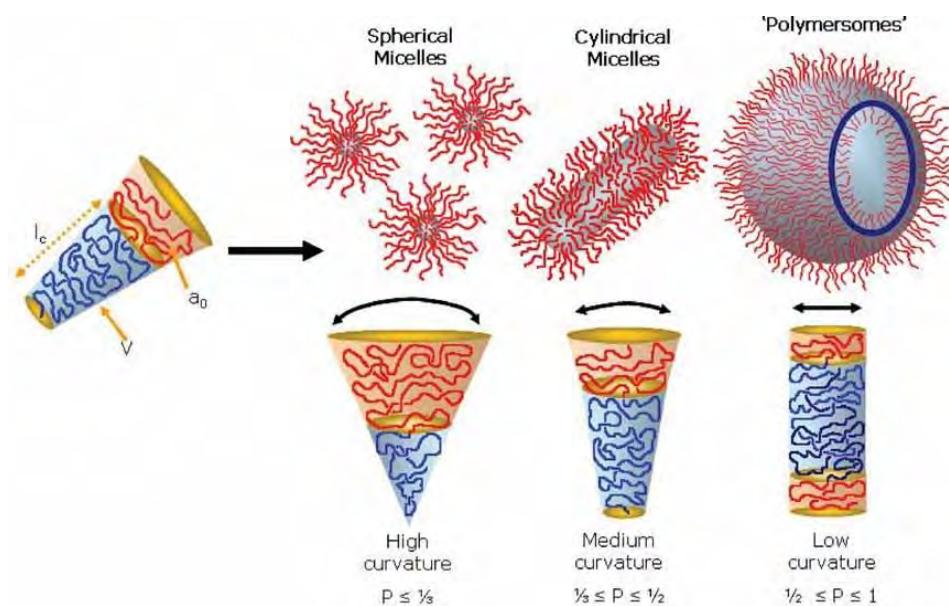


Figure 1.10. Different self-assemblies morphologies formed by amphiphilic copolymers. Reproduced from Blanazs et al. (2009) published in *Macromolecular Rapid Communications*.⁹²

An example of an amphiphilic system is the AA-BA block copolymer, which is pH-responsive in solution. This copolymer is soluble at high pH, then after a change in pH the copolymer starts to associate and finally at lower pH the AA block becomes hydrophobic and thus the copolymer precipitates. When the pH is brought back to its initial value the polymer is soluble again. In this case there are step changes rather than a dynamic response.

pH-responsiveness of PAA amphiphilic block copolymers

In amphiphilic block copolymers one of the blocks is hydrophobic and the other one is hydrophilic. In solution, they tend to self-assemble into micelles, in which the hydrophobic block forms the core and the hydrophilic block forms the corona of the micelle. AA has been polymerized with hydrophobic monomers like styrene or butyl acrylate in order to obtain block copolymers with self-assembly behavior responding to pH changes.^{93–95}

Colombani et al. analyzed $PnBA_{90}-b-PAA_{300}$ copolymer at different pH or degree of ionization (α).⁹⁶ DLS and SANS analysis revealed that neither the size (R_h , R_g) nor aggregation number (N_{agg}) showed any significant change from pH 10 ($\alpha = 1$) to pH 5 ($\alpha \sim 0.5$). At pH 3.5 ($\alpha \sim 0.2$) the spherical micelles tend to form clusters, and this is revealed by SANS curves (Figure 1.11), in which a minimum at $q = 0.04-0.05$ (indication of monodispersity) is observed for higher degrees of ionization ($\alpha = 1$, $\alpha \sim 0.5$), but not for $\alpha = 0.2$. In addition, an increase of intensity at low q was observed for $\alpha = 0.2$, this is

an indication of attractive interactions between particles and thus cluster formation. In order to study the reversibility of the micellization process, after the clustering, the pH was cycled 4 times between 10 ($\alpha \sim 1$) to 3 ($\alpha \sim 0$) by rapidly adding 0.4 M HCl and 2 M NaOH solutions and analyzed by DLS. This study showed that the clusters partially disaggregate when the pH is increased, hence the cluster formation and destruction is governed by slow dynamics over a period of several days or weeks.

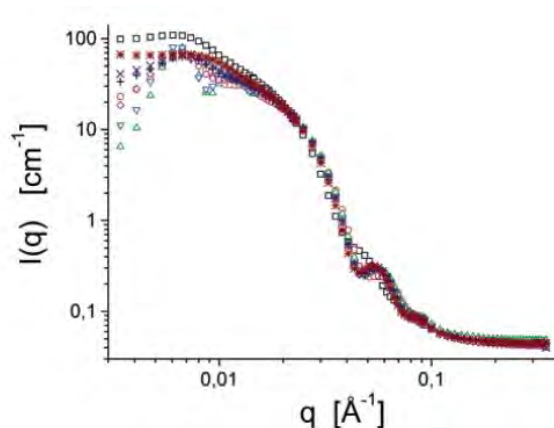


Figure 1.11. SANS curves for PnBA₉₀-PAA₃₀₀ block copolymer in D₂O at different degrees of ionization α : (\square) $\alpha = 0.2$, 0.1 M NaCl; (\circ) $\alpha = 0.5$, 0.1 M NaCl; (Δ) $\alpha = 1.0$, 0 M NaCl; (∇) $\alpha = 1.0$, 0.01 M NaCl; (\diamond) $\alpha = 1.0$, 0.1 M NaCl; (+) $\alpha = 1.0$, 0.3 M NaCl; (x) $\alpha = 1.0$, 0.5 M NaCl; (*) $\alpha = 1.0$, 1 M NaCl. Reproduced from Colombani et al (2007) published in *Macromolecules*.⁹⁶

In a similar study, Jacquin et al. investigated the solution properties of P(*n*-BA-*b*-AA) (3k–4k) copolymers at different pH or degree of ionization.⁹⁷ Cryo-TEM (Figure 1.12) and SANS showed that upon an increase of ionization from $\alpha = 0$ to $\alpha = 1$, a decrease in the core size was observed. Despite this finding, when α was decreased again to 0, the aggregate kept the same aggregation number as for higher ionization ($\alpha = 1$). Thus the structural changes in the core were not reversible and they were not in equilibrium.

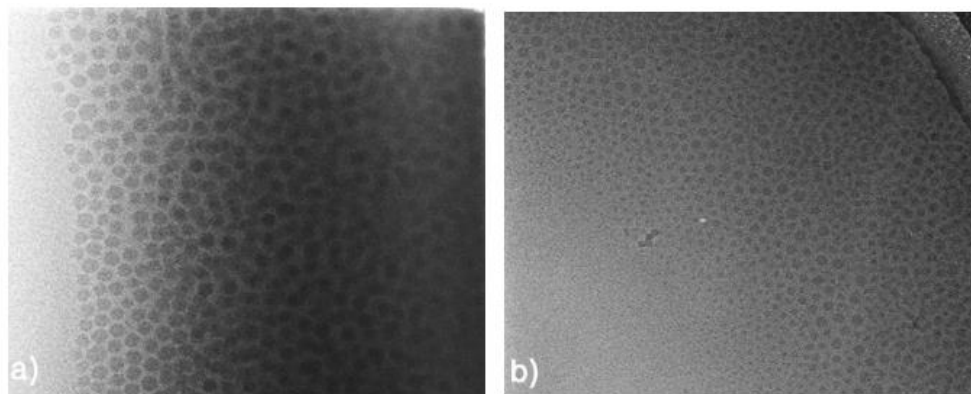


Figure 1.12. Cryo-TEM pictures of PBA-*b*-PAA 3k–4k at $C = 2$ wt% and degree of ionization a) $\alpha = 0$ and b) $\alpha = 1$. Reproduced from Jacquin et al (2007) published in *Journal of Colloid and Interface Science*.⁹⁷

The latter examples from Colombani and Jacquin, show a general picture of the self-assembly of amphiphilic pH-responsive block copolymers with PAA. Both studies demonstrated that micelles formed of PAA-*b*-PnBA, are kinetically frozen (weak change of size with pH) and that the micellization process has a slow or inexistent reversibility.

2.3 Thermoresponsive polymers

Thermoresponsive polymers are especially attractive because temperature can be reversibly applied and without adding anything to the system under observation. There are three kinds of temperature responsive polymers: shape-memory materials⁸³, liquid-crystalline materials and responsive polymer solutions.⁹⁸ In this context, only temperature responsive polymer solutions will be discussed.

Thermoresponsive polymers in solution experience phase transition upon increasing or decreasing temperature. Those polymers which, are miscible with the solvent at low temperatures and then become insoluble when increasing temperature, exhibit a lower critical solution temperature (LCST) behavior (Figure 1.13a). On the contrary, if the polymer becomes insoluble upon decrease of temperature, then it has an upper critical solution temperature (UCST) behavior (Figure 1.13b).⁹⁹ A few polymers exhibit closed loop behavior with both an LCST and UCST (Figure 1.13c). The best known is poly(ethylene glycol) which exhibit both UCST and LCST when heated far above the boiling point of water in closed vessels.¹⁰⁰

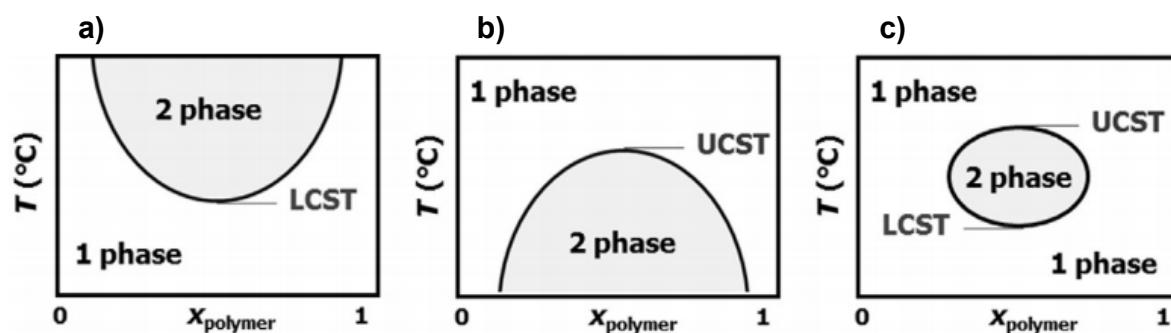


Figure 1.13. Schematic representation of the different thermoresponsive polymer phase diagrams. a) LCST behavior, b) UCST behavior and c) closed loop coexistence. Reproduced from Hoogenboom (2019) published in *Smart polymers and their applications*.⁹⁸

The terms cloud point temperature and LCST should not be confused. Cloud point temperature (T_{cp}) refers to the temperature where the polymer solution at a specific concentration undergoes a phase transition from a soluble to a collapsed state. Thus T_{cp} can be located at any position in the binodal curve and the polymer concentration needs to be specified. As observed in Figure 1.13a, the LCST is the minimal point on the binodal curve, that is, the lowest T_{cp} value.¹⁰¹

Polymers with LCST behavior

LCST polymers are miscible at low temperatures and become insoluble as the temperature increases. The change from a hydrophilic to hydrophobic state arises from hydrogen bonding between the polymer and water at low temperatures. Then upon an increase of temperature, the hydrogen bonds are weakened and the polymer chains become partially dehydrated which leads to aggregation.

In thermodynamic terms, for a polymer to be soluble at low temperature and insoluble at high temperature, the Gibbs free energy of dissolution ($\Delta G = \Delta H - T\Delta S$) must be negative at low temperature and positive at high temperature. For this to be possible, the enthalpy of dissolution must be negative, which is the result of favorable hydrogen bonding between water molecules and polymer chains. This also leads to a high ordering which contributes for the entropy of mixing to be negative. This means that when water is bound to the polymer chains it loses entropy.⁹⁸ When temperature increases, the enthalpy of mixing becomes smaller because of partial dehydration of polymer chains and most importantly the term $-T\Delta S$ becomes predominant which will lead to a positive free Gibbs energy. It is important to mention that polymer chains do not become totally dehydrated

during the LCST transition. This is dependent on the hydrophilicity of the polymer: the more hydrophilic the polymer the more water will be retained in its collapsed form.

Various types of polymers with LCST behavior have been investigated, including poly(*N*-alkyl substituted acrylamides)¹⁰², poly(*N*-vinylalkylamides)¹⁰³, poly(oligoethylene glycol methacrylates)¹⁰⁴ and more recently poly(oxazolines).¹⁰⁵ One of the most popular poly(*N*-alkyl substituted acrylamides) is poly(*N*-isopropylacrylamide) (PNIPAM) because its LCST occurs at 32 °C, which is very near to the body temperature and thus making this polymer very suitable for biomedical applications. As all thermoresponsive homopolymers, the repeating unit of PNIPAM contains both hydrophobic (isopropyl) and hydrophilic (amide) groups. Figure 1.14 shows some monomer structures used to synthesize thermoresponsive polymers. There are three types of LCST thermosensitive copolymers.

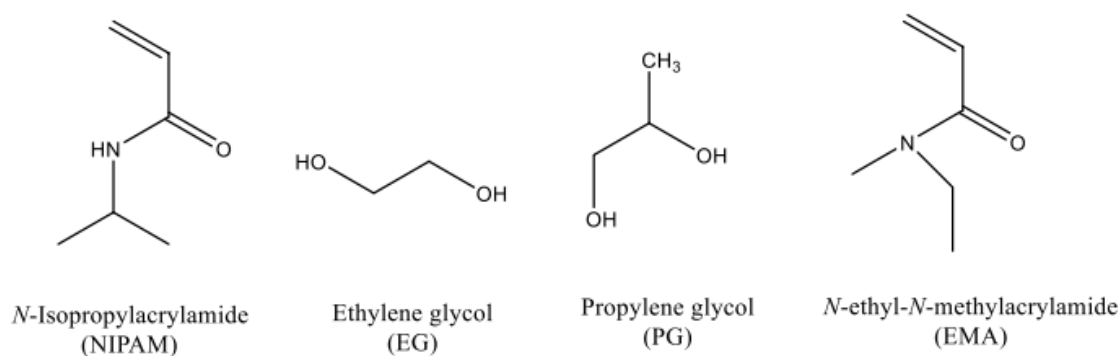


Figure 1.14. Monomer structures for the synthesis of thermoresponsive polymers.

The polymers of type I (Figure 1.15a) have a Flory-Huggins miscibility behavior, this means that the value of the critical point will shift towards a lower polymer concentration if the molar mass of the polymer increases.¹⁰⁶ The polymers of type II (Figure 1.15b) are weakly affected by a variation on the polymer chain length.¹⁰⁷ Type III systems have a bimodal phase diagram (Figure 1.15c) and possess two critical points; the first critical point positioned at low polymer concentration, has a classical Flory-Huggins behavior; the other critical point is almost unaffected by the chain length at high polymer concentration. Hence polymers type III combine behaviors corresponding to type I and type II.¹⁰⁸ PNIPAM is a type II polymer, which means that its LCST is nearly independent of the molar mass.¹⁰³ Phase diagrams corresponding to each polymer type are shown in Figure 1.15.

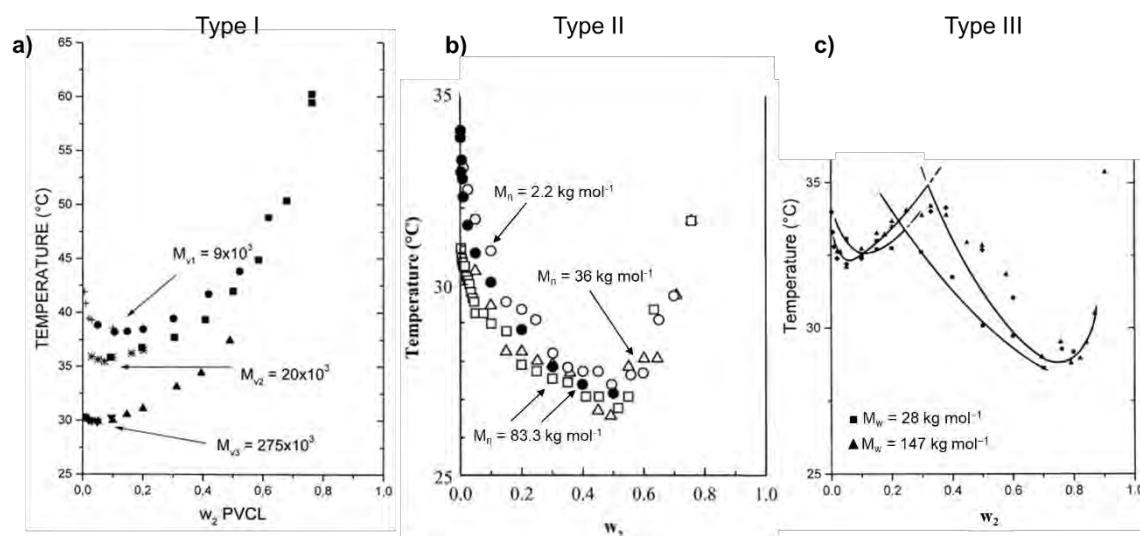


Figure 1.15. Phase diagrams of a) poly(*N*-vinylcaprolactam)¹⁰⁶ (LCST type I), b) poly(*N*-isopropylacrylamide)¹⁰⁷ (LCST type II) and c) poly(vinyl methyl ether)¹⁰⁸ (LCST type III) in water with different molar masses. In b) open symbols correspond to data obtained from DSC and closed symbols correspond to data obtained from turbidimetry.

The LCST can be modified by the copolymerization of the thermoresponsive polymer with hydrophilic or hydrophobic monomers, or, in the case of polymers of molar mass below 50 kg mol^{-1} ,¹⁰³ by incorporating low molar mass hydrophilic or hydrophobic end-groups. Hydrophilic end groups or comonomers result in a decrease in the LCST, while hydrophobic end groups or comonomers increase the LCST.

2.4 PNIPAM LCST modification with hydrophobic end-groups

Some groups have investigated the effect of tethering hydrophobic or hydrophilic end groups to PNIPAM with the aim to tune its LCST.^{109–113} For instance, the thermal behavior of PNIPAM oligomers with dodecyl and carboxylic acid end-groups (Figure 1.16) has been investigated.¹¹⁴ As observed in Figure 1.17, when PNIPAM chain is short (DP = 17) the LCST remains close to room temperature, while larger chains (DP = 60, 78, and 96) led to a LCST of $\sim 32 \text{ }^\circ\text{C}$, that of conventional PNIPAM. Thus the larger the chain it will be less affected by the end-group.¹⁰³ In addition the presence of dodecyl end-groups leads to the self-assembly of PNIPAM at low temperatures (10 and $20 \text{ }^\circ\text{C}$). Ionization of the carboxylic end group provokes the stabilization of PNIPAM aggregates, because phase separation above the LCST is suppressed, and micelles are still present above $50 \text{ }^\circ\text{C}$. But in the case of short PNIPAM chains (DP = 17 and 39) with ionized carboxylic acid group, the size of micelles remains nearly constant with the change of temperature. On the contrary, longer PNIPAM chains (DP ≥ 60) exhibit micelle elongation as in the

case of the non-ionized chains. Hence the hydrophilic end-group do not have a great influence on the self-assembly of PNIPAM at low temperatures, contrary to the behavior produced by hydrophobic end-group.

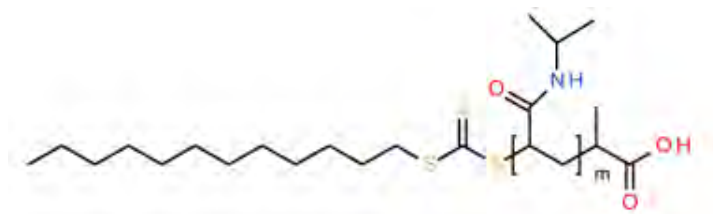


Figure 1.16. Structure of PNIPAM with dodecyl and carboxylic acid end-groups.

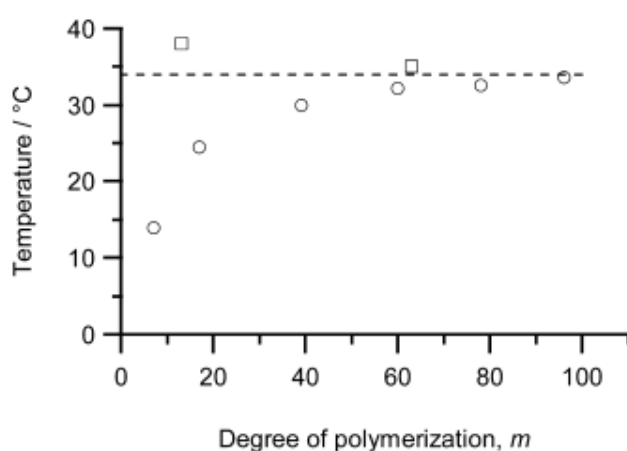


Figure 1.17. LCST for $C_{12}H_{25}$ -NIPAM $_m$ as a function of degree of polymerization (m). LCST of $C_{12}H_{25}$ -NIPAM $_m$ (○), LCST of PNIPAM oligomers reported from literature (□). Reproduced from FitzGerald et al (2014), published in Langmuir.¹¹⁴

The self-assembly of (PNIPAM, poly(N-propylacrylamide) (PNnPAM and poly(cyclopropylacrylamide) (PCPAM)) with ethyl and dodecyl terminal groups revealed that all the polymers with dodecyl end group as well as PCPAM with ethyl end group, are able to form micelles below their LCST. While PNIPAM and PNnPAM with ethyl end-groups exist as individual polymer chains. PNIPAM with dodecyl end group and PNCPAM with both end groups remained as dispersed micelles when temperature was near to their LCST.¹¹⁰ Thus, it is deduced that the effect of the end-group becomes more important when its molar mass is larger. In summary, by incorporating hydrophobic end-groups the miscibility of PNIPAM in water is reduced and so it is the entropy of mixing through micelles formation

2.5 PNIPAM LCST modification with hydrophilic or hydrophobic comonomers

Heating-induced micellization studies by DLS, DSC or turbidimetry have demonstrated that the LCST increases in PNIPAM random copolymers, by increasing the fraction of hydrophilic comonomer.^{115–118} This phenomenon has been studied in systems of NIPAM-DMA copolymers in which the turbidimetry analysis revealed that the increase of DMA content rises the LCST. For instance copolymers with 10% of DMA displayed an LCST of 36 °C while a copolymer with 50% DMA, exhibited an LCST of 63 °C.^{119,120} It was also demonstrated that with a content of 20% NIPAM, the copolymer did not display any LCST.

When comparing to block copolymers, the LCST of random copolymers is even larger, as shown in Figure 1.18, which indicates that the random distribution of hydrophilic units along the chains, not only has strong influence on the self-assembly of the NIPAM segments but it also increases the hydrophilicity of the whole polymer chains.¹²¹

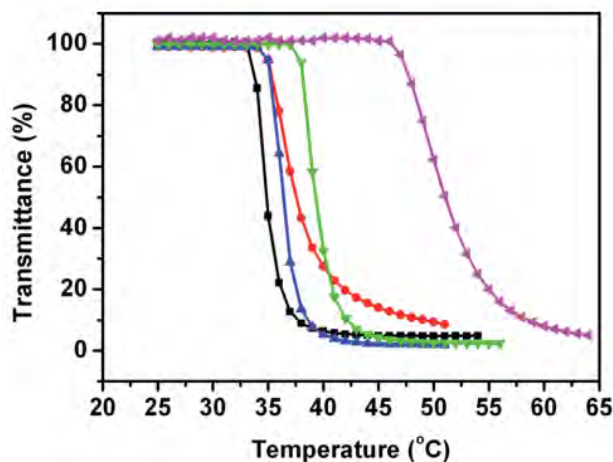


Figure 1.18. Turbidity curves of PNIPAM (black), mixture of PNIPAM and PVCL (red), diblock copolymer (blue), statistical copolymer (green) and PVCL (purple) in water upon heating at the concentration of 0.2 mg mL⁻¹. Reproduced from Hou et al. (2015) published in *Soft Matter*.¹²¹

In another example, the thermoresponsive analysis of DMA-NIPAM statistical copolymers containing one dodecyl end group, showed that the cloud point temperature (T_{cp}) for poly(N-co-D)₁₀₇-C12 containing 30 mol% DMA was 46 °C (Figure 1.19), which in comparison with the LCST of the PNIPAM homopolymer, is 14 °C larger.¹¹¹

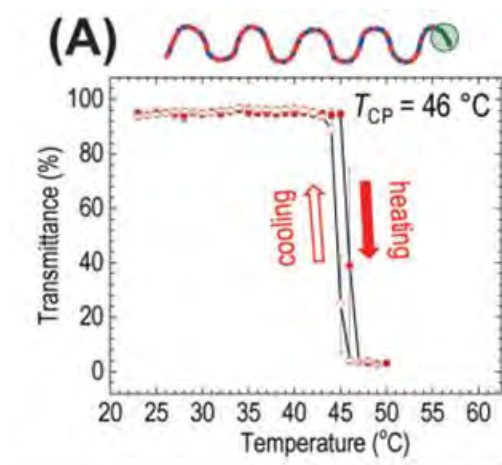


Figure 1.19. Turbidimetry curves of poly (NIPAM-co-DMA)₁₀₇-C12. Heating (filled, red circles and arrow) and cooling (open, red circles and arrow). Reproduced from Ohnsorg et al. (2019) published in *Polymer Chemistry*.¹¹¹

On the other hand, the LCST of PNIPAM decreases when the copolymerization is performed with hydrophobic monomers and it further decreases when the fraction of hydrophobic monomer is increased.¹²² As shown in Figure 1.20, the random distribution of hydrophobic units along the polymer chain produces a broadening of the LCST transition, in comparison with the pure PNIPAM.^{123,124}

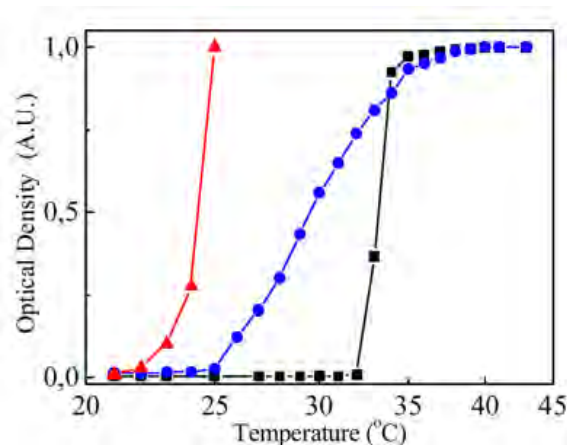


Figure 1.20. Optical density as a function of temperature of aqueous solutions (0.5% w/v) of PNIPAM (squares), P(NIPAM₉₀-co-NtBAM₁₀) (circles) and P(NIPAM₉₀-co-NtBAM₁₀) in NaCl 0.2 M (triangles). Reproduced from Iatrìdi et al. (2019) published in *Carbohydrate polymers*.¹²²

3 PROPERTIES OF ASYMMETRIC COPOLYMERS

Different properties can be obtained by varying the monomer distribution along the polymer chain. At the extreme, block copolymers present very different properties from those corresponding to statistical copolymers. Gradient copolymers typically present

properties that are intermediate between block and statistical copolymers, or similar to those of weakly segregating block copolymers. For instance broad glass transition temperatures (T_g) are characteristic of a gradient distribution,^{4,125} nevertheless weakly segregating A–B block copolymers, also exhibit this kind of thermal behavior². Some typical properties of asymmetric copolymers are displayed in Figure 1.21.

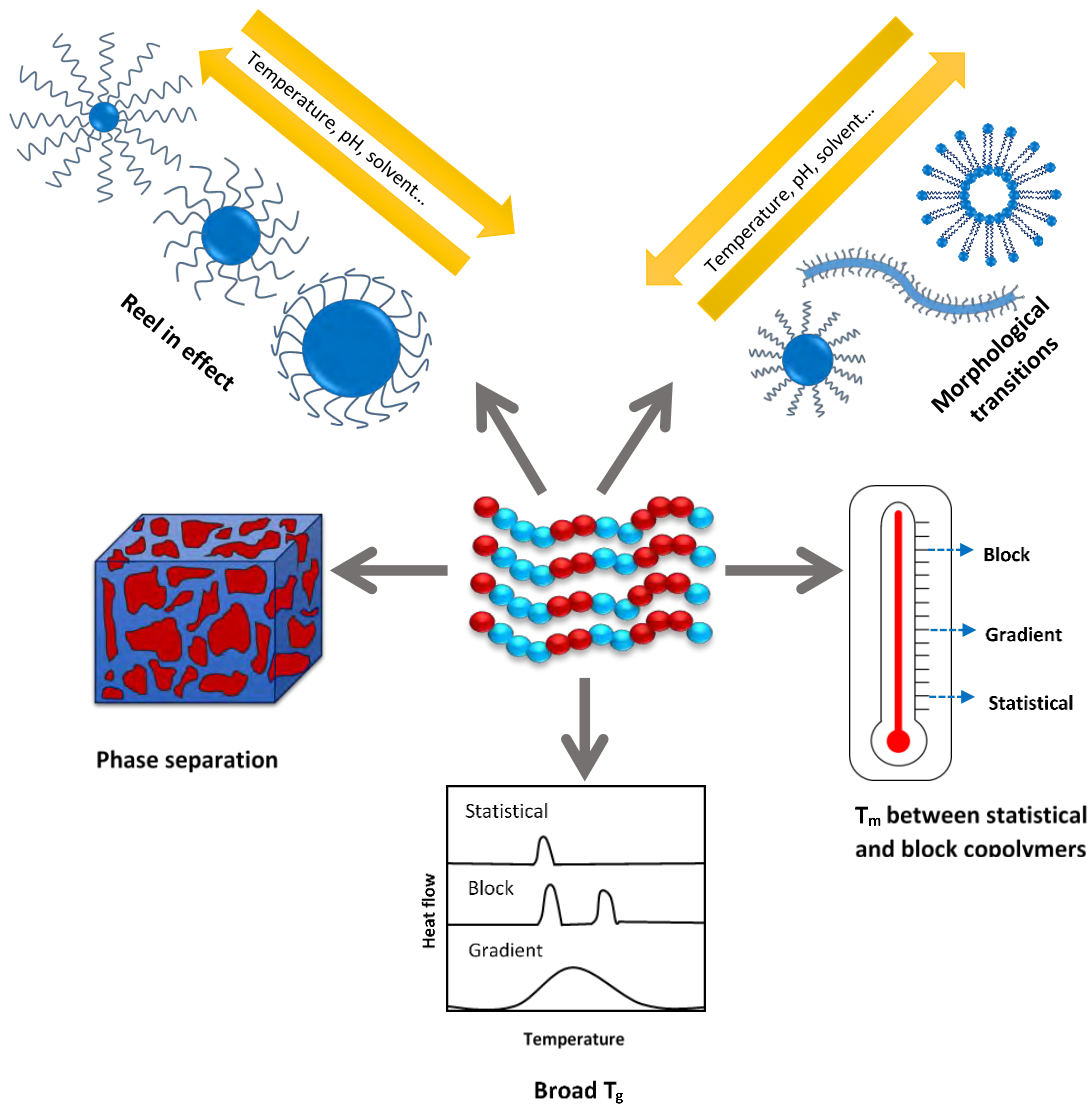


Figure 1.21. Properties of asymmetric copolymers in bulk and solution.

3.1 Critical micelle concentration and cloud point

Critical micelle concentration is the concentration of a surfactant (or amphiphilic copolymer) solution at which it starts to form micelles. Block copolymers tend to have

lower CMCs than gradient copolymers of the same overall composition.^{45,126–131} This is directly related to the fact that in block copolymers there is a well-defined transition between hydrophilic and hydrophobic segments. In a gradient copolymer, the hydrophobic region contains a fraction of hydrophilic units, which makes it more soluble than the pure hydrophobic section of a block copolymer.

There have been many investigations on NIPAM block copolymers with hydrophilic or hydrophobic monomers in order to modify the PNIPAM LCST.^{60,62,111,132–137}

Temperature-induced micellization studies of DMA-NIPAM multiblock copolymers have revealed that diblock copolymers go from molecularly dissolved unimers at low temperature to micelles above the LCST (Figure 1.22a). When temperature is increased above the LCST, the hydrodynamic size decreases which is attributed to further dehydration of aggregates. For the triblock polymers, shown in Figure 1.22b, only the larger copolymers form micelles and the smallest copolymers remained as dissolved unimers. It can also be observed that the smaller the NIPAM fraction in both diblock and triblock polymer micelles, the greater is the LCST. Heating and cooling cycles between revealed that the unimers and aggregate micelles remained approximately constant through the cycles, which means that the self-assembly process is reversible.⁶⁰

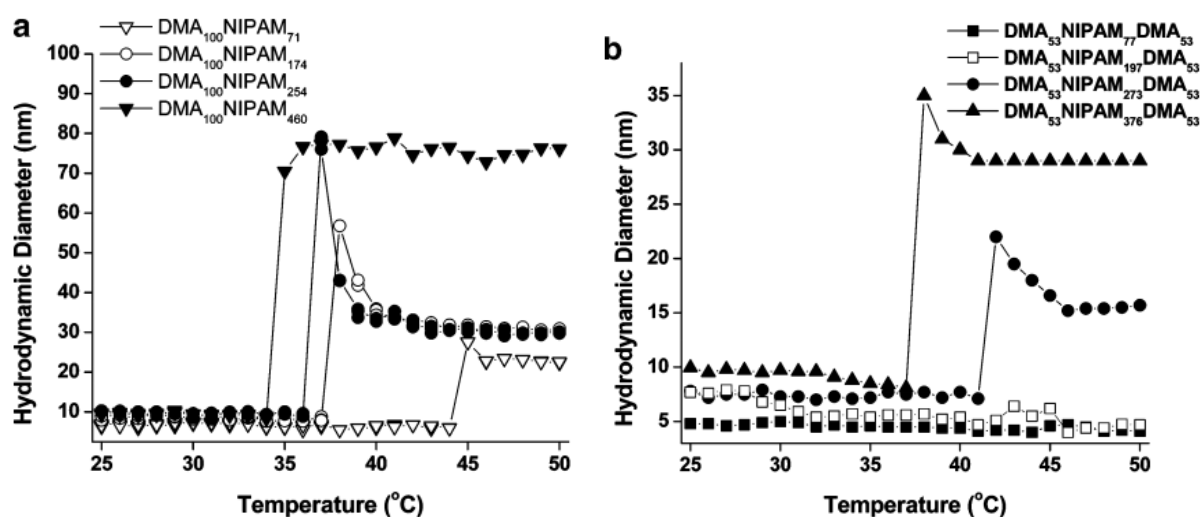


Figure 1.22. Hydrodynamic diameter as a function of temperature for a series of DMA-NIPAM a) diblock and b) triblock copolymers. Reproduced from Convertine et al. (2006) published in *Macromolecules*.⁶⁰

Studies on DMA-NIPAM multiblock copolymers with hydrophobic end groups¹¹¹ (Figure 1.23), revealed that a triblock copolymer (N₅₂D₅₀N₄₁-C12) displayed a T_{cp} of 45 °C,

attributed to a selective hydrophobic collapse of PNIPAM blocks when heating the triblock copolymer, which disrupts the hydrophobic end group to induce the formation of bigger aggregates upon heating. The hysteresis corresponding to this triblock copolymer (Figure 1.23a), takes place because the hydrophobic end group requires more time to form a stabilized core, solubilized by the hydrophilic chain. The unusual behavior of the turbidimetry curve for the pentablock with single hydrophobic chain end was explained using DLS analysis. This revealed that the polymer self-assembles at 31 °C into a single population of aggregates with $R_h = 99$ nm, swells to nearly twice this size at 36 °C, then the size decreases together with PDI ($R_h = 65$ nm) at 42 °C and finally form particles of 58 nm at 50 °C. Thus transmittance drops because a possible rearrangement of the particles when heating above 36 °C. On the other hand, the incorporation of two hydrophobic end groups reduced the T_{cp} in the three systems. Similar behavior was previously reported by Kujawa et al. for PNIPAM systems with double hydrophobic chain ends, which associated to form flower-like micelles.¹¹³ This is also in agreement with the flower-like micelles obtained from PS-PNIPAM-PS triblock copolymer reported by Papagiannopoulos et al.¹³⁶

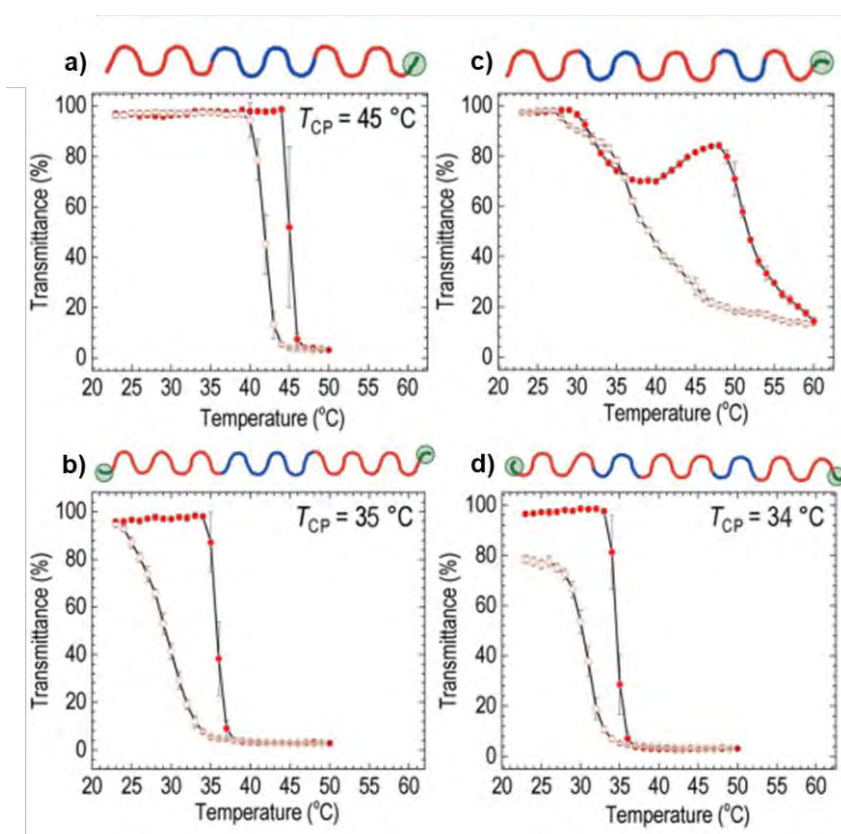


Figure 1.23. Turbidimetry curves of a) $N_{52}D_{50}N_{41}\text{-C12}$, b) $C12\text{-}N_{69}D_{60}N_{69}\text{-C12}$, c) $N_{35}D_{40}N_{42}D_{23}N_{22}\text{-C12}$, and d) $C12\text{-}N_{46}D_{29}N_{46}D_{29}N_{46}\text{-C12}$. Heating (filled, red circles) and cooling (open, red circles). Reproduced from Ohnsorg et al. (2019) published in *Polymer Chemistry*.¹¹¹

The cloud point of an asymmetric copolymer is typically between the cloud points of the corresponding block and statistical copolymers.^{56,138,139} By analyzing the thermoresponsive properties of block and gradient copolymers of 2-hydroxyethyl acrylate and 2-methoxyethylacrylate, it was observed that the cloud point of block copolymers were less dependent on the composition than those of the corresponding gradient copolymers. This is because the cloud point of block copolymers depends on the collapse of the pure hydrophobic block.¹³⁹ Cloud points of asymmetric copolymers are more sensitive to the hydrophilic content within the polymer than those for block copolymers.

The thermosensitive behavior of hyperbolic and linear gradient copolymers of 2-hydroxyethyl methacrylate (HEMA) and 2-(dimethylamino)ethyl methacrylate (DMAEMA) with different gradient strengths (the maximum difference in instantaneous composition along the polymer chain) was analyzed by DLS and it was observed that the onset of cloud point and the gradient strength have a linear relationship, (Figure 1.24). Hence, the more segregated the monomer units in a gradient copolymer, the lower will be the onset of the cloud point.^{140,141}

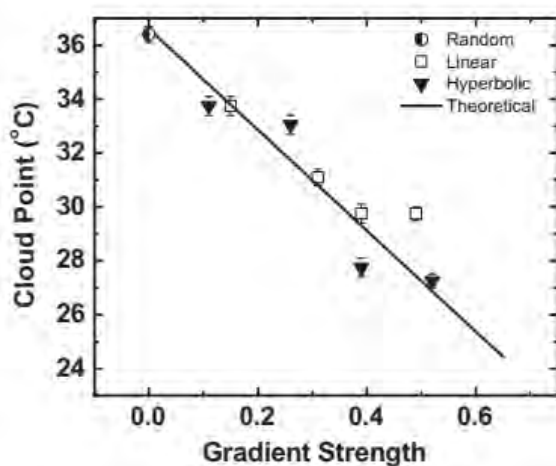


Figure 1.24. Cloud point temperatures of random, linear gradient and hyperbolic gradient copolymers of HEMA/DMAEMA, as a function of their corresponding gradient strength. The straight line denotes a linear fit of the theoretical cloud points. Reproduced from Gallow et al. (2012) published in *Polymer*.¹⁴⁰

3.2 Self-assembly of gradient copolymers

Generally, block copolymers in solution form aggregates which do not present any change with an external stimulus such as temperature, pH or solvent. These aggregates are said to be kinetically frozen. Block copolymer aggregates can also experience changes with varying the external conditions, but this evolution will not be continuous,

as in the case of AA-BA block copolymers. On the other hand, the aggregates of a gradient copolymer vary continuously with subtle changes on the environment, this is they have a continuous dynamic behavior. It is important to remark that a reversible self-assembly process can result in kinetically frozen aggregates.

For assemblies of block copolymers to be dynamic, polymer chains must be able to leave the aggregate. This requires the hydrophobic block to have a certain mobility within the micelle. Energy is required for this hydrophobic chain to migrate from the micelle to the solvent. This energy is defined as follows:

$$E_a = m^{2/3}\gamma$$

Where m represents the molar mass of the copolymer and γ is the surface tension between the hydrophobic block and the solvent. Thus, if m or γ are very high, the energy will be very elevated and it will be impossible for the hydrophobic block to escape from the aggregate.^{90,142} On the other hand, some block copolymers with a low molar mass¹⁴³ or low γ ¹⁴⁴ do possess dynamic behavior.

To overcome this issue more easily, incorporating hydrophilic units into the hydrophobic block results in an efficient way to decrease γ .^{39,145–148} Colombani et al. have investigated the effect of introducing different fractions of AA units into the poly(*n*BA) block of PAA-*b*-(*Pn*BA-*s*-PAA). These copolymers show dynamic behavior on the formation of aggregates through a wide range of ionization degrees, allowing a fine-tuning of pH range where a transition between visco-elastic solutions and self-supporting hydrogels occurs (Figure 1.25).

The self-assembly of asymmetric copolymers can be achieved by external stimulus such as varying the composition of the solvent¹⁴⁹, pH⁴³, temperature¹³¹ or in some cases multiple stimulus as temperature and pH.¹⁵⁰

In general, block copolymers undergo a stepwise transition while asymmetric copolymers have a continuous evolution with changing solvent characteristics.

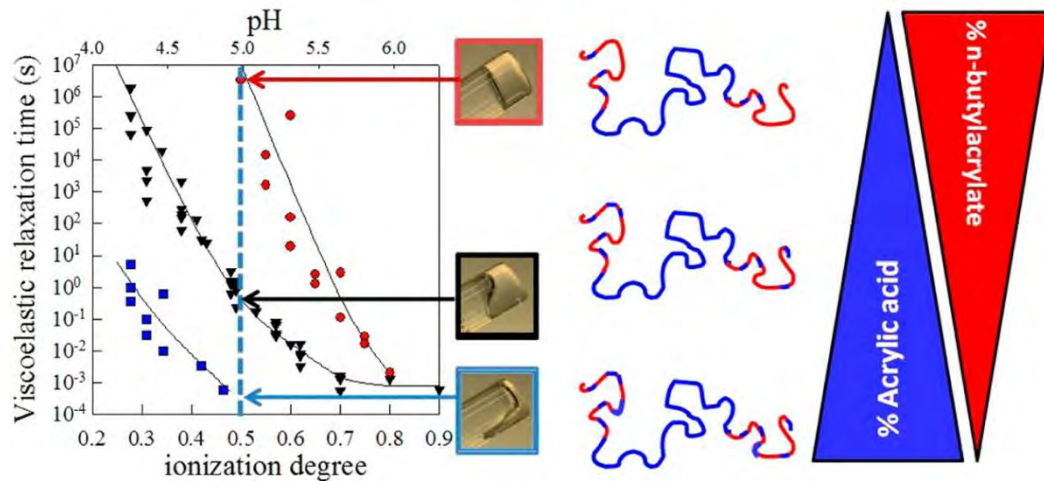


Figure 1.25. Dependence of the relaxation time on the ionization degree for amphiphilic copolyelectrolytes consisting of a central poly(acrylic acid) block and terminal poly(n-butyl acrylate-co-acrylic acid) blocks containing 40 (red), 50 (black), or 60 (blue) mol% of AA units. Reproduced from Shedge et al. (2014) published in *Macromolecules*.⁸¹

The reel-in effect

The continuous micellization process of gradient copolymers through the variation of solvent conditions has been explained by the reel-in effect. This is, the external chains that are part of the corona coil around the core when the quality of the solvent changes.¹⁵¹

Seno et al. studied the self-assembly of vinyl ether block and gradient copolymers in solution, as stimuli responsive systems and they observed how the gradient copolymers experience the reel-in effect. The size of gradient copolymer micelles decrease when the solution temperature is above the lowest critical solution temperature (LCST). On the other hand, the analogous micelles formed from block and random copolymers remained the same size through the variation of temperature (Figure 1.26).

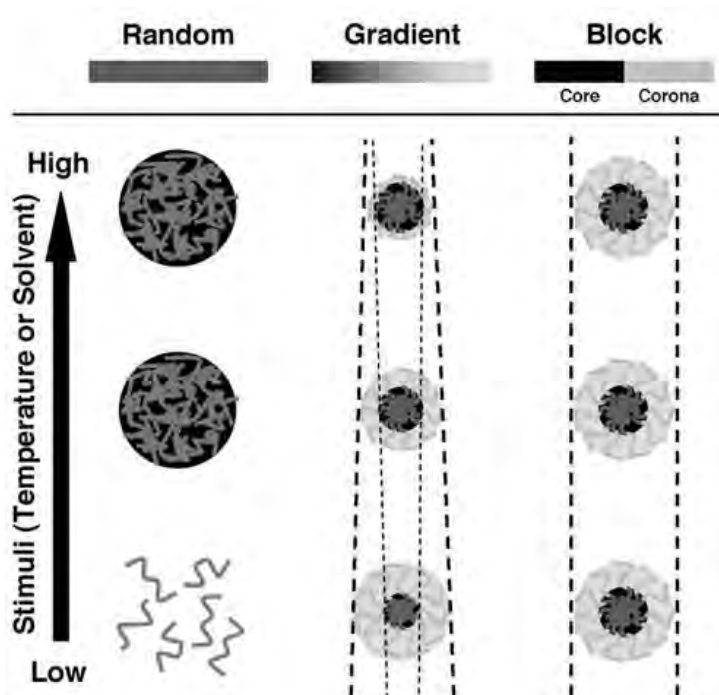


Figure 1.26. Differences in the micellization behavior of random, gradient and block copolymers depending on the temperature of the solvent. Reproduced from Seno et al. (2008) published in *J. Polym. Sci. Part A: Polym. Chem.*¹³⁸

In other works, light scattering and small angle neutron scattering (SANS) have been used in order to compare the micellization as a function of temperature in gradient and block copolymers. These studies showed a gradual microphase separation in the gradient copolymer solutions, which was attributed to the reel-in effect. On the contrary the block copolymer presented a stepwise micellization.^{151,152} In the work of Okabe et al., the micellization of 2-ethoxyethyl vinyl ether and 2-methoxyethyl vinyl ether (EOVE/MOVE) block and gradient copolymers was investigated by SANS at different temperatures. For the block copolymer they observed no significant variation on the size of the core or the shell. This was attributed to a stepwise change in the self-assembly of the block copolymer. In contrast, for the gradient copolymer the radius of the core increased and at the same time the size of the shell decreased, as shown in Figure 1.27. This phenomenon was due to a gradual partition of the gradient chains to core and corona.

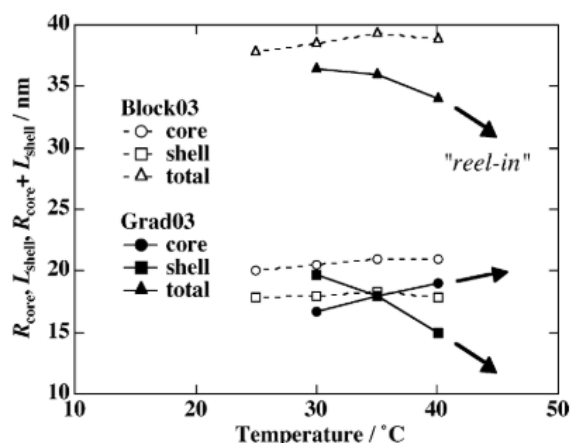


Figure 1.27. Temperature dependence of the sizes of micelle core and shell for block and gradient copolymers. Reproduced from Okabe et al. (2006) published in *Macromolecules*.¹⁵¹

Zheng et al. investigated the micellization process of styrene-methyl methacrylate gradient copolymers by changing the water content in water/acetone mixtures. Three main transitions could be detected, (Figure 1.28). At the lowest water content the dissolved unimers self-assembled into micelles. The second transition consisted on the decrease on size of the corona and increase of the core, resulting in a reel-in effect by worsening the quality of the solvent. Finally, at the higher water content the shrunken micelles underwent morphological transitions to cylindrical micelles and vesicles.

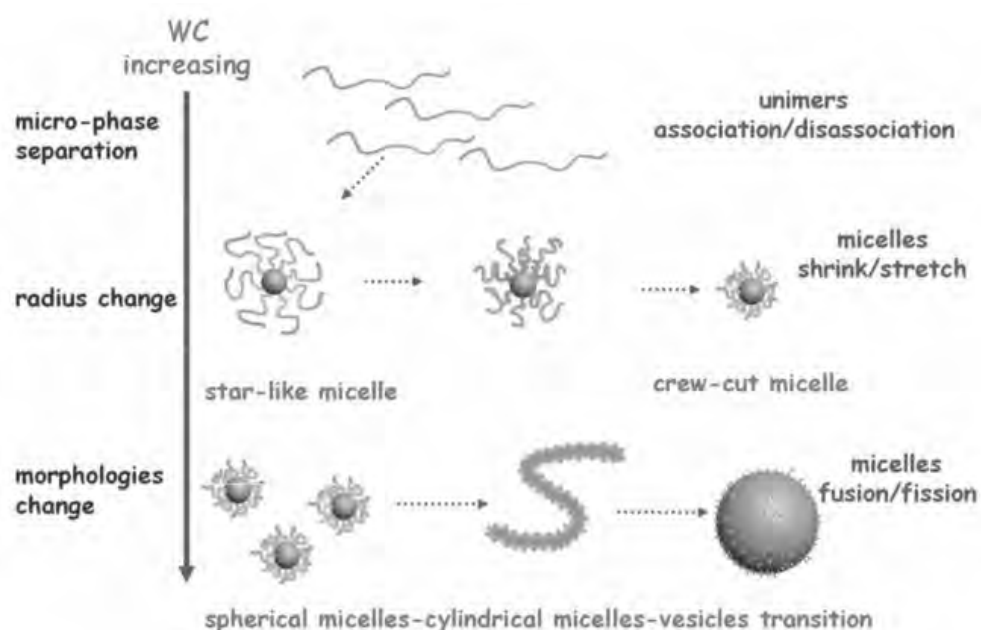


Figure 1.28. Schematic illustration of the overall transitions of the gradient copolymer micellar system via increasing the water content (WC) in acetone-water mixtures: a unimers to micelles transition; a star-like micelles to crew-cut micelles transition; and a morphological transition from spherical micelles to cylindrical micelles to vesicles. Reproduced from Zheng et al. (2013) published in *Macromolecular Rapid Communications*.¹⁴⁹

3.3 Microphase separation and thermal properties in bulk

Thermal properties of polymers in the bulk state are also of great importance, because the potential applications of the polymers will depend on this. Glass transition temperature (T_g) is one of the most important thermal properties of polymers and it is defined as the temperature where the polymer changes from a glassy to a rubbery state, directly affecting the mobility of chains. One of the most popular techniques to determine T_g , is differential scanning calorimetry (DSC) and the T_g can be obtained from the change of slope of the heating curve as a function of temperature. However, in the case of gradient copolymers the T_g ranges are very broad and this approach to measure T_g leads to mistaken values. In order to overcome this problem, the derivative of the heating curve is preferred for the accurately determination of polymers exhibiting breadth in T_g . In Figure 1.29, both approaches are compared and as it can be appreciated, the T_g in the derivative of the heat flow (Figure 1.29) is manifested as a strong peak.

The distribution of monomer units in an asymmetric polymer produces differences in thermal properties and microphase separation in the bulk state, in comparison with their analogous block copolymers. Due to microphase separation, typically block copolymers exhibit defined and separated T_g s. On the contrary, asymmetric copolymers have one single and extremely broad T_g s when the monomers which compose the polymer have a very strong segregation between them. In other words, the broad T_g is a result of the very different T_g s of the constituting homopolymers.^{4,55,125}

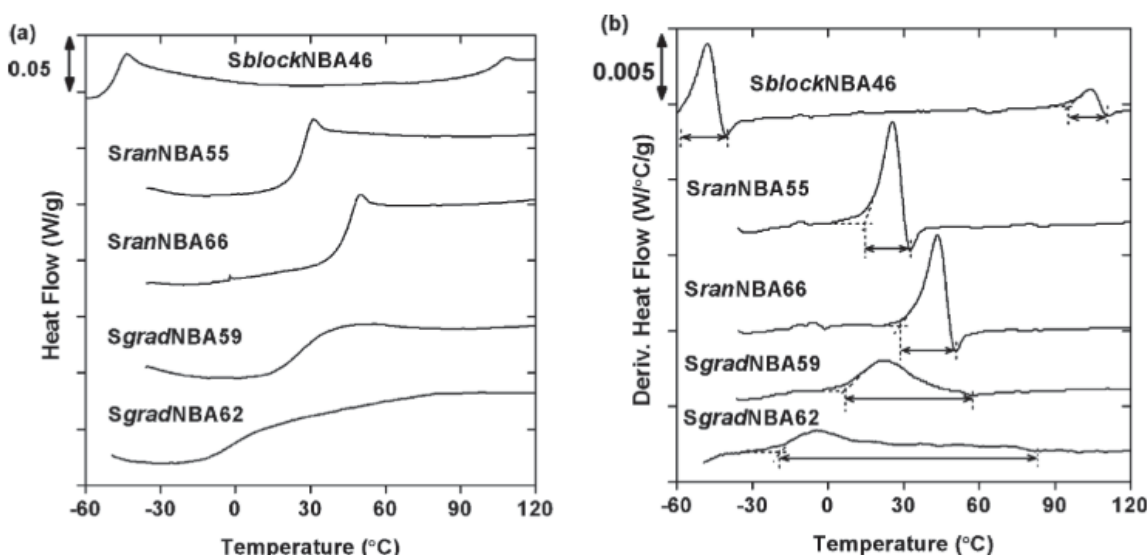


Figure 1.29. (a) DSC heating curves and (b) derivatives for Styrene/n butyl acrylate copolymers. From the derivative curve, the value for T_g onset (T_o) is defined by the onset of deviation in the curve from the baseline (e.g., 15.7 °C for *SranNBA55*), while the T_g endpoint (T_e) value is defined by the local minimum present due to enthalpic relaxations (e.g., 34.3 °C for *SranNBA55*). The difference between T_o and T_e yields the T_g breadth (e.g., 18.6 °C for *SranNBA55*). Reproduced from Mok et al. (2009) published in *Macromolecules*.⁴

It can be seen in Figure 1.29 that *St/nBA* block copolymer exhibits two well separated and narrow T_g s, each one corresponding to the T_g of PS and *PnBA*. This is a result of nanophase separation into ordered microdomains. In random copolymers all the units are mixed together and thus it only has one single and narrow T_g , which indicates a lack of nanoscopic heterogeneity. On the other hand, since the gradient copolymer has regions which are richer in PS, some other regions that are richer in *PnBA* and there are intermediate regions where both homopolymers are intimately mixed, it displays one single and broad T_g . This is produced by the incomplete microphase segregation leading to a compositional heterogeneous bulk material.

The T_g breadth in gradient copolymers depends on two factors: the segregation strength of the system (defined as χN , where χ is the Flory-Huggins interaction parameter and N is the average number of monomers per the chain) and the inherent difference in the homopolymers T_g values. Hence, by controlling the molar mass or chains length (N), the segregation strength and the gradient profile, it is possible to control the T_g breadths of gradient copolymers.

The relationship between the T_g breadths and the phase separation is explained with Figure 1.30, in which the gradient copolymer T_g breadths were compared with those obtained theoretically. In order to determine the dependence of T_g on composition the results obtained from a group of statistical copolymers were used. The equilibrium lamellar composition profiles, showed in Figure 1.30 consist of discrete points corresponding to determined set of compositions. It is thus assumed that all these volume fractions, $\Phi(z)$, contribute a T_g that corresponds to its distinctive composition. After, the derivative of *tanh* function (*tanh* functions were used to fit DSC heat flow curves) was used to represent these individual contributions (Figure 1.30b and c). It can be noted that the derivative of the *tanh* functions are narrow and symmetric peaks, very similar to the heat flow derivatives corresponding to homopolymers or statistical copolymers. Hence, it can be inferred that gradient copolymers contain a wide variety of dynamic environments.

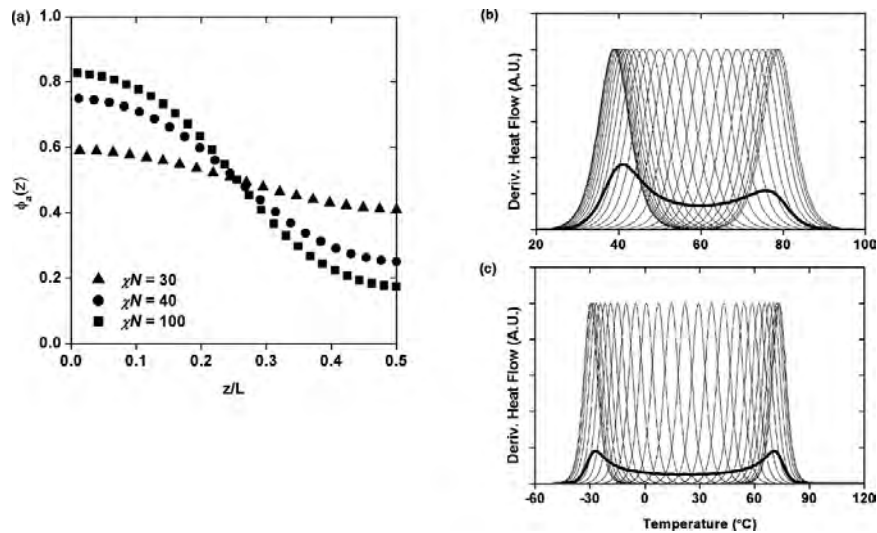


Figure 1.30. a) Equilibrium lamellar compositions for a symmetric linear gradient copolymer calculated at $\chi N = 30, 40,$ and 100 using self-consistent mean-field (SCMF) techniques. The period of the lamellar structure is L . Predicted differential scanning calorimetry (DSC) derivative heat flow curves for b) styrene/n-butyl methacrylate (S/BMA) and c) styrene/nBA linear gradient copolymers with $\chi N = 100$. The thin lines are the derivative heat flow traces corresponding to copolymers with the composition fractions predicted in the composition profile, while the bold line is the area-normalized summation of the individual composition fraction traces. Reproduced from Mok et al. (2009) published in *Macromolecules*.⁴

4 CONCLUSIONS

À partir de cette recherche bibliographique, il a été possible d'identifier les différences de structures et donc de propriétés, entre copolymères asymétriques, statistiques et à blocs. Dans les copolymères statistiques, les monomères sont statistiquement répartis le long de la chaîne et dans les copolymères à bloc la transition d'un segment à l'autre est bien définie. De plus, un copolymère asymétrique doit contenir au minimum deux segments de compositions significativement différentes. Différents profils de copolymères à gradient peuvent être obtenus grâce à la grande variété de voies de synthèse disponibles telles que la synthèse spontanée, forcée, par étapes et de catalyse en tandem. Dans la synthèse spontanée, il est nécessaire que les monomères aient des rapports de réactivité différents, tandis que dans une synthèse forcée les monomères peuvent avoir des rapports de réactivité similaires ou différents, puisque le profil de composition est ajusté en contrôlant la vitesse d'addition des monomères. La synthèse par étapes est effectuée par addition séquentielle des monomères et dans une polymérisation par catalyse en tandem, le monomère est simultanément polymérisé et converti en un nouveau monomère.

En raison de leurs structures uniques, les copolymères asymétriques possèdent des propriétés intéressantes (soit en solution ou en masse) parfois entre celles des copolymères à bloc et statistiques. C'est le cas notamment de la température de transition vitreuse. Les copolymères asymétriques s'auto-assemblent en structures dynamiques, capables de changer de taille ou de morphologie en raison d'un stimulus externe tel que le pH ou la température. Ils ont également des valeurs de CMC et de température de point de trouble plus élevées que les copolymères à blocs, et sont le résultat de la distribution asymétrique des monomères le long de la chaîne, ce qui a pour effet de réduire l'incompatibilité chimique entre les segments de chaîne. Une autre particularité est l'effet «reel-in», qui peut être attribué à la présence de plusieurs segments avec une composition graduellement variable.

4 CONCLUSIONS

Derived from this bibliographic research, it was possible to identify the differences in structures and thus in properties, between asymmetric, statistical and block copolymers. In statistical copolymers, the monomers are statistically distributed along the chain and in block copolymers the transition from one segment to another is well defined. By contrast, an asymmetric copolymer contains at least two segments of measurable different compositions.

Different profiles of gradient copolymers can be obtained thanks to the wide variety of synthetic routes available such as spontaneous, forced, stepwise and tandem catalysis synthesis. In the spontaneous synthesis, it is required that the monomers have different reactivity ratios, while in a forced synthesis the monomers may have, whether similar or different reactivity ratios, since the composition profile is adjusted by controlling the addition rate of the monomers. The stepwise synthesis is performed by sequential addition of the monomers and in a tandem catalysis polymerization, the monomer is simultaneously polymerized and converted into a new monomer.

Because of their unique structures, asymmetric copolymers possess intriguing properties (whether in solution or in bulk) sometimes in between the properties of block or statistical copolymers as in the case of the glass transition temperature. Asymmetric copolymers self-assemble into dynamic structures, which are capable of changing in size or morphology due to an external stimulus such as pH or temperature. They also have higher values of CMC and cloud point temperatures than block copolymers, and is a result of the asymmetric monomer distribution along the chain, which has the effect of reducing the chemical incompatibility between the chain segments. Another special characteristic is the “reel-in” effect, which can be attributed to the presence of multiple segments with gradually varying composition.

LITERATURE

- 1 J. Zhang, B. Farias-Mancilla, M. Destarac, U. S. Schubert, D. J. Keddie, C. Guerrero-Sanchez and S. Harrisson, *Macromol. Rapid Commun.*, 2018, **39**, 1800357.
- 2 R. Jiang, Q. Jin, B. Li, D. Ding, R. A. Wickham and A. C. Shi, *Macromolecules*, 2008, **41**, 5457–5465.
- 3 R. Wang, Y. Luo, B.-G. Li and S. Zhu, *AIChE J.*, 2007, **53**, 174–186.
- 4 M. M. Mok, J. Kim, C. L. H. Wong, S. R. Marrou, D. J. Woo, C. M. Dettmer, S. T. Nguyen, C. J. Ellison, K. R. Shull and J. M. Torkelson, *Macromolecules*, 2009, **42**, 7863–7876.
- 5 C. Charbonneau, C. Chassenieux, O. Colombani and T. Nicolai, *Macromolecules*, 2011, **44**, 4487–4495.
- 6 X. Gu, L. Zhang, Y. Li, W. Zhang, J. Zhu, Z. Zhang and X. Zhu, *Polym. Chem.*, 2018, **9**, 1571–1576.
- 7 V. S. Kravchenko and I. I. Potemkin, *J. Phys. Chem. B*, 2016, **120**, 12211–12217.
- 8 S. Harrisson, F. Ercole and B. W. Muir, *Polym. Chem.*, 2010, **1**, 326–332.
- 9 J. R. Brown, Y. Seo, S. W. Sides and L. M. Hall, *Macromolecules*, 2017, **50**, 5619–5626.
- 10 C. Guerrero-Sanchez, L. O'Brien, C. Brackley, D. J. Keddie, S. Saubern and J. Chiefari, *Polym. Chem.*, 2013, **4**, 1857–1862.
- 11 K. Matyjaszewski, *Macromolecules*, 2012, **45**, 4015–4039.
- 12 G. Moad, E. Rizzardo and S. H. Thang, *Aust. J. Chem.*, 2012, **65**, 985.
- 13 W. A. Braunecker and K. Matyjaszewski, *Prog. Polym. Sci.*, 2007, **32**, 93–146.
- 14 J. Nicolas, Y. Guillaneuf, D. Bertin, D. Gigmes and B. Charleux, *Prog. Polym. Sci.*, 2013, **38**, 63–225.
- 15 R. Wang, Y. Luo, B. Li, X. Sun and S. Zhu, *Macromol. Theory Simulations*, 2006, **15**, 356–368.
- 16 A. Clough, J. L. Sigle, A. Tapash, L. Gill, N. V Patil, J. Zhou and J. L. White, *ACS Publ.*, 2014, **47**, 2625–2631.
- 17 E. Vlassi and S. Pispas, *Macromol. Chem. Phys.*, 2015, **216**, 873–883.
- 18 M. Uchman, J. Hajduová, E. Vlassi, S. Pispas, M. S. Appavou and M. Štěpánek, *Eur. Polym. J.*, 2015, **73**, 212–221.
- 19 Y. Milonaki, E. Kaditi, S. Pispas and C. Demetzos, *J. Polym. Sci. Part A Polym. Chem.*, 2012, **50**, 1226–1237.
- 20 R. Hoogenboom, H. M. L. Thijs, M. W. M. Fijten, B. M. Van Lankvelt and U. S. Schubert, *J. Polym. Sci. Part A Polym. Chem.*, 2007, **45**, 416–422.
- 21 R. Hoogenboom, M. W. M. Fijten, S. Wijnans, A. M. J. Van Den Berg, H. M. L. Thijs and U. S. Schubert, *J. Comb. Chem.*, 2006, **8**, 145–148.
- 22 R. Hoogenboom, H. M. L. Lambermont-Thijs, M. J. H. C. Jochems, S. Hoepfener, C. Guerlain, C. A. Fustin, J. F. Gohy and U. S. Schubert, *Soft Matter*, 2009, **5**, 3590–3592.
- 23 P. Xiang and Z. Ye, *J. Polym. Sci. Part A Polym. Chem.*, 2013, **51**, 672–686.
- 24 Y. Liu, W. M. Ren, K. K. He and X. B. Lu, *Nat. Commun.*, , DOI:10.1038/ncomms6687.
- 25 C. M. Dettmer, M. K. Gray, J. M. Torkelson and S. T. Nguyen, *ACS Publ.*, 2004, **37**, 5504–5512.
- 26 A. B. Chang, T. P. Lin, N. B. Thompson, S. X. Luo, A. L. Liberman-Martin, H. Y. Chen, B. Lee and R. H. Grubbs, *J. Am. Chem. Soc.*, 2017, **139**, 17683–17693.

- 27 T. P. Lin, A. B. Chang, H. Y. Chen, A. L. Liberman-Martin, C. M. Bates, M. J. Voegtle, C. A. Bauer and R. H. Grubbs, *J. Am. Chem. Soc.*, 2017, **139**, 3896–3903.
- 28 K. O. Kim and T.-L. Choi, *ACS Publ.*, 2013, **46**, 33.
- 29 M. D. Lefebvre, C. M. Dettmer, R. L. Mcswain, C. Xu, J. R. Davila, R. J. Composto, S. T. Nguyen and K. R. Shull, *ACS Publ.*, 2005, **38**, 10494–10502.
- 30 K. E. Min, L. I. Mei and K. Matyjaszewski, *J. Polym. Sci. Part A Polym. Chem.*, 2005, **43**, 3616–3622.
- 31 B. S. Kim, H. K. Lee, S. Jeong, J. O. Lee and H. J. Paik, *Macromol. Res.*, 2011, **19**, 1257–1263.
- 32 A. M. Elsen, Y. Li, Q. Li, S. S. Sheiko and K. Matyjaszewski, *Macromol. Rapid Commun.*, 2014, **35**, 133–140.
- 33 B. Gu and A. Sen, 2002, 8913–8916.
- 34 J. He, Y. Wang, Q. Lin, L. Chen and X. Zhou, *J. Macromol. Sci. Part A Pure Appl. Chem.*, 2009, **46**, 405–411.
- 35 S. Qin, J. Saget, J. Pyun, S. Jia, T. Kowalewski and K. Matyjaszewski, *Macromolecules*, 2003, **36**, 8969–8977.
- 36 C. Lefay, B. Charleux, M. Save, C. Chassenieux, O. Guerret and S. Magnet, *Polymer (Guildf)*, 2006, **47**, 1935–1945.
- 37 M. Zaremski, I. Ereemeev, E. Garina, O. Borisova and B. Korolev, *J. Polym. Res.*, , DOI:10.1007/s10965-017-1303-7.
- 38 E. Mignard, T. Leblanc, D. Bertin, O. Guerret and W. F. Reed, *Macromolecules*, 2004, **37**, 966–975.
- 39 O. Borisova, L. Billon, M. Zaremski, B. Grassl, Z. Bakaeva, A. Lapp, P. Stepanek and O. Borisov, *Soft Matter*, 2012, **8**, 7649–7659.
- 40 C. Farcet, B. Charleux and R. Pirri, in *Macromolecular Symposia*, John Wiley and Sons Ltd, 2002, vol. 182, pp. 249–260.
- 41 D. I. Kalugin, M. Y. Zaremski, V. B. Golubev and E. S. Garina, *Polym. Sci. - Ser. B*, 2011, **53**, 307–312.
- 42 N. Cherifi, A. Issoulie, A. Khoukh, A. Benaboura, M. Save, C. Derail and L. Billon, *Polym. Chem.*, 2011, **2**, 1769–1777.
- 43 Z. Černochová, A. Bogomolova, O. V. Borisova, S. K. Filippov, P. Černocho, L. Billon, O. V. Borisov and P. Štěpánek, *Soft Matter*, 2016, **12**, 6788–6798.
- 44 M. Hurtgen, A. Debuigne, C. A. Fustin, C. Jérôme and C. Detrembleur, *Macromolecules*, 2011, **44**, 4623–4631.
- 45 X. Liu, M. Wang, S. Harrisson, A. Debuigne, J. D. Marty and M. Destarac, *ACS Sustain. Chem. Eng.*, 2017, **5**, 9645–9650.
- 46 R. Yañez-Macias, I. Kulai, J. Ulbrich, T. Yildirim, P. Sungur, S. Hoepfener, R. Guerrero-Santos, U. S. Schubert, M. Destarac, C. Guerrero-Sanchez and S. Harrisson, *Polym. Chem.*, 2017, **8**, 5023–5032.
- 47 K. J. Sykes, S. Harrisson, D. J. Keddie, K. J. Sykes, D. J. Keddie and S. Harrisson, 2016, 2310–2320.
- 48 C. Guerrero-Sanchez, S. Harrisson and D. J. Keddie, *Macromol. Symp.*, 2013, **325–326**, 38–46.
- 49 A. Tselepy, T. L. Schiller, S. Harrisson, C. Guerrero-Sanchez, G. Moad and D. J. Keddie, *Macromolecules*, 2018, **51**, 410–418.

- 50 X. Tang, J. Han, Z. Zhu, X. Lu, H. Chen and Y. Cai, *Polym. Chem.*, 2014, **5**, 4115–4123.
- 51 T. Ribaut, P. Lacroix-Desmazes, B. Fournel and S. Sarrade, *J. Polym. Sci. Part A Polym. Chem.*, 2009, **47**, 5448–5460.
- 52 T. Hardeman and G. Koeckelberghs, *Macromolecules*, 2015, **48**, 6987–6993.
- 53 P. Xiang and Z. Ye, *J. Polym. Sci. Part A Polym. Chem.*, 2013, **51**, 672–686.
- 54 Y. Liu, W. M. Ren, K. K. He and X. B. Lu, *Nat. Commun.*, 2014, **5**, 1–7.
- 55 Y. Guo, J. Zhang, P. Xie, X. Gao and Y. Luo, *Polym. Chem.*, 2014, **5**, 3363–3371.
- 56 K. I. Seno, I. Tsujimoto, T. Kikuchi, S. Kanaoka and S. Aoshima, *J. Polym. Sci. Part A Polym. Chem.*, 2008, **46**, 6151–6164.
- 57 K. Nakatani, T. Terashima and M. Sawamoto, *J. Am. Chem. Soc.*, 2009, **131**, 13600–13601.
- 58 K. Nakatani, Y. Ogura, Y. Koda, T. Terashima and M. Sawamoto, *J. Am. Chem. Soc.*, 2012, **134**, 4373–4383.
- 59 Y. Ogura, T. Terashima and M. Sawamoto, *Macromolecules*, 2017, **50**, 822–831.
- 60 A. J. Convertine, B. S. Lokitz, Y. Vasileva, L. J. Myrick, C. W. Scales, A. B. Lowe and C. L. McCormick, *Macromolecules*, 2006, **39**, 1724–1730.
- 61 F. Goto, K. Ishihara, Y. Iwasaki, K. Katayama, R. Enomoto and S. I. Yusa, *Polymer*, 2011, **52**, 2810–2818.
- 62 L. Hou and P. Wu, *Soft Matter*, 2014, **10**, 3578–3586.
- 63 C. Zheng, H. Huang and T. He, *Macromol. Rapid Commun.*, 2014, **35**, 309–316.
- 64 O. V. Borisova, L. Billon, Z. Cernochova, A. Lapp, P. Stepanek and O. V. Borisov, *Macromol. Symp.*, 2015, **348**, 25–32.
- 65 S. K. Filippov, A. Bogomolova, L. Kabarov, N. Velychkivska, L. Starovoytova, Z. Cernochova, S. E. Rogers, W. M. Lau, V. V. Khutoryanskiy and M. T. Cook, *Langmuir*, 2016, **32**, 5314–5323.
- 66 H. Matsuoka, S. Moriya and S. ichi Yusa, *Colloid Polym. Sci.*, 2018, **296**, 77–88.
- 67 S. K. Filippov, M. Hruby and P. Stepanek, in *Temperature-Responsive Polymers*, John Wiley & Sons Ltd, Chichester, UK, 2018, pp. 175–196.
- 68 J. Babin, M. Pelletier, M. Lepage, J. F. Allard, D. Morris and Y. Zhao, *Angew. Chemie - Int. Ed.*, 2009, **48**, 3329–3332.
- 69 J. Thévenot, H. Oliveira, O. Sandre and S. Lecommandoux, *Chem. Soc. Rev.*, 2013, **42**, 7099–7116.
- 70 G. Li, S. Song, L. Guo and S. Ma, *J. Polym. Sci. Part A Polym. Chem.*, 2008, **46**, 5028–5035.
- 71 Y. Huang, P. Yong, Y. Chen, Y. Gao, W. Xu, Y. Lv, L. Yang, R. L. Reis, R. P. Pirraco and J. Chen, *RSC Adv.*, 2017, **7**, 28711–28722.
- 72 O. V. Borisova, L. Billon, R. P. Richter, E. Reimhult and O. V. Borisov, *Langmuir*, 2015, **31**, 7684–7694.
- 73 L. Lauber, J. Santarelli, O. Boyron, C. Chassenieux, O. Colombani and T. Nicolai, *Macromolecules*, 2017, **50**, 416–423.
- 74 A. Choucair and A. Eisenberg, *Eur. Phys. J. E*, 2003, **10**, 37–44.
- 75 S. Pal, M. R. Hill and B. S. Sumerlin, *Polym. Chem.*, 2015, **6**, 7871–7880.

- 76 Q. Jin, L. P. Lv, G. Y. Liu, J. P. Xu and J. Ji, *Polymer (Guildf)*, 2010, **51**, 3068–3074.
- 77 L. García-Fernández, A. Mora-Boza and F. Reyes-Ortega, in *Smart Polymers and their Applications*, Elsevier, 2019, pp. 45–86.
- 78 Y. Zhao, Y. W. Luo, B. G. Li and S. Zhu, *Langmuir*, 2011, **27**, 11306–11315.
- 79 L. Lauber, C. Chassenieux, T. Nicolai and O. Colombani, *Macromolecules*, 2015, **48**, 7613–7619.
- 80 O. Colombani, E. Lejeune, C. Charbonneau, C. Chassenieux and T. Nicolai, *J. Phys. Chem. B*, 2012, **116**, 7560–7565.
- 81 A. Shedge, O. Colombani, T. Nicolai and C. Chassenieux, *Macromolecules*, 2014, **47**, 2439–2444.
- 82 L. Gao, Y. Sun, W. Zhang, D. Li, C. Hou and Y. Liu, *J. Polym. Res.*, 2015, **22**, 1–9.
- 83 S. J. Kim, C. K. Lee and S. I. Kim, *J. Appl. Polym. Sci.*, 2004, **92**, 1731–1736.
- 84 K. Nakamae, T. Nishino, K. Kato, T. Miyata and A. S. Hoffman, *J. Biomater. Sci. Polym. Ed.*, 2004, **15**, 1435–1446.
- 85 X. Han, X. Zhang, H. Zhu, Q. Yin, H. Liu and Y. Hu, , DOI:10.1021/la3036874.
- 86 Y. Hu, G. Cheng, J. Wang, G. Jiang and C. Kan, *Colloid Polym. Sci.*, 2014, **292**, 2611–2620.
- 87 N. González, C. Elvira and J. S. Román, *Macromolecules*, 2005, **38**, 9298–9303.
- 88 K. Fan, M. Bradley and B. Vincent, *J. Colloid Interface Sci.*, 2010, **344**, 112–116.
- 89 N. Sahiner and O. Ozay, *React. Funct. Polym.*, 2011, **71**, 607–615.
- 90 T. Nicolai, O. Colombani and C. Chassenieux, *Soft Matter*, 2010, **6**, 3111–3118.
- 91 J. N. Israelachvili, in *Intermolecular and Surface Forces*, Elsevier, 2011, pp. 503–534.
- 92 A. Blanzas, S. P. Armes and A. J. Ryan, *Macromol. Rapid Commun.*, 2009, **30**, 267–277.
- 93 E. Eghbali, O. Colombani, M. Drechsler, A. H. E. Müller and H. Hoffmann, *Langmuir*, 2006, **22**, 4766–4776.
- 94 X. Han, X. Zhang, H. Zhu, Q. Yin, H. Liu and Y. Hu, *Langmuir*, 2013, **29**, 1024–1034.
- 95 E. Lejeune, C. Chassenieux and O. Colombani, *Prog. Colloid Polym. Sci.*, 2010, **138**, 7–16.
- 96 O. Colombani, M. Ruppel, M. Burkhardt, M. Drechsler, M. Schumacher, M. Gradzielski, R. Schweins and A. H. E. Müller, *Macromolecules*, 2007, **40**, 4351–4362.
- 97 M. Jacquin, P. Muller, R. Talingting-Pabalan, H. Cottet, J. F. Berret, T. Fütterer and O. Théodoly, *J. Colloid Interface Sci.*, 2007, **316**, 897–911.
- 98 R. Hoogenboom, in *Smart Polymers and their Applications*, Elsevier, 2019, pp. 13–44.
- 99 J. Seuring and S. Agarwal, *Macromol. Rapid Commun.*, 2012, **33**, 1898–1920.
- 100 S. Saeki, N. Kuwahara, M. Nakata and M. Kaneko, *Polymer (Guildf)*, 1976, **17**, 685–689.
- 101 Q. Zhang, C. Weber, U. S. Schubert and R. Hoogenboom, *Mater. Horizons*, 2017, **4**, 109–116.
- 102 A. Kermagoret, C. A. Fustin, M. Bourguignon, C. Detrembleur, C. Jérôme and A. Debuigne, *Polym. Chem.*, 2013, **4**, 2575–2583.
- 103 A. Halperin, M. Kröger and F. M. Winnik, *Angew. Chemie - Int. Ed.*, 2015, **54**, 15342–15367.

- 104 J. F. Lutz, *J. Polym. Sci. Part A Polym. Chem.*, 2008, **46**, 3459–3470.
- 105 R. Hoogenboom and H. Schlaad, *Polym. Chem.*, 2017, **8**, 24–40.
- 106 F. Meeussen, E. Nies, H. Berghmans, S. Verbrugghe, E. Goethals and F. Du Prez, *Polymer (Guildf.)*, 2000, **41**, 8597–8602.
- 107 F. Afroze, E. Nies and H. Berghmans, *J. Mol. Struct.*, 2000, **554**, 55–68.
- 108 H. Schäfer-Soenen, R. Moerkerke, H. Berghmans, R. Koningsveld, K. Dušek and K. Šolc, *Macromolecules*, 1997, **30**, 410–416.
- 109 J. P. Patterson, E. G. Kelley, R. P. Murphy, A. O. Moughton, M. P. Robin, A. Lu, O. Colombani, C. Chassenieux, D. Cheung, M. O. Sullivan, T. H. Epps and R. K. O'Reilly, *Macromolecules*, 2013, **46**, 6319–6325.
- 110 X. Lang, A. D. Patrick, B. Hammouda and M. J. A. Hore, *Polymer (Guildf.)*, 2018, **145**, 137–147.
- 111 M. L. Ohnsorg, J. M. Ting, S. D. Jones, S. Jung, F. S. Bates and T. M. Reineke, *Polym. Chem.*, 2019, **10**, 3469–3479.
- 112 S. Furyk, Y. Zhang, D. Ortiz-Acosta, P. S. Cremer and D. E. Bergbreiter, *J. Polym. Sci. Part A Polym. Chem.*, 2006, **44**, 1492–1501.
- 113 P. Kujawa, F. Segui, S. Shaban, C. Diab, Y. Okada, F. Tanaka and F. M. Winnik, *Macromolecules*, 2006, **39**, 341–348.
- 114 P. A. Fitzgerald, S. Gupta, K. Wood, S. Perrier and G. G. Warr, *Langmuir*, 2014, **30**, 7986–7992.
- 115 K. Li and Y. Cao, *Soft Mater.*, 2010, **8**, 226–238.
- 116 K. Bauri, S. G. Roy, S. Arora, R. K. Dey, A. Goswami, G. Madras and P. De, *J. Therm. Anal. Calorim.*, 2013, **111**, 753–761.
- 117 O. O. Oyeneye, W. Z. Xu and P. A. Charpentier, *J. Polym. Sci. Part A Polym. Chem.*, 2017, **55**, 4062–4070.
- 118 I. Soutar, L. Swanson, P. G. Adamson and N. J. Flint, *Macromolecules*, 2009, **42**, 9153–9160.
- 119 I. C. Barker, J. M. G. Cowie, T. N. Huckerby, D. A. Shaw, I. Soutar and L. Swanson, *Macromolecules*, 2003, **36**, 7765–7770.
- 120 L. Cranitch, D. J. T. Hill and A. K. Whittaker, *Appl. Magn. Reson*, 2007, **32**, 51–62.
- 121 L. Hou and P. Wu, *Soft Matter*, 2015, **11**, 2771–2781.
- 122 Z. Iatridi, S. F. Saravanou and C. Tsitsilianis, *Carbohydr. Polym.*, 2019, **219**, 344–352.
- 123 A. García-Peñas, C. S. Biswas, W. Liang, Y. Wang, P. Yang and F. J. Stadler, *Polymers (Basel)*, 2019, **11**, 991.
- 124 Z. Cao, W. Liu, P. Gao, K. Yao, H. Li and G. Wang, *Polymer (Guildf.)*, 2005, **46**, 5268–5277.
- 125 J. Kim, M. M. Mok, R. W. Sandoval, D. J. Woo and J. M. Torkelson, *Macromolecules*, 2006, **39**, 6152–6160.
- 126 T. Ribaut, J. Oberdisse, B. Annighofer, B. Fournel, S. Sarrade, H. Haller and P. Lacroix-Desmazes, *J. Phys. Chem. B*, 2011, **115**, 836–843.
- 127 T. Ribaut, J. Oberdisse, B. Annighofer, I. Stoychev, B. Fournel, S. Sarrade and P. Lacroix-Desmazes, *Soft Matter*, 2009, **5**, 4962–4970.
- 128 K. R. Shull, *Macromolecules*, 2002, **35**, 8631–8639.

- 129 C. L. H. Wong, J. Kim, C. B. Roth and J. M. Torkelson, *Macromolecules*, 2007, **40**, 5631–5633.
- 130 R. W. Sandoval, D. E. Williams, J. Kim, C. B. Roth and J. M. Torkelson, *J. Polym. Sci. Part B Polym. Phys.*, 2008, **46**, 2672–2682.
- 131 S. K. Filippov, B. Verbraeken, P. V. Konarev, D. I. Svergun, B. Angelov, N. S. Vishnevetskaya, C. M. Papadakis, S. Rogers, A. Radulescu, T. Courtin, J. C. Martins, L. Starovoytova, M. Hruby, P. Stepanek, V. S. Kravchenko, I. I. Potemkin and R. Hoogenboom, *J. Phys. Chem. Lett.*, 2017, **8**, 3800–3804.
- 132 M. T. Cook, S. K. Filippov and V. V. Khutoryanskiy, *Colloid Polym. Sci.*, 2017, **295**, 1351–1358.
- 133 Y. Cui, X. Jiang, C. Feng, G. Gu, J. Xu and X. Huang, *Polym. Chem.*, 2016, **7**, 3156–3164.
- 134 B. Liu and S. Perrier, *J. Polym. Sci. Part A Polym. Chem.*, 2005, **43**, 3643–3654.
- 135 M. Khimani, S. Yusa, A. Nagae, R. Enomoto, V. K. Aswal, E. Kesselman, D. Danino and P. Bahadur, *Eur. Polym. J.*, 2015, **69**, 96–109.
- 136 A. Papagiannopoulos, J. Zhao, G. Zhang, S. Pispas and A. Radulescu, *Eur. Polym. J.*, 2014, **56**, 59–68.
- 137 L. Despax, J. Fitremann, M. Destarac and S. Harrisson, *Polym. Chem.*, 2016, **1**, 3375–3377.
- 138 K. I. Seno, I. Tsujimoto, S. Kanaoka and S. Aoshima, *J. Polym. Sci. Part A Polym. Chem.*, 2008, **46**, 6444–6454.
- 139 W. Steinhauer, R. Hoogenboom, H. Keul and M. Moeller, *Macromolecules*, 2013, **46**, 1447–1460.
- 140 K. C. Gallow, Y. K. Jhon, J. Genzer and Y. L. Loo, *Polymer (Guildf.)*, 2012, **53**, 1131–1137.
- 141 K. C. Gallow, Y. K. Jhon, W. Tang, J. Genzer and Y. L. Loo, *J. Polym. Sci. Part B Polym. Phys.*, 2011, **49**, 629–637.
- 142 A. Halperin and S. Alexander, *Macromolecules*, 1989, **22**, 2403–2412.
- 143 Q. T. Pham, W. B. Russel, J. C. Thibeault and W. Lau, *ACS Publ.*, 1999, **32**, 5139–5146.
- 144 C. Tsitsilianis, *Soft Matter*, 2010, **6**, 2372–2388.
- 145 O. Borisova, L. Billon, M. Zaremski, B. Grassl, Z. Bakaeva, A. Lapp, P. Stepanek and O. Borisov, *Soft Matter*, 2011, **7**, 10824–10833.
- 146 F. Dutertre, O. Boyron, B. Charleux, C. Chassenieux and O. Colombani, *Macromol. Rapid Commun.*, 2012, **33**, 753–759.
- 147 D. D. Bendejacq and V. Ponsinet, *J. Phys. Chem. B*, 2008, **112**, 7996–8009.
- 148 E. Lejeune, M. Drechsler, J. Jestin, A. H. E. Müller, C. Chassenieux and O. Colombani, *Macromolecules*, 2010, **43**, 2667–2671.
- 149 C. Zheng, H. Huang and T. He, *Macromol. Rapid Commun.*, 2013, **34**, 1654–1661.
- 150 M. Rabyk, A. Destephen, A. Lapp, S. King, L. Noirez, L. Billon, M. Hruby, O. Borisov, P. Stepanek and E. Deniau, *Macromolecules*, 2018, **51**, 5219–5233.
- 151 S. Okabe, K. I. Seno, S. Kanaoka, S. Aoshima and M. Shibayama, *Macromolecules*, 2006, **39**, 1592–1597.
- 152 S. Okabe, C. Fuse, S. Sugihara, S. Aoshima and M. Shibayama, *Phys. B Condens. Matter*, 2006, **385-386 I**, 756–758.

**CHAPTER 2. P(AA-*n*BA)
ASYMMETRIC
COPOLYMERS: A pH
RESPONSIVE SYSTEM**

CHAPITRE 2. COPOLYMERES ASYMETRIQUES DE P(AA-*n*BA) : UNE SYSTEME SENSIBLE AU pH

L'objectif de cette thèse est d'étudier l'effet du profil de composition des copolymères sur leurs propriétés. Les types de structures suivants ont été choisis : copolymères à bloc, asymétriques dibloc et tribloc, gradient et statistiques. L'ensemble des copolymères étudiés a la même composition globale (Figure 2.1). Ces structures et profils de composition seront utilisés tout au long de cette thèse.

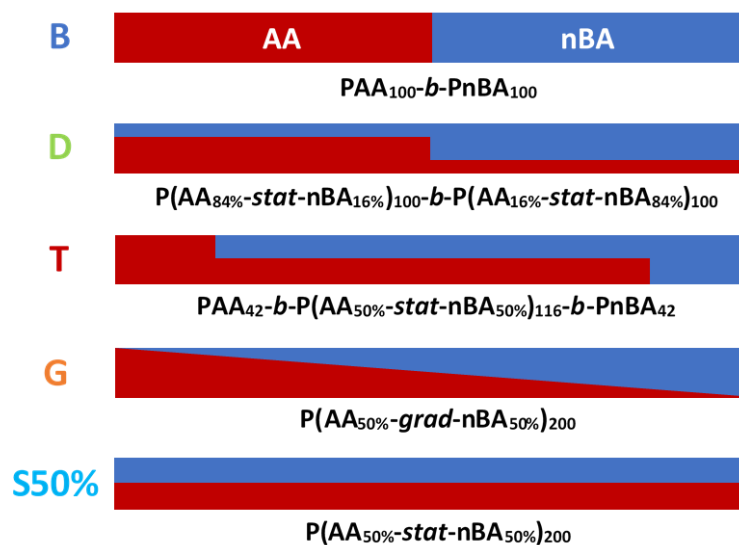


Figure 2.1. Profils de composition des copolymères bloc, dibloc, tribloc, gradient et statistique de degré de polymérisation 200, contenant la même quantité d'unités AA (50% en mole).

Les profils des copolymères asymétriques dibloc et tribloc ont été choisis comme des structures simples contenant seulement deux ou trois blocs qui imitent néanmoins étroitement le profil de composition du gradient. Dans cet objectif, des copolymères ont été conçus pour correspondre à la composition globale du copolymère à gradient (50 moles% d'acide acrylique, AA) mais également à l'emplacement moyen des unités d'AA dans la chaîne de polymère.

Le copolymère à gradient (G) a un profil de composition linéaire allant de 100 mol% AA à 0 mol% AA. Sa composition globale est de 50 mol% AA. La position moyenne des unités d'acide acrylique, mesurée à partir de l'extrémité riche en AA, est donnée par :

$$\bar{x}_G = \frac{\int_0^1 x(1-x) dx}{\int_0^1 (1-x) dx} = \frac{1}{3} \approx 0.33$$

Le copolymère asymétrique à dibloc (D) est constitué de deux blocs de la même longueur, contenant respectivement 84 et 16 mol% AA. Sa composition globale est de 50 mol% AA. La position moyenne des unités AA, mesurée à partir de l'extrémité riche en AA, est donnée par :

$$\bar{x}_D = \frac{\int_0^{0.5} 0.84x dx + \int_{0.5}^1 0.16x dx}{\int_0^{0.5} 0.84 dx + \int_{0.5}^1 0.16 dx} = 0.33$$

Le tribloc asymétrique (T) est constitué de deux blocs terminaux courts respectivement en poly (acide acrylique) (PAA) et en poly (acrylate de *n*-butyle) (P*n*BA), chacun correspondant à 21% en mole de la longueur totale du polymère. Le bloc central, correspondant aux 58% en moles restants du polymère, est un copolymère statistique à 50% en moles d'AA et de *n*BA. La composition globale d'AA est de 50%. La position moyenne des unités AA, mesurée à partir de l'extrémité riche en AA, est donnée par :

$$\bar{x}_T = \frac{\int_0^{0.21} x dx + \int_{0.21}^{0.79} 0.5x dx}{\int_0^{0.21} 1 dx + \int_{0.21}^{0.79} 0.5x dx} = 0.33$$

Ainsi, D, T et G partagent à la fois leur composition globale et l'emplacement moyen des unités d'AA dans la chaîne.

A titre de comparaison, l'emplacement moyen des unités AA dans le copolymère à bloc B constitué de parties égales de PAA et de P*n*BA est :

$$\bar{x}_B = \frac{\int_0^{0.5} x dx}{\int_0^{0.5} 1 dx} = 0.25$$

Alors que celui du copolymère statistique contenant 50 moles% d'unités AA ($S_{50\%}$) est :

$$\bar{x}_S = \frac{\int_0^1 0.5x dx}{\int_0^1 0.5 dx} = 0.5$$

Dans ce chapitre, certaines propriétés physiques des copolymères d'acide acrylique-acrylate de butyle en masse et en solution aqueuse sont étudiées. En masse, la

calorimétrie différentielle à balayage a été utilisée pour étudier l'effet du profil de composition sur la température de transition vitreuse des copolymères AA-BA. Cela donne un aperçu de leur comportement de séparation microphasique. En solution, l'accent est mis sur le comportement d'ionisation des copolymères AA-BA de profil de compositions variées en réponse aux changements de pH.

La synthèse des copolymères à bloc, asymétrique dibloc et tribloc a été réalisée par une polymérisation RAFT par étapes (addition séquentielle d'AA et *n*BA) et en ciblant des masses molaires de 10 et 20 kg mol⁻¹. Les synthèses ont été réalisées par Dr. Junliang Zhang dans un synthétiseur parallèle automatisé dans les installations du Jena Center for Soft Matter de l'Université de Jena Friedrich-Schiller. Les détails complets de la synthèse se trouvent dans la section expérimentale à la fin de ce chapitre.

Les polymères à profil de gradient, ont été obtenus par synthèse forcée en utilisant la polymérisation RAFT et en ciblant des masses molaires de 10 et 20 kg mol⁻¹. AA et *n*BA ont été ajoutés simultanément à une vitesse contrôlée au mélange réactionnel. Les synthèses ont été réalisées par le Dr Ihor Kulai et les détails de la synthèse sont expliqués dans la section expérimentale.

Les polymères à profil statistique ont été préparés par copolymérisation d'AA et de *n*BA. Deux ensembles de copolymères statistiques ont été préparés pour ce chapitre. Les polymères statistiques utilisés pour les expériences de calorimétrie différentielle à balayage ont été obtenus par le Dr. Ihor Kulai par copolymérisation RAFT et les masses molaires ciblées étaient de 10 et 20 kg mol⁻¹, et ils sont nommés S10K et S20K. Pour l'analyse des polymères en solution par modification du pH (titrages potentiométriques), un autre groupe de copolymères statistiques a été utilisé. Ceux avec la nomenclature S_{16%}, S_{30%}, S_{70%}, S_{84%} et PAA pur ont été synthétisés par Barbara Farias via la copolymérisation RAFT et ceux avec la nomenclature S_{40%}, S_{50%} et S_{60%} ont été synthétisés par Dr. Olivier Colombani via la copolymérisation ATRP.

Après leur purification, les polymères ont été soumis à une acidolyse sélective avec de l'acide trifluoroacétique (TFA) afin d'éliminer le groupe *t*-butyle pour donner des copolymères amphiphiles de AA-*n*BA.¹

Les caractéristiques macromoléculaires correspondant aux polymères sont présentées dans le tableau 1. Dans la nomenclature représentée dans le tableau 1, D10K par exemple, D représente le profil asymétrique à dibloc et 10K représente la masse molaire ciblée 10 kg mol⁻¹. Les masses molaires moyennes en nombre et les dispersités des deuxième et troisième blocs de copolymères blocs, diblocs asymétriques et triblocs, ont été calculées avec l'équation suivante : $\mathcal{D}_2 = 1 + [(\mu_{1+2})^2(\mathcal{D}_{1+2} - 1) - \mu_1^2(\mathcal{D}_{1+2} -$

1))/ $(\mu_{1+2} - \mu_1)^2$] (Equation 2.1). Où \mathcal{D}_2 est la dispersité du bloc ajouté, μ_1 et \mathcal{D}_1 sont la masse molaire moyenne en nombre et la dispersité du bloc initial et μ_{1+2} et \mathcal{D}_{1+2} sont la masse molaire moyenne en nombre et la dispersité du polymère final.

CHAPTER 2. P(AA-*n*BA) ASYMMETRIC COPOLYMERS: A pH RESPONSIVE SYSTEM

The objective of this thesis is to study the effect of the composition profile of copolymers over their properties. The following type of structures were chosen: block, asymmetric diblock and triblock, gradient, and statistical copolymers, all with the same overall composition (Figure 2.1). These structures and composition profiles will be used throughout this thesis.

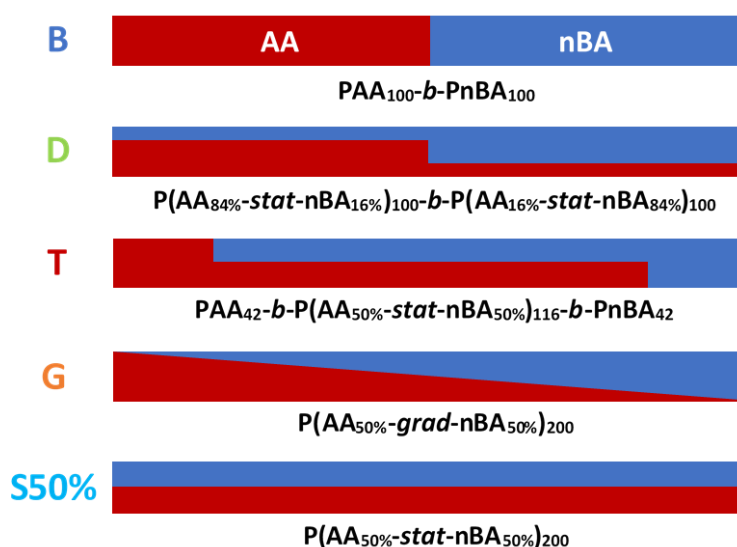


Figure 2.1 Composition profiles of block, diblock, triblock, gradient and statistical copolymers of degree of polymerization 200, containing the same amount of AA units (50 mol %).

The profiles of the asymmetric diblock and triblock copolymers were selected as simple structures containing only two or three blocks that nevertheless closely mimicked the gradient composition profile. In order to do so, copolymers were designed which matched both the overall composition of the gradient copolymer (50 mol % acrylic acid, AA) and also the average location of AA units within the polymer chain.

The gradient copolymer (G) has a linear composition profile ranging from 100 mol % AA to 0 mol % AA. Its overall composition is 50 mol % AA. The average position of the acrylic acid units, measured from the AA-rich terminus is given by:

$$\bar{x}_G = \frac{\int_0^1 x(1-x) dx}{\int_0^1 (1-x) dx} = \frac{1}{3} \approx 0.33$$

The asymmetric diblock (D) consists of two blocks of equal length, containing 84 and 16 mol % AA respectively. Its overall composition is 50 mol % AA. The average position of the AA units, measured from the AA-rich terminus is given by:

$$\bar{x}_D = \frac{\int_0^{0.5} 0.84x \, dx + \int_{0.5}^1 0.16x \, dx}{\int_0^{0.5} 0.84 \, dx + \int_{0.5}^1 0.16 \, dx} = 0.33$$

The asymmetric triblock (T) consists of two short terminal blocks of poly(acrylic acid) (PAA) and poly(*n*-butyl acrylate) (P*n*BA) respectively, each corresponding to 21 mol % of the total length of the polymer. The central block, corresponding to the remaining 58 mol % of the polymer, is a 50 mol % statistical copolymer of AA and *n*BA. The overall composition of AA is 50 AA%. The average position of the AA units, measured from the AA-rich terminus is given by:

$$\bar{x}_T = \frac{\int_0^{0.21} x \, dx + \int_{0.21}^{0.79} 0.5x \, dx}{\int_0^{0.21} 1 \, dx + \int_{0.21}^{0.79} 0.5x \, dx} = 0.33$$

Thus D, T and G share both their overall composition and the average location of AA units in the chain.

For comparison, the average location of the AA units in the block copolymer B consisting of equal parts PAA and P*n*BA is

$$\bar{x}_B = \frac{\int_0^{0.5} x \, dx}{\int_0^{0.5} 1 \, dx} = 0.25$$

While that of the statistical copolymer containing 50 mol % AA units ($S_{50\%}$) is:

$$\bar{x}_S = \frac{\int_0^1 0.5x \, dx}{\int_0^1 0.5 \, dx} = 0.5$$

In this chapter, some physical properties of acrylic acid-butyl acrylate copolymers in bulk and in aqueous solution are investigated. In bulk, differential scanning calorimetry has been used to investigate the effect of composition profile on the glass transition temperature of the AA-*n*BA copolymers. This in turn gives insights into their microphase separation behavior. In solution, the focus is on the ionization behavior of AA-*n*BA copolymers of varied composition profile in response to changes in pH.

The synthesis of block, asymmetric diblock, and asymmetric triblock copolymers was performed by a stepwise (sequential addition of AA and *n*BA) RAFT polymerization and

targeting molar masses of 10 and 20 kg mol⁻¹. The syntheses were carried out by Dr. Junliang Zhang in an automatized parallel synthesizer in the facilities of the Jena Center for Soft Matter at the University of Jena Friedrich-Schiller. The full details of the synthesis are in the experimental section at the end of this chapter.

The polymers with gradient profile, were obtained by forced synthesis using RAFT polymerization and targeting molar masses of 10 and 20 kg mol⁻¹. AA and *n*BA were simultaneously added at a controlled rate to the reaction mixture. The syntheses were carried out by Dr. Ihor Kulai and the details of the synthesis are explained in the experimental section.

The polymers with statistical profile were prepared by copolymerization of AA and *n*BA. Two sets of statistical copolymers were prepared for this chapter. The statistical polymers used for the differential scanning calorimetry experiments, were obtained by Dr. Ihor Kulai via RAFT copolymerization and the targeted molar masses were of 10 and 20 kg mol⁻¹, and they are named S10K and S20K. For the analysis of the polymers in solution by changing the pH (potentiometric titrations) another group of statistical copolymers were used. Those with nomenclature S_{16%}, S_{30%}, S_{70%}, S_{84%} and pure PAA were synthesized by Barbara Farias via RAFT copolymerization and those with nomenclature S_{40%}, S_{50%} and S_{60%} were synthesized by Dr. Olivier Colombani via ATRP copolymerization.

After their purification, the polymers were subjected to a selective acidolysis with trifluoroacetic acid (TFA) in order to remove the *t*-butyl group to yield amphiphilic copolymers of AA-*n*BA.¹

Macromolecular characteristics corresponding to the polymers are shown in Table 1. In the nomenclature depicted in Table 2.1, D10K for example, D represents the diblock profile and 10K represents the targeted molar mass 10 kg mol⁻¹. The number average molar masses and dispersities of the second and third blocks of block, asymmetric diblock and triblock copolymers, were calculated with the following equation: $\mathfrak{D}_2 = 1 + [(\mu_{1+2}^2(\mathfrak{D}_{1+2} - 1) - \mu_1^2(\mathfrak{D}_{1+2} - 1))/(\mu_{1+2} - \mu_1)^2]$ (Equation 2.1). Where \mathfrak{D}_2 is the dispersity of added block, μ_1 and \mathfrak{D}_1 are the number average molar mass and the dispersity of the initial block and μ_{1+2} and \mathfrak{D}_{1+2} are the number average molar mass and the dispersity of the final polymer.

Table 2.1 Macromolecular characteristics of the block, asymmetric diblock and triblock, gradient and statistical copolymers used in this chapter.

• Polymer	Profile	Overall			Component blocks		
		M_n ^[b] (σ ^[a]), kg.mol ⁻¹	\mathcal{D} ^[b]	%tBA ^[c]	M_n (σ ^[a]), kg.mol ⁻¹	\mathcal{D}	%tBA ^[c]
B10K	Block	10.9 (3.4)	1.10	52.3	5.7 ^[b] (1.6) 5.2 ^[d] (3.0)	1.08 ^[b] 1.34 ^[d]	100 0
B20K	Block	20.9 (6.9)	1.11	50.7	10.6 ^[b] (2.8) 10.3 ^[d] (6.3)	1.07 ^[b] 1.38 ^[d]	100 0
D10K	Asymmetric Diblock	10.8 (3.2)	1.09	50.7	4.9 ^[b] (1.6) 5.9 ^[d] (2.8)	1.11 ^[b] 1.23 ^[d]	85.4 16.0
D20K	Asymmetric Diblock	20.9 (6.6)	1.10	54.6	10.0 ^[b] (3.5) 10.9 ^[d] (5.7)	1.12 ^[b] 1.27 ^[d]	83.9 16.1
T10K	Asymmetric Triblock	9.7 (2.6)	1.07	52.7	1.7 (0.5) ^[b] 6.1 (2.1) ^[d] 2.2 (1.5) ^[d]	1.10 ^[b] 1.12 ^[d] 1.44 ^[d]	100 50 0
T20K	Asymmetric Triblock	20.1 (5.3)	1.07	55.8	4.1 (1.2) ^[b] 11.8 (4.1) ^[d] 4.2 (3.3) ^[d]	1.09 ^[b] 1.12 ^[d] 1.60 ^[d]	100 50.5 0
G10K	Gradient	7.4 (4.5)	1.37	48.6			
G20K	Gradient	26.0 (15.2)	1.34	56.1			
S_{16%}	Statistical	15.7	1.04	16			
S_{30%}	Statistical	11.7	1.05	30			
S_{40%}	Statistical	12.5	1.17	40			
S_{50%}	Statistical	12.5	1.10	51			
S_{60%}	Statistical	13.6	1.34	60			
S_{70%}	Statistical	11.7	1.06	70			
S_{84%}	Statistical	18.1	1.09	84			
PAA	Statistical	18.3	1.04	100			

a) Standard deviation of the molar mass number distribution, calculated as $\sigma = M_n \times \sqrt{(\mathcal{D}-1)^{2/3}}$ b) Measured by SEC (calibrated with PMMA standards) before acidolysis. c) from ¹H NMR analysis before acidolysis d) Calculated using Equation 2.1.²

1 STUDY OF PROPERTIES IN BULK: MICROPHASE SEPARATION OF COPOLYMERS

Microphase separation describes a type of chain segregation, which can occur in bulk or in a concentrated solution. Microphase separation occurs due to incompatible chemical components and they tend to form phase separation structures with microscopic length scales due to intramolecular phase separation.³

Glass transition temperature is the temperature region where a polymer changes from a glassy to a rubbery state and is due to the increased molecular mobility of the chains.

This is associated with a change in the heat capacity of the polymer, which can be revealed by differential scanning calorimetry (DSC).⁴

The study of thermal properties of gradient copolymers in bulk has been performed by DSC.⁵⁻⁸ In a typical DSC experiment the T_g is located where a clear change in slope of the heating curve as a function of temperature is observed. However, it is difficult to observe a change in slope when the glass transition occurs over a very broad temperature range, as it is the case for gradient copolymers. Another technique to determine the T_g involves the use of the first derivative of heat flow with respect to temperature. In this approach the T_g manifests as a strong positive peak followed by a small local minimum due to enthalpy relaxation.⁵ With this approach the location and breadth of the glass transition can be determined more accurately.

Figure 2.2 shows the derivative of heat curves for the PAA-*Pn*BA copolymers. The T_g breadths and positions are displayed in Table 2.2. As mentioned above, the statistical polymers S10K and S20K, were exclusively used for the differential scanning calorimetry analysis.

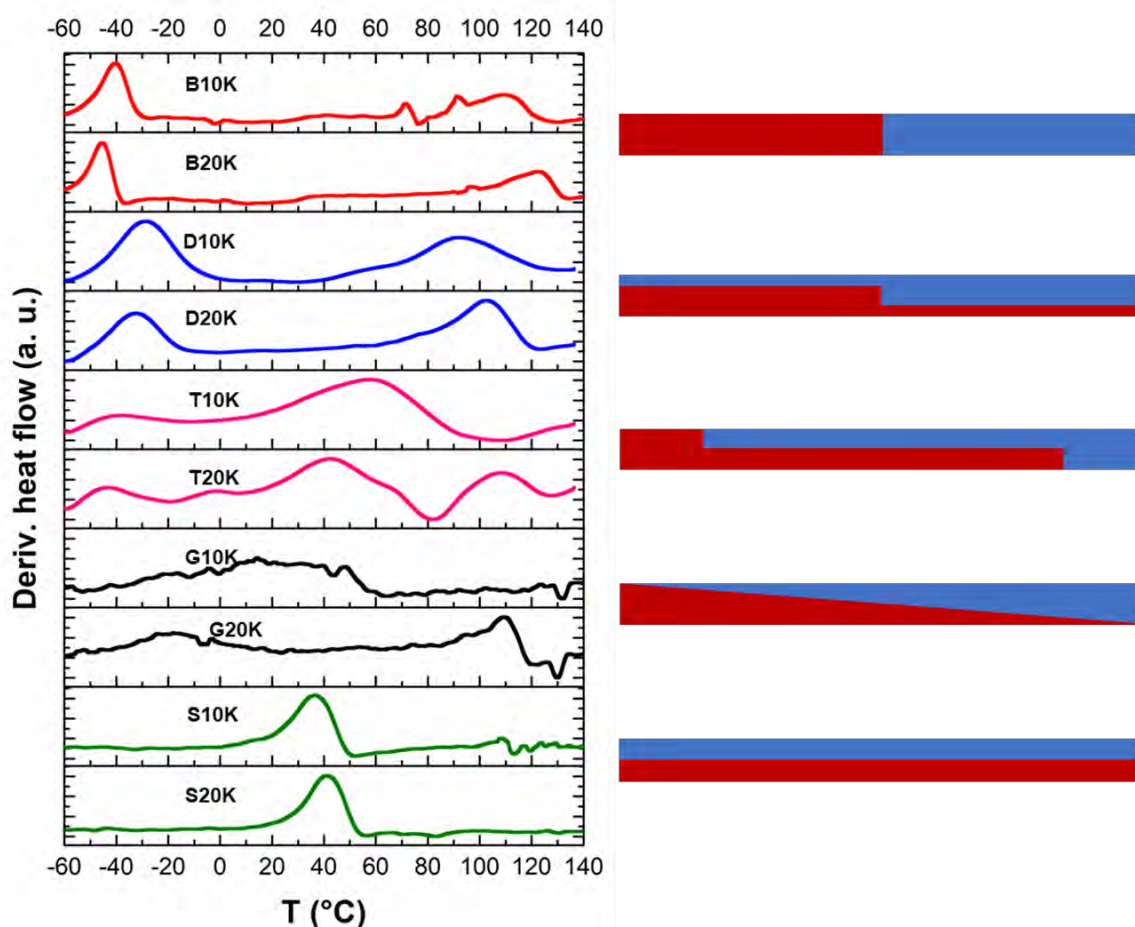


Figure 2.2. DSC derivatives of block, diblock, triblock, gradient and statistical copolymers of 10 and 20 kg mol⁻¹ with their corresponding structures.

Table 2.2 Summary of glass transition temperatures data for PAA-*Pn*BA copolymers

Copolymer	10 K		20 K	
	T_g (°C)	T_g breadth (°C) ^a	T_g (°C)	T_g breadth (°C) ^a
Block	-40.3	12	-45.3	9
	109.3	30	122.7	21
Diblock	-28.7	24	-32.3	22
	92.3	36	102.7	24
Triblock	-38.3	26	-43.3	18
	57.3	48	42.3	39
			108.3	26
Gradient	11	63	-18.3	36
			109.4	16
Statistical	36.7	18	41.2	16

a) Determined by measuring the peak width at half maximum.

For all copolymer structures, as molecular weight increases, the T_g breadths become narrower which is an indication of increased microphase segregation. In other words, the segments of different composition become less compatible as their molecular weights increase.

For both block copolymers (B10K and B20K) two well defined and separated T_g s are observed. The lowest values correspond to *Pn*BA and the highest values correspond to PAA. This is a result of microphases separation into two phases of nearly pure *Pn*BA and PAA. Similar PAA-*Pn*BA block copolymers have been observed to form ordered lamellar microphases.⁶ The statistical copolymers (S10K and S20K) have a single, relatively narrow T_g that is located between those corresponding to the blocks, corresponding to the homogeneous nature of the sample. The decrease in breadth of T_g going from 10K to 20K may be due to reduced variation in composition – as the chains get longer, there is less random variation in composition from one chain to another.

Like the statistical copolymers, gradient copolymer G10K also has a single T_g , but in this case it covers a much broader range of temperatures. This behavior is characteristic of gradient copolymers and is a result of weak segregation between the segments that are rich in acrylic acid and those that are rich in butyl acrylate. Unlike the block copolymer, in which microphase segregation leads to a sharp transition between AA-rich and BA-rich regions, the gradient copolymer presents a continuously varying composition, and hence a broad glass transition.⁶ For G20K, the higher molecular weight of the copolymer leads to stronger microphase separation, and greater segregation of AA and BA. As a

result two glass transitions are observed; a broad T_g at low temperatures and another narrower T_g is present at higher temperatures. The region between the two peaks appears elevated relative to the baseline, suggesting that there is a continuous variation of composition within the sample, as observed previously by Kim et al.⁵ for styrene-butyl methacrylate gradient copolymers.

Diblock copolymers (D10K and D20K) displayed two T_g s very close to the corresponding ones to *Pn*BA and PAA, as for the block copolymers, however the temperature ranges were broader. This behavior is in agreement with the copolymer compositions in which the first block is a statistical copolymer with 84 mol% *Pn*BA and the second block is also a statistical copolymer consisting of 84 mol % PAA. The increased breadth of the transitions compared to those of the block and statistical copolymers suggests weaker segregation of the AA-rich and BA-rich segments, but block-like behavior dominates.

The triblock copolymer T10K displays one T_g at low temperatures, corresponding to the T_g of *Pn*BA and another T_g within a similar range as for the statistical copolymers, but wider. This suggests that there is microphase separation of the poly(butyl acrylate) block, but relatively weak segregation of the AA/BA statistical block and the PAA homopolymer block. The breadth of the central glass transition, which is comparable to that of G10K, indicates significant mixing between the different phases. For triblock copolymer T20K three glass transitions can be observed: the first T_g corresponds to a BA-rich phase; the second, broad T_g is within a similar range as for the statistical copolymers and the last T_g is in the range corresponding to the AA-rich phase. Nonetheless, the central peak is still the most important, and it is still broad compared to the statistical copolymer. These results for the block, diblock, statistical and gradient copolymers demonstrate that it is possible to tune the glass transition behavior of copolymers by modifying their composition profile. The triblock results are of particular interest, as broad glass transitions similar to those typically associated with gradient copolymers can be obtained simply by adding short blocks of homopolymer to the ends of a statistical copolymer.

2 STUDY OF PROPERTIES IN SOLUTION: DEGREE OF IONIZATION

2.1 Ionization behavior of weak polyacids (polyelectrolytes)

In this section, block, gradient, statistical and asymmetric diblock and triblock copolymers, with targeted molar mass of 20 kg mol⁻¹, containing 50 mol% acrylic acid (AA) and 50 mol% *n*-butyl acrylate (*n*BA) are studied. The potentiometric titration study

is focused only on the polymers with targeted molecular weight of 20 kg mol⁻¹. Because of the presence of PAA, these copolymers are sensitive to pH changes in solution. This type of copolymer is known as a weak polyelectrolyte; a polymer in which a substantial portion of the units contain weak acidic or basic groups.⁹ Unlike strong electrolytes, which are fully ionized across the whole pH range, the degree of ionization of weak polyelectrolytes is pH-dependent. Because of their pH-responsive behavior, weak polyelectrolytes find applications as drug-delivery systems¹⁰, biosensors¹¹, pH-sensitive gelifiers or rheology modifiers.¹²

Classically the ionization reaction of a monoacid is represented as follows:



Where A⁻ is the conjugate base and H⁺ the dissociated charge which dissolves into the solution. The variation in the ionization behavior of a monoacid as a function of pH is described by its titration curve.¹³ The degree of ionization of a weak monoacid is defined by the Henderson-Hasselbach equation:

$$\text{pH} = \text{pK}a_0 + \log \frac{\alpha}{1 - \alpha} \quad \text{Equation 2.3}$$

Where α represents the degree of ionization (Equation 2.4) of the acid, which is the molar percentage of ionized units. $\text{pK}a_0 = -\log(\text{K}a_0)$ and $\text{K}a_0$ ($\text{K}a_0 = [\text{H}^+][\text{A}^-]/[\text{HA}]$), is the acidity constant which is a quantitative measurement of the strength of an acid in solution.

$$\alpha = \frac{[\text{A}^-]}{[\text{A}^-] + [\text{HA}]} \quad \text{Equation 2.4}$$

In dilute solution, the acidic groups of a monoacid remain well separated from each other and do not interact. Hence $\text{K}a_0$ does not vary along its ionization range. In a weak polyelectrolyte, the acidic groups are very close to each other and their interactions are significant. These interactions vary depending on α and produce deviations from ideal behavior (Equation 2.5):

$$\text{pH} = \text{pK}a_0 + \log \frac{\alpha}{1 - \alpha} + \Delta \quad \text{Equation 2.5}$$

Here Δ represents deviations in pH due to interactions between the ionizable units; these interactions vary depending on α .¹⁴ The effective pKa, $\text{pK}a_{\text{eff}}$, which also depends on α , is defined as the sum of $\text{pK}a_0$ and Δ :

$$\text{pH} = \text{pK}a_{\text{eff}} + \log \frac{\alpha}{1 - \alpha} \quad \text{Equation 2.6}$$

The $pK_{a\text{eff}}$ of weak polyacids increases with α because electrostatic interactions hinder the creation of charges close to already charged neighboring units. This sensitivity to α can be reduced by screening the charges through addition of monovalent salts, or by increasing the concentration of the polyacid, which also increases ionic strength. The sensitivity to α can also be reduced by increasing the distance between acidic units via copolymerization with a neutral monomer. Moreover, copolymerization will also affect $pK_{a\text{eff}}$ at a given α by changing the dielectric constant of the polymer chain. Thus, incorporating a non-polar hydrophobic monomer leads to an increase in $pK_{a\text{eff}}$.

The degree of ionization determines the effective quantity of charge in a polyelectrolyte and is pH dependent. The ionization of AA units depends on their surrounding environment, on the distribution of the acidic units and the vicinity of the charges along the polymer chain.¹⁵ The relevance of determining the degree of ionization is to understand how the distribution of acrylic acid (AA) units may directly affect the properties of the copolymers in solution. When the degree of ionization increases, more charges are created along the polymer chain, thus it becomes more difficult to further ionize the polyelectrolyte.

In various investigations it has been demonstrated that incorporation of weak acidic or basic units into the hydrophobic or hydrophilic blocks of amphiphilic copolymers, it is possible to control the dynamics of the self-assemblies by adjusting the pH of the solution.¹⁶⁻²¹

2.2 Study of degree of ionization

The analysis of degree of ionization (α) was performed by potentiometric titration of the copolymers in solution. Copolymers in aqueous solution were ionized with a NaOH solution. An excess of NaOH (10 mol %) was added in order to reach $\alpha = 1$, or in other words, to ensure that the totality of AA units were ionized. Then the copolymers were back titrated with a solution of HCl at NaCl concentration of 0.1 mol.L⁻¹. This provided that the amount of NaCl generated during the titration did not significantly change the ionic strength of the dispersion and, therefore, the titration curve¹⁵. The direct results obtained from the potentiometric titration are the evolution of pH as a function of the added volume of HCl, as depicted in Figure 2.3. This plot is divided into three regions: the first region (0–0.2 mL of HCl) in which pH decreases very rapidly, corresponds to the neutralization of the NaOH excess; the second region (0.2–1.7 mL), in which the pH

decreases more gradually is where HCl protonates all the ionized PAA units; and in the last region (1.7–2.1 mL) an excess of HCl is added to the solution.

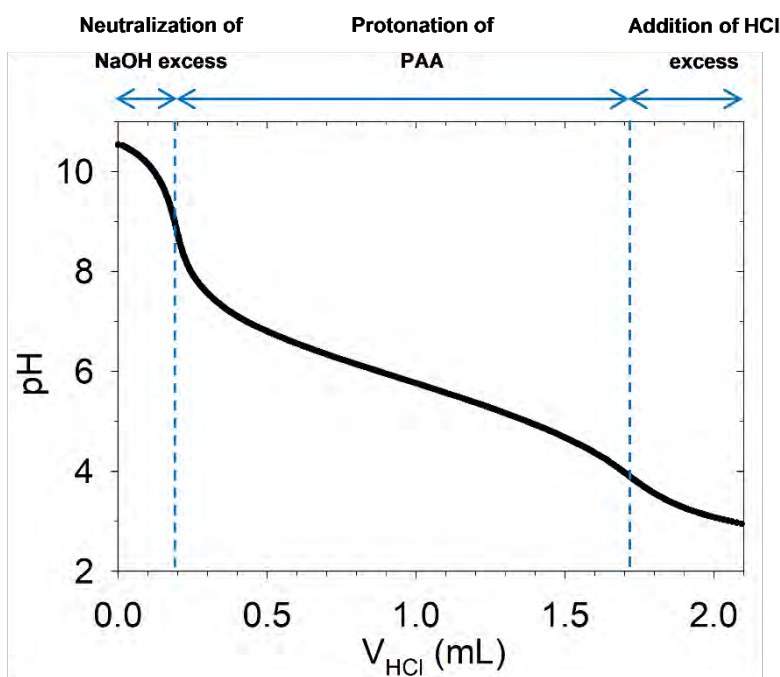


Figure 2.3. Raw potentiometric titration curve of gradient copolymer ($M_n = 20 \text{ kg}\cdot\text{mol}^{-1}$) at 1 g L^{-1} with HCl 0.1 M (addition rate = 0.1 mL min^{-1}) at a NaCl concentration of 0.1 M and starting with $\sim 10 \%$ excess of NaOH.

The macromolecular characteristics of asymmetric and block copolymers before and after the acidolysis, are displayed in Table 2.3. The number average molar mass (M_n) expected after acidolysis was calculated as depicted by Equation 2.7:

$$M_{n \text{ expected}} = M_{n1} \times \left(f_{tBA} \times \left(\frac{M_{AA}}{M_{tBA}} \right) + f_{nBA} \right) \quad \text{Equation 2.7}$$

Where M_{n1} represents the molar mass before the acidolysis, f_{tBA} and f_{nBA} are the mass fractions of *t*BA and *n*BA in the polymer before acidolysis which are equal to their molar fractions and were determined by ^1H NMR. After, the total amount of AA units was calculated from the number of moles of AA units (n_{AA}) titrated in a polymer mass ($m_{pol} \sim 30 \text{ mg}$) was determined by potentiometric titration. From that, the AA mol % was deduced as follows:

$$\%AA = \frac{n_{AA}}{\left(n_{AA} + \frac{(m_{pol} - n_{AA} \times M_{AA})}{M_{nBA}} \right)} \quad \text{Equation 2.8}$$

Where M_{AA} and M_{nBA} correspond to the respective molecular weights of AA or *n*BA units. The AA content in the polymers estimated by titration was consistent with the values calculated from the relative mass of the polymer segments and their composition by ^1H NMR (Table 2.3). This confirmed that all AA units along the polymer chains could be ionized.

Table 2.3. Macromolecular characteristics of block, asymmetric diblock and triblock, gradient and statistical copolymers before and after the acidolysis.

Copolymer	Before acidolysis			After acidolysis	
	M_n (kg mol^{-1}) ^c	\bar{D}^a	<i>t</i> BA mol % ^b	Expected M_n (kg mol^{-1}) ^c	AA mol % ^d
Block	20.9	1.11	51	16.3	49%
Asymmetric diblock	20.9	1.10	49	16.5	50%
Asymmetric triblock	20.1	1.07	50	15.7	53%
Gradient	26.0	1.34	56	20.3	51%
S _{16%}	15.7	1.04	16%	14.6	18%
S _{30%}	11.7	1.05	30%	10.2	31%
S _{40%}	12.5	1.17	40%	10.0	42%
S _{50%}	12.5	1.10	51%	10.0	51%
S _{60%}	13.6	1.34	60%	10.3	61%
S _{70%}	11.7	1.06	70%	9.7	63%
S _{84%}	18.1	1.09	84%	11.4	77%
PAA	18.3	1.04	100%	10.3	83%

a) Determined by size exclusion chromatography (SEC) in tetrahydrofuran (THF) before acidolysis for block, and gradient copolymers; determined by SEC in CHCl_3 before acidolysis for asymmetric diblock and triblock. SEC was calibrated with polystyrene (PS) and poly(methyl methacrylate) (PMMA) standards respectively. For S_{50%}, the analysis was performed on another column calibrated with PS standards, b) calculated from molar mass of each block, considering their composition obtained by proton nuclear magnetic resonance (^1H NMR), c) calculated from Equation 7, d) calculated from Equation 8.

2.2.1 Potentiometric titration reproducibility

The degree of ionization of copolymers was obtained from the raw data of potentiometric titrations, using Equation 2.3. The reproducibility of potentiometric titration experiments was verified, first by comparing curves of the triblock copolymer with different molecular weights and also by comparing statistical copolymers with different AA content. Figure 2.4a depicts pH as a function of α corresponding to the asymmetric triblock copolymer of 10 and 20 kg mol^{-1} . The curves overlap, indicating that the titrations were reproducible and did not significantly depend on the molar mass of the polymer, at least within the studied molar mass range. In Figure 2.4b it can be observed that the AA concentration had no significant influence on the titration curves for the statistical copolymers S_{30%} and

S_{84%}. The differences observed at the two distinct concentrations were slightly more pronounced close to $\alpha = 0$ or 1 where the determination of α becomes less accurate.

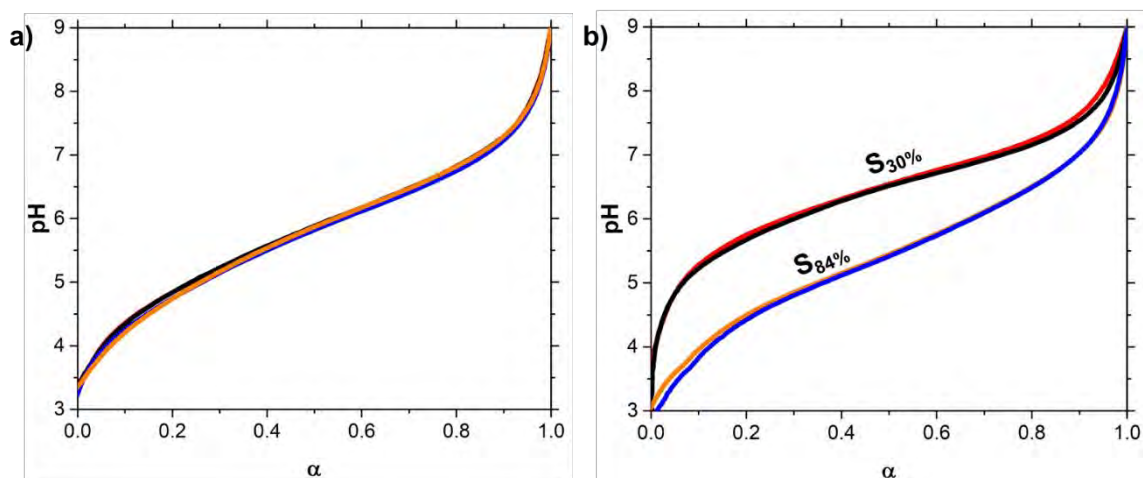


Figure 2.4. Reproducibility of titrations. a) Effect of molecular weight: Evolution of the pH as a function of α resulting from titrations of asymmetric triblock of (—, —) $M_n = 10 \text{ kg mol}^{-1}$ and (—, —) $M_n = 20 \text{ kg mol}^{-1}$. Titrations conducted from $\alpha = 1$ to $\alpha = 0$ with HCl 0.1 M at a polymer concentration of 1 g.L^{-1} and with 0.1 M NaCl. b) Effect of concentration: Evolution of the pH as a function of α resulting from titration of S_{30%} at 1 g L^{-1} (—) and 1.85 g L^{-1} (—) corresponding to $[\text{AA}] = 2.7 \times 10^{-3}$ or $5.0 \times 10^{-3} \text{ mol L}^{-1}$; S_{84%} at 1 g.L^{-1} (—) and 0.48 g.L^{-1} (—) corresponding to $[\text{AA}] = 10 \times 10^{-3}$ or $5.0 \times 10^{-3} \text{ mol L}^{-1}$. Titrations conducted from $\alpha = 1$ to $\alpha = 0$ with HCl 0.1 M.

2.2.2 Effect of the composition profile on the ionization behavior

Figure 2.5a shows pH as a function of α corresponding to statistical, block and gradient copolymers. Figure 2.5b shows the plot of $\text{pK}_{\text{a,eff}}$ as a function of α ($\text{pK}_{\text{a,eff}}$ was obtained from Equation 2.6) In Figure 2.5 it can be observed that the different distribution of AA units within the polymer chain directly affects the ionization behavior. For a fixed α , the block copolymer exhibits the lowest $\text{pK}_{\text{a,eff}}$ on the full α -range indicating that its AA units were more acidic than those of the gradient or the statistical copolymers. For both block and gradient copolymers, $\text{pK}_{\text{a,eff}}$ strongly increased with α , but for S_{50%} the relationship between pK_{a} and α was less pronounced.

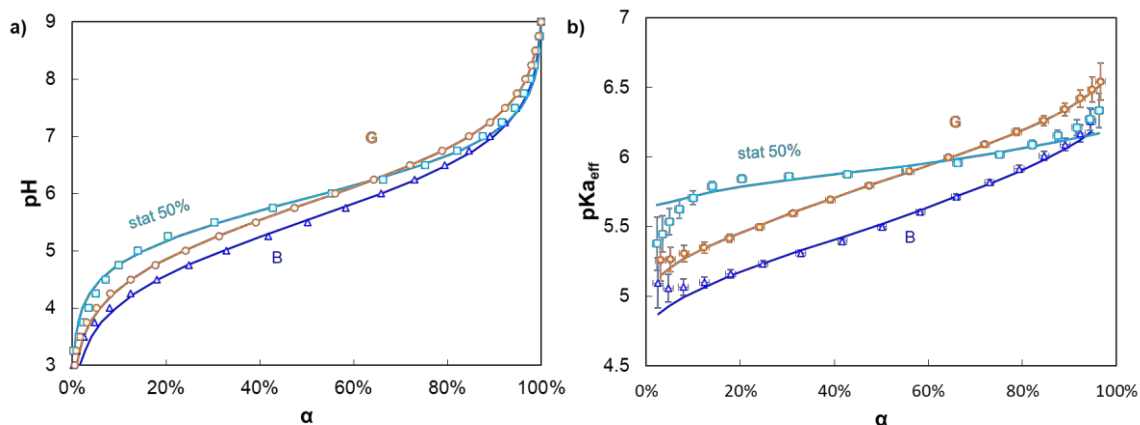


Figure 2.5. a) pH as a function of α . b) $pK_{a,eff}$ as a function of α , for B (\square , \triangle), G (\circ , \circ) and statistical (\square , \square) copolymers ($M_n = 20 \text{ kg mol}^{-1}$) showing the effect of composition profile on the ionization behavior. The symbols correspond to the experimental data, whereas the lines correspond to the best Gaussian fit. The titrations were conducted from $\alpha = 1$ to $\alpha = 0$ with HCl 0.1 M at a polymer concentration of 1 g L^{-1} and with 0.1 M NaCl.

These observations could be visualized in a more quantitative way by fitting the obtained experimental data from Figure 2.5 with a descriptive Gaussian model, in which the polyelectrolyte acid is treated as though it is made up of a mixture of ideal monoacids with pK_a s that follow a Gaussian distribution. The explanation of the Gaussian model is described in the experimental section at the end of the chapter. The fit parameters and an estimate of the standard error in the data points are shown in Table 2.4.

Table 2.4 Best fit parameters for Gaussian model.

Polymer	Mean pK_a (μ)	Standard deviation (σ)	Standard error in fit ^a
S _{50%}	5.92	0.49	0.011
Block	5.53	0.86	0.002
Gradient	5.83	0.87	0.004
Asymmetric diblock	5.65	0.79	0.007
Asymmetric triblock	5.78	0.89	0.002
S _{16%}	7.05	0.80	0.013
S _{30%}	6.46	0.57	0.013
S _{40%}	6.12	0.45	0.013
S _{60%}	5.69	0.64	0.005
S _{70%}	5.71	0.69	0.011
S _{84%}	5.44	0.97	0.003
PAA	5.43	1.08	0.009

a) Standard error in fit = $\sqrt{[SSR/(N-2)]}$, where SSR is the sum of squared residuals and N is the number of fitted data points. Roughly 70 % of measured α fall within this distance of the fitted line. The error in measuring pH was assumed to be negligible.

The Gaussian model has two parameters: An average value of pKa, which corresponds to the $pK_{a,eff}$ at $\alpha = 50\%$, and the standard deviation of the pKa distribution (σ). Hence, the stronger the deviation from monoacid-like behavior, the greater the standard deviation of the distribution. Despite having only two parameters, this empirical model fits the data well over nearly the entire α -range. The standard deviation followed the order $S_{50\%} < \text{gradient} \sim \text{block}$ (Figure 2.6), while the maximum of the distribution followed the order $\text{block} < \text{gradient} \sim S_{50\%}$. Thus, the statistical copolymer showed the smallest deviations (Table 2.4) from ideal monoacid-like behavior, while the gradient copolymer revealed qualitatively similar behavior to that of the block copolymer, but shifted to higher pH.

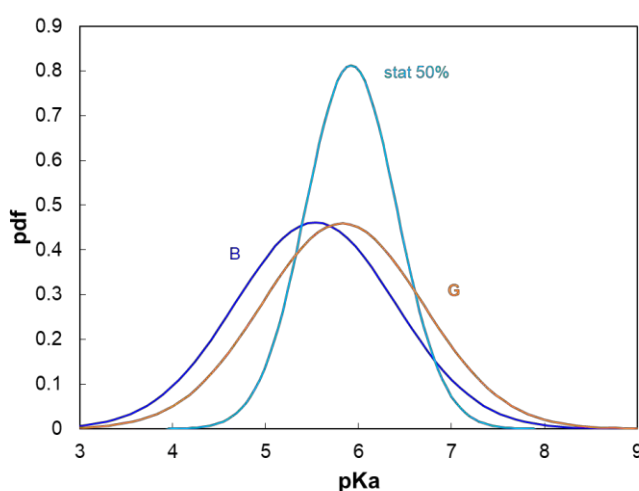


Figure 2.6. Fitted Gaussian distributions of pKa for block (B), gradient (G) and statistical (Stat_{50%}) copolymers ($M_n = 20 \text{ kg mol}^{-1}$) showing the effect of the composition profile on the ionization behavior.

2.2.3 Effect of AA content on the ionization behavior

In order to investigate how the AA content affects the ionization behavior of polyelectrolytes, statistical copolymers of different compositions were studied. Statistical copolymers $S_{16\%}$, $S_{30\%}$, $S_{70\%}$, $S_{84\%}$ and pure PAA were synthesized by RAFT copolymerization and those with nomenclature $S_{40\%}$, $S_{50\%}$ and $S_{60\%}$ were synthesized by ATRP copolymerization. Their macromolecular characteristics were obtained by SEC. Statistical copolymers were selectively acidolyzed using TFA, in order to yield amphiphilic copolymers of AA-*n*BA. Figure 2.7a and b depict the pH and $pK_{a,eff}$ as a function of α , respectively. Each copolymer exhibited a homogeneous composition along the chain but a different AA content ranging from 16% to 100 mol %. This allowed the effects of the local environment of the AA units and of α to be determined independently

of any composition variation along the polymer chain. From Figure 2.7b, three main deductions can be made: first, for a given α , the acidic character decreased with increasing *n*BA content ($pK_{a,eff}$ became larger); secondly, for a given *n*BA content, $pK_{a,eff}$ increased with α , and the variation of $pK_{a,eff}$ with α was the steepest for PAA, decreased with decreasing AA content (*i.e.*, increasing *n*BA content) until 40 mol % AA and increased again for even lower AA contents. These qualitative observations could be quantitatively described again by fitting the experimental data with a gaussian model. The behavior of these polymers was consistent with previously reported experimental and theoretical work on homogeneously distributed weak polyelectrolytes.¹⁴

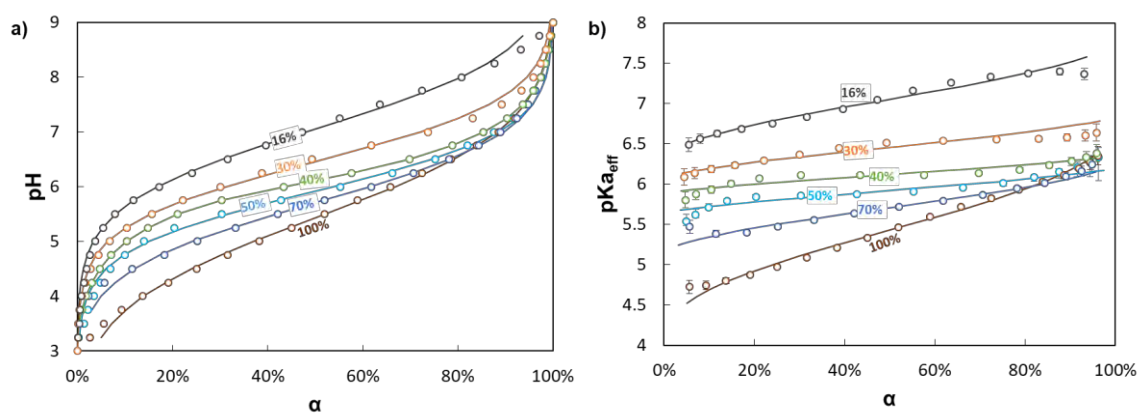


Figure 2.7. a) pH as a function of α , and b) $pK_{a,eff}$ as a function of α for statistical copolymers (S_{16%}, S_{30%}, S_{40%}, S_{50%}, S_{70%} and PAA) showing the effect of AA content on the ionization behavior. The symbols correspond to the experimental data, whereas the lines correspond to the best fit according to the model of Koper and Borkovec. The titrations were conducted from $\alpha = 1$ to $\alpha = 0$ with HCl 0.1 M at a polymer concentration of 1 g L⁻¹ and with 0.1 M NaCl

Qualitatively, the results summarized in Figure 2.7 could be interpreted as follows. For PAA, increase of α led to the formation of more and more charges within the polymer chains, which decreased the propensity of the remaining neutral AA units to ionize due to repulsive electrostatic interactions and caused a strong increase of $pK_{a,eff}$ with α . For the statistical copolymers, decreasing the amount of AA (*i.e.*, increasing *n*BA content) increased the hydrophobic character, resulting in a less polar environment where it was more difficult to create charges. This caused an increase of $pK_{a,eff}$ at a fixed α . Simultaneously, the AA units were further separated by the *n*BA units so that interactions between charges were weaker. This led to a shallower increase of $pK_{a,eff}$ with α with AA contents decreasing from 100 to 40 mol % (*i.e.*, *n*BA content increasing from 0 to 60 mol %). For AA \leq 30 mol %, the variation of $pK_{a,eff}$ with α became again slightly more pronounced with decreasing AA content, which could be attributed to a collapse of the

polymer chains forcing the AA units closer to one another and to interact slightly more than for S_{50%}. The variation of pK_{a,eff} with α was, however, never as steep as for PAA for any of the statistical copolymers. Globally, the effect of increasing the hydrophobic character of the chain on pK_{a,eff} dominated over the effect of separating the charges so that at a given α , pK_{a,eff} increased as the AA content of the statistical copolymers decreased (i.e., *n*BA content increased).

The titration curves could actually be well-fitted to a model described by Koper and Borkovec²² using two parameters: pK, which represents the acidic character of the AA units at $\alpha = 1$ and ϵ , which represents the extent of coupling between the neighboring AA units causing pK_{a,eff} to vary with α (Figure 2.8a and b, Table 2.5). The explanation of Koper and Borkovec's model can be found in the experimental section at the end of the chapter.

Table 2.5. Best fit parameters for Koper and Borkovec Site Binding model

Polymer	pK	ϵ	Standard error in fit ^a
S _{16%}	7.53	1.10	0.011
S _{30%}	6.69	0.52	0.011
S _{40%}	6.25	0.30	0.012
S _{50%}	6.14	0.49	0.012
S _{60%}	6.04	0.79	0.007
S _{70%}	6.09	0.89	0.011
S _{84%}	6.07	1.44	0.013
PAA	6.16	1.66	0.009

a) Standard error in fit = $\sqrt{[SSR/(N-2)]}$, where SSR is the sum of squared residuals and N is the number of fitted data points. Roughly 70% of measured α fall within this distance of the fitted line. The error in measuring pH was assumed to be negligible.

Best estimates for pK and ϵ are given in Table 2.5 for PAA and each of the statistical copolymers. The variations of pK and ϵ shown in Figure 2.8a are consistent with the qualitative interpretation of the results discussed above. To allow a quantitative comparison of the statistical copolymers to the copolymers with varying composition profiles represented in Figure 2.5, the titration curves in Figure 2.7 were also fitted to the Gaussian model (see Table 2.4) and the resulting distributions of pK_{a,eff} are displayed in Figure 2.8b. The deviations from ideal monoacid behavior were strongest for PAA and for S_{16%} as evidenced by the broad distributions of pK_a that result from the model fitting

procedure, while the smallest dependence of $pK_{a,eff}$ on α for $S_{40\%}$ leads to a narrower pK_a distribution.

In a statistical copolymer, all AA units have roughly the same immediate environment and, therefore roughly the same behavior regardless of their position in the chain. Their ionization behavior thus depends only on their overall composition and on α . In a gradient copolymer, however, the local environment of the AA units varies along the chain. Hence, it was hypothesized that the AA units at one end of a gradient copolymer would behave like an AA-rich statistical copolymer, while AA units further along the chain would behave like statistical copolymers with decreasing AA content. In other words, the gradient copolymer would behave like a combination of statistical copolymers of different composition.

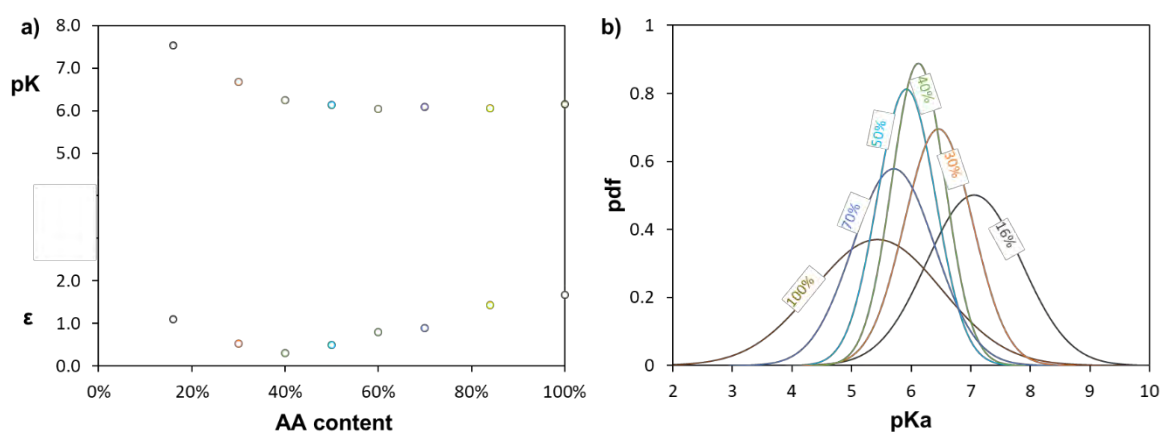


Figure 2.8. Impact of the AA content on the ionization behavior of statistical copolymers. a) Parameters of the model of Koper et al. used to fit the data. b) Gaussian distributions of pK_a . The titrations were conducted from $\alpha = 1$ to $\alpha = 0$ with HCl 0.1 M at a polymer concentration of 1 g L^{-1} and with 0.1 M NaCl.

In order to test this hypothesis, it was attempted to mimic the titration curves of the gradient copolymer as a combination of blocks with different composition. This was first tested by synthesizing a series of di- and tri-block copolymers with composition profiles that approximated ever more closely that of the gradient copolymer. These composition profiles consisted of: A block copolymer (B) of two blocks of equal length, containing 0 and 100 mol % of AA respectively; an asymmetric diblock copolymer (D) of two blocks of equal length containing 16 and 84 mol % of AA respectively; and an asymmetric triblock copolymer (T) of two blocks of equal length, containing 0 and 100 mol % of AA

respectively, separated by a central block of 50 mol % of AA statistical copolymer that accounted for 58 mol % of the total length of the polymer.

The structures of the corresponding block copolymers are represented in Figure 2.1, their macromolecular characteristics are summarized in Table 2.1 and their titration curves are displayed in Figure 2.9. Figure 2.9a and b revealed that block 20K was a very poor experimental mimic of the gradient copolymer. This result was already discussed above and is not surprising because of the abrupt variation of composition along the chain for B as compared to G. D, which resembled B but with a weaker variation of composition between each block behaved more closely to the gradient copolymer, but still did not capture faithfully its ionization behavior. Finally, T, which contains a central block of statistical P(AA-*n*BA) copolymer resulting in a smoother evolution of the AA content along the polymer chain, did behave very similarly to the gradient copolymer. Thus, these results support our initial hypothesis that the behavior of a complex gradient copolymer exhibiting a continuous variation of composition along the chain can be mimicked by asymmetrical block copolymers exhibiting a small number of step changes in their composition profile. From this, it is concluded that the broad distribution of $pK_{a_{eff}}$ highlighted in the fit of the Gaussian model to G (Figure 2.9c) reflects both the decrease in overall acidic character with increasing α due to repulsive electrostatic interactions, and the spatial heterogeneity of the individual acidic sites caused by the composition gradient in the polymer chain.

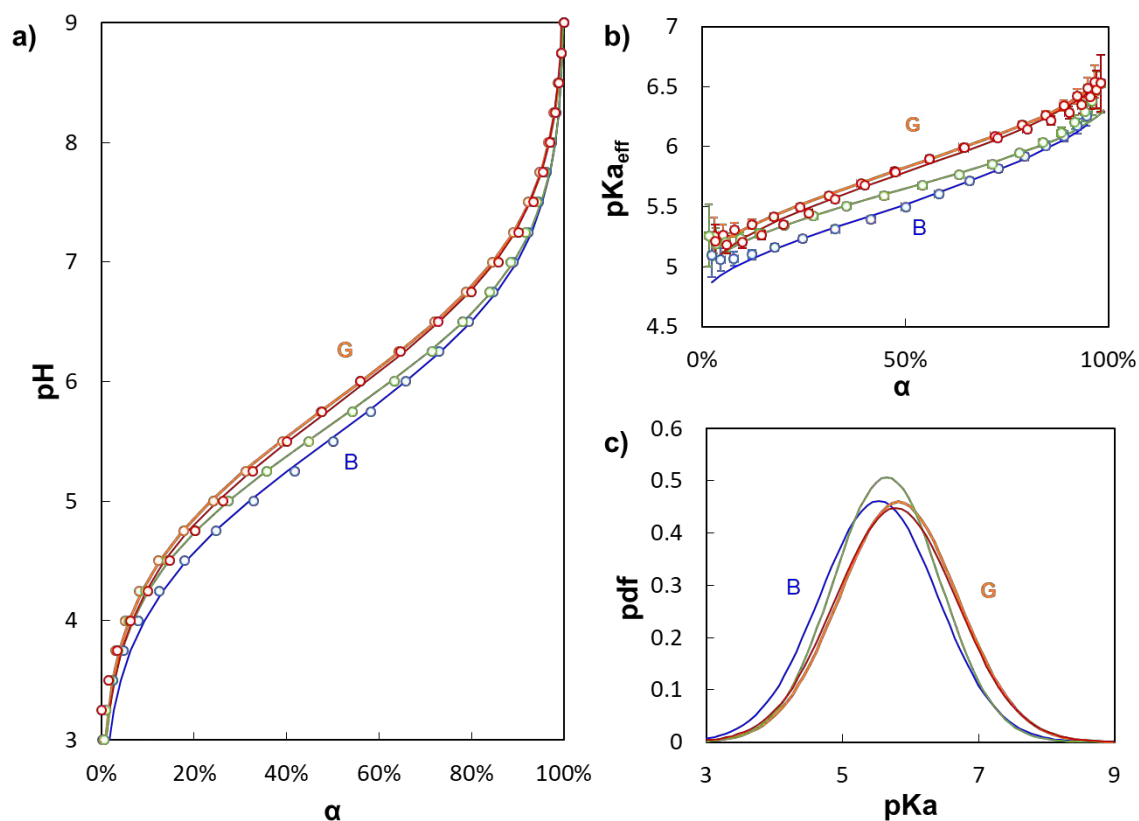


Figure 2.9. Comparison of the ionization behavior of model copolymers mimicking the behavior of the gradient. The titrations were conducted from $\alpha = 1$ to $\alpha = 0$ with HCl 0.1 M at a polymer concentration of 1 g.L^{-1} and with 0.1 M NaCl. a) pH vs α for B (\triangle), D (∇), T (\diamond) and G (\circ). The pH-axis was enlarged to highlight the small differences between the polymers. b) $pK_{a,eff}$ vs α for block 20K, diblock 20K, gradient 20K, triblock 20K. c) Gaussian distributions of $pK_{a,eff}$ for block 20K, diblock 20K, gradient 20K, triblock 20K. Lines in (a) and (b) correspond to Gaussian fits. The fitting parameters are given in Table 2.4.

To go one step further, the titration curves of each of these model copolymers (B, D, T) were mimicked by mathematically combining the titration curves of the statistical blocks they are composed of. This was done by taking into account the molar fraction of AA units contained in each of these blocks and assuming that the covalent bond between the different blocks did not change the titration behavior of their constituting blocks.

To calculate the ionization behavior of the polyelectrolytes exhibiting non homogeneous composition profiles based on that of the $S_{x\%}$ copolymers, it was assumed that connecting different blocks covalently did not affect their ionization behavior as compared to when each block is titrated independently. In that case, equation 2.9 can be used to calculate the average ionization degree $\alpha_{average}$ of the polymer at a given pH value.

$$\alpha_{average} = \sum_i f_i \times \alpha_i \quad \text{Equation 2.9}$$

Where, for the chosen pH value, f_i corresponds to the molar fraction of AA units contained in the statistical copolymer i and α_i corresponds to its degree of ionization.

In order to use equation 2.9, the experimental data of each polymer were interpolated from pH = 3 to 9 with a 0.25 step and $\alpha_{average}$ was calculated at each pH value. Then, $pK_{a,eff}$ was deduced from equation 6.

With these assumptions B should behave as a pure PAA homopolymer. However, this was not the case, as shown on Figure 2.10a which revealed a strong discrepancy between the experimental titration curve of B and the corresponding mathematical model at $\alpha \leq 50\%$. This discrepancy may be attributed to the fact that B self-assembled into spherical micelles in aqueous medium and, therefore, had a star-like architecture. Such an architecture has indeed been reported to result in an increase of $pK_{a,eff}$ compared to the corresponding linear PAA homopolymer.^{23,24}

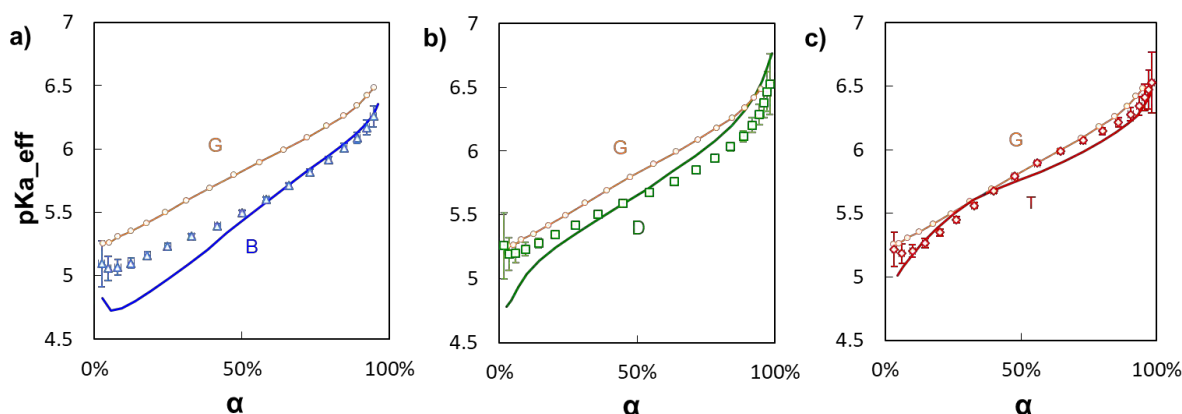


Figure 2.10. Mathematical modelling of the evolution of $pK_{a,eff}$ vs α for a) B (Δ), modelled as a pure PAA block (—), b) D (\square), modelled as 16 mol % $S_{16\%}$ + 84 mol % $S_{84\%}$ (—) and c) T (\diamond), modelled as 42 mol % PAA + 58 mol % $S_{50\%}$ (—). G (\circ) is also represented for comparison on each curve (the line connecting the points is only to guide the eye). The experimental data and conditions used in this figure are the same as in Figure 2.5.

D is mathematically modelled in Figure 2.10b as a combination of $S_{16\%}$ and $S_{84\%}$. The discrepancy between the mathematical model and the experimental data was still significant, but much less pronounced than for B at low α . The smaller discrepancy between the mathematical model and the experimental data was attributed to the fact that both $S_{16\%}$ and D are self-assembled in aqueous medium, so that the impact of self-assembly was not as strong as between PAA homopolymer (not self-assembled) and B (strongly self-assembled).

Finally, for T, the agreement between the mathematical model and the experimental curve was significantly improved. This result is extremely interesting from an application point of view because it allows to 1) predict the titration behavior of virtually any gradient profile in a simple way before having to actually synthesize the corresponding polymer, and/or 2) define the best suited composition profile along the chain to afford the targeted titration curve. Moreover, this simple model could also be used to adapt the existing theories and models currently valid for weak polyelectrolytes exhibiting a homogeneous composition profile to more complex weak polyelectrolytes.

3 CONCLUSIONS

Dans ce chapitre, les propriétés physiques en masse et en solution des copolymères de P(AA-*n*BA) ont été analysées.

Dans la première section, le DSC a été utilisé pour étudier la séparation en microphasique en masse des copolymères P(AA-*n*BA). Les résultats ont montré que les propriétés de séparation microphasique des copolymères asymétriques se situent entre celles correspondant aux copolymères séquencés et statistiques. Les copolymères à tribloc et gradient présentent un comportement thermique assez similaire car tous les deux présentent des larges amplitudes de T_g . Ceci est conforme à l'analyse de titrage, dans laquelle le copolymère à tribloc a un comportement d'ionisation similaire à celui du copolymère à gradient.

Dans la section des propriétés en solution, le comportement d'ionisation des copolymères P(AA-*n*BA) a été analysé par titrage potentiométrique. Dans la première section, l'effet du profil de composition a été étudié en comparant les courbes $pK_{a,eff}$ des copolymères séquencés, à gradient et statistiques. Le copolymère à blocs a présenté le $pK_{a,eff}$ le plus bas dans toute la gamme α , ce qui signifie que le copolymère à blocs a les unités d'AA les plus acides. Pour le copolymère à blocs et à gradient, le $pK_{a,eff}$ augmente constamment avec α , mais pour $S_{50\%}$, l'évolution du $pK_{a,eff}$ est moins prononcée. Les données expérimentales obtenues à partir des titrages potentiométriques ont été ajustées d'un modèle gaussien, qui considère deux paramètres: les valeurs moyennes de $pK_{a,eff}$ à $\alpha = 0,5$ et l'écart type de la distribution pK_a . Le $S_{50\%}$ a présenté la plus petite valeur d'écart type, ce qui indique qu'il a un faible écart par rapport au comportement d'un monoacide idéal.

Ensuite, l'impact du contenu en AA a été analysé en étudiant des copolymères statistiques avec différentes fractions d'AA. Pour le PAA, l'augmentation de α a conduit à la formation de plus de charges, ce qui a rendu difficile de continuer à ioniser les unités d'AA neutres restantes en raison d'interactions électrostatiques répulsives. Pour les copolymères statistiques avec 70 à 40 mol% d'AA, il a été observé que lorsque le contenu en AA diminue, le caractère acide des copolymères diminue également en raison de la génération d'un environnement plus hydrophobe. Il est donc plus difficile de créer des charges. Les copolymères statistiques, à gradient et à blocs ont également été ajustés du modèle de Koper et de Borkovec, dont les paramètres sont en accord avec ceux obtenus avec le modèle gaussien.

Enfin, le copolymère à gradient a été imité avec succès par des processus synthétiques et mathématiques. La voie de synthèse a montré que la distribution d'AA la plus similaire au copolymère à gradient est celle correspondant au copolymère tribloc asymétrique.

3 CONCLUSIONS

In this chapter the physical properties in bulk and in solution of P(AA-*n*BA) copolymers were analyzed.

In the first section DSC was utilized to investigate the microphase separation in bulk of the P(AA-*n*BA) copolymers. The results showed that the microphase separation properties of asymmetric copolymers lie in between those corresponding to block and statistical copolymers. Triblock and gradient copolymers show quite similar thermal behavior since both exhibit wide T_g breadths. This is in accordance with the titration analysis, in which the triblock copolymer has a similar ionization behavior to the gradient copolymer.

In the section of properties in solution, the ionization behavior of P(AA-*n*BA) copolymers was analyzed by potentiometric titration. In the first section the effect of the composition profile was investigated by comparing the $pK_{a_{eff}}$ curves of block, gradient and statistical copolymers. The block copolymer showed the lowest $pK_{a_{eff}}$ in all α -range, which means that the block copolymer has the most acidic AA units. For block and gradient copolymer, $pK_{a_{eff}}$ constantly increased with α , but for $S_{50\%}$ the evolution of $pK_{a_{eff}}$ was less pronounced. The experimental data obtained from potentiometric titrations was fitted with a Gaussian model, which considers two parameters: the average values of $pK_{a_{eff}}$ at $\alpha = 0.5$ and the standard deviation of the pK_a distribution. The $S_{50\%}$ presented the smallest standard deviation value, which indicates that it has a weak deviation from the ideal monoacid behavior.

Then the impact of the AA content was analyzed by studying statistical copolymers with different AA fractions. For PAA the increase of α led to the formation of more charges, which made difficult to keep ionizing the remaining neutral AA units due to repulsive electrostatic interactions. For statistical copolymers with 70 to 40 mol % AA, it was observed that when the AA content was diminished, the acidic character of the copolymers decreased due the generation of a more hydrophobic environment and it was more difficult to create charges. Statistical, gradient and block copolymers were also fitted with the Koper and Borkovec model, whose parameters were in agreement with those obtained by the Gaussian model.

Finally, the gradient copolymer was successfully mimicked by synthetic and mathematic processes. The synthetic route showed that the most similar AA distribution to the gradient copolymer was the corresponding to the asymmetric triblock copolymer.

4 MATERIALS AND METHODS

The P(*t*BA-*n*BA) diblock and triblock copolymers were synthesized at the University of Jena by Dr. Junliang Zhang. The PAA-P*n*BA gradient and block copolymers were synthesized at the IMRCP laboratory by Dr. Ihor Kulai. Once the initial batches of block and gradient copolymers were finished, new batches of 10 000 and 20 000 g mol⁻¹ were prepared. In order to simplify the description of copolymers a special notation is added at the end of their names. Those P(*t*BA-*n*BA) copolymers which contains at the end the letters **JZ** were synthesized by Dr. Junliang Zhang, copolymers containing **IK** at the end were synthesized by Dr. Ihor Kulai and copolymers containing **BF** at the end, were synthesized by Barbara Farias.

4.1 Materials

1,4-dioxane, dichloromethane (DCM), acetone, and methanol were purchased from TCI and used as received. 1,1'-Azobis(cyclohexanecarbonitrile) (ACHN), trifluoroacetic acid (TFA), azobisisobutyronitrile (AIBN), and anisole were purchased from Sigma Aldrich and used as received. *n*-Butyl acrylate (*n*BA) and tert-Butyl acrylate (*t*BA) were bought from TCI and stirred with inhibitor remover (purchased from Sigma Aldrich) for 30 minutes before use. Cyanomethyl dodecyl trithiocarbonate (chain transfer agent, CTA) were purchased from Strem Chemicals, Inc. and used as received. Methanol and distilled water were used for polymer precipitation. 1,3,5-trioxane was purchased from Sigma Aldrich and used as received. Deuterated chloroform (CDCl₃), deuterated dimethyl sulfoxide (DMSO-*d*₆), and acetone-*d*₆ obtained from Eurisotop were used as solvent for proton nuclear magnetic resonance (¹H NMR) analysis.

4.2 Size Exclusion Chromatography (SEC)

Number-average molar masses (*M*_n, SEC) and dispersities (*Đ*) of polymers were determined using SEC

SEC system at IMRCP laboratory: The SEC analyses were conducted on a system composed of Waters 515 HPLC pump, Agilent 1260 Autosampler, Varian ProStar 500 column valve module, set of three Waters columns (Styragel Guard Column, 20 μm, 4.6 mm × 30 mm, Styragel HR3, 5 μm, 7.8 mm × 300 mm and Styragel HR4E, 5 μm, 7.8 mm × 300 mm), Varian ProStar 325 UV-Vis detector set at 290 nm and Wyatt Optilab rEX differential refractive index detector using tetrahydrofuran (THF) as an eluent at a flow rate of 1.0 mL min⁻¹ (35 °C). The column system was calibrated with poly(methyl methacrylate) (PMMA) standards (ranging from 1120 to 138600 g mol⁻¹). Samples were

diluted to a concentration about 2 mg mL⁻¹ and filtered through 0.45 µm PTFE syringe filters before injection.

SEC system at IOMC, JCSM, Friedrich Schiller University Jena: The measurements were performed on a Shimadzu system equipped with a CBM-20A system controller, an LC-10AD VP pump, a RID-10A refractive index detector and a PSS SDV column. The eluent was a chloroform/isopropanol/trimethylamine (94%/2%/4%, v/v/v) solvent mixture. Samples were run at 1 mL min⁻¹ at 40 °C. PMMA, poly(styrene) (PS) and poly(ethylene glycol) (PEG) standards (molar mass range is ca. 400 – 100000 g mol⁻¹) were used for calibration. Analyzed samples were filtered through a PVDF membrane with 0.22 µm pore size before injection.

4.3 ¹H NMR

The proton NMR analyses were performed in an apparatus AVANCE Bruker 300 MHz. The P(*t*BA-*n*BA) copolymers were analyzed in CD₃Cl. After they were hydrolyzed to PAA-PBA, they were analyzed in deuterated DMSO.

4.4 Differential scanning calorimetry

The DSC analyses were performed in a FRS Mettler Toledo differential scanning calorimeter. Approximately 10 mg of copolymer was weighed into 40 µl aluminum capsules. The analyses were performed at a heat rate of 20 °C min⁻¹.

4.5 Synthesis of P(*t*BA-*n*BA) block copolymers (IK)

Stock solution A: Cyanomethyl dodecyl trithiocarbonate (1.27 g, 4.00 mmol) and AIBN (0.066 g, 0.40 mmol) were dissolved in 1,4-dioxane (29.5 g, 28.6 mL, 335 mmol) to yield a solution with a total volume of 30 mL. This stock solution was frozen at 3 °C and melted before use.

Stock solution B: AIBN (0.066 g, 0.40 mmol) was dissolved in 1,4-dioxane (30.8 g, 29.9 mL, 350 mmol) to yield a solution with a total volume of 30 mL. This stock solution was frozen at 3 °C and melted before use.

*n*BA (1.34 g, 1.5 mL, 10.45 mmol) was mixed with stock solution A (1.00 mL, 67 µmol RAFT agent, 6.7 µmol AIBN) in a 15 mL vial, adjusted with 1,4-dioxane (2.5 mL) to 5 mL volume and sealed with a rubber septum. The obtained solution was degassed by sparging with Ar for 15 minutes and immersed into a thermostated heating block at 60 °C for 8 hours. An aliquot was analyzed with ¹H NMR to determine the monomer

conversion (> 95%), then evaporated under vacuum and analyzed with SEC. The reaction mixture was concentrated under vacuum to remove the unreacted monomer, precipitated in a 10/90 (vol/vol) water/methanol mixture and dried under deep vacuum. This procedure resulted in a near quantitative yield of the originally added *n*BA to polymer. Then, the second monomer *t*BA (1.34 g, 1.5 mL, 10.45 mmol) and stock solution B (1.00 mL, 6.7 μ mol AIBN) were added, adjusted with 1,4-dioxane (2.00 mL) to 5 mL volume and polymerized as described above, with > 95% conversion of the *t*BA monomer.

4.6 Synthesis of P(*t*BA-*n*BA) linear gradient copolymers (IK, BF)

Gradient copolymer synthesis was performed in a batch reaction with continuous monomer addition. A stock solution with cyanomethyl dodecyl trithiocarbonate, 1,1'-azobis(cyclohexanecarbonitrile) (ACHN) and 1,3,5-trioxane (10 mg mL⁻¹), was prepared in dioxane and poured into a schlenk tube. The monomers, *t*-BA and *n*-BA, were transferred to vials and trioxane was added. Stock solution and monomers were degassed by argon bubbling during 30 min. Syringes were connected to a schlenk flask and then degassed with argon flow during 30 min. After degassing the schlenk flask with the stock solution, it was settled in an oil bath at 90 °C. The syringes, previously charged with the monomers, were installed on the master and secondary pumps. Later, the syringes were connected to the schlenk tube and a first amount of *t*-butyl acrylate was added. Immediately after the gradient addition profile was started. After 6 h the gradient addition finished and only *n*-butyl acrylate was added during 1.5 h. Samples were withdrawn each 0.5 h for their analysis by ¹H NMR and SEC. Finally, the reaction was stopped by quenching in liquid nitrogen.

The polymer was purified twice by precipitation in a methanol/water mixture (3:1 v/v). After it was allowed to dry at high vacuum during 6 h.

Table 2.6. Gradient copolymers synthesis and macromolecular characteristics.

Copolymer	<i>t</i> BA (mol L ⁻¹)	<i>n</i> BA (mol L ⁻¹)	Initiator (mol L ⁻¹)	RAFT agent (mol L ⁻¹)	Conversion (%)	<i>M_n</i> (kg mol ⁻¹)	<i>Đ</i>
G10K-BF	1.23	2.77	7.01E-3	5.2E-2	66	8.3	1.13
G20K-BF	1.41	3.26	3.98E-3	2.54E-2	65	21.0	1.20

4.7 Synthesis of P(*t*BA-*n*BA) diblock copolymers (JZ)

Stock solutions of cyanomethyl dodecyl trithiocarbonate (315 mmol L⁻¹) and azobisisobutyronitrile (AIBN, 12.18 mmol L⁻¹) were prepared in dioxane. *t*-butyl acrylate,

n-butyl acrylate and stock solutions were poured into separate containers inside the automatized synthesizer. The equipment was programmed to add the desired quantities of each reagent to the reactors. 1,3,5 trioxane was added as internal standard (10 mg mL⁻¹). Once all the reagents were introduced into the reactor, the mixture was degassed by bubbling N₂ during 15 min. After, the reaction was allowed to proceed at 60 °C during 8h. Samples were withdrawn each 2 h for the analysis by SEC and NMR. When the targeted molar mass was reached, the polymerization was stopped for its subsequent use without any purification.

Once the first block was obtained, the remaining quantity of monomer in the polymer was calculated and then more *n*-BA and *t*-BA were added in order to make the following block. Stock solution of AIBN (12.18 mmol L⁻¹) was also added and the mixture was degassed with N₂ during 15 min. The polymerization was allowed to run at 60 °C during 8 h. Aliquots were withdrawn each 2 h in order to analyze them by SEC and NMR. When the targeted molar mass was reached, the polymerization was stopped and the removed from the equipment. The polymers were recovered first by diluting with acetone and after by precipitation in a water/methanol mixture (1/3, v/v) and the procedure was repeated until the remaining monomer disappear from the ¹H NMR spectrum.

4.8 Synthesis of P(*t*BA-*n*BA) triblock copolymers (JZ)

Stock solutions of cyanomethyl dodecyl trithiocarbonate (315 mmol L⁻¹) and AIBN (12.18 mmol L⁻¹) were prepared in dioxane. *t*-BA and stock solutions were poured into separate containers inside the automatized synthesizer. The equipment was programmed to add the desired quantities of each reagent to the reactors. 1,3,5-trioxane was added as internal standard (10 mg mL⁻¹). Once all the reagents were introduced into the reactor, the mixture was degassed by bubbling N₂ during 15 min. After, the reaction was allowed to proceed at 60 °C during 8h. Samples were withdrawn each 2 h for the analysis by SEC and ¹H NMR. When the targeted molar mass was reached, the polymerization was stopped for its subsequent use without any purification.

Once the first block has been obtained, the remaining quantity of monomer in the polymer was calculated and then more *n*BA and *t*BA were added in order to make the following block. Stock solution of AIBN (12.18 mmol L⁻¹) was also added and the mixture was degassed with N₂ during 15 min. The polymerization was allowed to proceed at 60 °C during 8 h. Aliquots were withdrawn each 2 h in order to analyze them by SEC and ¹H NMR. When the targeted molar mass was reached, the polymerization was stopped and the removed from the equipment. The polymers were diluted with acetone and after

recovered by precipitation in a water/methanol mixture (1/3, v/v). The procedure was repeated until the remaining monomer was removed.

After the purification of the second block, it was dissolved in dioxane and *n*-BA was added to extend the third block. The stock solution of AIBN (12.18 mmol L⁻¹) was also added and the mixture was degassed with N₂ during 15 min. The reaction was allowed to proceed at 60 °C during 8h. Samples were withdrawn each 2 h for the analysis by SEC ¹H NMR and when the desired molar mass was reached, the polymerization was stopped. Finally, the polymers were purified twice by precipitation in a water/methanol mixture (1/3, v/v).

4.9 Synthesis of P(*t*BA-*n*BA) block copolymers (BF)

Stock solutions of cyanomethyl dodecyl trithiocarbonate (315 mmol L⁻¹) and AIBN (12.18 mmol L⁻¹) were prepared in dioxane. Certain amount of stock solutions were mixed with *t*-BA and dioxane (Table 2.7). The mixture was poured into a schlenk tube and it was degassed with argon during 30 min. The schlenk tube was placed in an oil bath at 70 °C during 3.5 h. The first blocks of 5 000 g mol⁻¹ and 10 000 g mol⁻¹ were analyzed by ¹H NMR and SEC. After, the polymers were purified twice by precipitating in a water/methanol mixture (1/3 v/v) and they were dried under high vacuum.

Once dried, the polymers were dissolved separately in dioxane and mixed with BA and AIBN stock solution in the described amounts in Table 2.7. The mixture was poured into a schlenk tube and it was degassed with argon during 30 min. The polymerization was allowed to proceed at 70 °C during 4 h.

Table 2.7. Synthesis and macromolecular characteristics of P(*t*BA-*n*BA) block copolymers

Copolymer	<i>t</i> BA (mmol L ⁻¹)	<i>n</i> BA (mmol L ⁻¹)	AIBN (mmol L ⁻¹)	RAFT or Macro RAFT (mmol L ⁻¹)	Conversion (%)	<i>M_n</i> (kg mol ⁻¹)	<i>Đ</i>
PtBA 5K-BF	3000	---	12.2	81.1	95	6.6	1.04
PtBA 10K-BF	3000	---	5.92	39.5	97	11.5	1.05
B10K-BF	---	2000	8.34	55.5	91	10.0	1.10
B20K-BF	---	2000	3.53	23.5	87.5	20.1	1.06

4.10 Synthesis of the different statistical S_x% copolymers

The synthesis of S_{40%}, S_{50%} and S_{60%} has been reported in a previous paper (they were named MH40, MH50 and MH60 in a previous study).²⁵ Additional statistical copolymers

(S_{16%}, S_{30%}, S_{70%}, S_{84%}) and a sample of PAA homopolymer were prepared according to the following typical procedure (procedure for S_{30%} is reported).

Stock solutions of cyanomethyl dodecyl trithiocarbonate (55 mg mL⁻¹ in dioxane) and AIBN (2 mg mL⁻¹ in dioxane) were prepared. These stock solutions, *t*BA (12 mmol, 1.54 g), *n*BA and (28mmol, 3.60 g) were poured into a schlenk tube equipped with a magnetic stirrer. Dioxane was also added until 10 mL. The mixture was degassed by four freeze-pump-thaw cycles and the tube was then filled with argon. The schlenk tube was placed into a pre-heated oil bath at 60 °C for 6h. After this time the polymerization was quenched by immersing the tube in liquid nitrogen. A sample was withdrawn and analysed by ¹H NMR and SEC to obtain monomer conversion (69 %) and molar mass (11.7 kg.mol⁻¹), respectively. The polymers were purified by two precipitations in a water/methanol (1/3, v/v) solvent mixture.

Acidolysis of block, gradient, diblock and triblock copolymers

Each polymer was first dissolved in 5 mL of DCM, then 5-fold excess (mol % corresponding to the amount (mol) of *t*BA units) of TFA was added at once. The reaction mixture was stirred at room temperature for 72 hours, rotary evaporated, dissolved in 10 mL of 1,4-dioxane and rotary evaporated again, washed with 10 mL of deionized water and dried under vacuum.

4.11 Acidolysis of S_{16%}, S_{30%}, S_{70%}, S_{84%} and PAA

Each polymer was first dissolved in 5 mL of DCM, then 5-fold excess (relative to the *t*BA units) of TFA was added at once. Reaction mixture was stirred at room temperature for 72 hours. Afterwards, this mixture was rotary evaporated and subjected to deep vacuum. Then it was dissolved with 10 mL of dioxane and rotary evaporated again. Finally it was subjected to deep vacuum to eliminate the remaining solvent.

Table 2. 8. Macromolecular characteristics of the Sx% statistical copolymers of AA and *n*BA.

Copolymer	Before acidolysis			After acidolysis	
	M_n (kg mol^{-1})	\bar{D}^a	tBA mol % ^b	Expected M_n (kg mol^{-1})	AA mol % ^d
S _{16%}	15.7	1.04	16%	14.6	18%
S _{30%}	11.7	1.05	30%	10.2	31%
S _{40%}	12.5	1.17	40%	10.0	42%
S _{50%}	12.5	1.10	51%	10.0	51%
S _{60%}	13.6	1.34	60%	10.3	61%
S _{70%}	11.7	1.06	70%	9.7	63%
S _{84%}	18.1	1.09	84%	11.4	77%
PAA	18.3	1.04	100%	10.3	83%

4.12 Potentiometric titration experiments

4.12.1 Preparation of polymer solutions

For the titration of polymers containing 50 mol % of AA units in the chain, 30 mL of polymer solution at $C_{\text{polymer}} = 1 \text{ g L}^{-1}$ (corresponding to $[\text{AA}] = 5 \cdot 10^{-3} \text{ mol L}^{-1}$) and $[\text{NaCl}] = 0.1 \text{ M}$ were prepared as follows. The degree of ionization α of the polymers in their solid form was 0. The polymers were first dissolved in water in the presence of ~ 1.1 equivalent of NaOH relative to the total amount of AA units, which was calculated from the chemical structure of the polymer. After stirring for at least one night, the polymers were fully dispersed resulting in transparent solutions. The NaCl concentration was then adjusted using a 4 M NaCl solution. For the statistical copolymers with varying contents of AA, the solutions were prepared in the same way but either at $C_{\text{polymer}} = 1 \text{ g.L}^{-1}$ of polymer or at constant $[\text{AA}] = 5 \cdot 10^{-3} \text{ mol.L}^{-1}$.

4.12.2 Titration experiments.

The polymer solutions were back titrated at room temperature with $[\text{HCl}] = 0.1 \text{ M}$ using an automatic titrator (TIM 856, Radiometer Analytical) controlled by the TitraMaster 85 software following a published procedure¹⁵. The addition of HCl titrant was done at a constant speed of 0.1 mL min^{-1} .

4.13 Gaussian model

The Gaussian model is derived as follows:

For a weak acid, the degree of ionization, α , is given by the equation 2.10

$$\alpha = \frac{10^{pH}}{10^{pH} + 10^{pKa}} \quad \text{Equation 2.10}$$

For a mixture of acids, each with a different pKa, the total degree of ionization is the sum of the degrees of ionization of the individual acids:

$$\alpha = \sum_i f_i \cdot \frac{10^{pH}}{10^{pH} + 10^{pKa_i}} \quad \text{Equation 2.11}$$

Where f_i is the mole fraction of the acid with $pKa = pKa_i$. This can be extended to a mixture of acids with a continuous distribution of pKa, with probability distribution function f :

$$\alpha = \int_{-\infty}^{\infty} f(pKa) \cdot \frac{10^{pH}}{10^{pH} + 10^{pKa}} dpKa \quad \text{Equation 2.12}$$

If the pKas are normally distributed, with mean μ and standard deviation σ , the degree of ionization is given by:

$$\alpha = \frac{1}{\sigma\sqrt{\pi}} \int_{-\infty}^{\infty} \frac{10^{pH}}{10^{pH} + 10^x} e^{-\frac{(x-\mu)^2}{2\sigma^2}} dx \quad \text{Equation 2.13}$$

Setting $z = (x - \mu)/\sigma$ gives

$$\alpha = \frac{1}{\sqrt{\pi}} \int_{-\infty}^{\infty} \frac{1}{1 + 10^{\mu + \sigma z - pH}} e^{-\frac{z^2}{2}} dz \quad \text{Equation 2.14}$$

This equation can be fitted to the data with the help of numerical integration. These equations were used to fit the Gaussian model to the experimental degree of ionization data, taking pH as the independent variable and assuming negligible error in this measurement relative to the error in the degree of ionization measurement, using a nonlinear least squares fitting procedure.

4.14 Koper and Borkovec's model

Koper and Borkovec's model²² considers equally spaced acidic sites along a linear chain that interact with each other through pairwise interactions. In the case of an infinitely long chain, the degree of protonation, θ (equal to $1 - \alpha$), is given by:

$$\theta = 1 - \alpha = \frac{1 - u + \lambda u}{2 + (\lambda/z)(1 - zu)} \quad \text{Equation 2.15}$$

In this equation,

$$\lambda = \frac{1 + zu}{2} + \sqrt{z + \frac{(1 - uz)^2}{4}} \quad \text{Equation 2.16}$$

$$z = Ka_H = 10^{pK - pH} \quad \text{Equation 2.17}$$

$$u = 10^{-\varepsilon} \quad \text{Equation 2.18}$$

pK is the logarithm of the binding constant for protonation of the fully deprotonated polyacid, and corresponds to the pK_a for dissociation of the final proton from the polyacid. The parameter ε is due to pairwise interactions between the binding sites. The resulting titration curve resembles that of a diprotic acid due to the stability of the state in which every second site is protonated, although the protonation steps are broader.

This equation was fitted to the experimental titration curve (pH vs α) data using nonlinear least squares fitting assuming negligible error in the measurement of pH. Due to the complexity of the equation, the partial derivatives $\partial\alpha/\partial pK$ and $\partial\alpha/\partial\varepsilon$ were estimated as:

$$\frac{\partial\hat{\alpha}}{\partial pK} \approx \frac{\hat{\alpha}(1.01 \times pK) - \hat{\alpha}(pK)}{0.01 \times pK} \quad \text{Equation 2.19}$$

$$\frac{\partial\hat{\alpha}}{\partial\varepsilon} \approx \frac{\hat{\alpha}(1.01 \times \varepsilon) - \hat{\alpha}(\varepsilon)}{0.01 \times \varepsilon} \quad \text{Equation 2.20}$$

LITERATURE

- 1 O. Colombani, M. Ruppel, F. Schubert, H. Zettl, D. V. Pergushov and A. H. E. Müller, *Macromolecules*, 2007, **40**, 4338–4350.
- 2 S. Harrisson, *Polym. Chem.*, 2018, **9**, 1366–1370.
- 3 R. A. Brown, A. J. Masters, C. Price and X. F. Yuan, in *Comprehensive Polymer Science and Supplements*, Elsevier, 1989, pp. 155–198.
- 4 D. W. VAN KREVELEN, in *Properties of Polymers*, Elsevier, 1997, pp. 129–187.
- 5 J. Kim, M. M. Mok, R. W. Sandoval, D. J. Woo and J. M. Torkelson, *Macromolecules*, 2006, **39**, 6152–6160.
- 6 M. M. Mok, J. Kim, C. L. H. Wong, S. R. Marrou, D. J. Woo, C. M. Dettmer, S. T. Nguyen, C. J. Ellison, K. R. Shull and J. M. Torkelson, *Macromolecules*, 2009, **42**, 7863–7876.
- 7 W. Jakubowski, A. Juhari, A. Best, K. Koynov, T. Pakula and K. Matyjaszewski, *Polymer (Guildf)*, 2008, **49**, 1567–1578.
- 8 M. K. Gray, H. Zhou, S. B. T. Nguyen and J. M. Torkelson, *Macromolecules*, 2004, **37**, 5586–5595.
- 9 L. García-Fernández, A. Mora-Boza and F. Reyes-Ortega, in *Smart Polymers and their Applications*, Elsevier, 2019, pp. 45–86.
- 10 J. Jagur-Grodzinski, *Polym. Adv. Technol.*, 2010, **21**, 27–47.
- 11 F. S. H. Krismastuti, W. L. A. Brooks, M. J. Sweetman, B. S. Sumerlin and N. H. Voelcker, *J. Mater. Chem. B*, 2014, **2**, 3972–3983.
- 12 C. Chassenieux and C. Tsitsilianis, *Soft Matter*, 2016, **12**, 1344–1359.
- 13 I. Borukhov, D. Andelman, R. Borrega, M. Cloitre, L. Leibler and H. Orland, *J. Phys. Chem. B*, 2000, **104**, 11027–11034.
- 14 J. Landsgesell, L. Nová, O. Rud, F. Uhlík, D. Sean, P. Hebbeker, C. Holm and P. Košovan, *Soft Matter*, 2019, **15**, 1155–1185.
- 15 O. Colombani, E. Lejeune, C. Charbonneau, C. Chassenieux and T. Nicolai, *J. Phys. Chem. B*, 2012, **116**, 7560–7565.
- 16 O. Borisova, L. Billon, M. Zaremski, B. Grassl, Z. Bakaeva, A. Lapp, P. Stepanek and O. Borisov, *Soft Matter*, 2012, **8**, 7649–7659.
- 17 G. Laruelle, J. François and L. Billon, *Macromol. Rapid Commun.*, 2004, **25**, 1839–1844.
- 18 M. Rabyk, A. Destephen, A. Lapp, S. King, L. Noirez, L. Billon, M. Hruby, O. Borisov, P. Stepanek and E. Deniau, *Macromolecules*, 2018, **51**, 5219–5233.
- 19 C. Charbonneau, C. Chassenieux, O. Colombani and T. Nicolai, *Macromolecules*, 2011, **44**, 4487–4495.
- 20 C. Charbonneau, C. Chassenieux, O. Colombani and T. Nicolai, *Macromolecules*, 2012, **45**, 1025–1030.
- 21 C. Charbonneau, T. Nicolai, C. Chassenieux, O. Colombani and M. Miriam De Souza Lima, *React. Funct. Polym.*, 2013, **73**, 965–968.
- 22 G. J. M. Koper and M. Borkovec, *Polymer (Guildf)*, 2010, **51**, 5649–5662.
- 23 F. A. Plamper, H. Becker, M. Lanzendörfer, M. Patel, A. Wittemann, M. Ballauff and A. H. E. Müller, *Macromol. Chem. Phys.*, 2005, **206**, 1813–1825.

- 24 Y. Xu, F. Plamper, M. Ballauff and A. H. E. Müller, in *Complex Macromolecular Systems II*, Springer, Berlin, Heidelberg, 2009, pp. 1–38.
- 25 L. Lauber, C. Chassenieux, T. Nicolai and O. Colombani, *Macromolecules*, 2015, **48**, 7613–7619.

**CHAPTER 3. P(AA-*n*BA)
ASYMMETRIC
COPOLYMERS: SELF-
ASSEMBLY BEHAVIOR**

CHAPITRE 3. COPOLYMERES ASYMETRIQUES DE P(AA-*n*BA) : COMPORTEMENT D'AUTO-ASSEMBLAGE

Le but de ce chapitre est d'étudier le comportement d'auto-assemblage de copolymères asymétriques de P(AA-*n*BA) en solution. Les structures de copolymères utilisées dans ce chapitre sont les mêmes que dans le chapitre 2. L'analyse des copolymères a été réalisée par cryo-TEM, diffusion dynamique de la lumière (DLS) et diffusion de neutrons aux petits angles (SANS). Les copolymères ont été analysés par DLS par deux voies : 1) en dissolvant directement les copolymères dans des solutions tampons à différents pH et 2) par titrage potentiométrique.

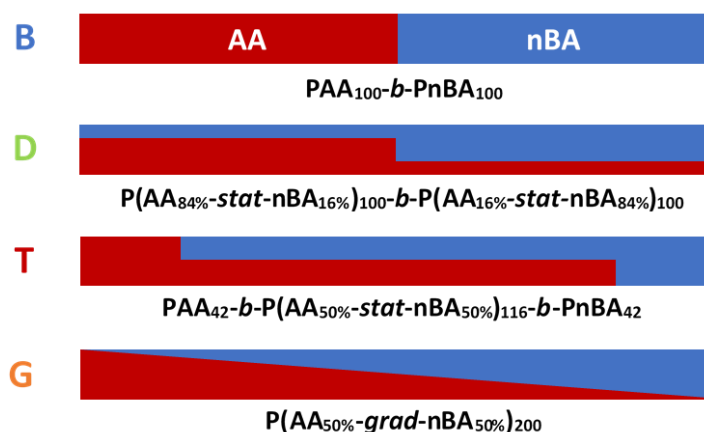


Figure 3.1. Profils de composition ciblés de copolymères à bloc (B), de copolymères à gradient linéaire (G) et de copolymères asymétriques à dibloc (D) et à triblocs (T).

Comme mentionné au chapitre 2, quatre profils de composition ont été ciblés, chacun contenant 50% de BA et 50% d'AA (Figure 3.1) : un copolymère à blocs poly (AA-*bloc*-*n*BA) (B); un copolymère à gradient poly (AA-*grad*-*n*BA) (G) de profil de composition nominale linéaire; un copolymère asymétrique dibloc (D) constitué de deux blocs poly (AA-*stat*-BA) de longueurs égales comprenant 16% et 84% AA, respectivement; et un copolymère asymétrique tribloc (T) constitué d'un bloc court de poly (AA), d'un bloc plus long de poly (AA-*stat*-BA) comprenant 50% d'AA, et d'un bloc court de poly (*n*BA). Les longueurs de blocs de T étaient dans la proportion 21:58:21. Le profil à gradient a été obtenu en utilisant un procédé semi-batch avec addition en flux continue des deux monomères, tandis que les profils asymétriques dibloc et tribloc ont été obtenus par des polymérisations séquentielles en utilisant un synthétiseur robotique parallèle. Les

structures asymétriques D et T ont été choisis pour imiter le profil de gradient linéaire en utilisant un nombre minimal d'étapes. Chaque profil de composition a été réalisé à des masses molaires moyennes en nombre ciblées de 10 et 20 kg.mol⁻¹. Tous les détails du profil de composition et de la distribution des poids moléculaires sont donnés dans le tableau 2.1 du chapitre 2 (p. 64).

1. ANALYSE DLS

L'auto-assemblage des différentes structures de copolymères en solution est provoqué par le changement de pH. Dans cette étude, la modification du pH est réalisée par deux voies : en dissolvant directement les copolymères dans des solutions tampons à différents pH ; et par titrage potentiométrique dans lequel le polymère est d'abord dissous dans une solution aqueuse à un pH déterminé et après que le pH est modifié in situ en titrant la solution avec une solution acide.

1.1 Analyse d'auto-assemblage par DLS en solutions tampons

Les polymères ont été directement dissous dans des solutions tampons à pH de 10, 8, 7, 6, 5 et 4. Ces solutions ont été analysées par DLS. A pH 4, les polymères ne se dissolvent pas spontanément dans l'eau et des dispersions sont obtenues par chauffage avec irradiation micro-ondes. Les tendances de distribution de taille pour les copolymères à bloc, dibloc, tribloc et gradient à 10 et 20 kg mol⁻¹ sont affichées dans la Figure 3.2.

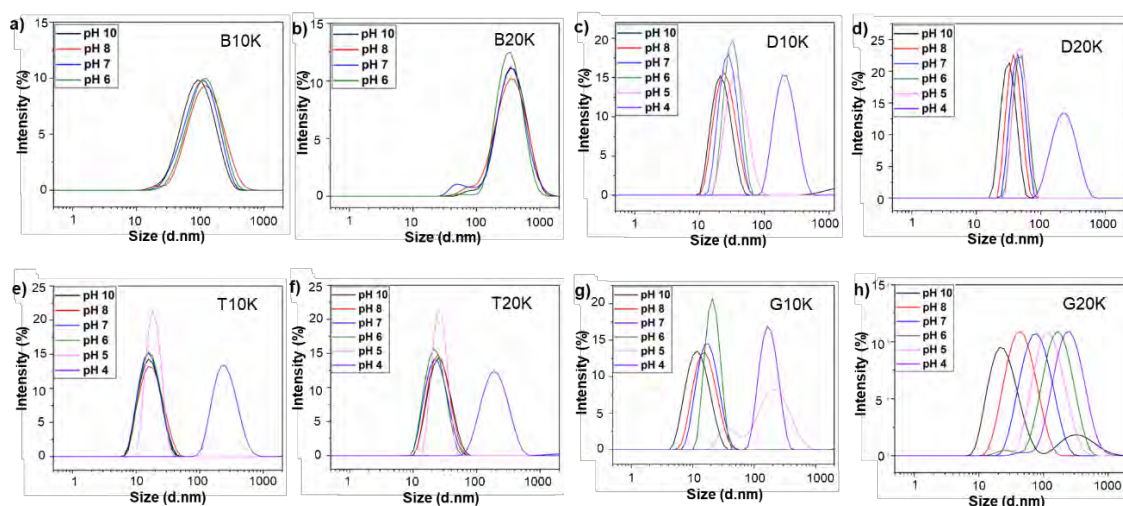


Figure 3.2. Distributions de taille obtenues par DLS pour des copolymères de structures différentes à 10 et 20 kg mol⁻¹. a) bloc 10K b) bloc 20K, c) dibloc 10K, d) dibloc 20K, e) tribloc 10K, f) tribloc 20K, g) gradient 10K, h) gradient 20K.

Dans presque tous les cas, les distributions de taille observées sont unimodales et relativement étroites en termes de distribution. B10K et B20K affichent des distributions de tailles monomodales, mais celles correspondant à B20K sont plus étroites. D10K et D20K montrent également des distributions monomodales et affichent des comportements similaires dans toutes les gammes de pH, mais de manière similaire aux copolymères blocs, les distributions de D20K sont relativement plus étroites que celles pour D10K. T10K et T20K affichent également un comportement similaire de distribution de taille. Pour les deux, les distributions sont monomodales et étroites mais la distribution la plus étroite se manifeste à pH 6. G10K et G20K présentent le comportement de distribution de taille le plus différent de polymères analogues. Pour G10K en diminuant le pH, les distributions monomodales se rétrécissent, sauf dans le cas du pH 5 dans lequel une distribution bimodale apparaît, indiquant un mélange de petites et grandes particules. Dans G20K, les distributions sont très larges, presque comme celles qui correspondent à B10K. À pH 10, une distribution bimodale est observée indiquant un mélange de petits et grands agrégats. En diminuant le pH, les distributions sont maintenant monomodales et plus larges.

Dans quelques cas (D10K, pH 10; G20K, pH10), une population de faible intensité et de grand diamètre (> 100 nm) est observée en plus de la population majeure de diamètre beaucoup plus petit. Celles-ci pourraient être attribuées à une contamination par des particules de poussière ou à une fraction pondérale négligeable de fausses agrégats.¹⁻⁵ Dans le cas de la population bimodale observée à pH 5 pour G10K (Figure 3.2g) et à pH10 pour G20K (Figure 3.2h), la distribution montrée peut ne pas être une représentation précise de la distribution de taille réelle en raison des limites de l'algorithme d'ajustement lorsqu'il est appliqué à des distributions bimodales.

La principale différence qui peut être observée entre les différents profils de composition est que la distribution de taille des deux copolymères à blocs, B10K et B20K (Figures 3.2a et 3.2b), reste presque constante dans toute la gamme de pH, tandis que celles des copolymères blocs à gradient et asymétriques sont dépend du pH. Ceci est résumé sur la Figure 3.3 qui présente les diamètres hydrodynamiques (D_h) en fonction du pH. La taille des particules et le PDI sont résumés à l'annexe 2, tableau A2.1.

CHAPTER 3. P(AA-*n*BA) ASYMMETRIC COPOLYMERS: SELF-ASSEMBLY BEHAVIOR

The aim of this chapter is to study the self-assembly behavior of P(AA-*n*BA) asymmetric copolymers in solution. The copolymer structures used in this chapter are the same as in chapter 2. The analysis of the copolymers was performed by cryo-TEM, dynamic light scattering (DLS) and small angle neutron scattering (SANS). The copolymers were analyzed by DLS by two routes: 1) directly dissolving the copolymers in buffer solutions at different pH and 2) by potentiometric titration.

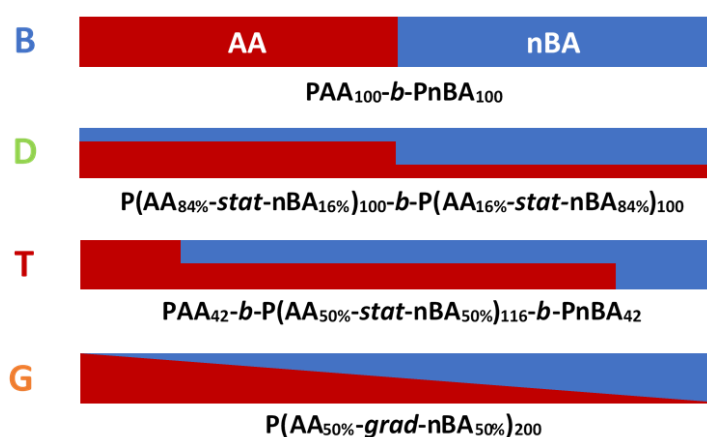


Figure 3.1. Targeted composition profiles of block copolymers (**B**), linear gradient (**G**) copolymers and asymmetric diblock (**D**) and triblock (**T**) copolymers.

As mentioned in chapter 2, four composition profiles were targeted, each containing 50% BA and 50% AA (Figure 3.1): a poly(AA-*block*-BA) block copolymer (**B**); a poly(AA-*grad*-BA) gradient copolymer (**G**) of nominally linear composition profile; an asymmetric diblock copolymer (**D**) consisting of two poly(AA-*stat*-BA) blocks of equal lengths comprising 16% and 84% AA, respectively; and an asymmetric triblock copolymer (**T**) consisting of a short block of poly(AA), a longer block of poly(AA-*stat*-BA) comprising 50% AA, and a short block of poly(BA). The block lengths of **T** were in the proportion 21:58:21. The gradient profile was obtained using a starved feed semibatch process with continuous addition of both monomers, while the asymmetric diblock and triblock profiles were obtained via sequential polymerizations using a robotic parallel synthesizer. The asymmetric structures **D** and **T** were chosen to mimic the linear gradient profile using a minimal number of steps. Each composition profile was realized at overall targeted number average molar masses of 10 and 20 kg.mol⁻¹. Full details of the composition profile and molecular weight distribution are given in Table 2.1 of Chapter 2 (p. 64).

1 DLS ANALYSIS

The self-assembly of the different copolymer structures in solution is triggered by the change of pH. In this investigation pH modification was accomplished by two routes: 1) by directly dissolving the copolymers in buffer solutions at different pHs and 2) by potentiometric titration, in which the polymer is first dissolved in an aqueous solution at basic pH and after the pH is modified by titrating with an acidic solution. It is important to mention that in the experiments carried out in buffer solutions the self-assemblies had longer time to equilibrate at each pH under study than in the case of the potentiometric titration experiments.

1.1 Self-assembly analysis by DLS in buffer solutions

The polymers were directly dissolved in buffer solutions at pH of 10, 8, 7, 6, 5 and 4. These solutions were analyzed using DLS. At pH 4, the polymers did not dissolve spontaneously in water, and dispersions were obtained by heating with microwave irradiation. The size distribution trends for block, diblock, triblock and gradient copolymers at 10 and 20 kg mol⁻¹ are displayed in Figure 3.2.

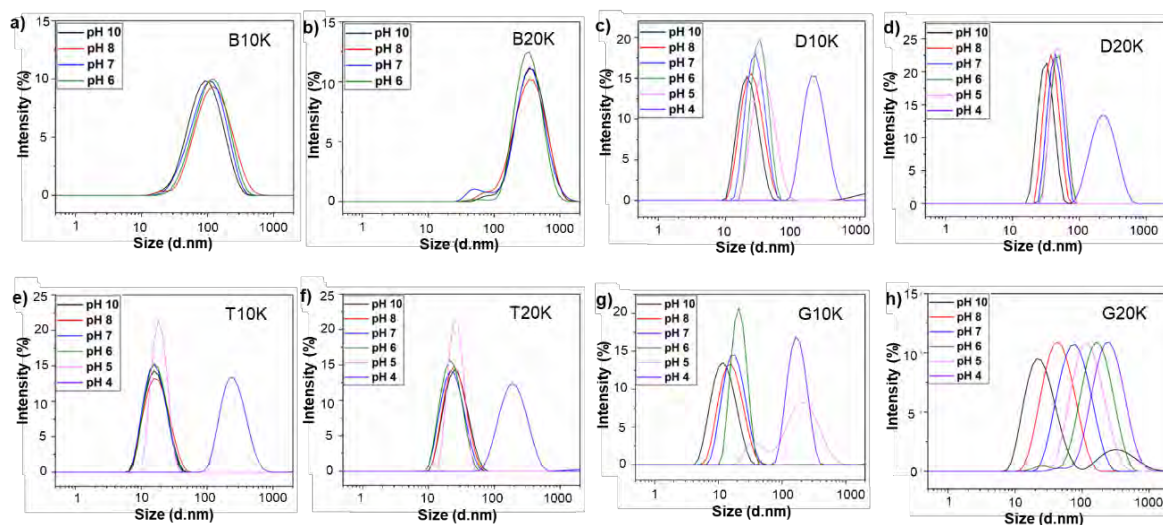


Figure 3.2. Size distributions obtained by DLS for copolymers with different structures at 10 and 20 kg mol⁻¹. a) Block 10K b) block 20K, c) diblock 10K, d) diblock 20K, e) triblock 10K, f) triblock 20K, g) gradient10K, h) gradient 20K.

In nearly all cases, the observed particle size distributions are unimodal and relatively narrow in dispersity. B10K and B20K display monomodal size distributions, but those corresponding to B20K are narrower. D10K and D20K also show monomodal distributions and display similar behaviors in all pH range, but similarly to block

copolymers, the distributions of D20K are relatively narrower than those for D10K. T10K and T20K also display similar behavior of size distribution. For both, distributions are monomodal and narrow but the narrowest distribution is manifested at pH 6. G10K and G20K display the most different behavior of size distribution from their analogous polymers. For G10K by decreasing pH, the monomodal distributions get narrower, except in the case of pH 5 in which a bimodal distribution appears, indicating a mixture of small and large particles. In G20K distributions are very broad, almost as the corresponding ones to B10K. At pH 10 a bimodal distribution is observed indicating mixture of small and large aggregates. By decreasing pH, the distributions are now monomodal and broader.

In a few cases (D10K, pH 10; G20K, pH10) a low intensity, large diameter (> 100 nm) population is observed in addition to the major population of much smaller diameter. These could be attributed to contamination by dust particles or to a negligible weight fraction of spurious aggregates.¹⁻⁵ In the case of the bimodal population observed at pH 5 for G10K (Figure 3.2g) and at pH10 for G20K (Figure 3.2h), the distribution shown may not be an accurate representation of the true size distribution due to the limitations of the fitting algorithm when applied to bimodal distributions;

The major difference that can be observed between the different composition profiles is that the size distribution of both block copolymers, B10K and B20K (Figures 3.2a and 3.2b), remain almost constant in all pH range, while those of the gradient and asymmetric block copolymers are dependent on the pH. This is summarized in Figure 3.3 which presents the hydrodynamic diameters (D_h) as a function of pH. The particle sizes and PDI are summarized in Appendix 2, Table A2.1.

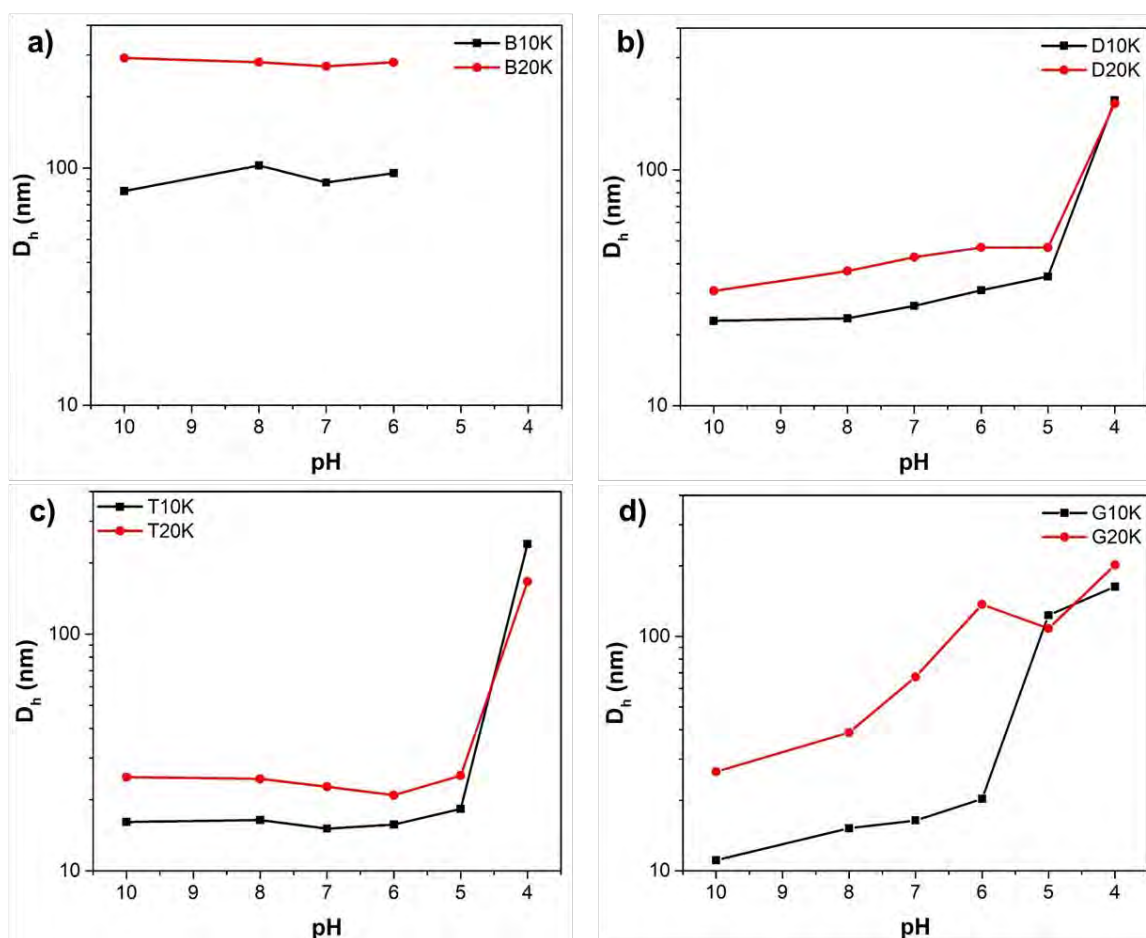


Figure 3.3. Hydrodynamic diameter as a function of pH for a) block copolymers, b) asymmetric diblock copolymers, c) asymmetric triblock copolymers and d) gradient copolymers of 10 and 20 g mol^{-1} .

In Figures 3.3b it is observed that the size trends for D10K and D20K shift towards higher particle size when decreasing pH from 10 to 5, and then at pH 4 they both form aggregates larger than 100 nm. For triblock copolymers (Figure 3.3c), there is no variation on the size distribution from pH 10 to pH 6, then at pH 4 both T10K and T20K formed larger aggregates. The near constant hydrodynamic size behavior at higher pH is very similar to that of block copolymers, and could be ascribed to the *Pn*BA block in the triblock copolymers. For the case of G10K, the size trend first shifts towards larger particle size as the pH decreases from 10 to 6, then at pH 5 and 4 larger aggregates are formed. G20K exhibits a size trend which continuously shifts towards larger particle size.

Hence, unlike block copolymers, the hydrodynamic diameter of aggregates of asymmetric diblock, triblock and gradient copolymers, varies in response to changes in pH, with gradient copolymers being most sensitive to changes in pH, followed by the asymmetric diblock copolymers, and finally the triblock copolymers, whose relative lack

of sensitivity may be related to the presence of a block of P*n*BA homopolymer in the composition profile.

1.2 Self-assembly analysis by DLS by potentiometric titration

The polymers were directly dissolved into 0.1 M NaOH solution at a concentration of 0.2 wt%, ensuring their complete ionization. The solution was titrated with 0.1 M HCl until it became turbid (around pH ~ 4). It was then back titrated with aqueous NaOH to return to high pH. DLS measurements were obtained at regular intervals during titration, and a selection of the intensity-average particle size distributions obtained are shown in Figure 3.4. The particle size distributions were monomodal in nearly all cases, with PDIs ranging from less than 0.1 in the case of D20K to a maximum of 0.46 in the case of G20K at pH 4.45. The full set of D_h and PDI are shown in Appendix 2, Tables A2.2 to A2. 9.

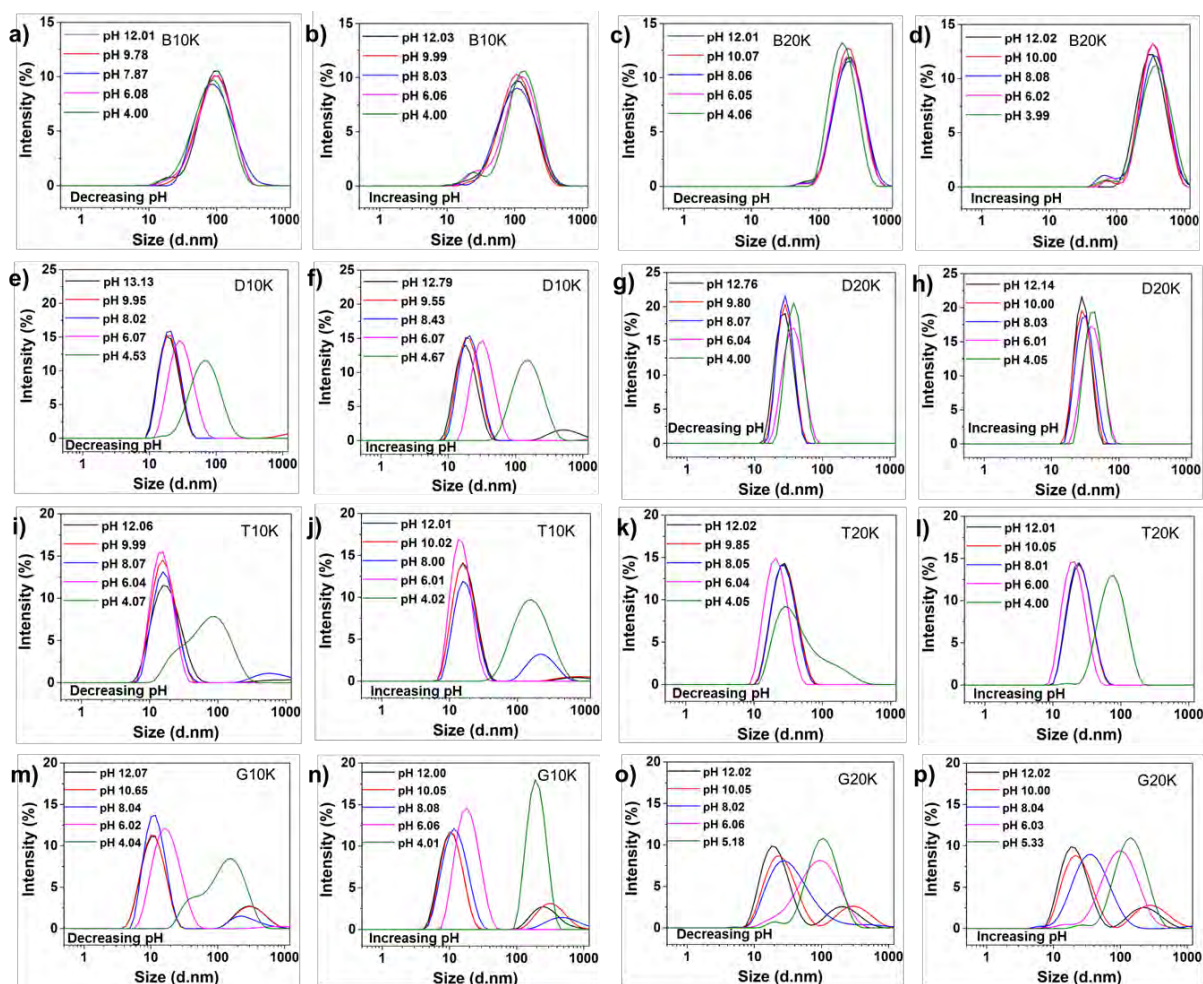


Figure 3.4. Size distributions obtained by DLS for the potentiometric titration study of P(AA-*n*BA) copolymers ($M_n = 10 \text{ kg mol}^{-1}$ and 20 kg mol^{-1}). 10K block copolymer a) decreasing pH b) increasing pH, 20K block copolymer c) decreasing pH d) increasing pH, 10K diblock copolymer e) decreasing pH f) increasing pH, 20K diblock copolymer g) decreasing pH h) increasing pH, 10K triblock copolymer i) decreasing pH j) increasing pH, 20K triblock copolymer k) decreasing pH l) increasing pH, 10K gradient copolymer a) decreasing pH b) increasing pH and 20K gradient copolymer a) decreasing pH b) increasing pH. (Decrease of pH by adding HCl solution and increase of pH by adding NaOH solution).

As in the analysis previously discussed, the self-assemblies of the block copolymers B10K (Figures 3.4a and b) and B20K (Figures 3.4c and d) were unaffected by changes in pH for pH > 5. At pH 5, the polymer precipitated. Significant differences in D_h were observed in the forward and back titrations, indicating that the self-assemblies were kinetically trapped, non-equilibrium species in agreement with earlier results from the literature⁶⁻⁸.

In contrast, the hydrodynamic diameters of the gradient copolymers and asymmetric diblock copolymers were sensitive to pH, steadily increasing from 10 to 30 nm at pH greater than 7 to around 100 nm at pH of 4 to 5 (Figure 3.5).

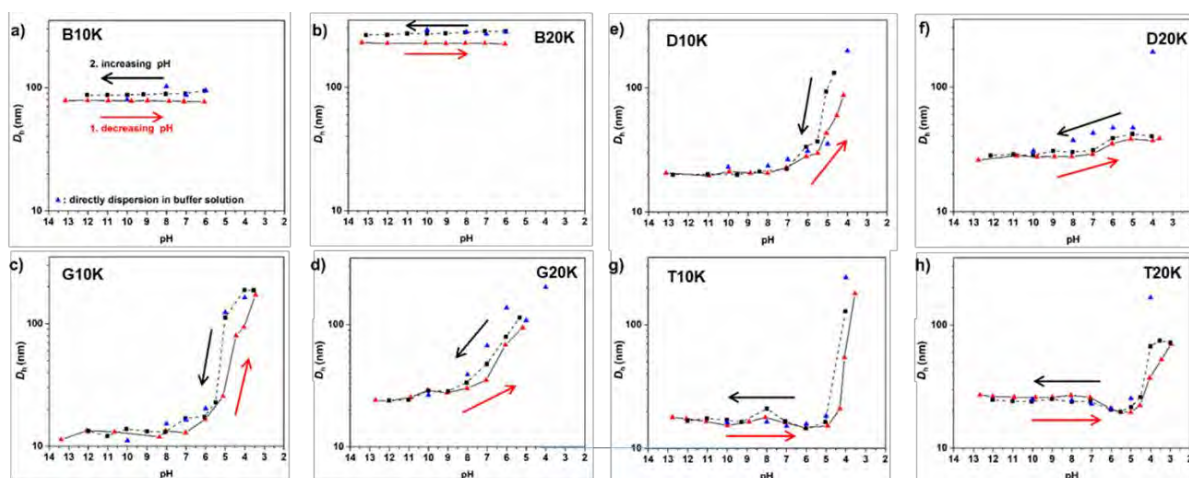


Figure 3.5. Z-average hydrodynamic diameters obtained by DLS for different types of copolymers with molar mass of 10 and 20 kg mol⁻¹ using two different methods (directly dispersed in different pH buffers (blue triangles) and titration study (decreasing pH: red triangles; increasing pH: black squares)): a) B10K b) B20K c) G10K d) G20K e) D10K f) D20K g) T10K h) T20K.

In the potentiometric titration analysis for D10K (Figures 3.4e and 3.5e), the size distribution remained roughly within the same values while decreasing pH 12 to pH 8, but at pH 6 the trend shifted to larger sizes. Finally, at pH 4 larger aggregates (~100 nm) were formed. A similar range of particle size distributions was displayed while increasing the pH (Figure 3.4f). The results obtained from the potentiometric titration experiments do not exactly display the same results as for the buffered solutions at pH > 6, they do are in agreement below pH 6. The low intensity, large diameter (≥ 200 nm) populations observed at pH value 9.95 (Figure 3.4e) and pH value 6.07 (Figure 3.4f) are probably either due to contamination by dust particles or to a negligible weight fraction of spurious aggregates.¹⁻⁵ For D20K (Figures 3.4g and 3.5f) the size distribution remained roughly constant when pH was decreased from 12 to 8, and then at pH < 6 there was a slight shift of the peak to higher size regions (both, by decreasing and increasing pH). The

large aggregates observed at pH 4 in the analysis of buffered solutions did not appear in the titration experiment at pH 4, neither by decreasing nor increasing pH (Figure 3.4h).

For T10K the analysis from the potentiometric titration are roughly in accordance with the analysis of buffered solutions. Figures 3.4i and 3.5g depict that size trends remain constant while decreasing pH from 12 to 6, and then at pH 4 larger aggregates (~100 nm) appear, as it occurred in the analysis of buffered solutions. At pH 4 the corresponding size distribution exhibit a bimodal character, indicating that not all the aggregates could rearrange into larger particles. The titration by increasing pH is in agreement with the size distributions from the analysis of buffered solutions. The low intensity, large diameter (≥ 200 nm) populations observed at pH > 11 (Figure 3.4i) and pH > 10 and pH value 8 (Figure 3.4j) are most probably either due to contamination by dust particles or to a negligible weight fraction of spurious aggregates.¹⁻⁵ In the case of T20K as in the analysis of buffered solutions, there is no significant change in size trends with decrease of pH. Then at pH 4 a bimodal distribution is observed, which indicates that not all the aggregates could self-assemble into larger particles. In Figure 3.4l it is observed that the size distributions are quite similar to those obtained in the analysis of buffered solutions, with a narrow and monomodal distribution at pH 4 and when pH increases the trends shift to smaller particle size region.

For G10K (Figures 3.4m and 3.5c) size distributions remain within the same values by decreasing the pH from 12 to 8, then at pH 6 the size trend shifts towards larger particle size, and at pH 4 a bimodal distribution is observed, and as for the triblock copolymers, this indicates that not all the particles could self-assemble into larger aggregates. In Figure 3.4n it is observed that at pH 4 the size trend of G10K is narrow and very similar to the distribution observed in the analysis of buffered solutions, and then when the pH is increased the size trends slightly shift to shorter particle sizes. The low intensity, large diameter (≥ 200 nm) populations observed at pH > 6 could be either due to contamination by dust particles or to a negligible weight fraction of spurious aggregates. In the titration of G20K, by decreasing the pH (Figures 3.4o and 3.5d) from 12 to 8 there is a slight shift of the trends to larger particle regions and the distribution gets wider as the pH decreases. At pH 6 the wide trend shifts to a particle size of ~ 100 nm and finally at pH 5 the size remains within the same values but with a narrower distribution. Then by increasing the pH of G20K (Figure 3.4p) it can be noted the gradual and continuous evolution of the trends towards smaller particle size.

Due to the limitations of the fitting algorithm when applied to bimodal distributions, the resulting D_h for T10K (Figure 3.4i), T20K (Figure 3.4k) and G10K (Figure 3.4m) may not be an accurate representation of the true size distribution.

Something interesting to note is that when the titration is made by increasing the pH of the polymer solutions, the behavior exhibits more similarities to the results obtained by the analysis of buffered solutions than when the titration is made by decreasing the pH.

The titration curves shown in Figure 3.5 were reversible and generally in good agreement with hydrodynamic diameters obtained by direct dissolution in buffer solution. Hysteresis was observed for pH less than ~ 5 , suggesting that equilibration is slow or nonexistent when the degree of ionization is low, which is consistent with previous observations of block copolymers of polyacrylic acid and poly(acrylic acid-*stat*-styrene).^{9,10} Finally, the D_h of the asymmetric triblock copolymers remained constant or decreased slightly as the pH decreased, before abruptly increasing at pH 4. Again, the changes in size were reversible and independent of the method of preparation for pH > 4.

2 SELF-ASSEMBLY ANALYSIS BY cryo-TEM

Selected samples (B20K, G20K, D10K and T10K, prepared by direct dispersion in buffer) were subsequently analyzed by cryogenic transmission electron microscopy (Cryo-TEM), with representative images displayed in Figure 3.6. These images were generally consistent with the trends in particle size observed by DLS, but allowed direct evaluation of particle morphology.

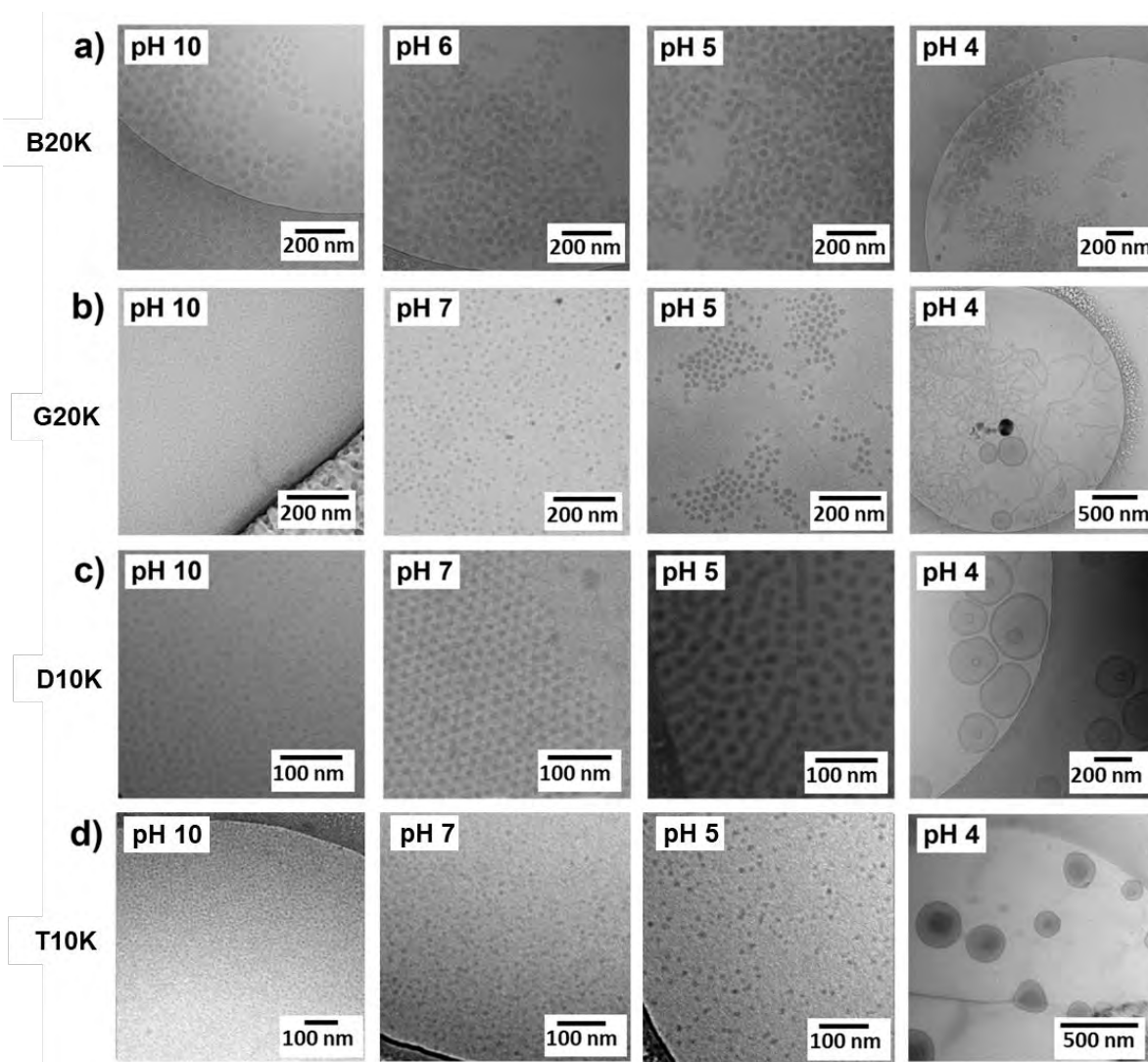


Figure 3.6. Representative Cryo-TEM images of the self-assemblies of different types of copolymers directly dispersed in different pH buffers: a) B20K; b) G20K; c) D10K; and d) T10K.

Cryo-TEM images of B20K displayed spherical particles with diameters of ~ 40 nm. At all pHs, they are densely packed in larger clusters of bigger size, which explains the larger particle diameters obtained by DLS. More ill-defined, highly polydisperse spherical particles dominate at pH 4, although some larger particles including wormlike micelles and vesicles, were also observed (Figure 3.6a and Figure 3.7) and some macroscopic phase separation occurs.

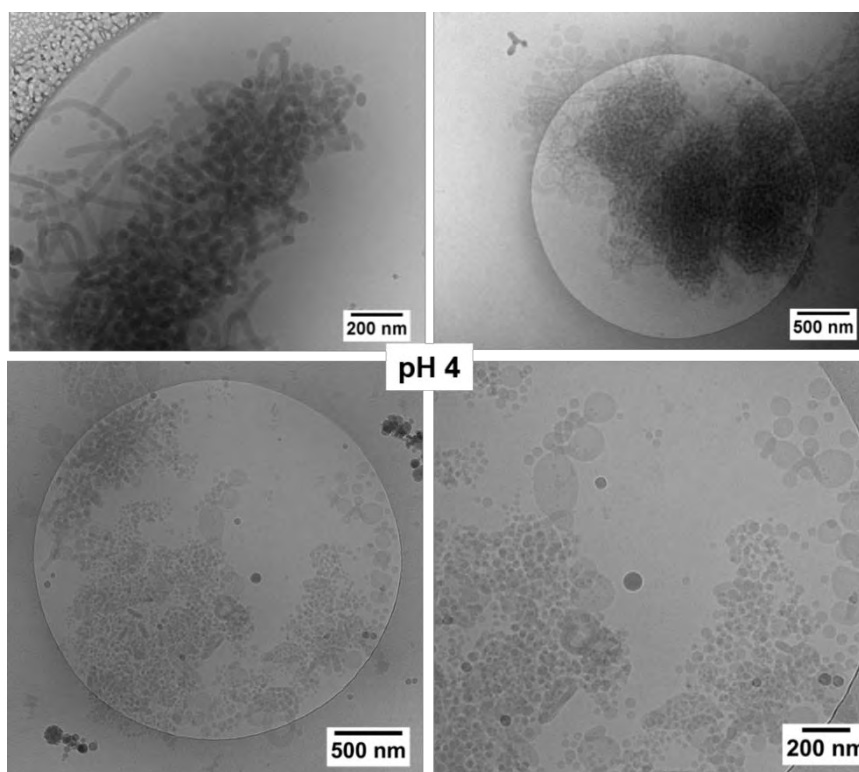


Figure 3.7. Cryo-TEM images of block copolymer B20K (20 kg mol^{-1}) directly dispersed in buffer of pH 4.

By contrast, spherical assemblies of G20K and D10K increased in size as the pH decreased from 10 (fully ionized) to 7 (degree of ionization, $\alpha = 80\text{-}90\%$). At pH 5 ($\alpha = 20$ to 40%), D10K exhibited a mixture of wormlike and spherical structures, while at pH 4 ($\alpha < 10\%$) vesicles dominated. For G20K, aggregates of spherical assemblies were observed at pH 5, while at pH 4 a mixture of vesicles and wormlike micelles was observed. The presence of wormlike micelles and vesicles rather than purely vesicles as in the other structures may be related to the greater dispersity of the gradient copolymer, as increased dispersity is known to displace the phase diagrams of block copolymers,¹¹⁻¹⁵ for example pushing the cylinder/lamellar phase boundary of polystyrene-*block*-polyisoprene-*block*-polystyrene elastomers to higher volume fractions of polystyrene.¹⁵ Wormlike structures have previously been observed in aqueous dispersions of block copolymers of *n*BuA and AA prepared at low pH; these irreversibly transform into spheres when the pH is raised.^{7,16}

Finally, assemblies of T10K remained small and spherical from pH 10 to pH 5, while only vesicles of 100 to 300 nm in diameter were observed at pH 4.

The asymmetric diblock, triblock and gradient structures showed broad similarities in their response, forming spherical structures at high pH and vesicles at low pH, with a

dynamic and reversible response to changes in pH (at least for $\text{pH} \geq 5$) that was absent from the block copolymers B10K and B20K. While the triblock copolymers were superficially more similar in composition profile to the linear gradient copolymers, it was the shorter asymmetric diblock copolymer D10K that most closely mimicked the size and morphological transitions observed for gradient copolymers. This may be due to the presence of a segment of poly(butyl acrylate) homopolymer in the triblock copolymers, which could be expected to significantly retard exchange between micelles.^{6,7,17}

The observed transformations of D10K seemed particularly noteworthy, as this copolymer forms spheres of varying size worms or vesicles in response to changes in pH, with evidence of reversibility at least for $\text{pH} > 5$. Such a range of structures is uncommon for any single polymer composition, and in this case the effect of varying the spatial distribution of hydrophobic and hydrophilic units is particularly apparent.

3 SANS ANALYSIS

While cryo-TEM analysis provided directly the morphology and size for each polymer structure studied at different pH, these cannot be taken as the absolute characteristics of the self-assemblies formed by the polymers. Many pictures must be taken and analyzed to ensure that they are truly representative of the sample, and thus giving good statistics of the particles.¹ A complementary technique to electronic microscopy is small angle neutron scattering (SANS). Hence, in order to have a more quantitative analysis of the self-assemblies, SANS was used, which gives good statistics of the analyzed particles ($> 10^9$ particles). A further advantage is that the analysis can be performed in solution where there is a minimal effect on the sample.

SANS analysis was carried out in buffer solutions. The polymers were directly dissolved in buffers (prepared in D_2O) at different pH.

3.1 Self-assembly analysis by small angle neutron scattering

The samples analyzed by SANS were D10K, D20K, T10K, T20K and G20K at pH 4, 5, 7 and 10. From the block copolymers only B20K was analyzed and due to its frozen behavior, the analysis was performed only at pH 4 and 10. D10K results are firstly discussed in order to exemplify how the data analysis was performed and to explain the models used to fit the SANS curves.

The results of SANS for D10K are shown in Figure 3.8, which shows the scattering intensity (integrated over all angles) as a function of the scattering wave vector, q defined in Equation 3.1:

$$q = \frac{4\pi \sin(\theta/2)}{\lambda} \quad \text{Equation 3.1}$$

Where θ and λ are the scattering angle and the wavelength, respectively.

At pH 10 and 7 a plateau at low q values is observed, indicating small quasi spherical nano-objects. For pH 5 and 4, at low q (Guinier regime), the scattering intensity $I(q)$ is proportional to q^{-1} and q^{-2} respectively and indicate the presence of large cylindrical and lamellar species.

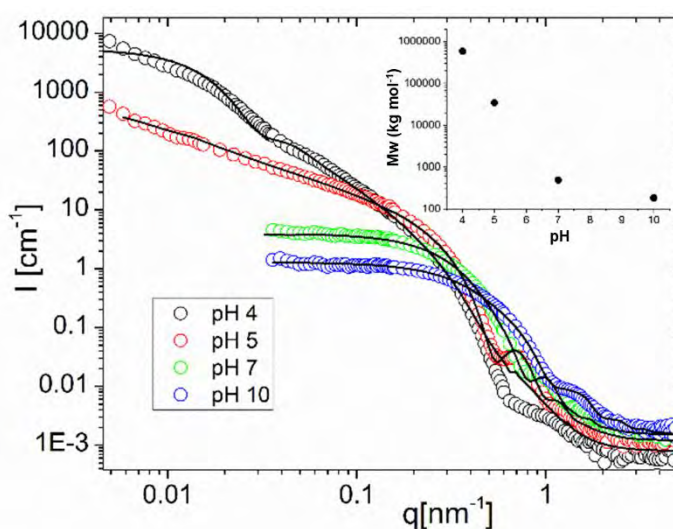


Figure 3.8. Small angle neutron scattering patterns for D10K as a function of pH for pH4, 5, 7 and 10. The black lines are the fitting curves. The shift in the scattering pattern to lower q with decreasing pH together with the increase of the forward scattering are consistent with an increase in particle size (inset), while the changing shape of the scattering patterns corresponds to a transition from slightly elongated micelles (pH 10 and 7) to long cylindrical micelles (pH 5) and vesicles (pH 4).

These qualitative observations are confirmed by fitting the data over the whole q range, which suggest that the sample comprised slightly elongated micelles at pH 10 and 7, long cylinders at pH 5, and predominantly vesicles at pH 4. The sizes of these self-assemblies are shown in Table 3.1.

Table 3. 1 Values of the characteristic sizes of the nano-objects according to fit results (D10K). R_v and d , are the radius and the bilayer thickness of the vesicles L and R_c are the length and radius of the elongated micelles, long or flexible cylinders. R_g is the radius of gyration of the single polymer chains. Also the molar mass of the aggregates is depicted.

pH	Type of self-assembly	Size (nm)		Molar mass (kg mol ⁻¹)
		R_v		
4	Vesicles		89	589 000
		d	11	
5	Long cylinders ^a	L	> 600	34 500
		R_c	7.1	
7	Elongated micelles	L	17	490
		R_c	5.1	
10	Elongated micelles	L	14	185
		R_c	3.5	
	Polymer chains	R_g	2.5	

a) A slightly improved fit could be obtained by incorporating a contribution from spheres of radius 12 nm, accounting for 6% of the total scattering intensity.

The scattering curves of D10K at pH 5, 7 and 10 were fitted using a cylindrical model according to the following relationship for the particle form factor, $P(q)$, of randomly oriented particles:

$$P(q) = \int_0^{\pi/2} F^2(q, \alpha) \sin \alpha \, d\alpha = \int_0^1 F^2(q, u) \, du \quad \text{Equation 3.2}$$

with

$$F(q) = \frac{2J_1(qR_c \sin \alpha) \sin\left(\frac{qL}{2} \cos \alpha\right)}{qR_c \sin \alpha \left(\frac{qL}{2} \cos \alpha\right)} \quad \text{Equation 3.3}$$

$J_1(x)$ represent the first order Bessel function, R_c et L are the radius and the length of the cylinder, respectively. The polydispersity of the radius and the length of the anisotropic assemblies was described with a Gaussian function.¹⁸

At pH 10 a contribution for free polymer chains had to be added to the cylinder model in order to account for the scattering intensity at high q . A model for polymer chains undergoing excluded volume interactions was used. The analytical form developed by Hammouda¹⁹ is:

$$P(q) = \frac{1}{vU^{1/2v}} \gamma\left(\frac{1}{2v}, U\right) - \frac{1}{vU^{1/v}} \gamma\left(\frac{1}{v}, U\right) \quad \text{Equation 3.4}$$

Where:

$$\gamma(x, U) = \int_0^U dt e^{-t} t^{x-1} \quad \text{Equation 3.5}$$

$$U = \frac{q^2 R_g^2 (2\nu + 1)(2\nu + 2)}{6} \quad \text{Equation 3.6}$$

R_g is the radius of gyration of the polymer and ν the excluded volume parameter (in this case $\nu = 3$).

At pH 5, the fit could be slightly improved by incorporating a contribution from spherical particles of radius 12 ± 2 nm, accounting for 6% of the total scattering intensity. A comparison of the two curves (cylinders + spheres versus cylinders only) is shown in Figure 3.9. While this indicates that the observed scattering is consistent with a mixture of cylindrical and spherical particles, the total scattering is dominated by the larger cylinders, and the parameters associated with contribution of the spherical particles should be interpreted with caution.

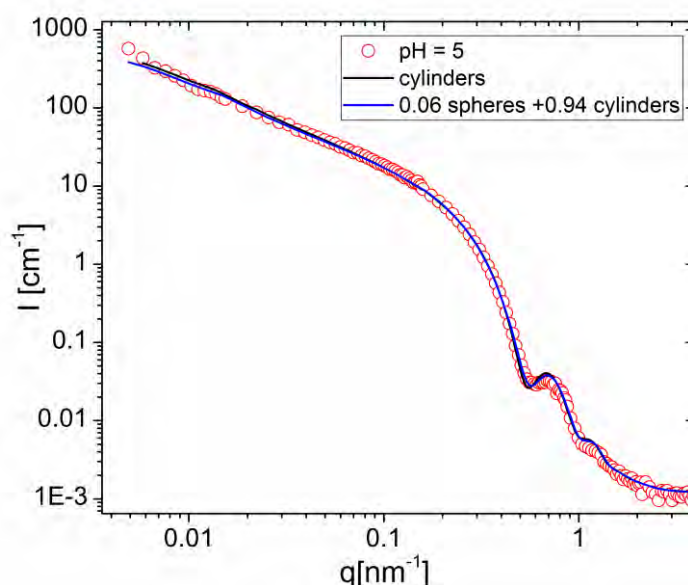


Figure 3.9. Comparison of cylinder only (black line) and cylinder + sphere (blue line) models applied to experimental neutron scattering data (open circles) from D10K at pH 5.

At pH 4, the vesicles were described as hollow spheres. A core-shell spherical model was used where the core was replaced by the solvent to account for the presence of the internal aqueous pool and the shell was the polymer bilayer:

$$F(q) = \frac{3}{V_{TOT}} \left[\frac{V_c(\rho_s - \rho_{sh})j_1(qR_c)}{qR_c} + \frac{V_{TOT}(\rho_{sh} - \rho_s)j_1(qR_{TOT})}{qR_{TOT}} \right] \quad \text{Equation 3.7}$$

V_{TOT} is the volume of the whole nano-object, V_c is the volume of the core (aqueous pool), R_c is the radius of the core (aqueous pool) and $R_{TOT} = R_c + d$ (d is the shell thickness), ρ_s and ρ_{sh} are the scattering length density of the solvent and the shell respectively. j_1 is the first order spherical Bessel function. The polydispersity of the radius and the length of the anisotropic assemblies was described with a Gaussian function.

The presence of other morphologies (worm-like micelles for example) as shown by cryo-TEM images is the reason that the model does not exactly reproduce the data. However, the main features (the bilayer size at $q \sim 0.6 \text{ nm}^{-1}$ and the overall size at $q \sim 0.25 \text{ nm}^{-1}$) of the vesicles could be described.

It is possible to evaluate the molar mass of the self-assemblies from the value of the forward scattering (at the limit as q approaches zero) using the following formula obtained from the Guinier approximation:

$$I(q = 0) = \frac{C\Delta\rho^2 M_w}{N_A d^2} \quad \text{Equation 3.8}$$

Where C is the copolymer concentration, $\Delta\rho = \rho_{polymer} - \rho_{solvent}$ with $\rho_{polymer}$ and $\rho_{solvent}$ the scattering length density of the copolymer and the solvent, respectively, d the copolymer density, N_A the Avogadro number and M_w the molar mass of the aggregates in solution. The results indicate an increase of three orders of magnitude of the molar mass of the self-assemblies going from pH 10 to pH 4 (inset in Figure 3.8).

Figure 3.10 shows the SANS curves and the respective fit lines for T10K, T20K, D20K and G20K. Also, an inset is included in each figure, which depicts the evolution of the molar mass of aggregates as a function of pH. The increase of intensity at low q values by decreasing pH, indicates that the size of the aggregates is increasing and the change on the shape of the curve is directly related with the change of the aggregate morphologies. All the polymers were fitted with a vesicle model for pH 4 and an elongated micelle model for pH 5, 7 and 10.

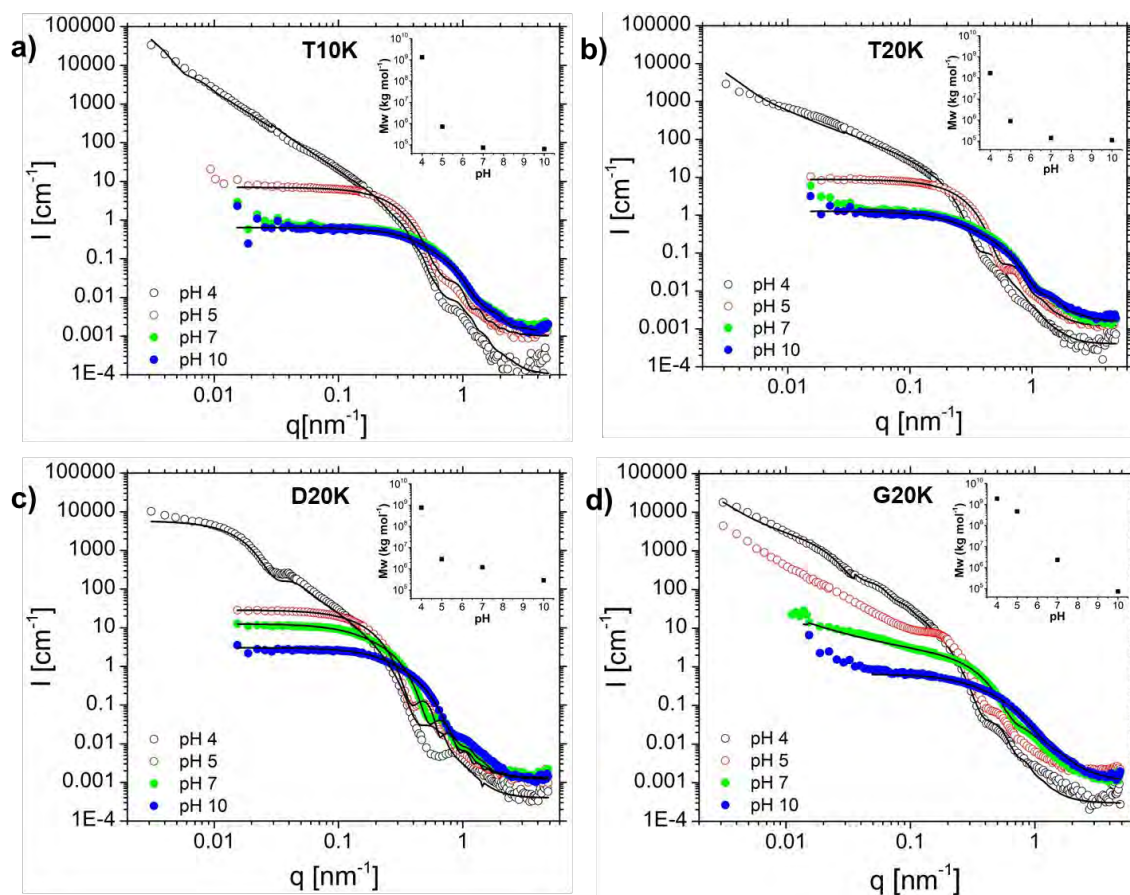


Figure 3.10. Small angle neutron scattering patterns as a function of pH for pH 4, 5, 7 and 10, for a) triblock copolymer T10K, b) triblock copolymer T20K, c) diblock copolymer D20K and d) gradient G20K. The black lines are the fitting curves. The inset in the figures show the molar mass of the aggregates as a function of pH.

Figures 3.10a and 3.10b depict the SANS curves corresponding to the T10K and T20K respectively. Both polymers behave very similarly in all pH range. The increase of intensity in the low q values for the curve at pH 4, reveals the presence of very large objects. Although T10K has a lower molar mass than T20K, T10K displays higher forward scattering than T20K, which indicates that larger objects are formed by T10K than the objects from T20K. Then the curves at pH 5, 7 and 10 for T10K and T20K exhibit a plateau at low q values (Guinier region), indicating the presence of small quasi spherical aggregates. The curves at pH 7 and pH 10 are nearly identical, revealing that the morphologies and sizes at these pHs are very similar. For both T10K and T20K, the inset reveals that the molar mass of the nano-objects decreases by three orders of magnitude as the pH increases from 4 to 7. By comparing both insets it is observed that the molar mass of the aggregates of T20K at pH 4 is effectively lower than the molar mass of the aggregates of T10K. Then the molar mass at pH 10 is roughly the same that at pH 7, which is in agreement with the overlap of the curves at these pH. The fit of the

curve at pH 4 was performed with a vesicle model. The scattering curves corresponding to pH 5, 7 and 10 were fitted using a cylindrical model adding contributions from spherical aggregates for pH 5 and polymer chains for pH 7 and pH 10.

Figure 3.10c shows the SANS curves as a function of pH for D20K. The very high intensity for the curve at pH 4 reveals the formation of large aggregates. Then, similarly to triblocks, the scattering curves at pH 5, 7 and 10 manifest a plateau in the Guinier region, attributed to the presence of quasi spherical nano-objects. The scattering curves at pH 5, 7 and 10 display similar shapes, but they differ in their forward scattering which decreases with increase of pH, indicating that smaller aggregates are formed when pH increases. The inset for D20K shows that the molar mass of the aggregates decays three orders of magnitude by going from pH 4 to pH 5. After, from pH 5 to pH 10 the molar mass slightly decreases only one order of magnitude. The evolution of molar mass with pH confirms the observations from the scattering curves. D20K was fitted with a vesicle model for pH 4 and elongated micelles with contribution of spheres for pH 5, 7 and 10.

Figure 3.10d depicts the SANS curves at different pH for G20K. As for the other polymers the high scattering intensity for the curve at pH 4 reveals that the largest objects are formed at this pH. The curve at pH 5 displays a different behavior from the other polymers at this pH. G20K was not very soluble in the pH 5 buffer, thus some precipitate was present in the sample when the measure in SANS was performed. Hence the peak at approximately 0.1 nm^{-1} is attributed to interactions between assemblies in larger aggregates. Despite the interaction peak of the curve at pH 5, it has several common features with the curve at pH 4. The curves at pH 4 and pH 5 follow the same power law within the Guinier region, indicating that at both pHs large objects of similar morphology are being formed. For the scattering curves at pH 7 and pH 10 it can be clearly seen that they do not have the plateau as in the case other polymers at the same pHs. This tendency to slightly increase in intensity at low q , is attributed to the formation of larger objects than for the triblocks or the diblock copolymers. The fit of the curve at pH 4 was performed with a vesicle model adding a contribution of elongated micelles. For the curves at pH 7 and 10 the elongated micelles model was used, adding contributions from spheres and polymer chains to improve the fit.

Table 3.2 presents a summary with the type of self-assemblies and sizes for T10K, T20K, D10K, D20K and G20K, obtained from the fitting of the SANS curves.

Table 3.2. Values of the characteristic sizes of the nano-objects according to fit results (T10K). R_v and d , are the radius and the bilayer thickness of the vesicles. L and R_c are the length and radius of the elongated micelles, long or flexible cylinders. R is the radius of spheres and R_g is the radius of gyration of the single polymer chains.

			T10K	T20K	D10K	D20K	G20K
<i>pH</i>	Type of self-assembly		Size (nm)				
4	Vesicles	R_v	> 600	400	89	87.0	72.0
		d	9.5	14.1	11	15.5	24.7
	Elongated micelles	L	----	900	----	----	> 1000
		R_c	----	10.6	----	----	10.1
5	Elongated micelles	L	16.4	15.8	> 600	29.0	ND*
		R_c	6.7	7.0	7.1	13.0	ND*
	Spheres	R	6.1	----	----	11.8	ND*
7	Elongated micelles	L	12.0	22.4	17	36.0	600
		R_c	2.6	3.4	5.1	8.2	5.0
	Spheres	R	----	----	----	8.2	6.4
	Polymer chains	R_g	1.5	4.8	----	----	3.0
10	Elongated micelles	L	12	24.1	14.0	20	17.3
		R_c	2.6	3.4	3.50	5.2	3.0
	Spheres	R	----	----	----	4.5	----
	Polymer chains	R_g	1.5	4.8	2.5	----	3.8

*The fit for G20K at pH 5 is not defined.

At pH 4 T10K and T20K self-assembled into vesicles, including elongated micelles for T20K. The objects generated from T10K are larger than those of T20K. At pH 5 elongated micelles are formed for both triblock copolymers, with spherical micelles for the T10K. At pH 7 and pH 10 the sizes of the self-assemblies for both T10K and T20K, are very similar, as expected from the observations of the scattering curves. It was not necessary to add contributions from spheres to the fits of triblocks for pH 7 and 10, despite the shape of the curves (Figures 3.10a and 3.10b) and the cryo-TEM images (Figure 3.6d) that indicated the formation of quasi spherical objects. It can be noted that these elongated micelles at pH 7 and 10 are not very long thus the aspect ratio (2:1) is close to a spherical morphology. Hence in this way the fit of the scattering curve of T10K and T20K at high pH did confirm the presence of quasi spherical objects. At pH 4, D10K and D20K both self-assemble into vesicles, which are smaller than those vesicles formed by the triblocks. At pH 5, 7 and 10, D10K tends to form only elongated micelles, unlike D20K which in addition to elongated micelles, also forms spheres. Finally, vesicles and very large elongated micelles are formed by G20K at pH 4. Although the fit for the curve at

pH 5 was not determined, from the similarities with the curve at pH 4, it could be assumed that also very long elongated micelles are formed at pH 5. It might be possible that these elongated micelles are sufficiently large to interact with each other, which is the probable cause of the interaction peak ($0.1 - 0.3 \text{ nm}^{-1}$) in the curve at pH 5. Then at pH 7 there is a mixture of elongated micelles, spheres and polymer chains. Interestingly the elongated micelles are much longer (600 nm) than those obtained at pH 7 for the other structures ($\sim 10\text{-}40 \text{ nm}$). Finally, at pH 10 only elongated micelles and polymer chains are produced and the size of elongated micelles are in agreement with the elongated micelles for the other polymers.

Although, the model of elongated micelles was used to perform the fitting of all the curves at $\text{pH} > 4$, in most of the cases these micelles were not very long, displaying rather a rice grain-like morphology. Only in the cases of D20K and G20K, very long elongated micelles were produced at pH 5.

It is interesting to compare the different asymmetric copolymers: the diblocks D10K and D20K, triblocks T10K and T20K and G20K. The diblock copolymers D10K and D20K, like G20K, show a definite increase in size as the pH changes from 10 to 7, while the triblock copolymers T10K and T20K form practically identical assemblies at pH 10 and pH 7. On the other hand, the diblock copolymers form relatively small vesicles at pH 4, with radii of approximately 90 nm, while the triblock and gradient copolymers at pH 4 form much larger structures, either wormlike micelles or vesicles with dimensions of $> 600 \text{ nm}$.

At high pH, the similarity between asymmetric diblock and gradient copolymers might be attributed to their broadly similar composition profile, with the presence of hydrophilic acrylic acid units within the hydrophobic segment allowing a dynamic exchange between micelles that enables the micelles to change size in response to changing pH. By contrast, the triblock copolymers contain short segments of poly(butyl acrylate) homopolymer, which may freeze the polymer chains within the micelles and hinder their pH response.

At pH 4, it is likely that all the polymer chains are frozen as the acrylic acid units are nearly fully protonated. Under these conditions, the structures formed by the triblock copolymers are closer to those formed by the gradient copolymers as the overall composition profile of the triblock copolymers is closer to that of the gradient copolymers. Hence, the self-assembly properties of triblock copolymers seem to be in between the block copolymers, because of the frozen state at high pH, and gradient copolymers, because of the formation of long elongated micelles.

As the self-assemblies formed by the block copolymers B10K and B20K were unresponsive to changes in pH, only a limited SANS analysis was carried out on B20K. Figure 3.11 shows the SANS curves corresponding to B20K at the two extreme pH values investigated (pH 4 and 10). At both pH values a power-law behavior, $I(q) \propto q^{-x}$ with $x = 2.9$ and 2.5 for pH value 10 and 4 respectively, is observed indicating the presence of fractal clusters whose size exceed the one accessible in our experiment (size larger than $1 \mu\text{m}$). The lower size measured through DLS experiments is due to the fact that they were conducted on filtered solution, so the obtained values are those of the bigger clusters which passed through filters (400 nm).

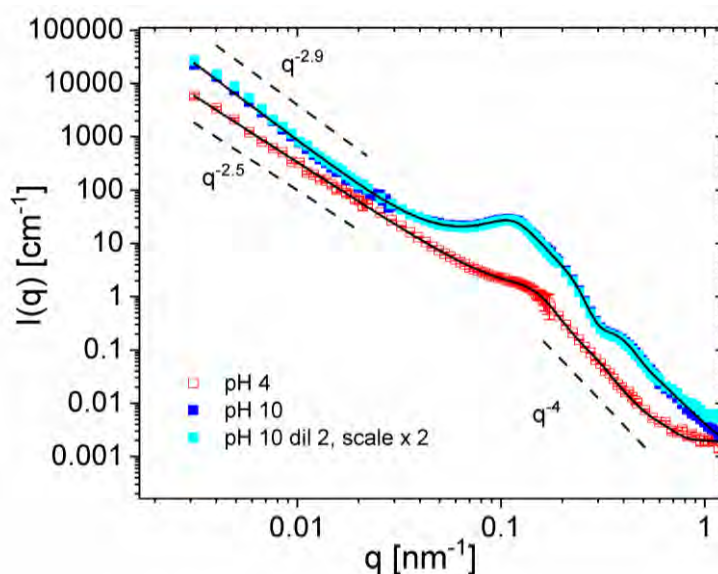


Figure 3.11. Small angle neutron scattering patterns for B20K at pH 4 and 10. The black lines are the fitting curves.

A peak is visible at intermediate q values, more pronounced in the case of pH 10. This is expected as the correlation peak must be due to electrostatic interactions and the polymer is almost neutral at pH 4.

Both curves could be described as polydisperse spheres densely packed in fractal aggregates.²⁰ To emulate the effect of electrostatic interactions, a hard sphere model was used, allowing the excluded radius to be larger than the particle radius, adding a transparent shell of constant thickness^{21–23}.

$$I(q) = I_{pHS}(q) \cdot S_f(q)$$

Equation 3.9

A simple structure factor for fractals has been used

$$S_f(q) = 1 + aq^{-b}$$

Equation 3.10

The exponent b is close to the fractal dimension D_f of the aggregates. The values for the fits are reported in Table 3.3 and are in good agreement with the cryo-TEM images (Figure 3.6a and Figure 3.7). Interestingly, dilution at pH 10 has no effect on the structure of the clusters, it just has the effect to dilute them (as the overall scattering intensity decreases proportionally to the concentration). Macroscopic phase separation occurs at pH 4, meaning that the scattering spectra are representative of the polymer left in solution.

Table 3. 3. Values of the fit parameters of the nano-objects formed for B20K at pH value 4 and 10. b is the power-law exponent; R_c and $(R_c + R_s)$ are the spherical micelles radius and the center to center distance between adjacent micelles in the clusters; ϕ is the volume fraction inside the clusters.

	pH 10	pH 4
B	2.87	2.47
R_c (nm)	13.8±2.5	7.7±1.8
R_s (nm)	10.9	11.2
ϕ	0.04	0.016

4 CONCLUSIONS

Les études réalisées par DLS en dissolvant directement les polymères dans des solutions tampons, ont révélé que les agrégats de copolymères séquencés restent constants ou figés dans toute la gamme de pH. Ensuite, les agrégats des copolymères à diblocs ont subi une légère augmentation de taille en diminuant le pH, et à pH 4, de plus grands agrégats se sont formés. Les agrégats de copolymères à triblocs sont restés assez constants presque dans toute la gamme de pH (ce qui indique un état figé à pH élevé), sauf à pH 4 où des agrégats plus gros se sont à nouveau formés. Les copolymères à gradient ont présenté quant à eux un changement plus continu avec la variation de pH, ce changement étant plus significatif pour G20K que pour G10K. Enfin, comme pour les autres structures asymétriques, à pH 4, des agrégats plus gros sont apparus. Ainsi, les copolymères à blocs ne sont pas affectés par le changement de pH et les copolymères à gradient et les copolymères à blocs asymétriques, se sont révélés plus dépendants du changement de pH et l'ordre de cette dépendance est le suivant: gradient > dibloc > tribloc. Les résultats du titrage ont révélé la réversibilité du processus de micellisation et les D_h sont en accord avec les résultats obtenus par l'analyse des solutions tamponnées. Il est intéressant de noter que les résultats de la distribution de taille obtenus à partir du titrage en augmentant le pH, ont montré des caractéristiques plus communes avec le polymère directement dissous dans les solutions tampons, que lorsque le titrage est effectué en diminuant le pH.

À partir d'expériences de cryo-TEM, des micelles sphériques de même taille dans toute la gamme de pH ont été observées pour les copolymères à blocs, ce qui est conforme aux résultats de DLS. Pour les structures à gradient et diblocs asymétriques, différentes morphologies ont été obtenues à différents pH. À pH 4, les diblocs asymétriques ont formé des vésicules et dans le cas du gradient, un mélange de vésicules et de micelles vermiculaires a été obtenu. Ensuite, à un pH plus élevé, des sphères ont été observées pour G20K et T10K et un mélange de sphères et de micelles vermiculaires a été observé pour D10K.

Enfin, avec l'analyse SANS, la dépendance de l'auto-assemblage au pH a également été étudiée. Premièrement, l'augmentation de l'intensité aux faibles valeurs de q en diminuant le pH a été une indication de l'augmentation de la taille des agrégats. Le changement de forme des courbes de diffusion indique également un changement de morphologie. La comparaison qualitative des courbes et des paramètres obtenus en ajustant ces courbes a permis de retrouver des caractéristiques similaires entre les auto-assemblages de copolymères à blocs, à gradient et asymétriques. Par exemple, les deux

copolymères à diblocs asymétriques changent continuellement de taille et de forme tout au long de la gamme de pH, comme dans le cas du copolymère à gradient, ce qui indique que les deux structures ont une réponse dynamique au pH. Cela pourrait être dû à leurs structures similaires, dans lesquelles les unités d'AA sont mélangées avec les unités de *n*BA, et que ni le gradient ni le dibloc ne contiennent une section de *Pn*BA pur. Ensuite, les structures triblocs et à gradient partagent la caractéristique commune que les deux ont tendance à s'auto-assembler en très grandes micelles vermiculaires, ce qui pourrait s'expliquer par leur profil de composition similaire. En revanche, les copolymères à triblocs ne sont pas affectés par les changements de pH à pH élevé, ce qui pourrait être attribué au bloc de *Pn*BA pur dans leur structure. Ainsi les auto-assemblages triblocs partagent les caractéristiques d'un copolymère à gradient et d'un copolymère à bloc.

Les trois techniques ont révélé que les copolymères à diblocs et à triblocs asymétrique et à gradient ont tendance à s'auto-assembler en gros agrégats à pH 4 et aussi elles montrent la diminution de la taille des agrégats au-dessus de pH 4. Ainsi, les résultats de DLS, cryo-TEM et SANS sont cohérents car ils mettent effectivement en évidence la variation du profil de composition avec l'auto-assemblage.

4 CONCLUSIONS

The DLS studies by directly dissolving the polymers in buffer solutions, revealed that the block copolymer aggregates remain constant or frozen in all pH range. Then the aggregates from the diblock copolymers experienced a slight increase of size by decreasing pH and at pH 4 larger aggregates were formed. The aggregates of triblock copolymers remained fairly constant almost in all pH range (which indicates a frozen state at high pH), except at pH 4 in which larger aggregates were formed. Gradient copolymers displayed a more continuous change with change on pH, being more significant for G20K than for G10K. Finally, as for the other asymmetric structures, at pH 4 larger aggregates appeared. Thus, block copolymers remained unaffected by the change of pH, and gradient and asymmetric blocks were more dependent on the change of pH and the order of this dependency is as follows: gradient > diblock > triblock. The titration results revealed the reversibility of the micellization process and the D_h are in agreement with the results obtained by the analysis of buffered solutions. Interestingly the results of size distribution obtained from the titration by increasing the pH, showed more common features with the directly dissolved polymer in the buffer solutions, than when the titration is made by decreasing the pH.

From cryo-TEM experiments, spherical micelles of the same size through all the pH range were observed for block copolymers, which is in accordance with the results from DLS. For the gradient and asymmetric copolymers, it was observed that different morphologies were obtained at the different pH. At pH 4 the asymmetric blocks formed vesicles and in the case of the gradient there was a mixture of vesicles en wormlike micelles. Then at higher pH, spheres were observed for G20K and T10K and mixture of spheres and wormlike micelles were observed for D10K.

Finally, with the SANS analysis, the self-assembly dependence on pH was also studied. First, the increase of intensity at the low q values by decreasing pH was an indication of the increase in size of aggregates and the change in shape of the scattering curves indicates a change in morphology. The qualitative comparison of the curves and the parameters obtained by fitting these curves allowed to find similar characteristics between the self-assemblies of gradient and asymmetric block copolymers. For instance, both diblock copolymers continuously change in size and shape in all pH range, as in the case of the gradient copolymer, which indicates that both structures have a dynamic response to pH. This could be due to their similar structures, in which the units of AA are mixed with the units of *n*BA, and that neither the gradient nor the diblock contain a section of pure *Pn*BA. Then triblock and gradient structures share the common feature that both

tend to self-assemble into very large wormlike micelles, which could be due to their similar composition profile. By contrast, triblock copolymers remained unaffected by changes in pH at high pH, which might be attributed to the block of pure *Pn*BA within their structure. Thus, the triblock self-assemblies share characteristics of a gradient copolymer and of a block copolymer.

The three techniques revealed that the diblocks, triblocks and gradient polymers tend to self-assemble into large aggregates at pH 4 and then the decrease of the size of the aggregates above pH 4. Hence, altogether the results from DLS, cryo-TEM and SANS are consistent as they picture the changing composition profile with self-assembly.

5 MATERIALS AND METHODS

The synthesis and characterization methods of block, asymmetric diblock, asymmetric triblock and gradient copolymers are presented in the section of materials and methods of chapter 3.

5.1 Dynamic Light Scattering (DLS)

Hydrodynamic diameters (D_h) and size distributions were determined by DLS on a MALVERN Zetasizer Nano ZS operating at 20 °C with a 633 nm laser module. Measurements were made at a detection angle of 173° (back scattering). Measurements were repeated three times with automatic attenuation selection and measurement position. The average result of these three measurements was used for the manuscript. The results were analyzed using Malvern DTS 6.20 software, using the multiple narrow modes setting. Size distributions were obtained using the CONTIN algorithm. The Z-average diameter (D_h) and the width of the distribution as the polydispersity index of the particles (PDI) were obtained by the cumulants method assuming a spherical shape of the particles.

5.1.1 DLS study of polymer solutions prepared by direct dissolution in buffers

A 0.2 wt. % solution of the polymers was prepared by dispersing each polymer sample in pH buffers (0.1 M pH 10, 8, 7, 6, 5, and 4). The pH 10 buffer (0.1 M) was made using Na_2CO_3 and NaHCO_3 . The pH 8, 7, and 6 buffers (0.1 M) were made using NaH_2PO_4 and Na_2HPO_4 . The pH 5 and 4 buffers (0.1 M) were made using sodium acetate and acetic acid. As the polymers could not be dissolved in pH 4 buffer at room temperature, the dispersions at pH4 were prepared by heating to 100 or 120 °C using a microwave reactor. The polymer solutions were filtered through a Nylon 66 membrane with 0.45 μm pore size before being analyzed by DLS.

5.1.2 DLS pH Titration Study

Solutions containing 0.2% weight of each polymer were prepared by dissolving them into a 0.1 M NaOH aqueous solution separately. The polymer solutions were filtered through a Nylon 66 membrane with 0.45 μm pore size before the titration study and were not filtered during the titration study. Each polymer solution was first titrated with an HCl solution (6 M and 1M) to lower the pH until the solution became cloudy. The same solution was then titrated with a NaOH solution (1 M and 0.1 M) to increase the pH value. As the HCl or NaOH solution concentrations were relatively high, only a small amount of

HCl or NaOH solution was needed to change the pH value. Therefore, the concentration of the polymer stayed relatively constant during the titration. The hydrodynamic diameters (D_h) and size distributions were determined using DLS as demonstrated above

5.2 Cryogenic Transmission Electron Microscopy (Cryo-TEM)

The polymer solutions (2 mg mL^{-1}) obtained by direct dispersion into buffers were used for Cryo-TEM imaging directly. The measurements were performed on an FEI Tecnai G2 20 platform with a LaB6 filament at 200 kV acceleration voltage. Samples were prepared on Quantifoil grids (R2/2) which were treated with Ar plasma prior to use for hydrophilization and cleaning. $8.5 \text{ }\mu\text{L}$ of the solutions (2 mg mL^{-1}) was applied onto the grids utilizing an FEI Vitrobot Mark IV system (offset: -5 mm , blotting time: 1 s). After blotting, the samples were immediately plunged into liquid ethane to obtain vitrification. Samples were transferred to a Gatan cryo stage and subsequently into a Gatan cryo holder (Gatan 626) and were transferred into the microscope by always maintaining a temperature below $-168 \text{ }^\circ\text{C}$ during the whole transfer and measurement process after vitrification. Images were acquired with a Mega View (OSIS, Olympus Soft Imaging Systems) or an Eagle 4k CCD camera.

Due to the amount of effort required for the Cryo-TEM measurements and the large number of samples, only selected samples were imaged by Cryo-TEM. Based on the DLS results, B20K, G20K, D10K, and T10K were selected for the Cryo-TEM.

5.3 Small-Angle Neutron Scattering

Small-angle neutron scattering (SANS) was performed at the D11 beamline of the Institut Laue-Langevin (ILL) in Grenoble, France. The SANS patterns were collected using a 2D detector then integrated to obtain the scattering intensity as a function of scattering vector $q = 4\pi \sin(\theta/2)/\lambda$, where θ is the angle between the incident beam and the detector and λ is the neutron wavelength. The measured SANS profiles were normalized to an absolute scale using H_2O as a secondary standard. A combination of four configurations with three different sample-to-detector distances 1.4 m , 8 m and 39 m and two wavelengths ($\lambda = 5 \text{ \AA}$ and 20 \AA , FWHM 9%) was employed, covering a total q -range from $5 \cdot 10^{-3}$ and 5 nm^{-1} . The solutions (all in D_2O) were loaded in 2 mm quartz cells. The background sample (D_2O) was subtracted from the experimental data. Sample concentration was 2 mg mL^{-1} .

The software package BerSANS²⁴ was used to integrate and merge the data acquired at all configurations and subtract the background. In this way the absolute scattering intensity $d\sigma(q)/d\Omega$ is obtained (equation 10):

$$\frac{d\sigma(q)}{d\Omega} = n\Delta\rho^2V^2P(q) \quad \text{Equation 3.11}$$

Where n is the particle number density, $\Delta\rho$ the difference between the scattering length density of the self-assemblies and the solvent, V the volume of the nano-objects. $P(q)$ is the particle form factor.

LITERATURE

- 1 J. P. Patterson, M. P. Robin, C. Chassenieux, O. Colombani and R. K. O'Reilly, *Chem. Soc. Rev.*, 2014, **43**, 2412–2425.
- 2 S. Han, E. Nicol, F. Niepceron, O. Colombani, S. Pensec and L. Bouteiller, *Macromol. Rapid Commun.*, 2019, **40**, 1800698.
- 3 C. Charbonneau, M. M. De Souza Lima, C. Chassenieux, O. Colombani and T. Nicolai, *Phys. Chem. Chem. Phys.*, 2013, **15**, 3955–3964.
- 4 C. Lefay, B. Charleux, M. Save, C. Chassenieux, O. Guerret and S. Magnet, *Polymer (Guildf.)*, 2006, **47**, 1935–1945.
- 5 E. Lejeune, C. Chassenieux and O. Colombani, *Prog. Colloid Polym. Sci.*, 2010, **138**, 7–16.
- 6 O. Colombani, M. Ruppel, M. Burkhardt, M. Drechsler, M. Schumacher, M. Gradzielski, R. Schweins and A. H. E. Müller, *Macromolecules*, 2007, **40**, 4351–4362.
- 7 M. Jacquin, P. Muller, R. Talingting-Pabalan, H. Cottet, J. F. Berret, T. Fütterer and O. Théodoly, *J. Colloid Interface Sci.*, 2007, **316**, 897–911.
- 8 B. K. Johnson and R. K. Prud'homme, *Phys. Rev. Lett.*, 2003, **91**, 118302.
- 9 C. Charbonneau, C. Chassenieux, O. Colombani and T. Nicolai, *Macromolecules*, 2011, **44**, 4487–4495.
- 10 A. Shedge, O. Colombani, T. Nicolai and C. Chassenieux, *Macromolecules*, 2014, **47**, 2439–2444.
- 11 R. Whitfield, N. P. Truong, D. Messmer, K. Parkatzidis, M. Rolland and A. Anastasaki, *Chem. Sci.*, 2019, **10**, 8724–8734.
- 12 J. Listak, W. Jakubowski, L. Mueller, A. Plichta, K. Matyjaszewski and M. R. Bockstaller, *Macromolecules*, 2008, **41**, 5919–5927.
- 13 J. M. Widin, A. K. Schmitt, A. L. Schmitt, K. Im and M. K. Mahanthappa, *J. Am. Chem. Soc.*, 2012, **134**, 3834–3844.
- 14 D. T. Gentekos and B. P. Fors, *ACS Macro Lett.*, 2018, **7**, 677–682.
- 15 S. I. Rosenbloom and B. P. Fors, *Macromolecules*, 2020, [acs.macromol.0c00954](https://doi.org/10.1021/acs.macromol.0c00954).
- 16 E. Eghbali, O. Colombani, M. Drechsler, A. H. E. Müller and H. Hoffmann, *Langmuir*, 2006, **22**, 4766–4776.
- 17 O. Colombani, M. Ruppel, F. Schubert, H. Zettl, D. V. Pergushov and A. H. E. Müller, *Macromolecules*, 2007, **40**, 4338–4350.
- 18 J. S. Pedersen, *Adv. Colloid Interface Sci.*, 1997, **70**, 171–210.
- 19 B. Hammouda and M. H. Kim, *J. Mol. Liq.*, 2017, **247**, 434–440.
- 20 M. Muthig, S. Prévost, R. Orglmeister and M. Gradzielski, *J. Appl. Crystallogr.*, 2013, **46**, 1187–1195.
- 21 W. L. Griffith, R. Triolo and A. L. Compere, *Phys. Rev. A*, 1987, **35**, 2200–2206.
- 22 L. Blum and G. Stell, *J. Chem. Phys.*, 1979, **71**, 42–46.
- 23 L. Blum and G. Stell, *J. Chem. Phys.*, 1980, **72**, 2212.
- 24 U. Keiderling, *Appl. Phys. A Mater. Sci. Process.*, 2002, **74**, s1455–s1457.

**CHAPTER 4. P(DMA-NIPAM)
COPOLYMERS: A
THERMORESPONSIVE
SYSTEM**

CHAPITRE 4. COPOLYMÈRES DE P(DMA-NIPAM) : UN SYSTÈME SENSIBLE À LA TEMPÉRATURE

Alors que les chapitres précédents traitaient de l'effet du profil de composition sur un système sensible au pH, à savoir les copolymères d'acide acrylique et d'acrylate de butyle, dans ce chapitre un système sensible à la température sera examiné. Les copolymères étudiés dans ce chapitre sont composés de diméthylacrylamide (DMA) et de *N*-isopropylacrylamide (NIPAM) et la fraction molaire ciblée de chaque monomère est de 0,50. Le PNIPAM et le PDMA sont des polymères hydrophiles à température ambiante, mais le PNIPAM devient hydrophobe au-dessus de 32 °C¹.

Ce phénomène est dû au fait que les PNIPAM possèdent des groupements hydrophiles et hydrophobes. Lorsque la température de la solution est inférieure à la LCST, les groupes hydrophiles sont solvatés et les chaînes polymères existent sous forme de pelote. Au contraire, si la température est supérieure à la LCST, des agrégats de polymère commencent à apparaître². Les polymères NIPAM purs ne présentent pas de changements sur la LCST en modifiant la masse molaire du polymère.

La LCST des copolymères thermosensibles peut être modifiée par incorporation de groupes terminaux ou comonomères hydrophiles ou hydrophobes. Des structures de copolymères différentes induisent également des différences par rapport à la LCST. Lorsqu'un polymère avec une LCST est copolymérisé avec un polymère hydrophile, sa LCST augmente. La littérature comporte des études dans lesquelles le NIPAM a été copolymérisé avec le monomère hydrophile diméthylacrylamide (DMA) et l'augmentation de la teneur en DMA augmente la LCST. Par exemple, les copolymères contenant 20% et 50% de DMA ont affiché des LCST de 39 °C et 63 °C respectivement.³ La teneur en DMA a été augmentée jusqu'à un point où la fraction de NIPAM (~ 20%) était insuffisante dans le copolymère pour que celui-ci présente des propriétés de LCST^{3,4}. Au contraire, l'incorporation de monomères hydrophobes tend à diminuer la LCST. Lorsque le PNIPAM est prolongé avec des monomères hydrophiles tels que le diméthylacrylamide⁵ ou l'acide acrylique⁶, formant ainsi des copolymères à blocs double-hydrophiles sensibles à la température, la micellisation se produit à des températures supérieures à la LCST du copolymère.

Comme pour le système P(AA-*n*BA), les copolymères P(DMA-NIPAM) étudiés dans ce chapitre partagent la même composition globale, mais diffèrent dans la répartition des monomères le long de la chaîne. Copolymères à blocs, à dibloc asymétrique, à tribloc

asymétrique et copolymères statistiques de DMA et NIPAM (Figure 4.1) de composition globale constante, ont été synthétisés en utilisant des polymérisations radicalaires contrôlées séquentielles ou semi-discontinues. Leur comportement d'auto-assemblage en solution aqueuse a été analysé en fonction de la température par spectroscopies DLS, SANS et RMN. Ces trois techniques ont été sélectionnées pour fournir des informations à plusieurs échelles de la matière. En effet, la DLS fournit des informations sur la taille moyenne des particules et la distribution de la taille des particules, la SANS sur la morphologie des particules et la structure interne, et la RMN au niveau des monomères individuels.

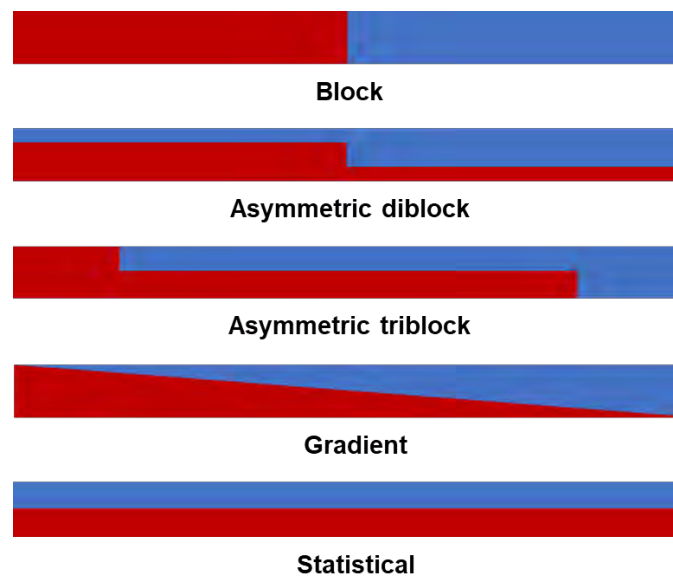


Figure 4.1. Différentes structures pour les copolymères P(DMA-NIPAM).

Sur la base des recherches précédentes sur les copolymères P(DMA-NIPAM), et considérant que les blocs constitutifs présentent un comportement indépendant, certaines hypothèses peuvent être faites. Pour le polymère à bloc, on s'attend à ce que le bloc PNIPAM s'effondre au-dessus de 32 °C. Dans le cas du dibloc asymétrique, car il est composé de deux blocs de copolymères statistiques, le premier bloc à 16% de NIPAM ne présenterait aucune transition tandis que le bloc à 84% de NIPAM présenterait une transition à ~ 39 °C. Pour le copolymère tribloc asymétrique, il y aurait deux transitions à 32 °C et ~ 63 °C, correspondant respectivement à l'homopolymère séquencé de NIPAM et au bloc statistique avec 50% de NIPAM.

Le but de ce chapitre est d'étudier l'influence des blocs voisins au sein de chaque structure sur la transition de température, puisque les polymères étudiés ont des distributions de monomères différentes le long de la chaîne

CHAPTER 4. P(DMA-NIPAM) COPOLYMERS: A THERMORESPONSIVE SYSTEM

While the previous chapters dealt with the effect of composition profile on a pH-responsive system, namely copolymers of acrylic acid and butyl acrylate, in this chapter a temperature responsive system will be examined. The copolymers studied in this chapter are composed of dimethyl acrylamide (DMA) and *N*-isopropylacrylamide (NIPAM) and the targeted molar fraction of each monomer is 0.50. PNIPAM and PDMA are hydrophilic polymers at room temperature, but PNIPAM becomes hydrophobic above 32 °C¹.

This phenomenon is due to the fact that PNIPAM possess hydrophilic and hydrophobic moieties. When the solution temperature is low, hydrophilic groups are solvated and polymer chains exist as coils. On the other hand, if the temperature is higher than the LCST, polymer aggregates start to appear². Pure PNIPAM polymers do not exhibit changes on the LCST by modifying the molar mass of the polymer.

The LCST of thermoresponsive copolymers can be modified by incorporation of hydrophilic or hydrophobic end groups or comonomers. Also different copolymer structures provoke differences over the LCST. When a polymer with an LCST is copolymerized with a hydrophilic polymer, its LCST will increase. There have been studies in which NIPAM has been copolymerized with hydrophilic monomer dimethylacrylamide (DMA) and the increase of DMA content rises the LCST. For instance, copolymers with 20% and 50% of DMA, displayed LCSTs of 39 °C and 63 °C respectively.³ DMA content was increased until a point where the fraction of NIPAM (~20%) was insufficient to trigger the copolymer LCST.^{3,4} On the contrary the incorporation of hydrophobic monomers will decrease the LCST. When PNIPAM is chain extended with hydrophilic monomers such as dimethyl acrylamide⁵ or acrylic acid,⁶ forming temperature responsive double hydrophilic block copolymers, micellization occurs at temperatures above the LCST of the copolymer.

As for the P(AA-*n*BA) system, the P(DMA-NIPAM) copolymers studied in this chapter share the same overall composition, but differ in the distribution of monomers along the chain. Block, asymmetric diblock, asymmetric triblock and statistical copolymers of DMA and NIPAM (Figure 4.1) of constant overall composition were synthesized using sequential or semi-batch controlled radical polymerizations. Their self-assembly behavior in aqueous solution was analyzed as a function of temperature using DLS,

SANS and NMR spectroscopy. These three techniques were selected to provide information on a range of length scales, as DLS provides information about the average particle size and particle size distribution, SANS about the particle morphology and internal structure, and NMR at the level of individual monomers.

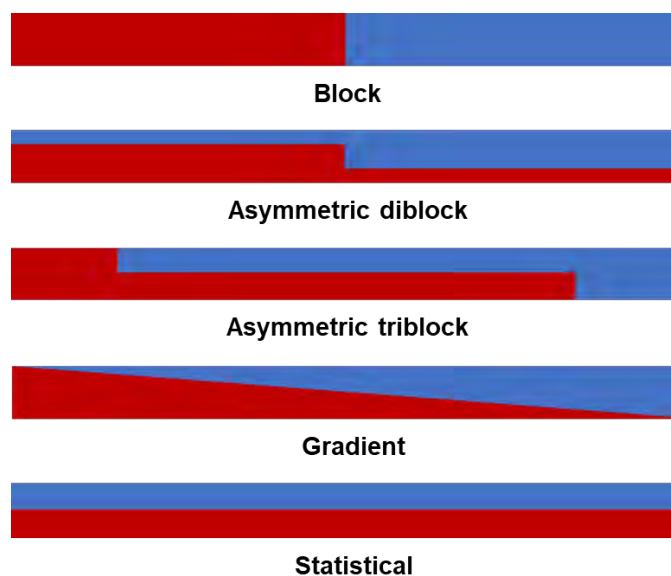


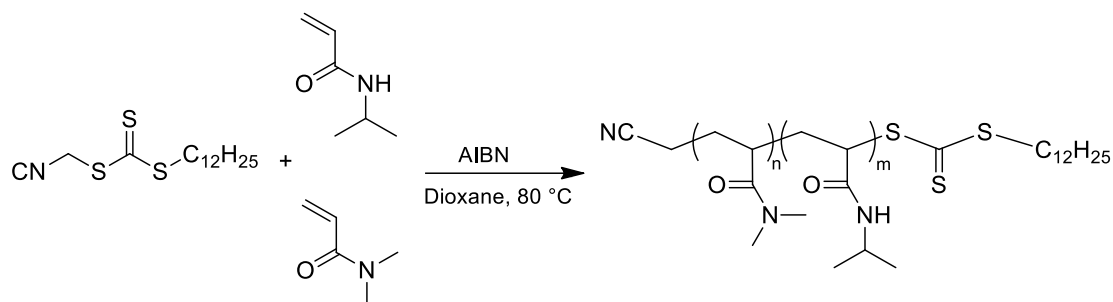
Figure 4.1. Different structures for P(DMA-NIPAM) copolymers.

Based on previous investigations on P(DMA-NIPAM) copolymers, and considering that the constituent blocks would display an independent behavior, some hypothesis can be made. For the block polymer it is expected that the PNIPAM block collapses above 32 °C. In the case of the asymmetric diblock, as it is composed by two blocks of statistical copolymers, the first block with a content of 16% NIPAM would not exhibit any transition while the block with 84% NIPAM would present a transition at ~39 °C. For the asymmetric triblock copolymer there would be two transitions at 32 °C and ~63 °C, corresponding to the block homopolymer of NIPAM and to the statistical block with 50% NIPAM, respectively.

The aim of this chapter is to investigate the influence of the neighboring blocks within each structure on the temperature transition, since the polymers under study have different monomer distributions along the chain.

1 SYNTHESIS OF POLY(DMA_{50%}-GRAD-NIPAM_{50%}) COPOLYMERS

For the synthesis of P(DMA-NIPAM) gradient copolymers the procedure of P(AA-*n*BA) gradient copolymers was taken as a base. The general reaction scheme for the synthesis is presented in scheme 4.1:



Scheme 4.1. Synthesis of poly(dimethylacrylamide—*N*-isopropylacrylamide) (P(DMA-NIPAM)) gradient copolymer via RAFT polymerization mediated by cyanomethyl dodecyl trithiocarbonate at 80 °C.

A diagram showing a set up for the synthesis of gradient copolymers is depicted in Figure 4.2. The stock solution with RAFT agent and initiator was poured into the reactor, then this was placed into a pre-heated oil bath. After, monomer charged syringes installed on the addition pumps, were connected with needles to the reactor sealed with a rubber septum. Immediately after DMA solution was added in a single shot and later the addition of DMA and NIPAM solution with gradient profile was started and allowed to proceed during 6h. At the end of this time, only NIPAM solution was constantly added during 1.5 h.

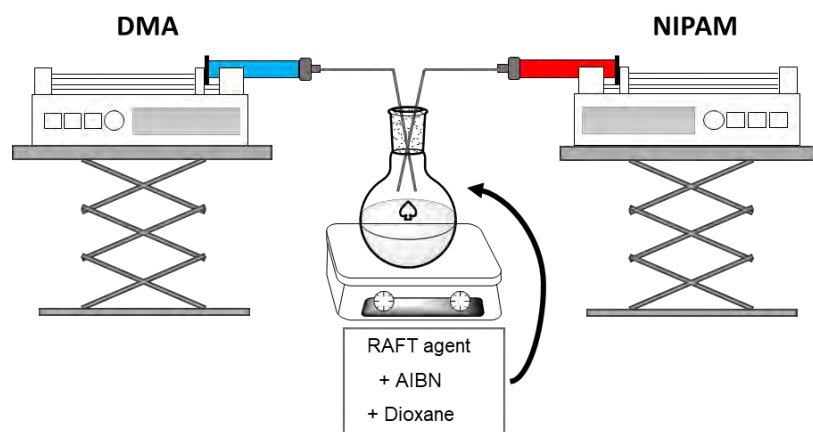


Figure 4.2. Diagram of the set up used for the synthesis of gradient copolymers.

Table 4.1 depicts representative experiments of DMA and NIPAM gradient polymerizations. The first attempts to synthesize the gradient copolymer were made with NIPAM and DMA separately with the aim to know how each monomer would behave. A first formulation was prepared with NIPAM (BF34), at 70 °C during 7.5 h. This polymerization presented an inhibition period of 4.5 h. Inhibition or retardation periods are undesirable as in a forced polymerization the composition and the structure of the

copolymer strongly depend on the adequate evolution of conversion with time. Increasing the concentration while keeping other conditions constant (BF36) led to a decrease in the inhibition period to 1 h and a final conversion of 84% after 7.5 hours of reaction (Table 4.1). For the following experiment (BF38) temperature was increased in order to increase the rate of polymerization. Unexpectedly the final conversion was lower than for BF36. However, the inhibition period was less than 1 h and the molar mass was in agreement with the expected value. Later, a similar approach was used with DMA (BF41) and its polymerization proceeded without an induction period. Although the molar mass was lower than expected, the dispersity was relatively low. The relatively low conversions obtained at 80 °C may be due to the consumption of AIBN in the early stages of polymerization. At 80 °C, the half-life (the time required to reduce the initial concentration of an initiator by 50%) of AIBN is equal to 1h. Thus, for instance within a period of 4h. With this in mind, in subsequent experiments only 20% of the total AIBN was initially present in the reactor, with the remainder added during the course of the reaction as part of the monomer solution.

Table 4.1 Details of NIPAM and DMA polymerizations with the procedure for gradient copolymers.

Exp.	T (°C)	DMA/NIPAM (mmol L ⁻¹)	AIBN (mmol L ⁻¹)	CTA (mmol L ⁻¹)	t (h)	Conv. ^a (%)	M _{n,theo} ^b (g mol ⁻¹)	M _n ^c (g mol ⁻¹)	Đ ^c
BF34	70	0/2000	2.33	23.3	7.5	70	7.20	6.5 ^d	ND
BF36	70	0/2000	3.50	23.3	7.5	84	8.5	12.0	1.11
BF38	80	0/2000	3.50	23.3	7.5	66	6.8	10.1	1.39
BF41	80	2000/0	3.40	22.7	7.5	70	6.4	7.4	1.20

a) Determined from ¹H NMR, b) Determined from $M_n = ([M]_0 \cdot \rho \cdot M_M) / [CTA]_0 + M_{CTA}$, where $[M]_0$ is the initial concentration of the monomer, ρ is the conversion of the monomer, M_M is the molar mass of the monomer, $[CTA]_0$ is the initial concentration of the RAFT agent and M_{CTA} is the molar mass of the RAFT agent c) Determined by SEC in DMF/LiBr d) M_n of BF34 was determined by ¹H NMR.

After these preliminary experiments, gradient copolymerizations were attempted, using separate feeds of DMA and NIPAM. In a typical experiment, a degassed solution of DMA, chain transfer agent and AIBN was placed in an oil bath at 80 °C. Polymerization commenced after an induction time of 1 h. After 1h, solutions of DMA and NIPAM were added by syringe pump over a period of 7.5 h. The rates of addition were adjusted so that the fraction of NIPAM in the monomer feed increased linearly, while the total rate of monomer addition remained constant. Regular samples were taken for analysis by NMR and SEC. NMR analysis revealed that the concentration of unreacted monomer in the reactor remained roughly constant at approximately 1 mol L⁻¹ (Figure 4.3a). As shown in Figure 4.3b, the fraction of DMA in the reaction ($f_{DMA} = [DMA] / ([DMA] + [NIPAM])$)

decreased in an approximately linear fashion from 1 to near 0, while the cumulative fraction of DMA in the copolymer decreased linearly from 1 to approximately 0.5, indicating that a linear gradient composition profile was formed. As it can be observed in Figure 4.3d, M_n increased linearly with conversion, while the dispersity remained relatively low. However, the molecular weight distributions broadened (Figure 4.3c) over the course of the reaction due to a build up of dead polymer chains resulting from termination reactions.

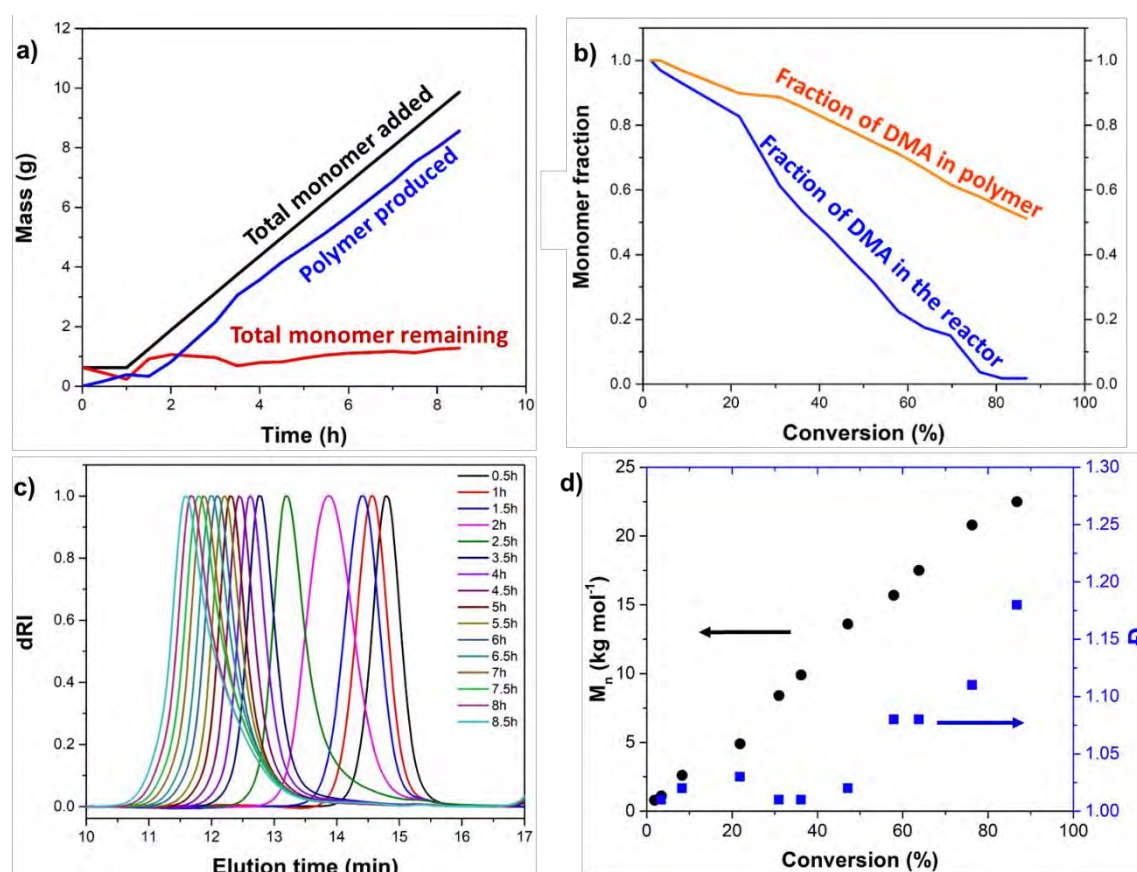


Figure 4.3. Kinetic characteristics of P(DMA-NIPAM) gradient copolymer G20K ($M_n = 20 \text{ kg mol}^{-1}$) a) composition of the reaction mixture over the course of the polymerization, b) Monomer fraction in the polymer and in the reactor, c) SEC traces evolution over the course of the polymerization, d) Evolution of M_n and \bar{D} over the course of the polymerization.

P(DMA-NIPAM) gradient copolymers with number average molecular weights ranging from 10 to 32 kg mol⁻¹ (Table 4.2) were prepared using a similar protocol; increases in molecular weight were achieved by reducing the concentration of CTA. Dispersities remained relatively low with the exception of the 32 kg mol⁻¹ copolymer which had a dispersity of 1.36.

Table 4.2. Details of P(DMA-NIPAM) gradient copolymer synthesis and their macromolecular characteristics. (T = 80 °C, time = 8.5 h)

<i>Exp.</i>	<i>DMA</i> (mmol L ⁻¹)	<i>NIPAM</i> (mmol L ⁻¹)	<i>AIBN</i> (mmol L ⁻¹)	<i>CTA</i> (mmol L ⁻¹)	<i>Conv.</i> ^a %	<i>M_n</i> ^b (kg mol ⁻¹)	<i>Đ</i> ^b
BF62	960	1040	3.30	21.70	83	10.0	1.24
G10K	1440	1560	4.90	32.60	91	14.2	1.09
G20K	1390	1510	2.90	19.33	87	22.5	1.19
G30K	1390	1510	1.28	8.53	73	32.4	1.36

a) Determined from ¹H NMR, b) Determined by SEC in LiBr/DMF.

Asymmetric diblock and asymmetric triblock copolymers were obtained by a stepwise synthesis by Dr. Junliang Zhang at the facilities of the Jena Center for Soft Matter in the University of Jena Friedrich-Schiller. Full details are in the experimental section. Copolymerizations were performed in a Chemspeed Accelerator SLT automated parallel synthesizer using a sequential reagent addition and similar experimental protocols as reported in previous investigations.⁷⁻⁹

The macromolecular characteristics of the copolymers are displayed in Table 4.3. In the nomenclature shown in Table 4.3, for example in T10K, T represents the composition profile of asymmetric triblock copolymer and 10K is the targeted molar mass 10 kg mol⁻¹.

Table 4.3. Macromolecular characteristics of P(DMA-NIPAM) copolymers.

<i>Copolymer</i>	<i>Profile</i>	<i>Overall</i>		<i>Component blocks</i>	
		<i>M_n</i> ^a (kg mol ⁻¹) ^a	<i>Đ</i> ^a	<i>M_n</i> ^a (kg mol ⁻¹) ^a	<i>Đ</i> ^a
S10K	Statistical	10.10	1.05		
S20K	Statistical	19.20	1.07		
B10K	Block	10.0	1.07	5.0 5.0	1.10 1.07
B20K	Block	20.80	1.07	9.5 11.3	1.10 1.07
D10K	Asymmetric diblock	9.30	1.09	4.5 4.8	1.09 1.09
D20K	Asymmetric diblock	18.90	1.11	9.0 9.9	1.11 1.10
T10K	Asymmetric triblock	12.70	1.10	2.3 7.2 3.2	1.09 1.09 1.10
T20K	Asymmetric triblock	26.10	1.12	4.4 15.1 6.6	1.09 1.10 1.10
G10K	Gradient	14.20	1.10		
G20K	Gradient	22.50	1.20		
G30K	Gradient	32.40	1.35		

a) Determined by SEC. For gradient and statistical copolymers DMF/LiBr was used as eluent and for the rest of the polymers CHCl₃ was used.

2 DYNAMIC LIGHT SCATTERING EXPERIMENTS

In order to obtain a first general picture about the effect of temperature on the aggregation behavior of the P(DMA-NIPAM) copolymers, DLS analysis as a function of temperature was performed within a range of 25-70 °C.

The DLS results are shown in terms of hydrodynamic size and derived count rate as a function of temperature. The derived count rate measures the intensity of light scattering, and it increases when particle size becomes larger or if particle concentration becomes higher.¹⁰ Also, the size distribution as a function of temperature was analyzed.

As the RAFT agent used to synthesize all the series of copolymers contains a dodecyl group in its structure, the copolymers also contain the dodecyl end group in the NIPAM-richer region, as depicted in Scheme 4.1. These dodecyl groups drive aggregation of the copolymers into micelles, even at room temperature.¹¹⁻¹⁴

In Figure 4.4 it can be seen that both statistical copolymers have very similar behaviors. For instance, both form micelles at room temperature and D_h remains constant through temperature variation and then at 60 °C they both precipitate, which can be considered the cloud point temperature of these statistical copolymers. This observation is consistent with the reported LCST (63 °C) for statistical copolymers with 50% NIPAM.³ Light scattering shows the gradual increase of the aggregate concentration with temperature and at 60 °C it drops to very low values indicating precipitation of the polymer aggregates. The size distribution at different temperatures (Figure 4.4c and d). The size distribution of S10K shows two populations from 25 to 55 °C. In fact, the population with the larger particles is on the same region of the size distribution at 65 °C. Despite the large size of this population, the low intensity reveals that the fraction of these particles within the sample is not very significant. On the contrary the S20K has a single population which stays roughly constant through the change of temperature. Since the size of both S10K and S20K is very similar, there is no effect of molar mass over the size of the aggregates in the specific case of statistical copolymers. Hence, the behavior of statistical copolymers in this aspect is similar to that of the pure PNIPAM, which cloud point temperature is not affected by the chain length.

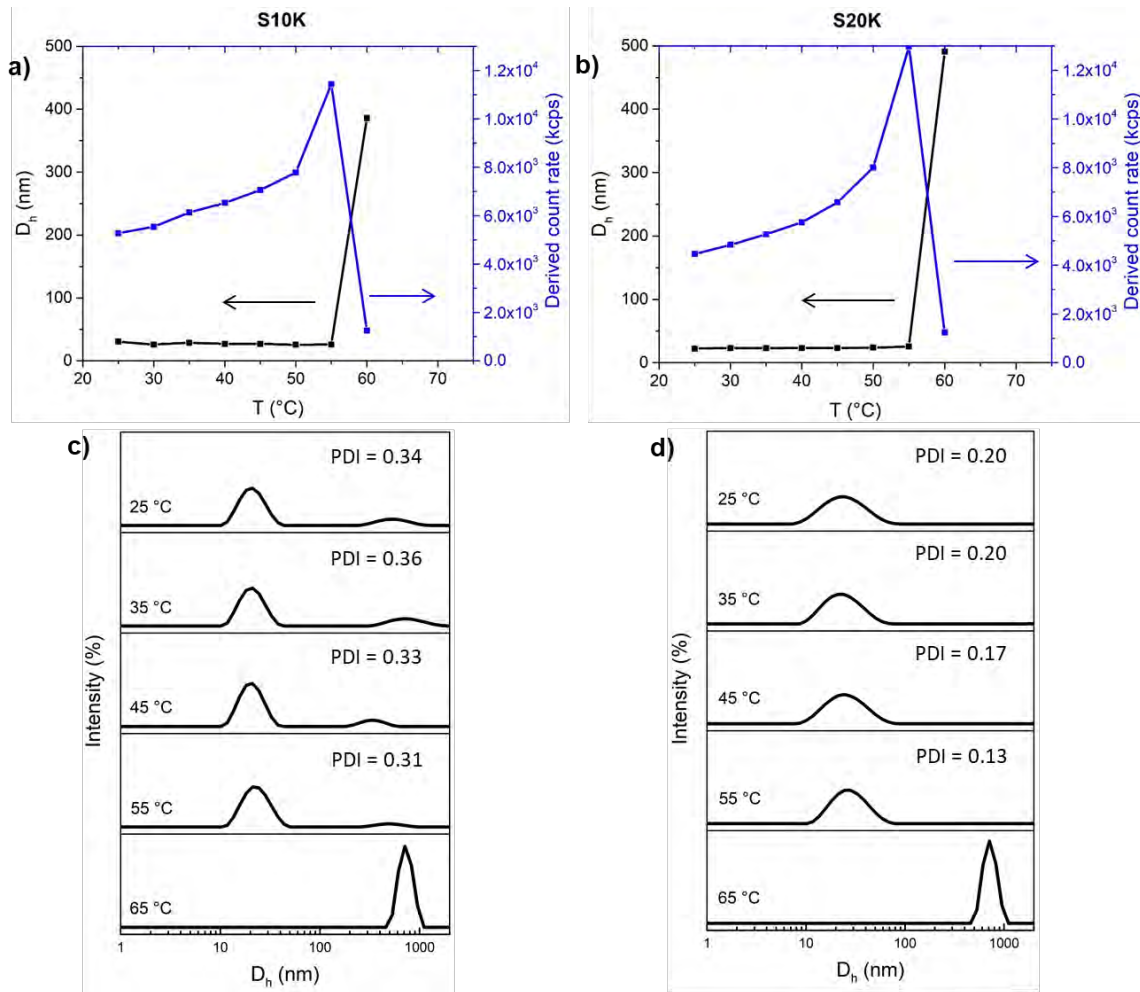


Figure 4.4. Hydrodynamic diameter and light scattering as a function of temperature for P(DMA-NIPAM) statistical copolymers of a) S10K ($M_n = 10 \text{ kg mol}^{-1}$) and b) S20K ($M_n = 20 \text{ kg mol}^{-1}$). Size distribution at selected temperatures of c) S10K and d) S20K. Prepared in H_2O $c = 1 \text{ wt } \%$.

Figure 4.5 shows D_h and light scattering intensity as a function of temperature for block 10K and 20K. The obtained hydrodynamic size does not correspond to the size of dissolved unimers ($1\text{-}10 \text{ nm}$)¹⁵, thus it is inferred there are aggregates already formed at 25 °C due to association of the dodecyl end group. For B10K (block copolymer, $M_n = 10 \text{ kg mol}^{-1}$) shown in Figure 4.5a, both D_h and scattering intensity start to increase around 35 °C. In the case of B20K (Figure 4.5b) there is a very steep increase in size after 35 °C. When the temperature reaches 45 °C the hydrodynamic diameter remains constant. This plateau has been observed in other studies with PNIPAM block copolymers.⁵ Then the increase in scattering intensity is due to the presence of a higher number of polymer aggregates in the solution. For both polymers B10K and B20K, the increase in scattering intensity with temperature seems roughly consistent with the change in size hence the change in concentration over the temperature range is not very significant. B20K ($M_n = 20 \text{ kg mol}^{-1}$) produces larger micelles than B10K ($M_n = 10 \text{ kg mol}^{-1}$), as expected due to

its higher molar mass.⁵ Regarding the size distribution results of B10K and B20K (Figure 4.5c and d), the intensity peak shifts towards larger sizes and becomes narrower with increasing temperature. This is the result of the progressive hydrophobic transformation of the PNIPAM block in the micelle core. Differently from statistical copolymers, block copolymers undergo changes in size with increase of temperature and remain in solution when they are heated above 60 °C, indicating that their aggregates are stabilized by the poly(dimethyl acrylamide) block which remains water soluble.

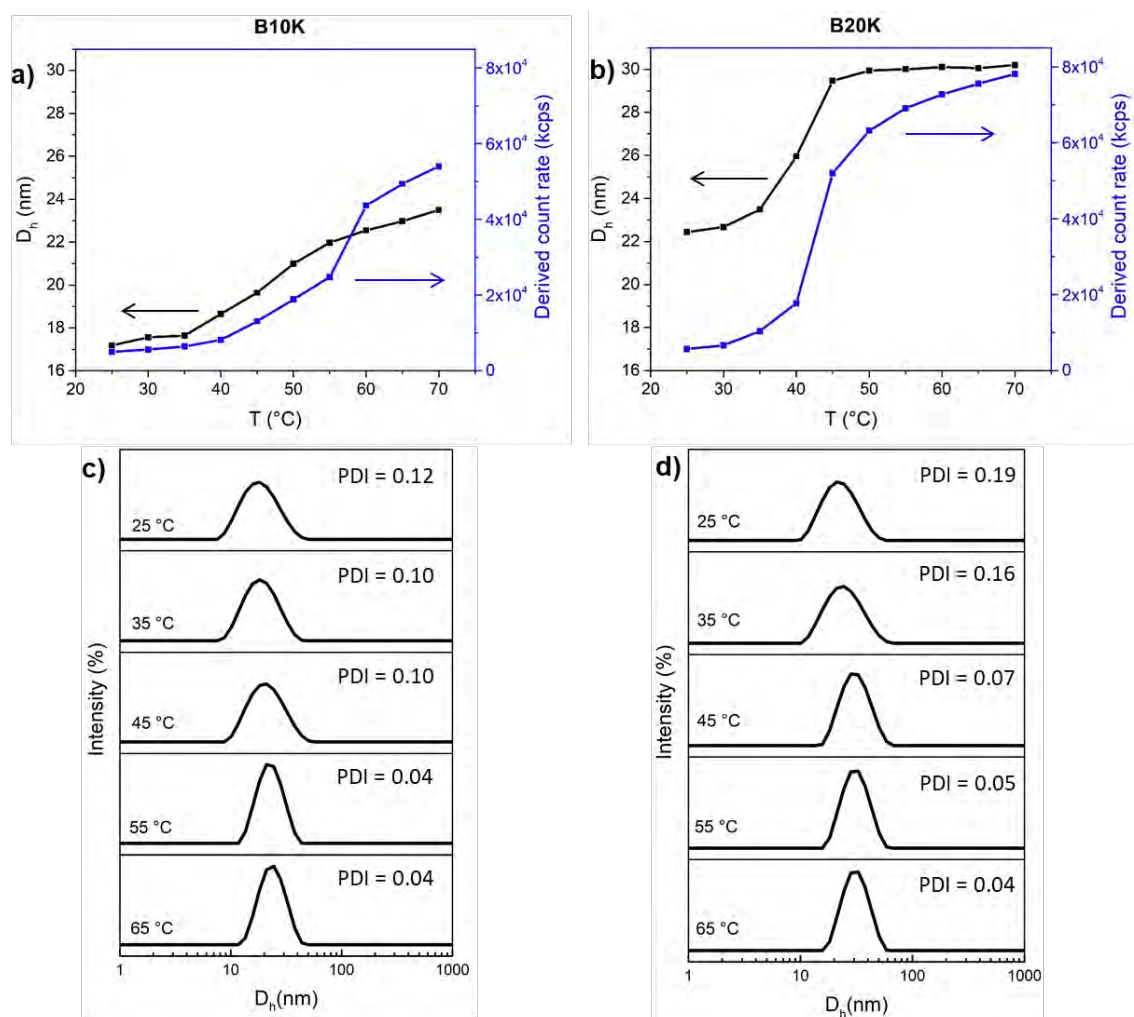


Figure 4.5. Hydrodynamic diameter and light scattering as a function of temperature for P(DMA-NIPAM) block copolymers of a) B10K ($M_n = 10 \text{ kg mol}^{-1}$) and b) B20K ($M_n = 20 \text{ kg mol}^{-1}$). Size distribution at selected temperatures of c) B10K and d) B20K. Prepared in H_2O $c = 1 \text{ wt } \%$.

DLS results of D10K and D20K are shown in Figure 4.6. As in the previous cases, both diblock copolymers form micelles at 25 °C due to the association of dodecyl end-group. D20K forms larger aggregates than D10K, as was mentioned before this effect is

produced because of the higher molar mass of D20K. In both copolymers, light scattering seems to increase at the same rate as D_h . For D10K the evolution of D_h from 25 to 50 °C is not very significant; D_h remains almost constant within this range of temperature. A similar situation occurs for D20K, between 25 and 35 °C the size remains constant but above 35 °C it gradually increases. The size distribution for D10K and D20K is monomodal and it gets slightly narrower with increase of temperature.

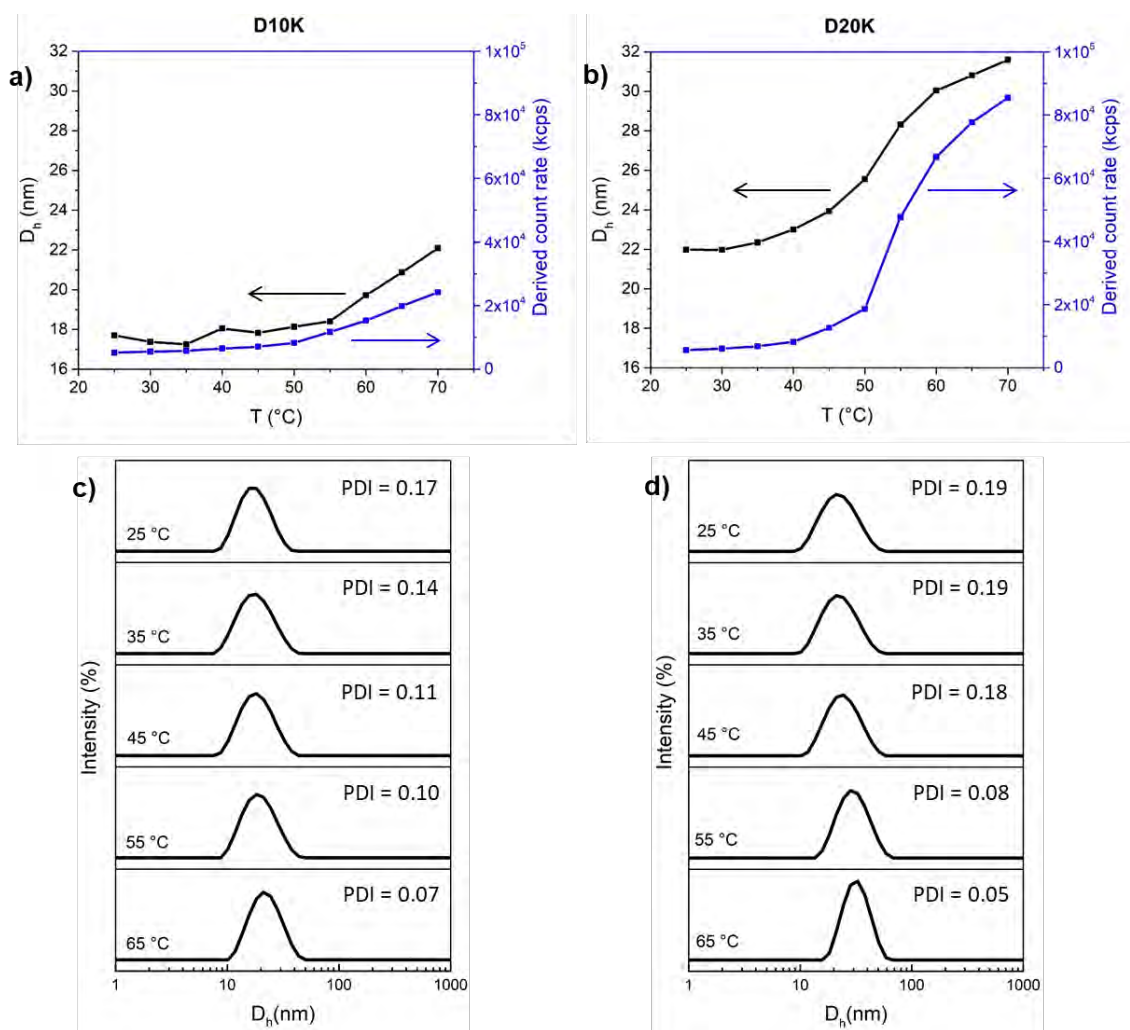


Figure 4.6. Hydrodynamic diameter and light scattering as a function of temperature for P(DMA-NIPAM) asymmetric diblock copolymers of a) D10K ($M_n = 10 \text{ kg mol}^{-1}$) and b) D20K ($M_n = 20 \text{ kg mol}^{-1}$). Size distribution at selected temperatures of c) D10K and d) D20K. Prepared in H_2O $c = 1 \text{ wt } \%$.

DLS results of T10K and T20K are shown in Figure 4.7. As for the previous polymers, no dissolved unimers are observed but only micelles, due to the presence of the hydrophobic end-group. The effect of molar mass can be observed as the aggregates formed by T20K are larger than those of T10K. For T10K (Figure 4.7a) the increase of

D_h from 25 to 45 °C is not very significant, thus the aggregates of T10K are not affected within this range of temperature. Furthermore the total increase of D_h is approximately of 5 nm, which is not a very substantial increase as, in the case of the 10K block and diblock copolymers. In T20K (Figure 4.7b) D_h increases smoothly from 30 to 55 °C, however above this temperature the size of aggregates remains fairly constant, which is a very similar behavior to that of B20K. This could be attributed to the PNIPAM block within the triblock copolymer, but since the block is not very large as for B20K, the plateau is not so marked in T20K. Besides the plateau in B20K started at 45 °C. Both triblock copolymers display monomodal size distributions which get narrower with increase of temperature.

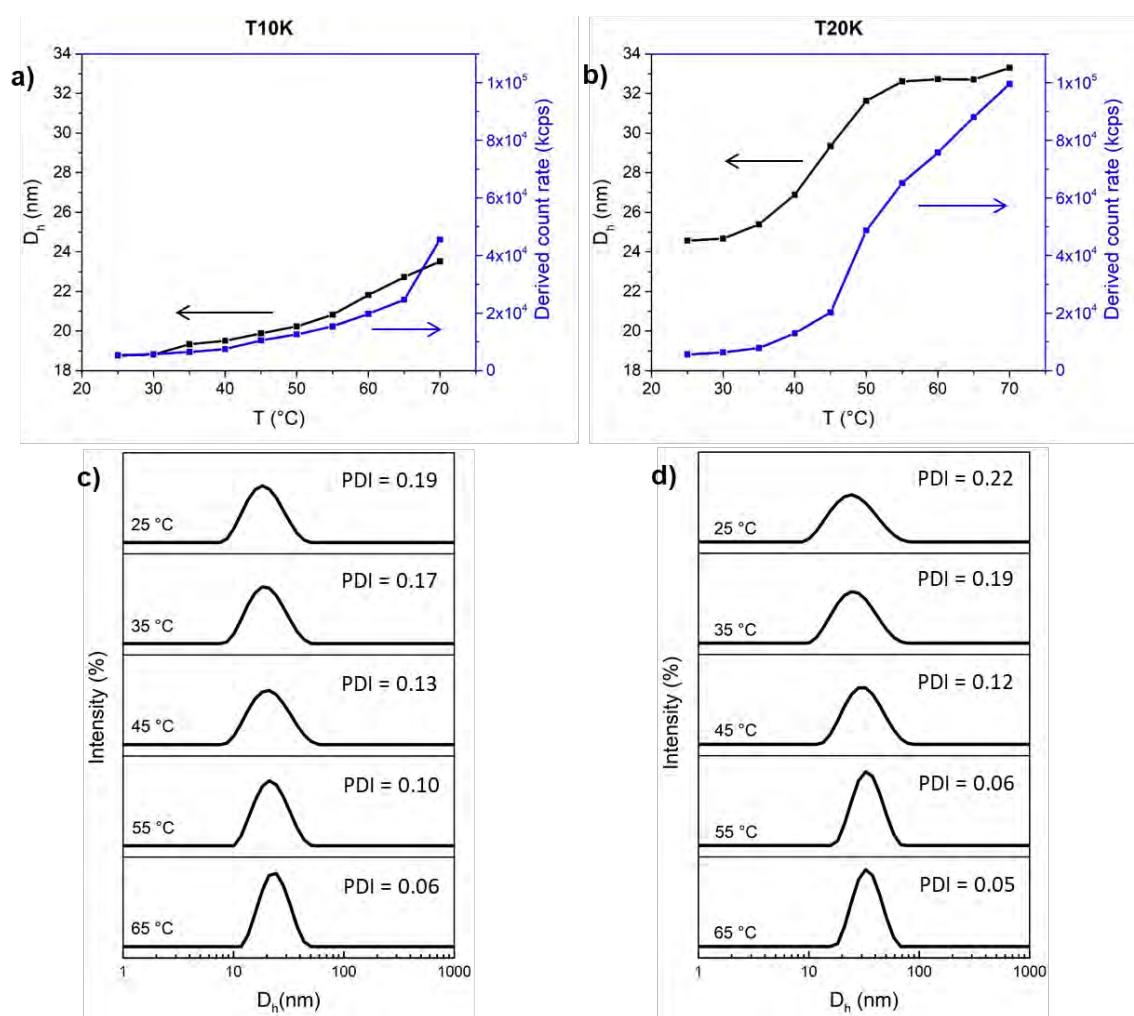


Figure 4.7. Hydrodynamic diameter and light scattering as a function of temperature for P(DMA-NIPAM) asymmetric triblock copolymers of a) T10K ($M_n = 10 \text{ kg mol}^{-1}$) and b) T20K ($M_n = 20 \text{ kg mol}^{-1}$). Size distribution at selected temperatures of b) T10K and c) T20K. Prepared in H_2O $c = 1 \text{ wt } \%$.

For the set of gradient copolymers, another polymer (G30K, $M_n = 30 \text{ kg mol}^{-1}$) was synthesized with the aim to study the effect of a higher molar mass. In the case of G10K showed in Figure 4.8a, D_h does not increase very significantly from 25 to 45 °C, then above 45 °C there is a steeper increase of D_h . As for the other copolymers, the size distribution analysis of G10K is monomodal and by increasing the temperature it shifts to larger particle size and becomes narrower. The aggregation behavior of G20K (Figure 4.8b) and G30K (Figure 4.8c) is very different from the other asymmetric copolymers even from the same G10K. In both cases there is a sharp increase in D_h , however with a further increase of temperature (above 40 °C) D_h starts to decrease. This probably is an indication of the “reel-in” effect, in which above 40 °C NIPAM-rich segments of the chains of the corona start collapsing around the core, causing the D_h to diminish. This phenomenon could also be attributed to further dehydration of the PNIPAM which provokes the core to be more compact and thus the size diminishes. G20K and G30K also show similar size distribution behavior, which are presented in Figure 8e and Figure 8f respectively. For both polymers, at 25 °C and 35 °C there is a bimodal distribution.

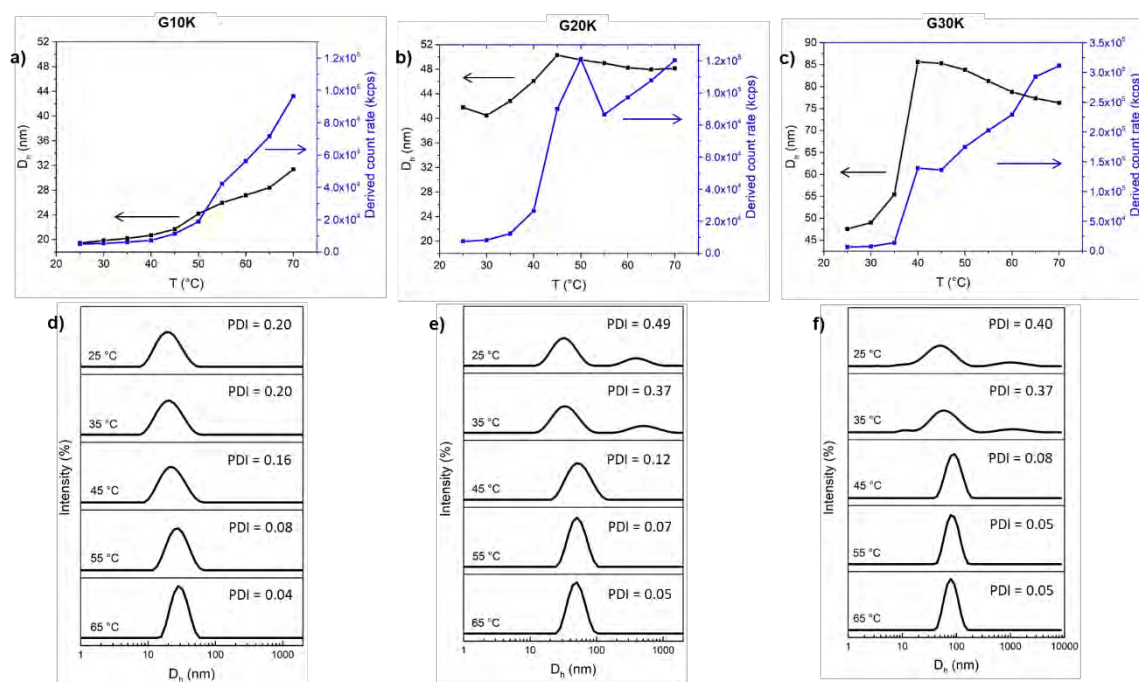


Figure 4.8. Hydrodynamic diameter and light scattering as a function of temperature for P(DMA-NIPAM) gradient copolymers of a) G10K ($M_n = 10 \text{ kg mol}^{-1}$), b) G20K ($M_n = 20 \text{ kg mol}^{-1}$), c) G30K ($M_n = 30 \text{ kg mol}^{-1}$) Size distributions at selected temperatures of d) G10K and e) G20K and f) G30K. Prepared in H_2O $c = 1 \text{ wt } \%$.

From 45 °C there is only one population and it becomes more intense and narrower with increase of temperature. This bimodal distribution at 25 °C and 35 °C is also manifested

by the statistical copolymer S10K. The presence of two populations in thermoresponsive gradient copolymers was previously reported in the investigation of Ogura et al.¹⁶ They studied the self-assembly behavior of MMA/EGMA gradient, block and statistical copolymers by DLS and found that the gradient structures had bimodal size distributions at room temperature, as did the statistical copolymer. It must be noted that D_h of G20K are larger than for the rest of 20K polymers, which might be attributed to the bimodal particle size distribution. D_h are the Z-average diameters obtained by cumulant method, which gives good results if the particles in the sample are monodisperse. Hence the cumulant analysis of G20K and G30K, takes into account both distributions and that could be the reason of the larger D_h for G20K than for the other 20K polymers.

2.1 Comparison by molar mass

The comparison of hydrodynamic diameter of the different copolymer aggregates as a function of temperature is shown in Figure 4.9. With the exception of G10K, the copolymers of 10 kg mol^{-1} form aggregates which do not vary largely in size when temperature increases. This is not the case for the G10K, because above $45 \text{ }^\circ\text{C}$ D_h increases more abruptly than for B10K, D10K and T10K. In the case of copolymers of 20 kg mol^{-1} it can be observed that B20K, D20K and T20K, remain approximately within the same range of D_h , nevertheless G20K produces larger aggregates. The difference between the size of the aggregates formed by the G10K and the rest of the 10K copolymers may be due to the difference in molar mass. For G10K M_n is 14.7 kg mol^{-1} (see Table 4.3) while for the other polymers the molar mass is closer to 10 kg mol^{-1} . And as explained in the section of gradient copolymers, the difference in D_h between G20K and the other 20K polymers is due to the bimodal distribution and the analysis method used to determine the average size.

Interestingly T20K displays a very similar behavior to B20K, which can be attributed to the presence of the PNIPAM block in the triblock structure. Even at $45 \text{ }^\circ\text{C}$ block and triblock copolymers (both 10K and 20K) produce aggregates of the same size.

There is a clear change on size of the 20K polymers which takes place near the cloud point temperature of pure PNIPAM. In the B20K, T20K and G20K this transition occurs between 30 and $50 \text{ }^\circ\text{C}$ and for the D20K it happens from 45 to $60 \text{ }^\circ\text{C}$.

The 10K polymers exhibit a different behavior from the 20K. The transition corresponding to B10K (35 - $55 \text{ }^\circ\text{C}$) seems to be broader than for B20K, while for D10K and T10K the size remains roughly within the same values and then at $55 \text{ }^\circ\text{C}$, their aggregates start to

increase, and differently from the 20K polymers, the size trends do not display a plateau at higher temperatures. G10K begins to increase in size at 45 °C, and it appears to keep increasing at 70 °C. These results may suggest that the shorter (10K) copolymers, particularly the asymmetric ones (D, T, G) behave to some extent like statistical copolymers. For the longer copolymers, it seems that the DMA-rich segments are far enough from the NIPAM-rich segments so they can continue to stabilize the aggregates, even above the cloud point temperature of statistical copolymers with 50 % DMA.

As it was discussed in chapter 1, since PNIPAM is a type II thermoresponsive polymer, molar mass does not affect strongly the T_{cp} , but this is not true for copolymers and block copolymers of PNIPAM, which are strongly affected by the molar mass due to presence of hydrophilic units.

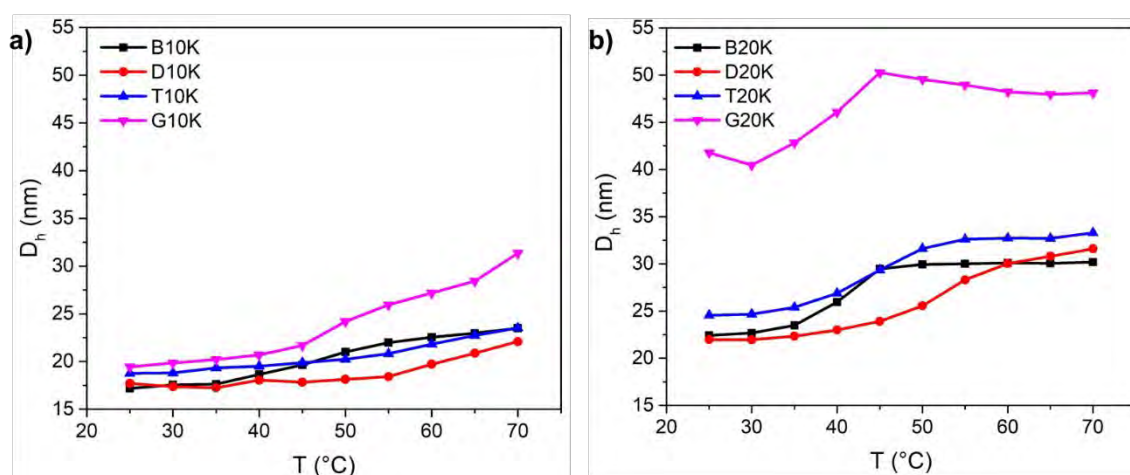


Figure 4.9. Hydrodynamic diameter as a function of temperature, comparing the different structures of P(DMA-NIPAM) copolymers of a) 10 kg mol⁻¹ and b) 20 kg mol⁻¹.

3 SANS AS A FUNCTION OF TEMPERATURE

SANS experiments were carried out with the aim to investigate the self-assembly behavior as a function of temperature of the P(DMA-NIPAM) copolymers. Polymer solutions of 1 wt % (10 mg mL⁻¹) were prepared in D₂O at room temperature. Figure 4.10 contains the SANS curves of statistical copolymer 20K at 25 and 55 °C. Since there were almost no differences between the behavior of S10K and S20K, only S20K was studied by SANS. Furthermore, as the size of the aggregates produced by the statistical copolymers remained constant between 25 and 55 °C, only these two temperatures were analyzed for the S20K. The curves are almost superimposed and the forward

scattering is nearly identical, which indicates that the size and morphology of this copolymer remain constant at these temperatures, which is in agreement with the constant D_h trend observed by DLS between 25 and 55 °C.

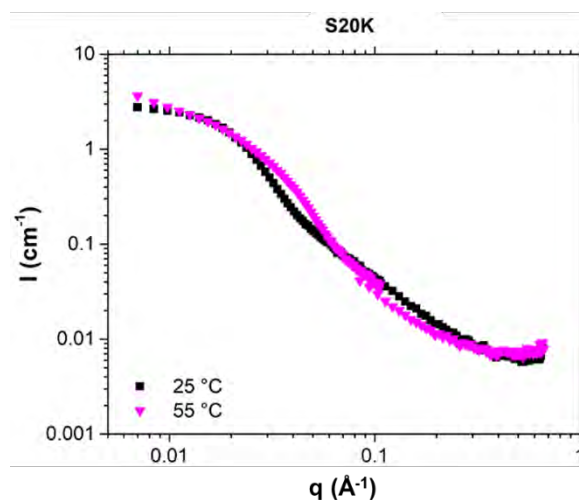


Figure 4.10. SANS curves at 25 °C and 55 °C for the statistical copolymer of 20 kg mol⁻¹. Concentration = 1 wt% in D₂O.

SANS curves for all the remaining polymers exhibit an increase of intensity at the low q values when temperature is increased, indicating increase of the aggregate size.¹⁷ As it was mentioned at the beginning of the chapter, all the polymers possess a dodecyl end-group in the side of the PNIPAM richer region, which produces aggregates at 25 °C because of the association of the hydrophobic end groups. This can be clearly observed in the intensity of the SANS curves at low q values. For all the series of copolymers, at 25 °C the intensity at low q values is $\sim 2 \text{ cm}^{-1}$. For dissolved unimers (Gaussian chains), intensities of $\sim 0.18 \text{ cm}^{-1}$ are typically reported.¹² Similar aggregation behavior was reported in the work of Fitzgerald et al., in which PNIPAM oligomers with dodecyl end groups were analyzed by SANS and it was observed that the intensity at low q values was higher than the corresponding to Gaussian chains.¹²

Figure 4.11 shows the SANS curves of block copolymers B10K and B20K. The intensity of the curves at low q values for B10K increases with the increase of temperature, which reveals that the aggregates are becoming larger. This is in accordance with the inset in Figure 4.11a, in which the molar mass of the aggregates increases with temperature. The curves of B20K (Figure 4.11b) also exhibit increase of intensity at low q , by increasing the temperature. However above, 45 °C the curves are very similar in shape and forward scattering, and even the curve at 65 °C is totally superimposed with the curve at 55 °C, indicating that self-assemblies with nearly the same size are produced

above 45 °C. The inset in Figure 4.11b also reveals that the molar mass of the aggregates remains constant above 45 °C. These observations are consistent with the results obtained from DLS.

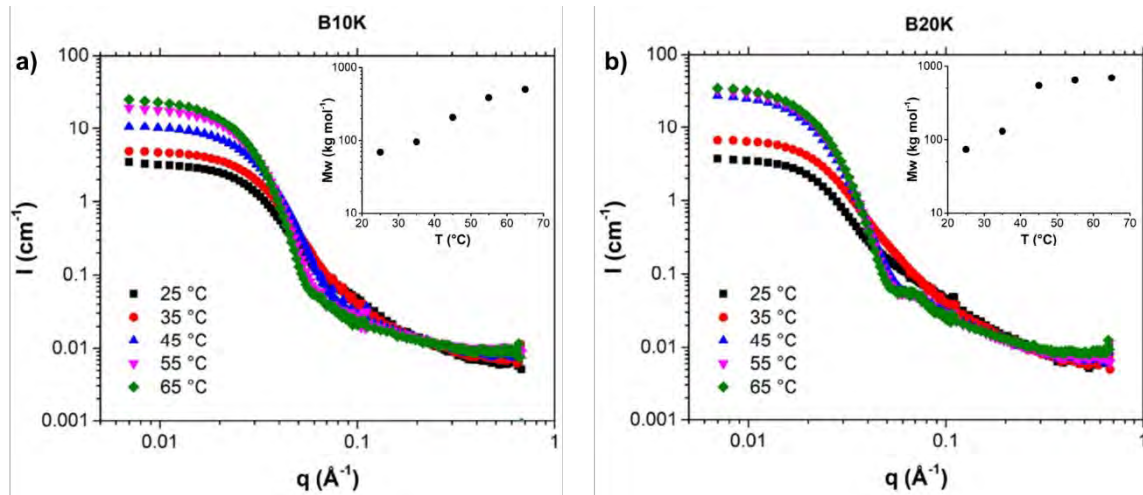


Figure 4.11. SANS curves at different temperatures for block copolymers a) 10 kg mol⁻¹ and b) 20 kg mol⁻¹. Concentration = 1 wt% in D₂O.

The scattering curves of D10K (Figure 4.12a) display a slight but continuous increase in forward scattering by increasing the temperature and it is consistent with the molar mass evolution of the aggregates as a function of temperature depicted in the inset of Figure 4.12a. The intensity of the curves of D20K (Figure 4.12b) at 25 and 35 °C slightly increases (which is a similar behavior to that of D10K), and then above 35 °C the increase on intensity becomes more important. Finally, at 65 °C the intensity at low q values, remains very close to the intensity of the curve at 55 °C. The effect of molar mass of the polymer is better appreciated in the range of 45 to 65 °C, as it can be observed that the forward scattering is higher for the curves of D20K than the curves of D10K. Besides, in the inset of Figure 4.12b it is observed that the molar masses of the aggregates are higher than for D10K.

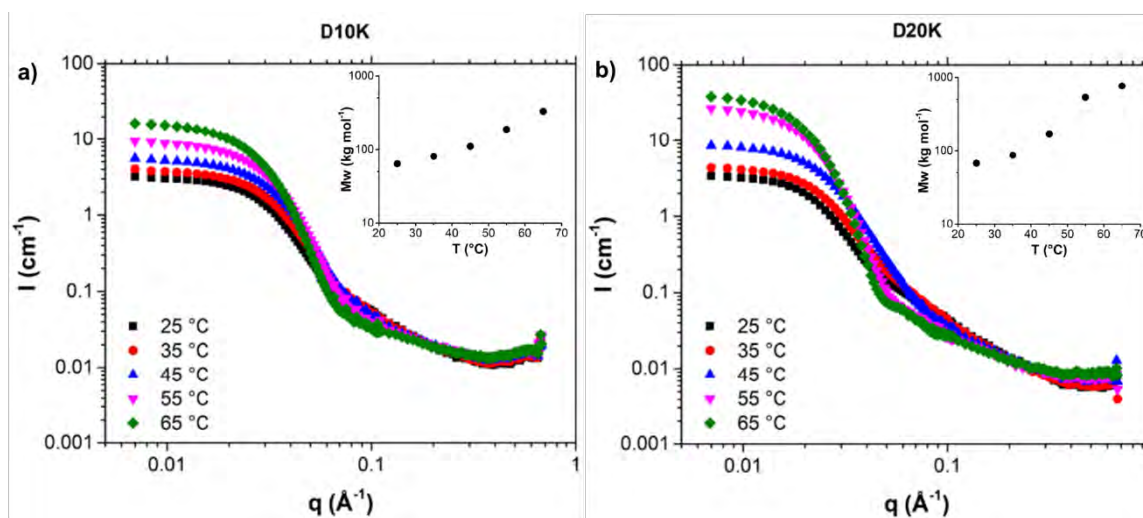


Figure 4.12. SANS curves at different temperatures for diblock copolymers a) 10 kg mol^{-1} and b) 20 kg mol^{-1} . Concentration = 1 wt% in D_2O .

Very similarly to D10K, the scattering curves of T10K, displayed in Figure 4.13a slightly increase in intensity as the temperature increases, even the molar mass of the aggregates as a function of temperature has a similar trend to that of D10K. These observations are in agreement with the DLS results. The curves of T20K (Figure 4.13b) also shifts to higher intensities in the low q values when temperature is increased, but at $45 \text{ }^\circ\text{C}$ the intensity abruptly increases, having very similar forward scattering values as T10K which indicates. Thus T10K at $65 \text{ }^\circ\text{C}$ and T20K at $45 \text{ }^\circ\text{C}$ form aggregates of nearly the same size. Then above $55 \text{ }^\circ\text{C}$ intensity keeps increasing, until at $65 \text{ }^\circ\text{C}$ it reaches a forward scattering similar to that of D20K. In the inset in Figure 4.13b it is observed that the trend of molar mass of T20K is very similar to the behavior of D20K.

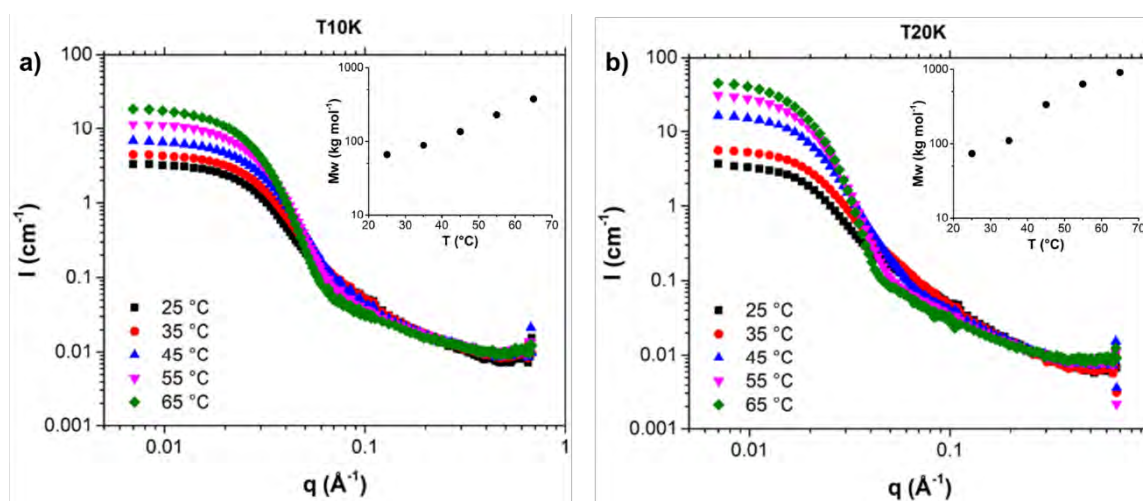


Figure 4.13. SANS curves at different temperatures for triblock copolymers a) 10 kg mol^{-1} and b) 20 kg mol^{-1} . Concentration = 1 wt% in D_2O .

SANS curves of G10K shown in Figure 4.14a, also shifts to higher intensities at low q values as temperature increases, but differently from the other polymers, the curve at 65 °C seems to keep increasing in intensity at low q , while for the other polymers at 65 °C the curves exhibit a plateau. This singular characteristic in the slope of G10K at 65 °C, might indicate a slight difference in the morphology of the produced self-assemblies. For the G20K (Figure 4.14b) the intensity abruptly increases and then the increase appears to be slower for the curves at 55 °C and 65 °C. This can also be observed by the slight increase of molar mass in the inset of Figure 4.14b. For the scattering curves of G30K (Figure 4.14c), the increase of intensity is continuous and quite large from 25 to 45 °C in comparison with the other polymers, which reveals that larger objects are being formed by G30K at 35 and 45 °C. This might be due to the difference in molar mass. However, above 45 °C the increase of intensity is not very significant, and finally the curve at 65 °C is almost overlapping the curve at 55 °C, indicating that similar aggregates are produced at these temperatures. This is a similar behavior to that of B20K, in which also above 45 °C the intensity of the curves at low q remained roughly constant. The similarities between G30K and B20K are can also be observed in the inset of Figure 4.14c, where the evolution of molar mass with temperature appears to be similar to that of B20K.

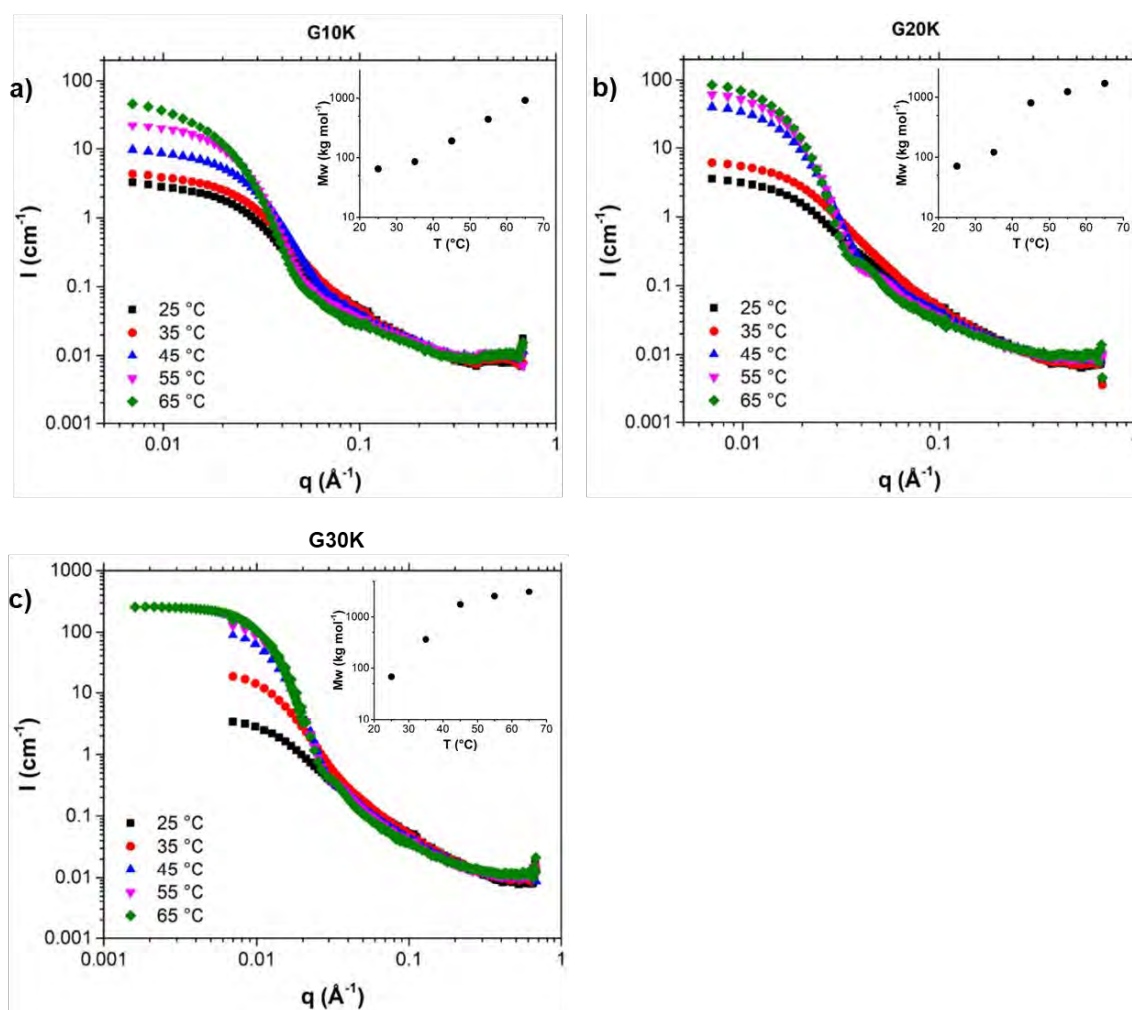


Figure 4.14. SANS curves at different temperatures for gradient copolymers a) 10 kg mol^{-1} , b) 20 kg mol^{-1} and c) 30 kg mol^{-1} . Concentration = 1 wt% in D_2O .

It is interesting to note that the molar mass of the 10K polymers, seems to continually increase with temperature but for the 20K polymers at high temperatures, the molar mass appears to reach a plateau. These observations are consistent with the increase in D_h observed in DLS.

In Figure 4.15 the SANS curves of copolymer series of 10K and 20K are compared at 25, 45 and 65 $^{\circ}\text{C}$. As it can be observed at 25 and 65 $^{\circ}\text{C}$, the curves corresponding to 10K and 20K, are very similar, they have roughly the same intensity at low q values and at 25 $^{\circ}\text{C}$ the curves are superimposed. This is an indication of the similarities between the structures that are generated from all the polymers at the extreme temperatures of the SANS experiment. At 25 $^{\circ}\text{C}$ all the structures form micelles of approximately the same size.

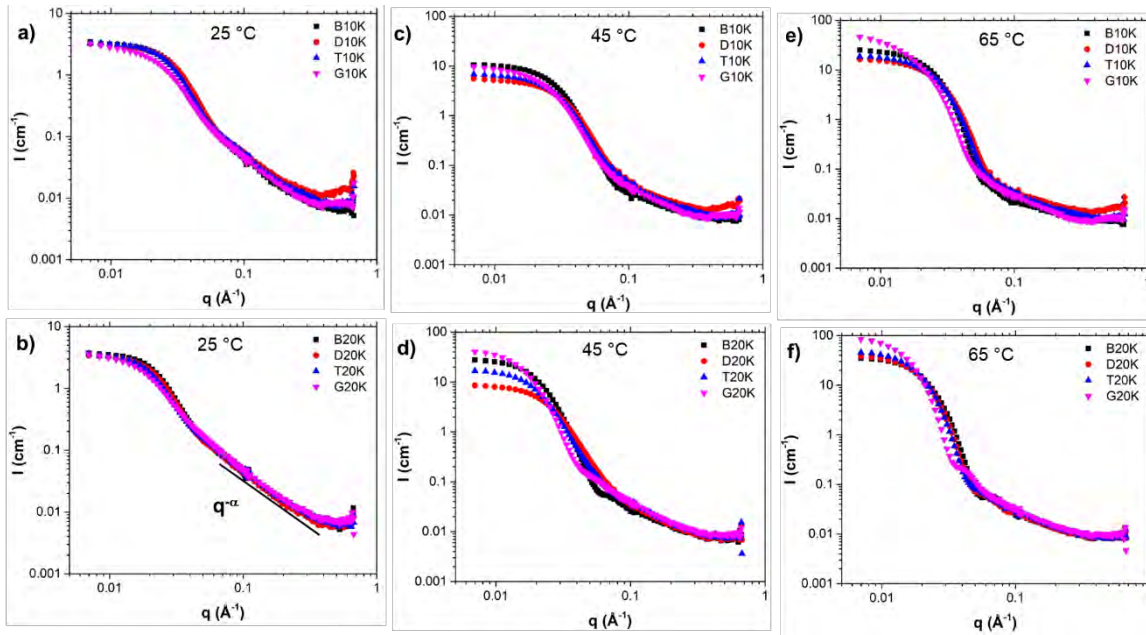


Figure 4.15. Comparison of SANS curves at a), b) 25 °C, c), d) at 45 °C and e), f) 65 °C for copolymers of 10 kg mol⁻¹ and 20 kg mol⁻¹. (b) shows an example of a porod region section fitted to a power law $I \propto q^{-\alpha}$

At 45 °C the scattering curves of the 10K polymers display a slight difference in intensity at the low q values, which indicates a small difference in size of the aggregates formed by each polymer. The lower intensity at low q corresponds to D10K and then T10K has slightly higher intensity. Interestingly the scattering curves of B10K and G10K are very similar, but the intensity at low q of B10K is slightly higher than G10K. Thus at 45 °C the order of aggregate size of 10K polymers is $B > G > T > D$. Notably, the largest difference of intensity in the low q region is displayed by the 20K polymers at 45 °C. Hence, at 45 °C the set of 20K polymers produce aggregates of different size in the following order: $G > B > T > D$. Then at 65 °C the curves for both set of polymers (10K and 20K) do not exhibit a very significant difference in the intensity at the low q region, which indicates that their aggregates are roughly the same size. However, there is a small difference between the gradient copolymers and the rest of the polymers. At low q values, the intensity is higher for both gradient copolymers, which indicates that the aggregates formed by G10K and G20K are larger than the aggregates of the other polymers. It is important to note that the forward scattering of B20K at 65 °C, remains roughly in the same region as the curve of D20K, while at 45 °C B20K displayed higher intensity than D20K, which is consistent with the comparison of D_h obtained by DLS.

3.1 Parameters obtained from Guinier region and forward scattering

The models to fit the neutron scattering curves usually involve a large number of parameters, hence it is necessary to impose some of these parameters in order to obtain reliable results from the fitting. First of all, the scattering length density (SLD) of NIPAM, DMA and D₂O were obtained with a calculator in the software SAS view.¹⁸ SLD is a measure of the scattering power of a material and it increases with the physical density and for the case of SANS, it arises from the nuclear scattering lengths. SLD of NIPAM, DMA and D₂O are shown below.

$$\text{SLD NIPAM} = 8.14 \text{ E-07 } \text{\AA}^{-2}$$

$$\text{SLD DMA} = 8.61 \text{ E-07 } \text{\AA}^{-2}$$

$$\text{SLD D}_2\text{O} = 6.34 \text{ E-06 } \text{\AA}^{-2}$$

After, the volumes of NIPAM, DMA, and the groups corresponding to the RAFT agent (dodecyl (C₁₂H₂₅), trithiol (CS₃) and cyanomethyl (CH₂CN)) were calculated with Equation 4.1, and the values are shown in Table 4.4.

$$Vol_{\text{monomer}} = \frac{M_{\text{monomer}}}{N_A * d} \quad \text{Equation 4.1}$$

Where M_{monomer} represents the molar mass of the monomer in g mol⁻¹, N_A is the Avogadro's number and d is the density of the material in g cm⁻³.

Table 4. 4 Physical properties of NIPAM and DMA used for the fitting.

Functional group	d (g cm ⁻³)	M_{monomer} (g mol ⁻¹)	Vol. (Å ³)
NIPAM	1.10	113	170.6
DMA	0.96	99.13	171.5
CS ₃	1.0	108	179.3
CH ₃ CN	1.0	42	69.7
C ₁₂ H ₂₅	0.75	169	375.0

By using these volumes it is possible to calculate the corresponding volumes to the PNIPAM and PDMA sections¹².

$$Vol_{\text{PNIPAM}} = (m * vol_{\text{NIPAM}}) + vol_{\text{CS}_3} + vol_{\text{C}_{12}\text{H}_{25}} \quad \text{Equation 4.2}$$

$$Vol_{\text{PDMA}} = (m * vol_{\text{DMA}}) + vol_{\text{CH}_3\text{CN}} \quad \text{Equation 4.3}$$

Where m is the number of monomer units.

From the scattering data of SANS experiments, it is possible to evaluate the molar mass of the self-assemblies from the value of the forward scattering using Equation 4.4 obtained from the Guinier approximation¹⁹:

$$I(q = 0) = \frac{C \Delta \rho^2 M_w}{N_A d^2} \quad \text{Equation 4.4}$$

Where C is the copolymer concentration, $\Delta \rho = \rho_{\text{polymer}} - \rho_{\text{solvent}}$ with ρ_{polymer} and ρ_{solvent} the scattering length density of the copolymer and the solvent, respectively, d the copolymer density, N_A the Avogadro number and M_w the molar mass of the aggregates in solution.

The concentration of particles (n_{density} will be used to refer to this term) in the sample can be calculated according to Equation 4.5:

$$n_{\text{density}} = \frac{c * N_A}{N_{\text{agg}} * M_{\text{polymer}}} \quad \text{Equation 4.5}$$

Where c is the concentration of the polymer in g mL^{-1} , N_{agg} is the aggregation number and M_{polymer} is the molar mass of the polymer.

From the Guinier region it is possible to extract information about the overall size of the particle¹¹ (Figure 4.16). The fitting of this region, performed by using the software SasView, allowed to obtain the radius of gyration (R_g) of the aggregate. The porod region corresponds to the scattering from the local structure of the aggregate and is followed by a power law behavior where $I \propto q^{-\alpha}$, and the scaling factor α will give information about the morphology.

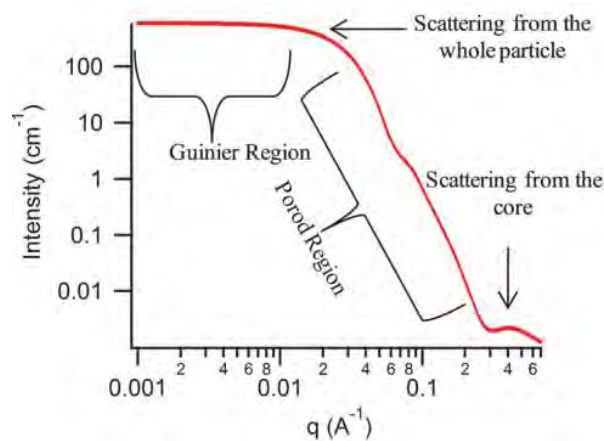


Figure 4.16. SANS model showing intensity as a function of scattering vector (q), for a polydisperse spherical particle. Reproduced from Patterson et al. (2014) published in Chemical society reviews.¹¹

In Appendix 3, tables A3.5 to A3.8 contain the parameters obtained from the Guinier region and forward scattering for all the series of copolymers.

Table 4.5. α values obtained from the fitting of porod regime with $I \rightarrow q^\alpha$ at 25 and 65 °C for the 20K polymers.

	α	
	25 °C	65 °C
B20K	1.54	0.90
D20K	1.50	0.93
T20K	1.50	1.0
G20K	1.50	1.0

It can be seen from Table 4.5 that the 20K copolymers at 25 °C have the same value of α , which is in accordance with the comparison of the SANS curves at 25 °C (Figure 4.15d) for the 20K polymer series. This similarity is an indication of similar particle morphologies at 25 °C. Since NIPAM and DMA are very similar monomers, it is thus expected that the molar mass and morphology of the aggregates obtained from their polymers display similar features. Also, from Table 4.5 it is observed that the scale factor α , slightly decreases from 1.5 to ~ 1.0 , which might indicate a change in the morphology of the aggregates.

Aggregation number (N_{agg}) as a function of temperature is shown in Figure 4.17a and b, and it is observed that the aggregation number at 25 °C is very similar for both sets of polymers (10K and 20K). In addition, it is noted that molar mass has a weak effect on N_{agg} . However, for the block copolymers N_{agg} is bigger when molar mass is low. It has been reported^{11,13} that in hydrophobically modified PNIPAM aggregates, N_{agg} decreases slightly with the decrease of M_n , which is attributed to increased shielding of the micelle core as the chains become longer. Conversely, for gradient copolymers the effect is the opposite above 45 °C: with increase of molar mass, N_{agg} also increases. This could be attributed to the distribution of NIPAM units along the chain, however this does not occur for the diblock and triblock copolymers, which aim to mimic the distribution of NIPAM units of a gradient copolymer.

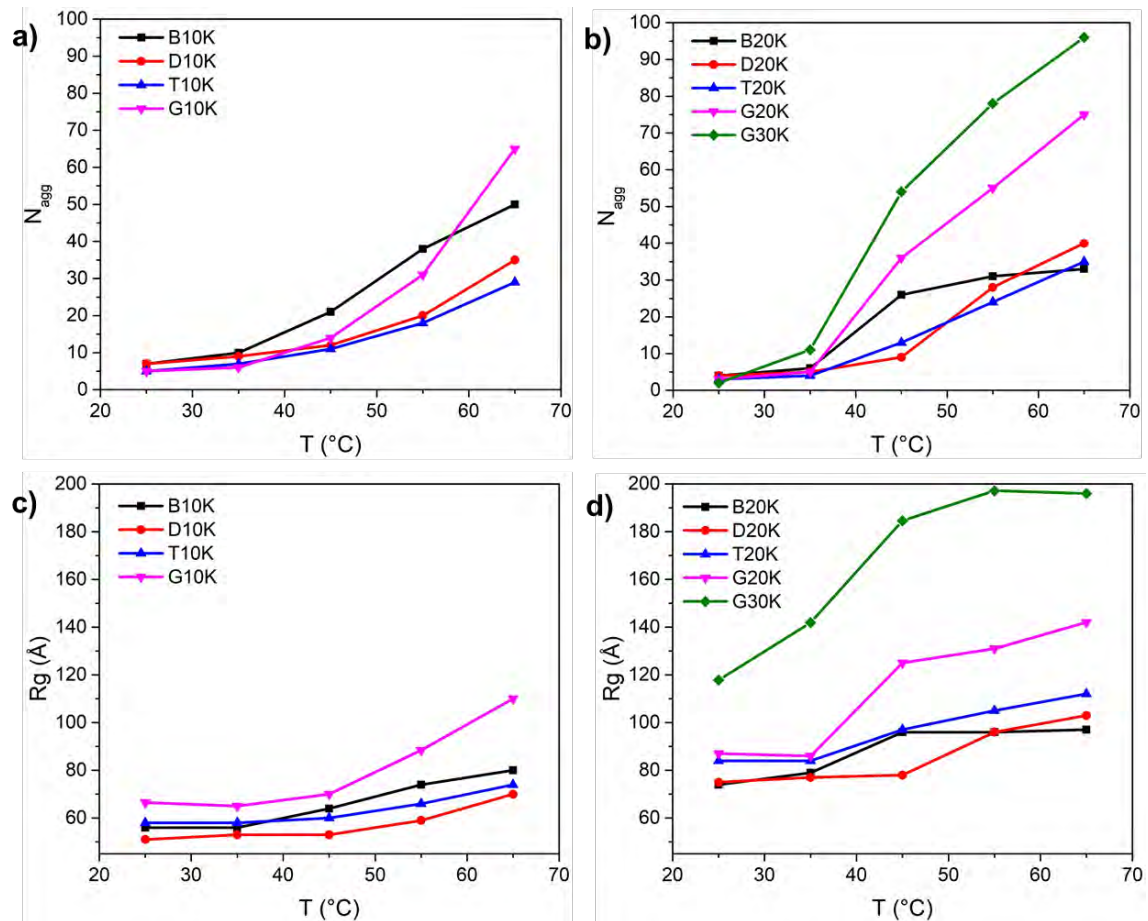


Figure 4.17. Aggregation number (N_{agg}) as a function of temperature comparing polymers at a) 10 kg mol⁻¹ and b) series of 20 kg mol⁻¹ and G30K. Radius of gyration (R_g) as a function of temperature comparing polymers of c) 10 kg mol⁻¹ and d) series of 20 kg mol⁻¹ and G30K

In Figure 4.17 b and c is depicted the evolution of R_g (obtained from the Guinier regime) with temperature. It can be observed that the R_g dependency with temperature is in agreement with the D_h obtained by DLS. G10K and G20K form the larger aggregates compared to their respective 10K and 20K analogous polymers. R_g corresponding to B20K remains constant above 45 °C, which was also revealed by D_h obtained in DLS.

It is worth to mention that the effect of temperature on the polymer chains must be taken as a cooperative phenomenon, requiring the concerted action of an entire segment of polymer. From Figure 4.17a and b it is appreciated that the N_{agg} trend of B10K has a similar behavior to that of G20K. This might be due to the fact that in B10K the length scale of the chains is short enough that NIPAM units are more affected by the DMA. Thus, the polymer chain behaves as if NIPAM and DMA were mixed together as in a statistical copolymer or a gradient-like copolymer.

The SANS curves were fitted to a polymer micelle model with spherical core, calculated according to the equation given by Perdersen²⁰

$$F(q) = N^2 \beta_s^2 F_s(q) + N \beta_c^2 F_c(q) + 2N^2 \beta_s \beta_c S_{sc}(q) + N(N-1) \beta_c^2 S_{cc}(q) \quad \text{Equation 4.6}$$

Where N represents the aggregation number of the micelle and β_s and β_c are the total excess scattering length of a block in the core and in the corona respectively and they are calculated from

$$\beta_s = v_s (\rho_s - \rho_{solv}) \quad \text{Equation 4.7}$$

$$\beta_c = v_c (\rho_c - \rho_{solv}) \quad \text{Equation 4.8}$$

where V_s and V_c are the total volumes in the core and in the corona ρ_s and ρ_c are the corresponding scattering length density and ρ_{solv} is the scattering length density of the solvent.

The normalized self-correlation term [$F_s(q=0)=1$] for the spherical core with radius R is given by Rayleigh (1911):

$$F_s(q) = \left(\frac{3[\sin(qR) - qR\cos(qR)]}{(qR)^3} \right)^2 \quad \text{Equation 4.9}$$

The chains in the corona have a radius of gyration R_g and the self-correlation terms of the Gaussian chains is given by the Debye²¹ function:

$$F_c(q) = \frac{2[e^{-q^2 R_g^2} - 1 + q^2 R_g^2]}{q^4 R_g^4} \quad \text{Equation 4.10}$$

The interference cross term between the core and the chains is:

$$S_{sc}(q) = \left[\frac{3[\sin(qR) - qR\cos(qR)]}{(qR)^3} \right] \left[\frac{1 - e^{-q^2 R_g^2}}{q R_g} \right] \left[\frac{\sin(q[R + dR_g])}{q[R + dR_g]} \right] \quad \text{Equation 4.11}$$

The interference term between the chains in the corona is:

$$S_{cc}(q) = \left[\frac{1 - e^{-q^2 R_g^2}}{q^2 R_g^2} \right]^2 \left[\frac{\sin(q(R + dR_g))}{q(R + dR_g)} \right]^2 \quad \text{Equation 4.12}$$

The fit of all the polymer series at 10K and 20K and G30K was carried out by fixing the N_{agg} and $n_{density}$ (obtained from the information of the forward scattering), then V_s , V_c , R and R_g were allowed to vary. Nonetheless, as it can be observed in Figure 4.18a, the fits

of the curves of T10K are not adequate in the region between $\sim 0.05 - 0.13 \text{ \AA}^{-1}$. This might be corrected by adding a contribution from polydispersity or even a contribution from other type of morphology. Similarly, the fitting of the other polymers were not in agreement with the corresponding scattering curves, as for the case of T10K. For instance in Figure 4.18b the fits corresponding to B20K are shown, and as it is observed in the q region $\sim 0.04 - 0.10 \text{ \AA}^{-1}$, the fit is even more unstable than in the case of T10K. Hence, the parameters obtained from the fit of the curves are probably inaccurate.

The rest of the polymers with their fits and the parameters obtained can be found in Appendix 3 in Figures A3.1 to A3.4 and Tables A3.10 to A3.13.

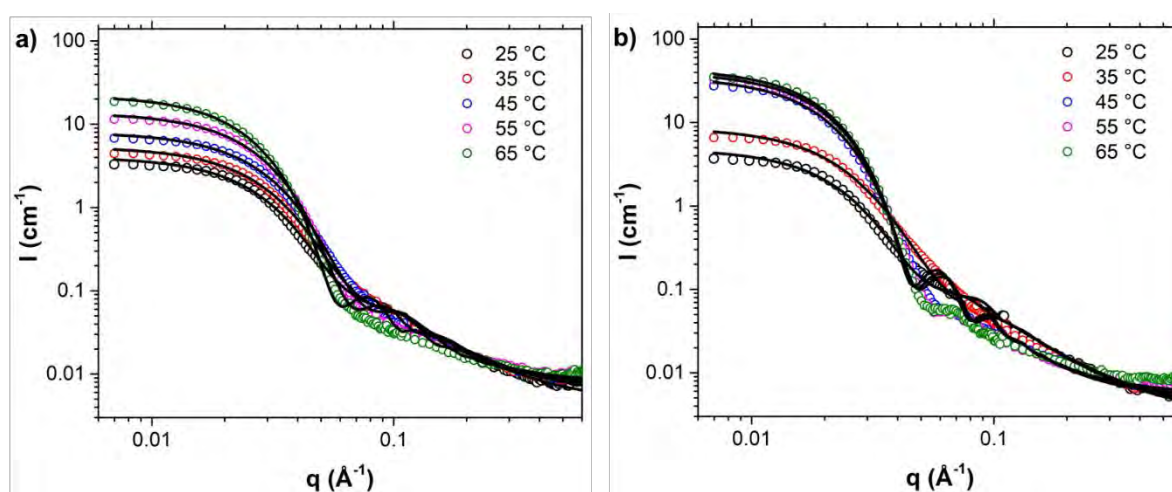


Figure 4.18. Small angle neutron scattering curves at 25, 35, 45 55 and 65 °C, of a) T10K and b) B20K. The black lines are the fit curves.

4 ^1H NMR AS A FUNCTION OF TEMPERATURE

NMR spectroscopy is a very valuable technique, which can provide information about the phase transition of thermoresponsive polymers. Previous studies have reported the use of ^1H NMR as a function of temperature to study block structures of PNIPAM and PDMA-containing copolymers.^{3-5,22-25} It is easy to observe the changes that the polymer experiments through the variation of temperature. Heat-induced micellization of polymers in solution ($c = 1 \text{ wt\%}$) was analyzed by monitoring changes in the peak integral areas as a function of temperature. A solution of 3-(trimethylsilyl) propionic acid-D4 10 mM was used as internal standard, in order to have a reference signal which remained constant through the change of temperature.

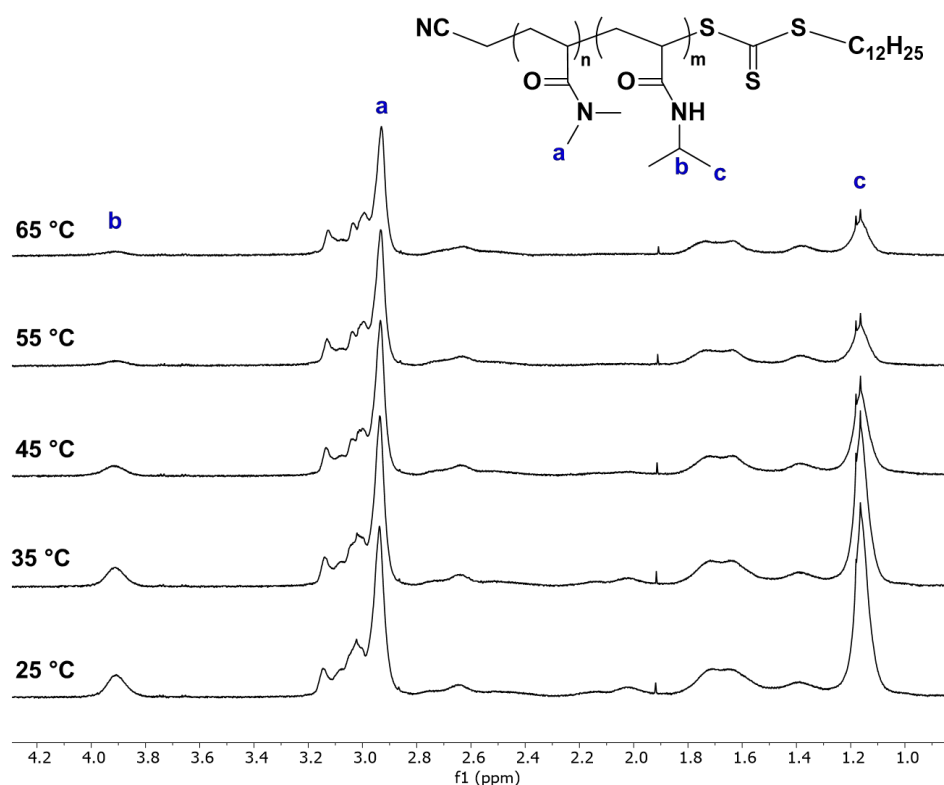


Figure 4.19. ^1H NMR spectra of P(DMA-NIPAM) asymmetric diblock copolymer D20K ($M_n = 20 \text{ kg mol}^{-1}$) as a function of temperature. Analysis performed in D_2O , $c = 1 \text{ wt}\%$.

Figure 4.19 shows an example of a ^1H NMR spectra as a function of temperature corresponding to the asymmetric diblock copolymer D20K. It can be observed that the increase of temperature produces the decrease of the methyne proton peak (3.9 ppm) in PNIPAM, while the methyl protons peak (2.97 ppm) corresponding to PDMA remains fairly constant. The ^1H NMR peak integral areas of PNIPAM methyne proton and PDMA methyl protons were measured from 25 to 70 °C on intervals of 5 °C. The change in normalized peak area as a function of temperature for all polymers is shown in Figure 4.20.

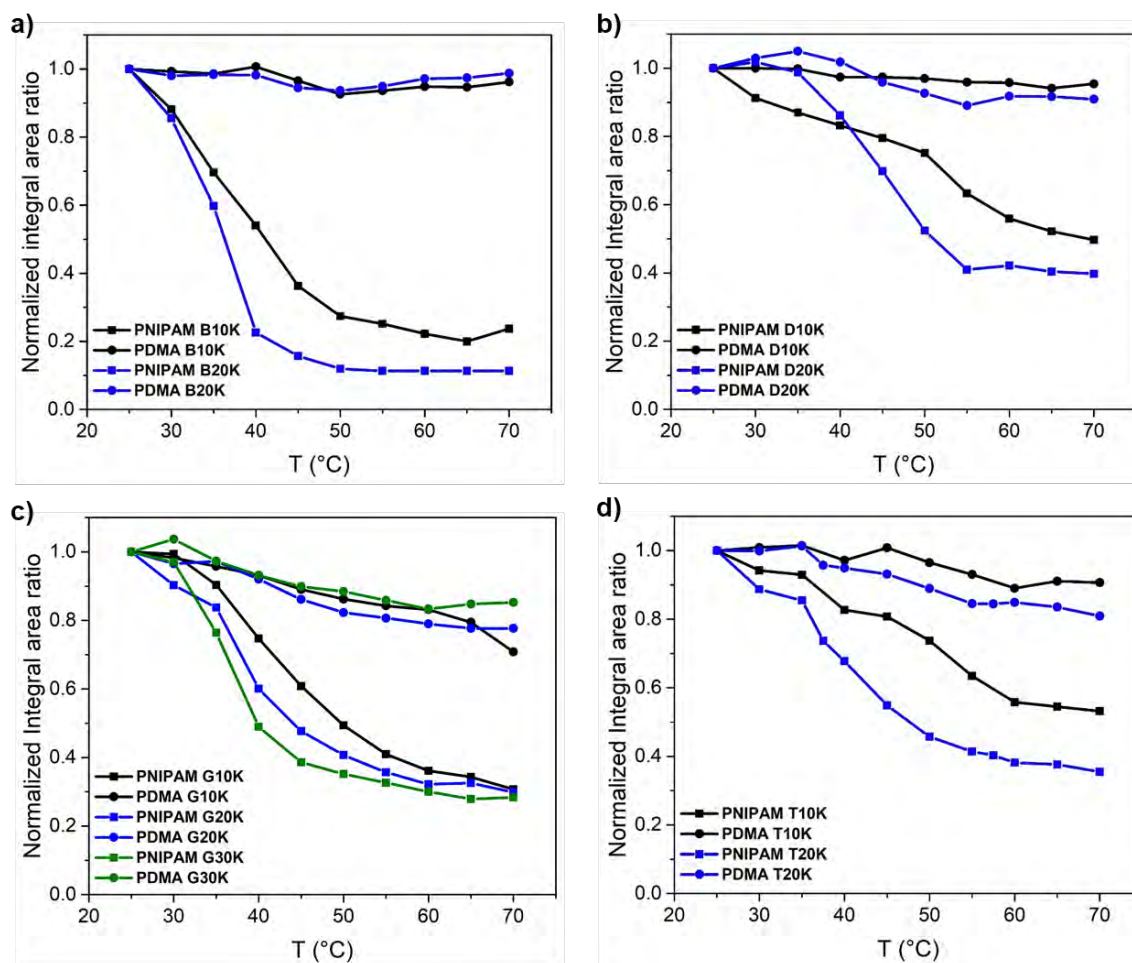


Figure 4.20. Normalized integral area as a function of temperature, derived from ¹H NMR experiments. Comparison of PNIPAM and PDMA in a) block copolymers of 10 and 20 kg mol⁻¹, b) diblock copolymers of 10 and 20 kg mol⁻¹, c) gradient copolymers of 10, 20 and 30 kg mol⁻¹ and d) triblock copolymers of 10 and 20 kg mol⁻¹,

In Figure 4.20a it can be seen that the integral area of PNIPAM in block 20K decreases very sharply between 25 and 40 °C, and after it remains constant. In the case of block 10K this change is less steep, and the decrease occurs between 25 and 45 °C. This difference in the integrated signal can be attributed to the differences in molar mass. In both block copolymers, the isopropyl protons are considerably lower above 45 °C than at 25 °C, which is a result of restricted motion of the NIPAM segment at elevated temperatures.²⁴ In both copolymers, PDMA integral area remains constant through temperature variation. Gao et al. reported that the high steric hindrance of hydrophobic blocks produces restricted motion of hydrophobic blocks leading to weaker ¹H NMR signals.²⁶ On the contrary the characteristic signals of PDMA remain constant. Goto et al. observed similar results with PMPC-*b*-P(NIPAM/DMA) copolymer solutions from 22 to 68 °C.²² ¹H NMR results are in agreement with the DLS results for both block polymers,

but this is better appreciated for B20K because above 40 °C, D_h remains constant, as in this case the integral area is also constant above 40 °C.

PNIPAM peak integrals corresponding to diblock copolymers have a very different behavior from that of the blocks. As it can be seen in Figure 4.20b, there is a gradual decrease in the signal of PNIPAM in diblock10K. On the other hand, the integral of PNIPAM in diblock 20K, starts to decrease after the 35 °C, and in this case is steeper than the diblock 10K.

Differently from block copolymers, in the case of diblock, triblock and gradient copolymers a slight decrease on the methyl proton signal corresponding to PDMA can be observed. This is due to the way that the DMA units are distributed along the polymer chain. In the block copolymer a limit is defined between DMA and NIPAM segments. On the other hand, the asymmetric copolymers contain regions of copolymer which both NIPAM and DMA units mixed together. In the case of the diblock copolymer, collapse of the NIPAM rich segment will lead to a reduction in the DMA signal, corresponding to the DMA in this segment. Meanwhile the NIPAM present in the DMA-rich segment remains visible in the NMR spectrum. That is why the signal integral of PNIPAM at 70 °C, for diblock, triblock and gradient copolymers, does not decay, but remains approximately in a value of 0.40. The effect of the dodecyl end group has a major effect on the polymers of lower molar mass. This can be observed in the transitions of the curves to higher temperatures when the molar mass decrease.

As observed in Figures 4.20a and 20c, B10K and G20K display similar behaviors. As discussed previously in the section of SANS results, this similarity can be due to the length scale of the block 10K: since the molar mass is relatively low, the NIPAM is more affected by the presence of DMA units. Also B20K and G30K exhibit similar behaviors, but in this case is the gradient which probably has a blocky behavior. In a gradient copolymer with a length scale long enough, probably there will be some sections behaving like a block copolymer.

D10K, T10K display similar behaviors in their transitions to that of G10K. However, the fraction of NIPAM at 70 °C is higher for the D10K and T10K than for the gradient. This indicates that the NIPAM is more affected by the DMA units in an asymmetric diblock or triblock structure than in a gradient copolymer.

D20K, T20K and G20K are also very similar, which can be attributed to the similarities in composition profile, and in comparison with the B20K, the transitions for the asymmetric polymers are broader and they are shifted to higher temperatures. Hence in the asymmetric structures the units of NIPAM appear to be more affected by the presence

of the DMA than in a block copolymer. Overall, the behavior of the polymers suggests that the chain collapse on heating through the cloud point involves a significant number of monomer units. The collapse of any particular segment of a chain will take place at a temperature that corresponds to the average composition of all the monomers in that segment. This is schematically illustrated in Figure 4.21 for the structures B10K, B20K and T20K.

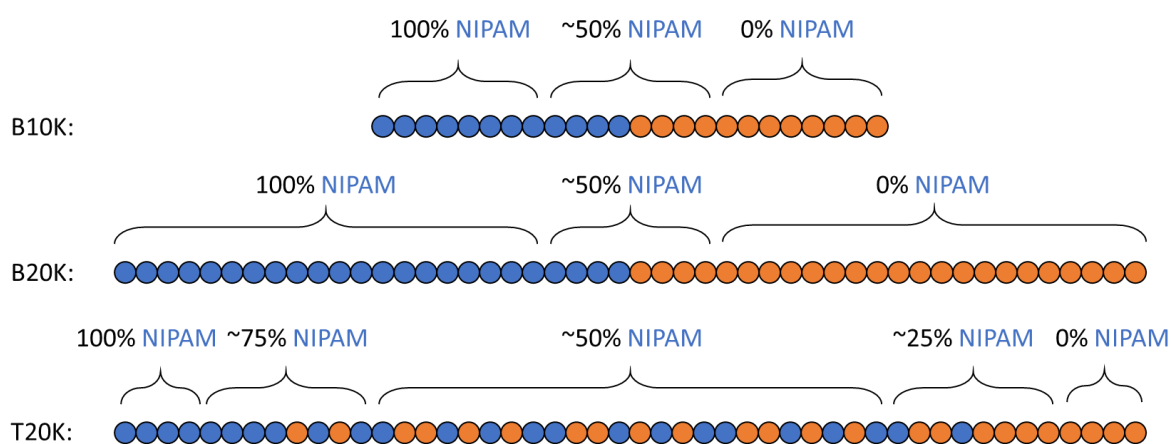


Figure 4.21. Differences between structures of B10K, B20K and T20K. The chains are divided into sections to illustrate the effect of NIPAM distribution.

For the block copolymers B10K and B20K, the DMA block has a significant influence on the collapse of the NIPAM block. In the region around the transition from one block to another, this influence causes the effective composition of the copolymer to change gradually from 100% NIPAM to 100% DMA. However, this effect is proportionately greater for the shorter B10K polymer, as in this case the transitional region accounts for a greater proportion of the total length of the copolymer. The effect of this is that, rather than showing a sharp transition from soluble to collapsed that corresponds to the LCST of PNIPAM, the block copolymers show a more gradual transition that is more similar to that expected from a gradient copolymer. The solubility transition sharpens as the molecular weight of the polymer increases.

This effect is also apparent for the asymmetric copolymers, whose changes in composition are equally blurred as a result of the influence of neighboring blocks. As illustrated for the copolymer T20K, the effect is to smooth out the steps in the composition profile, leading to an effective composition profile that is closer to that of a gradient. This may explain the similarities in behavior between the triblock and gradient copolymers, and the failure to observe separate transitions corresponding to the PNIPAM

homopolymer and PNIPAM/DMA statistical copolymer segments for the triblock copolymers.

As for the block copolymers, this smoothing effect is more pronounced at lower molecular weight. The 10K copolymers, in particular the asymmetric ones (D, T, G) behave to some extent like statistical copolymers. For the 20K copolymers, it seems that the DMA-rich segments are far enough from the NIPAM-rich segments so they can continue to stabilize the aggregates, even above the cloud point temperature of statistical copolymers with 50 % DMA.

5 CONCLUSIONS

Dans ce chapitre, les copolymères de P(DMA-NIPAM) sensibles à la température ont été étudiés. Différentes structures telles que les copolymères dibloc asymétriques et tribloc copolymères statistiques, copolymères à blocs et gradient avec des masses molaires globales de 10 et 20 kg mol⁻¹, ont été analysées par DLS, SANS et RMN ¹H en fonction de la température. Un copolymère à gradient supplémentaire de 30 kg mol⁻¹ a également été étudié.

Le comportement de micellisation en fonction de la température a d'abord été étudié par DLS, grâce à quoi il a été observé la formation de micelles à 25 °C, du fait de la présence du groupement terminal dodécyle dans les copolymères. Les copolymères statistiques (S10K et S20K) sont restés constants de 25 à 55 °C et ils ont leur T_{cp} à 60 °C. Les polymères 20K ont formé des agrégats plus gros que les polymères 10K (à l'exception des copolymères statistiques), ce qui est un effet de la masse molaire des polymères. Ensuite, au-dessus de 50 °C, les tendances de taille des polymères 20K ont présenté un plateau, contrairement aux polymères 10K dont la taille des agrégats a commencé à augmenter à ~ 55 °C. Les polymères 10K n'ont pas montré de D_h constant en fonction de la température comme c'était le cas pour les polymères 20K. Par conséquent, les résultats DLS pourraient indiquer que les plus petits copolymères asymétriques (D10K, T10K et G10K) se comportent comme des copolymères statistiques puisque leur taille est restée constante et au-delà d'une certaine température, ils ont subi une transition. Dans le cas des polymères 20K, le segment riche en DMA est suffisamment éloigné de la section riche en NIPAM pour qu'il continue de stabiliser les agrégats même lorsque la température est supérieure au T_{cp} d'un copolymère statistique avec 50% de NIPAM.

Par l'analyse SANS en fonction de la température, l'intensité croissante des courbes à faibles valeurs q a indiqué l'augmentation de taille des agrégats, ce qui est également confirmé par l'augmentation de la masse molaire des agrégats. Bien que l'ajustement des courbes ne soit pas totalement en accord avec les courbes de diffusion correspondantes, des informations importantes ont pu être extraites de la diffusion vers l'avant et de la région de Guinier, comme R_g et N_{agg}. Les tendances de R_g sont cohérentes avec le D_h obtenu par DLS. Il est intéressant de noter que la tendance N_{agg} de B10K a montré un comportement similaire à celui correspondant à G20K, qui pourrait être attribué à l'échelle de longueur courte de B10K, où les unités NIPAM et DMA sont suffisamment proches pour que le NIPAM soit très affecté par le DMA.

Enfin, la micéllisation induite par la température a également été analysée par RMN ¹H en fonction de la température, ce qui, de manière similaire au SANS, a révélé les

ressemblances entre B10K et G20K ainsi qu'entre B20K et G30K. Le comportement similaire de B10K et G20K a la même explication que dans l'analyse SANS : les chaînes B10K sont suffisamment courtes pour que les unités de NIPAM soit très affecté par celles de DMA, comme si les deux monomères étaient mélangés ensemble, à l'image d'un copolymère statistique ou à gradient. Pour les comportements similaires de B20K et G30K, la situation se concentre sur l'échelle de longueur de G30K dans laquelle les chaînes sont suffisamment longues pour que certaines sections aient un comportement de type bloc.

5 CONCLUSIONS

In this chapter P(DMA-NIPAM) thermally responsive copolymers were studied. Different structures such as statistical, block, gradient, and asymmetric diblock and triblock copolymers with targeted molar masses of 10 and 20 kg mol⁻¹, were analyzed by DLS, SANS and ¹H NMR as a function of temperature. An additional gradient copolymer of 30 kg mol⁻¹ was also under study.

The micellization behavior as a function of temperature was first studied by DLS, in which it was observed the formation of micelles at 25 °C due to the presence of the dodecyl end group in the copolymers. The statistical copolymers (S10K and S20K) remained constant from 25 to 55 °C and they have their T_{cp} at 60 °C. 20K polymers produced larger aggregates than the 10K polymers (except the statistical copolymers), which was an effect of the molar mass of the polymers. Then, above 50 °C the size trends of the 20K polymers exhibited a plateau and differently, the size of the 10K polymer aggregates started to increase at ~55 °C and they did not display the constant D_h as in the 20K polymers. Hence, the DLS results might indicate that the smaller asymmetric copolymers (D10K, T10K and G10K) behave somehow as statistical copolymers since the size of both remains constant and above certain temperature they experience a transition. In the case of the 20K polymers the DMA-rich segment is far enough from the NIPAM-rich section so it keeps stabilizing the aggregates even when the temperature is above the T_{cp} of a statistical copolymer with 50% NIPAM.

By SANS analysis as a function of temperature, the increasing intensity of the curves at low q values, indicated the increase of size of the aggregates, confirmed by the increase of molar mass of the aggregates. Despite the fit of the curves were not totally in agreement with the corresponding scattering curves, important information could be extracted from the forward scattering and the Guinier region, such as R_g and N_{agg} . The trends of R_g were roughly consistent with the D_h obtained by DLS. Interestingly, the N_{agg} trend of B10K displayed a similar behavior to the corresponding one to G20K, which could be attributed to the short length scale of B10K, where NIPAM and DMA units are close enough that NIPAM is very affected for DMA.

Finally, the heat-induced micellization was also analyzed by ¹H NMR as a function of temperature, which similarly to SANS, revealed the similarities between B10K and G20K and also between B20K and G30K. The similar behavior of B10K and G20K has the same explanation as in SANS: B10K chains are short enough so that NIPAM units are very affected by DMA units, as if both monomers were mixed together as in a statistical or gradient copolymer. For the similar behaviors of B20K and G30K the situation focuses

on the length scale of G30K in which the chains are long enough that some sections would have block-like behavior.

6 MATERIALS AND METHODS

6.1 Proton Nuclear Magnetic Resonance (^1H NMR)

Conventional ^1H NMR

^1H NMR spectra for the analysis of copolymer conversions were obtained on a Bruker Avance 400 MHz with 3 channels, equipped with an autosampler (NMRcase). Number of accumulation (NS = 32). Samples were analyzed in CDCl_3 .

^1H NMR as a function of temperature

^1H NMR experiments as a function of temperature were performed on a Bruker Avance III HD 400 MHz spectrometer equipped with a 5mm TBO probe. The parameters used are as follows: Pulse sequence zgpr (program with pre saturation of the water signal). Number of accumulation (NS = 32). Relaxation time (D1 = 2s). Acquisition time (AQ = 4s). Temperature range 298K-343K. PDMA-PNIPAM solutions were prepared in D_2O at a concentration of 1 wt%. 3(trimethylsilyl)-propionic acid- D_4 (10 mM) was used as chemical shift internal reference (0 ppm) and as internal standard.

6.2 Size exclusion chromatography (SEC)

Molar mass and molar mass distribution were obtained by SEC in DMF/LiBr (10mM). SEC analyses were performed in an Agilent 1260 Autosampler, Varian ProStar 500 column valve module, set of two Tosoh alpha columns (TSKgel Alpha-2500 and TSKgel Alpha-3000; Media: Polymer; Particle: 7 micrometer; 7.8mm I.D. x 30cm Length; Stainless Steel), a Wyatt Optilab rEX differential refractive index detector and a Dawn Heleos II MALS detector using LiBr/DMF (10 mM) as eluent at a flow rate of 1.0 mL min^{-1} (35 °C). The column system was calibrated with PMMA standards (ranging from 1120 to $138\,600 \text{ g mol}^{-1}$). Samples were prepared in LiBr/ DMF (10 mM) and filtered through $0.45 \mu\text{m}$ PTFE filters.

6.3 Dynamic Light Scattering (DLS)

Hydrodynamic diameter and size distribution were determined by DLS on a Malvern Zetasizer Nano ZS equipped with a 633 nm laser module and a detection angle of 173° (backscattering). Measurements were triplicated, each one with a duration of 300 s. Solutions of 1 wt % of PDMA-PNIPAM copolymers were prepared in distilled water.

6.4 Small Angle Neutron Scattering

The SANS instrument used for this experiments was KWS-1 which is at the research reactor FRM II (Jülich Centre for Neutron Science).

The neutron scattered intensity $I(q)$ is obtained as a function of the scattering vector (q), which depends on the neutron wavelength (λ) and scattering angle (θ).

$$q = \frac{4\pi}{\lambda} \sin \frac{\theta}{2}$$

Solutions of 1 wt % (10 mg mL⁻¹) were prepared in D₂O and stirred overnight at room temperature.

6.5 Synthesis of copolymers

Materials

Dimethylacrylamide (DMA, Sigma-Aldrich, 99%) was purified by passing through a basic alumina column, N-isopropylacrylamide (NIPAM, VWR, >98%) was recrystallized from n-hexane. Azobisisobutyronitrile (AIBN, Acros organics, >98%) was recrystallized from methanol. Cyanomethyl dodecyl trithiocarbonate (TCI chemicals, >98%), dioxane (Sigma Aldrich, ACS reagent, 99%), diethyl ether (Sigma Aldrich, 99%), 1,3,5-trioxane (Sigma Aldrich, ≥99%) and deuterated chloroform (EurisoTop, 99%) were used as received

Block, diblock and triblock copolymers were synthesized in a Chemspeed Accelerator SLT automated parallel synthesizer at the University of Jena, using a sequential reagent addition and similar experimental protocols as reported elsewhere.^{7-9,23}

6.5.1 Synthesis of block copolymers poly(DMA_{50%}-*b*-NIPAM_{50%})

First block: A stock solution of cyanomethyl dodecyl trithiocarbonate and AIBN (100 mg mL⁻¹ and 2 mg mL⁻¹ respectively) was prepared in dioxane. The stock solution, pure DMA and dioxane were poured into adequate vessels and collocated in the chemspeed synthesizer. The desired quantities of each reagent were dispensed by the equipment into the reactors. 1,3,5-Trioxane (10 mg mL⁻¹) was also added as internal standard to follow the conversion by ¹H NMR. The mixtures were degassed by bubbling N₂ during 15 min and then after the reactors were sealed and the temperature was set to 60 °C. When the temperature was reached, the polymerizations started and they were allowed to proceed during 6 h. Samples were withdrawn each 0.5 h for their analysis by ¹H NMR

and SEC. Once the targeted molar mass was reached, the polymerizations were quenched by decreasing the temperature to 10 °C and opening the reactors. The polymers were dissolved with dichloromethane and recovered by precipitating twice in diethyl ether, to remove remaining monomer and solvent.

Second block: The obtained copolymers in the last step were first solubilized with dioxane and after the desired amounts of NIPAM solution (0.33 g mL⁻¹ in dioxane) and AIBN stock solution (2 mg mL⁻¹), were dispensed by the equipment into the reactors. 1,3,5-Trioxane (10 mg mL⁻¹) was added as internal standard to follow the conversions by ¹H NMR. The mixtures were degassed by bubbling N₂ during 15 min and then after the reactors were sealed and the temperature was set to 60 °C. When the temperature was reached, the polymerizations started and they were allowed to proceed during 6h. Samples were withdrawn each 0.5 h for their analysis by ¹H NMR and SEC. When the targeted molar masses were reached, the polymerizations were quenched by decreasing the temperature to 10 °C and opening the reactors. The polymers were dissolved with dichloromethane and recovered by precipitating twice in diethyl ether, to remove remaining monomer and solvent. Finally, the copolymers were dried in a vacuum oven at 40 °C.

6.5.2 Synthesis of diblock copolymers poly(DMA_{84%}-s-NIPAM_{16%})_{50%}-b-poly(DMA_{16%}-s-NIPAM_{84%})_{50%}

First block: A stock solution of cyanomethyl dodecyl trithiocarbonate and AIBN (100 mg mL⁻¹ and 2 mg mL⁻¹ respectively) was prepared in dioxane. The stock solution, DMA, NIPAM solution (0.33 g mL⁻¹) and dioxane were poured into adequate vessels and collocated in the chemspeed synthesizer. The desired quantities of each reagent were dispensed by the equipment into the reactors. 1,3,5-Trioxane (10 mg mL⁻¹) was added as internal standard to follow the conversion by ¹H NMR. The mixtures were degassed by bubbling N₂ during 15 min and then after the reactors were sealed and the temperature was set to 60 °C. When the temperature was reached, the polymerizations started and they were allowed to proceed during 6h. Samples were withdrawn each 0.5 h for their analysis by ¹H NMR and SEC. Once the targeted molar masses were reached, the polymerizations were quenched by decreasing the temperature to 10 °C and opening the reactors.

Second block: The remaining monomers in the first blocks were calculated from the added monomer amounts and the conversions. Then the monomer concentrations for the next blocks were calculated. The first blocks were used as obtained to make the chain extensions. NIPAM solution (0.33 g mL⁻¹ in dioxane), pure DMA and AIBN stock

solution (2 mg mL^{-1}) were dispensed by the equipment into the reactors. 1,3,5-Trioxane (10 mg mL^{-1}) was added as internal standard to follow the conversion by $^1\text{H NMR}$. The mixtures were degassed by bubbling N_2 during 15 min and then after the reactors were sealed and the temperature was set to $60 \text{ }^\circ\text{C}$. When the temperature was reached, the polymerizations started and they were allowed to proceed during 6h. Samples were withdrawn each 0.5 h for their analysis by $^1\text{H NMR}$ and SEC. When the targeted molar masses were reached, the polymerizations were quenched by decreasing the temperature to $10 \text{ }^\circ\text{C}$ and opening the reactors. The polymers were dissolved with dichloromethane and recovered by precipitating twice in diethyl ether, to remove remaining monomer and solvent. Finally, the copolymers were dried in a vacuum oven at $40 \text{ }^\circ\text{C}$.

6.5.3 Synthesis of triblock copolymers poly(DMA)_{21%}-*b*-poly(DMA_{50%}-*s*-NIPAM_{50%})_{58%}-*b*-poly(NIPAM)_{21%}

First block: A stock solution of cyanomethyl dodecyl trithiocarbonate and AIBN (100 mg mL^{-1} and 2 mg mL^{-1} respectively) was prepared in dioxane. The stock solution, pure DMA and dioxane were poured into adequate vessels and collocated in the chemspeed synthesizer. The desired quantities of each reagent were dispensed by the equipment into the reactors. 1,3,5-Trioxane (10 mg mL^{-1}) was added as internal standard to follow the conversion by $^1\text{H NMR}$. The mixtures were degassed by bubbling N_2 during 15 min and then after the reactors were sealed and the temperature was set to $60 \text{ }^\circ\text{C}$. When the temperature was reached, the polymerizations started and they were allowed to proceed during 6h. Samples were withdrawn each 0.5 h for their analysis by $^1\text{H NMR}$ and SEC. Once the targeted molar masses were reached, the polymerizations were quenched by decreasing the temperature to $10 \text{ }^\circ\text{C}$ and opening the reactors.

Second block: The remaining DMA in the first blocks was calculated from the added DMA amounts and the conversions. Then the monomer concentrations for the next blocks were calculated. The first blocks were used as obtained to make the chain extensions. NIPAM solution (0.33 g mL^{-1} in dioxane), pure DMA and AIBN stock solution (2 mg mL^{-1} in dioxane) were dispensed by the equipment into the reactors. 1,3,5-Trioxane (10 mg mL^{-1}) was added as internal standard to follow the conversion by $^1\text{H NMR}$. The mixtures were degassed by bubbling N_2 during 15 min and then after the reactors were sealed and the temperature was set to $60 \text{ }^\circ\text{C}$. When the temperature was reached, the polymerizations started and they were allowed to proceed during 6 h. Samples were withdrawn each 0.5 h for their analysis by $^1\text{H NMR}$ and SEC. When the targeted molar masses were reached, the polymerizations were quenched by decreasing the

temperature to 10 °C and opening the reactors. The polymers were dissolved with dichloromethane and recovered by precipitating twice in diethyl ether, to remove remaining monomer and solvent. Finally, the copolymers were dried in a vacuum oven at 40 °C.

Third block: The obtained copolymers in the last step were first solubilized with dioxane and after the desired amounts of NIPAM solution (0.33 g mL⁻¹ in dioxane) and AIBN stock solution (2 mg mL⁻¹), were dispensed by the equipment into the reactors. 1,3,5-Trioxane (10 mg mL⁻¹) was also added as internal standard to follow the conversions by ¹H NMR. The mixtures were degassed by bubbling N₂ during 15 min and then after the reactors were sealed and the temperature was set to 60 °C. When the temperature was reached, the polymerizations started and they were allowed to proceed during 6h. Samples were withdrawn each 0.5 h for their analysis by ¹H NMR and SEC. When the targeted molar masses were reached, the polymerizations were quenched by decreasing the temperature to 10 °C and opening the reactors. The polymers were dissolved with dichloromethane and recovered by precipitating twice in diethyl ether, to remove remaining monomer and solvent. Finally the copolymers were dried in a vacuum oven at 40 °C.

6.5.4 Synthesis of gradient copolymers poly(DMA_{50%}-*grad*-NIPAM_{50%})

Stock solutions of cyanomethyl dodecyl trithiocarbonate (114 mg mL⁻¹) and AIBN (2 mg mL⁻¹) were prepared in dioxane. Stock solutions of DMA and NIPAM were also prepared in dioxane (0.33 g mL⁻¹) and 1,3,5-trioxane (10 mg mL⁻¹) was added to each one. Each solution was mixed with 40% of the total amount of the initiator required for the polymerization. The remaining 20% of the initiator was reserved for the solution in the reactor.

CTA and AIBN stock solutions and 1,3,5-trioxane (10 mg mL⁻¹) were poured into a schlenk tube and it was sealed with a rubber septum. This mixture and the monomer solutions were degassed with Ar during 30 min. The syringes used to inject the monomers were also purged with Ar during 30 min. Then the syringes were charged with the monomer solutions and installed on the master and secondary pumps. The schlenk tube was placed in an oil bath at 80 °C and the syringes were connected to the tube with needles. DMA solution (1.88 mL, 6.55 mmol of DMA) was added in one shot to the reactor and it was allowed to polymerize for 1 h. After, the addition of the gradient profile was started. The addition rate of each monomer was adjusted so that the addition rate of DMA decreased linearly from 3.77 to 0 mL/h within 6 h and on the contrary the addition rate of NIPAM solution increased linearly from 0 to 3.77 mL/h over 6 h. At the final stage

of the reaction, 5.66 mL of NIPAM were added during 1.5 h at 3.77 mL/h. Samples were withdrawn each 30 min for the analysis by ^1H NMR and SEC.

6.5.5 Synthesis of statistical copolymers poly(DMA_{50%}-*stat*-NIPAM_{50%})

Stock solutions of cyanomethyl dodecyl trithiocarbonate (103.6 mg mL^{-1} and 51.5 mg mL^{-1} to obtain molecular weights of 10 kg mol^{-1} and 20 kg mol^{-1} respectively) and AIBN (2 mg mL^{-1}) were prepared. These stock solutions, DMA (14.4 mmol , 1.42 g), NIPAM and (15.6 mmol , 1.77 g) were poured into a schlenk tube equipped with a magnetic stirrer. Dioxane was also added until 10 mL . The mixture was degassed by bubbling with Ar during 15 min . The schlenk tube was placed into a pre-heated oil bath at $70 \text{ }^\circ\text{C}$ for 6 h . After this time the polymerization was quenched by immersing the tube in liquid nitrogen. A sample was withdrawn and analysed by ^1H NMR and SEC to obtain monomer conversion (92%) and molar mass ($19\,200 \text{ g}\cdot\text{mol}^{-1}$), respectively. The polymers were purified by two precipitations in diethyl ether.

LITERATURE

- 1 A. Halperin, M. Kröger and F. M. Winnik, *Angew. Chemie - Int. Ed.*, 2015, **54**, 15342–15367.
- 2 J. Li, S. Mizutani, S. I. Sato, A. Narumi, O. Haba, S. Kawaguchi, M. Kikuchi, T. Kakuchi and X. Shen, *Polym. Chem.*, 2020, **11**, 2346–2359.
- 3 I. C. Barker, J. M. G. Cowie, T. N. Huckerby, D. A. Shaw, I. Soutar and L. Swanson, *Macromolecules*, 2003, **36**, 7765–7770.
- 4 L. Cranitch, D. J. T. Hill and A. K. Whittaker, *Appl. Magn. Reson*, 2007, **32**, 51–62.
- 5 A. J. Convertine, B. S. Lokitz, Y. Vasileva, L. J. Myrick, C. W. Scales, A. B. Lowe and C. L. McCormick, *Macromolecules*, 2006, **39**, 1724–1730.
- 6 G. Li, S. Song, L. Guo and S. Ma, *J. Polym. Sci. Part A Polym. Chem.*, 2008, **46**, 5028–5035.
- 7 J. J. Haven, C. Guerrero-Sanchez, D. J. Keddie and G. Moad, *Macromol. Rapid Commun.*, 2014, **35**, 492–497.
- 8 J. J. Haven, C. Guerrero-Sanchez, D. J. Keddie, G. Moad, S. H. Thang and U. S. Schubert, *Polym. Chem.*, 2014, **5**, 5236–5246.
- 9 C. Guerrero-Sanchez, S. Harrisson and D. J. Keddie, *Macromol. Symp.*, 2013, **325–326**, 38–46.
- 10 Q. Jin, L. P. Lv, G. Y. Liu, J. P. Xu and J. Ji, *Polymer (Guildf.)*, 2010, **51**, 3068–3074.
- 11 J. P. Patterson, E. G. Kelley, R. P. Murphy, A. O. Moughton, M. P. Robin, A. Lu, O. Colombani, C. Chassenieux, D. Cheung, M. O. Sullivan, T. H. Epps and R. K. O'Reilly, *Macromolecules*, 2013, **46**, 6319–6325.
- 12 P. A. Fitzgerald, S. Gupta, K. Wood, S. Perrier and G. G. Warr, *Langmuir*, 2014, **30**, 7986–7992.
- 13 X. Lang, A. D. Patrick, B. Hammouda and M. J. A. Hore, *Polymer (Guildf.)*, 2018, **145**, 137–147.
- 14 M. L. Ohnsorg, J. M. Ting, S. D. Jones, S. Jung, F. S. Bates and T. M. Reineke, *Polym. Chem.*, 2019, **10**, 3469–3479.
- 15 M. Khimani, S. Yusa, A. Nagae, R. Enomoto, V. K. Aswal, E. Kesselman, D. Danino and P. Bahadur, *Eur. Polym. J.*, 2015, **69**, 96–109.
- 16 Y. Ogura, T. Terashima and M. Sawamoto, *Macromolecules*, 2017, **50**, 822–831.
- 17 A. Papagiannopoulos, J. Zhao, G. Zhang, S. Pispas and A. Radulescu, *Eur. Polym. J.*, 2014, **56**, 59–68.
- 18 M. Doucet, J. H. Cho, G. Alina, J. Bakker, W. Bouwman, P. Butler, K. Campbell, M. Gonzales, R. Heenan, A. Jackson, P. Juhas, S. King, P. Kienzle, J. Krzywon, A. Markvardsen, T. Nielsen, L. O'Driscoll, W. Potrzebowski, R. Ferraz Leal, T. Richter, P. Rozycko and A. Washington, , DOI:10.5281/ZENODO.438138.
- 19 A. Guinier and G. Fournet, *Small Angle Scattering of X-Rays*, New York : Wiley, 1955.
- 20 J. S. Pedersen, *J. Appl. Crystallogr.*, 2000, **33**, 637–640.
- 21 P. Debye, *J. Phys. Colloid Chem.*, 1947, **51**, 18–32.
- 22 F. Goto, K. Ishihara, Y. Iwasaki, K. Katayama, R. Enomoto and S. I. Yusa, *Polymer (Guildf.)*, 2011, **52**, 2810–2818.
- 23 R. Yañez-Macias, I. Kulai, J. Ulbrich, T. Yildirim, P. Sungur, S. Hoepfener, R. Guerrero-Santos, U. S. Schubert, M. Destarac, C. Guerrero-Sanchez and S. Harrisson, *Polym.*

- Chem.*, 2017, **8**, 5023–5032.
- 24 S. I. Yusa, Y. Shimada, Y. Mitsukami, T. Yamamoto and Y. Morishima, *Macromolecules*, 2004, **37**, 7507–7513.
- 25 B. Liu and S. Perrier, *J. Polym. Sci. Part A Polym. Chem.*, 2005, **43**, 3643–3654.
- 26 Z. Gao, X.-F. Zhong and A. Eisenberg, *Chain Dynamics in Coronas of Ionomer Aggregates*, 1994, vol. 27.

GENERAL CONCLUSIONS

The aim of this thesis was to analyze the effect of different monomer distribution of two groups of polymers, on their physical and self-assembly properties. The polymers under study were P(AA-*n*BA) and P(DMA-NIPAM) with an overall composition of 50% AA or 50% NIPAM and targeted molecular weights of 10 kg mol⁻¹ and 20 kg mol⁻¹. The structures with different monomer distribution were block, statistical, gradient, asymmetric diblock and triblock copolymers. The last three type of structures are classified as asymmetric copolymers and the asymmetric diblock and triblock structures aim to mimic the behavior of the gradient copolymer.

From the first part of the thesis it was possible to have an insight of the relationship structure-properties for asymmetric copolymers in comparison with block and statistical copolymers. Derived from the bibliographic investigation, it was observed that some properties of asymmetric copolymers are between those corresponding to block and statistical copolymers, as in the case of the glass transition temperature.

The physical properties in bulk of P(AA-*n*BA) copolymers were analyzed by DSC and it was effectively found that the T_g of the asymmetric structures displayed features of both block and statistical copolymers. While block copolymers display two separated and defined T_g s, due to microphase separation, the statistical copolymers showed one single and narrow T_g . The gradient copolymers exhibited one single and broad T_g , while the diblock structures displayed two T_g s similar to those of block copolymer, but in this case with broader temperature ranges. And finally the triblock is of particular interest, since it displayed a broad glass transition similar to that obtained from gradient copolymer. The similarities between asymmetric structures are attributed to the weak microphase segregation inherent to their structure.

Then the ionization behavior of the P(AA-*n*BA) copolymers, with targeted molar mass of 20 kg mol⁻¹, was analyzed by potentiometric titrations. A set of statistical copolymers was analyzed and it was shown that the higher the content of *n*BA units within the polymer chain, it was more difficult to create charges along the chain. Regarding the results of the asymmetric structures revealed that the diblock copolymer behaved similarly to a gradient copolymer, but did not totally capture its ionization behavior. And finally it was shown that the triblock copolymer mimicked the ionization behavior of the gradient copolymer.

The self-assembly as a function of pH of the P(AA-*n*BA) copolymers revealed that the block copolymers produced frozen aggregates over the entire pH range and then below pH 6 these aggregates collapse. On the contrary the self-assemblies corresponding to the asymmetric structures displayed dynamic behavior in which they changed in size and morphology as a function of pH. Differently from the potentiometric titrations of chapter 2, also diblock copolymers exhibited some common features with the gradient copolymer, as their continuous change in size and shape. Then both, triblock and gradient copolymers, produced very large wormlike micelles at low pH. However, in this case, the triblock also displayed characteristics of block copolymers, since their aggregates remained frozen at high pH. The similarities between the asymmetric structures were attributed to their similar composition profiles.

Finally, the temperature-induced self-assembly of the P(DMA-NIPAM) copolymers was studied. All the P(DMA-NIPAM) polymer structures formed micelles already at 25 °C because of the association of the dodecyl end groups in the polymers. DLS showed that micelles from statistical copolymers remained constant in size from 25 to 55 °C and they manifest a T_{cp} at 60 °C. Also, DLS results indicated that the 10K asymmetric copolymers shared some characteristics of statistical copolymers, since assemblies of both polymers remain constant in size before experiencing a broad transition around 60 °C. The 20K polymers remain stable at high temperatures because their chains are long enough, so that the DMA-rich segment is far enough from the NIPAM-rich section to keep stabilizing the aggregates even above the T_{cp} of statistical copolymers. After, the results observed by SANS and ^1H NMR, showed that the 10K block copolymers and the 20K gradient copolymers displayed similar behaviors. This was attributed to the length scale of the block copolymer, in which the NIPAM and DMA are close enough that NIPAM is strongly affected by the DMA units.

Globally, it can be concluded from chapters 2, 3 and 4 that the asymmetric diblock and triblock do mimic the properties of gradient copolymers. In chapter 2 it was observed that the diblock captured some characteristics of the gradient copolymer, while the structure of triblock conferred the ability to faithfully mimic the ionization behavior of the gradient copolymer. In comparison, the results from chapter 3 showed that both diblock and triblock share some features of the gradient copolymer, for the diblock the continuous variation of size and shape and for the triblock the generation of long wormlike micelles at low pH. Similarly to chapter 2, the results in chapter 4 showed the ability of P(DMA-NIPAM) triblock copolymers to mimic the thermoresponsive properties corresponding to the gradient structures.

Something to remark is that while the pH-responsiveness of P(AA-*n*BA) copolymers involves the protonation and deprotonation of individual monomer units, the thermal responsive phenomenon of P(DMA-NIPAM) copolymers is rather a cooperative process where the chain collapse on heating through the cloud point involves a significant number of monomer units. As a result, even block copolymers of DMA and NIPAM may show characteristics that are typically associated with gradient copolymers, such as broad transitions between solvated and collapsed states in the lower molecular weight (10K) block copolymers.

Based on the results obtained through this thesis, it can be said that asymmetric diblock and triblock structures effectively behave like a gradient copolymer. In some properties they are able to display most of the characteristics of a gradient copolymer and in few cases they share properties with gradient copolymers but also with block copolymers. This suggests that many of the desirable properties associated with linear gradient copolymers, which can be difficult to synthesize, can be obtained using more readily-accessible stepwise gradient copolymers such as the asymmetric diblock and triblock structures investigated here.

APPENDIX 1: SCATTERING TECHNIQUES FOR POLYMER ANALYSIS

The most used techniques for the analysis of polymers in solution are dynamic and static light scattering (DLS and SLS), and small angle X-ray and neutron scattering (SAXS and SANS). In each case, the analysis consists in irradiating the sample with a known wavelength and to detect the scattered intensity by the particles in the sample. Since in this work only DLS and SANS were used for the study of the copolymers, only these two techniques will be discussed.

Dynamic light scattering

The particles are constantly moving due to Brownian motion. Brownian motion is defined as the movement of particles due to random collisions with the molecules of the liquid surrounding the particle. Something of great importance is that small particles move more rapidly than large particles. The relationship among particle size and diffusion coefficient D , is established by the Stokes-Einstein equation.

$$R_H = \frac{K_B T}{6\pi\eta D}$$

Where R_H is the hydrodynamic radius, K_B represents the Boltzmann's constant, T is the absolute temperature of the solution and η is the viscosity of the solvent. Is very important to mention that R_H , obtained from DLS instrument, refers to the radius of a hard sphere which has the same diffusion coefficient as the particle analyzed.

Since particles are constantly in motion, the speckle pattern will also appear to move. The distance among the scattering particles in solution is constantly changing with time, which results in the fluctuation of the intensity of scattered light. With the aim to obtain information about the particles in motion, the time scale of scattered light intensity fluctuations need to be analyzed by a mathematical process called autocorrelation. The autocorrelation function represents the comparison of the signal with itself over a period of time. If a signal intensity is compared with itself, then there will be a perfect match and hence perfect correlation, which is reported with a value of 1. Within a very short period of time the signals are very similar among them, nonetheless the correlation is decaying. After a longer time delay the signals will have no relation to each other due to the particles are moving randomly and correlation will tend to 0. When a small particle is measured, a quickly correlation reduction will be observed. On the contrary, a large particle will

produce a slow correlation reduction. The normalized autocorrelation function is established by the following equation:

$$g(\tau) = \frac{\langle I(t)I(t + \tau) \rangle}{\langle I(t) \rangle^2}$$

Where $I(t)$ is the intensity as a function of time t , $\langle I(t) \rangle^2$ is the average scattered intensity squared, τ is a delay time, and the brackets indicate averaging over all t .

In the case of a monodisperse sample, the autocorrelation function can be demonstrated as an exponential function with a single relaxation time. In order to obtain the size distribution information, the cumulant analysis is used, and this assumes a monomodal distribution of relaxation times with a given dispersity. In contrast, for polydisperse systems, the CONTIN analysis is preferred, in which the data is fitted with a regularization method and produces a smooth distribution of relaxation times, allowing the analysis of multimodal systems.

Small Angle Neutron Scattering

SANS has impacted polymer solutions characterization because it is possible to obtain information about the conformation, morphology and thermodynamics of the polymer.

The most important feature of SANS is that the range in which the polymer can be studied is 1-100 nm. Figure A1.1 depicts the typical SANS curves, in which different polymer conformations are represented. As it can be observed, the guinier regime is followed by the middle q -range which is governed by a power law of $q^{-\alpha}$. α represents a law exponent that contains information about the conformation of the polymer particle and it is related to the Flory exponent (ν) in the following equation $\alpha = 1/\nu$.

When $\alpha = 2$ it reveals a macromolecule in gaussian conformation. The range of $\alpha = 1.5$ -2 show the presence of excluded volume effects or electrostatic interactions as in the case of polyelectrolytes. If $\alpha > 2$ this suggests that there is a more compact conformation. And for polymers with globular conformation α varies between 3 and 4.

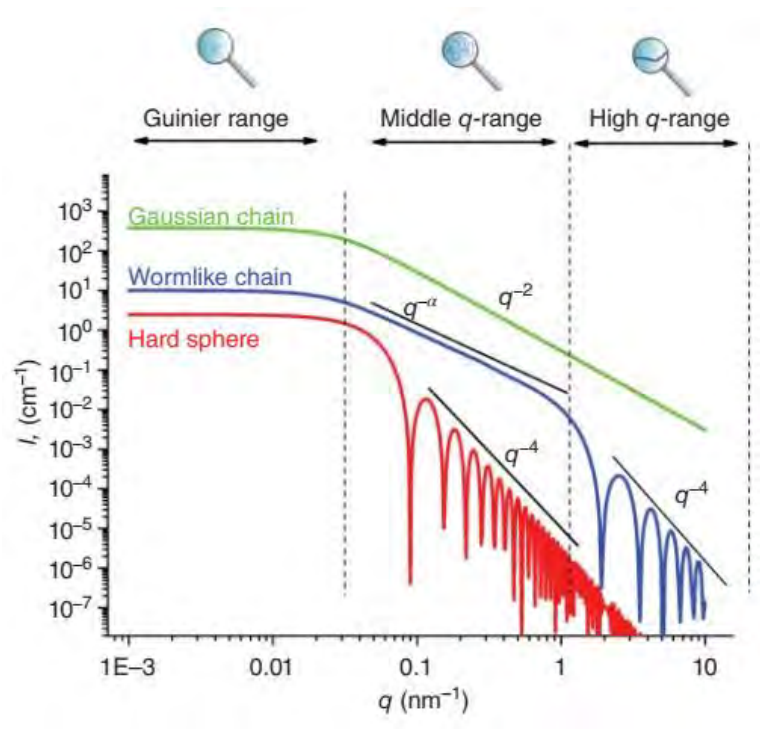


Figure A1.1. Typical SANS curves. Reproduced from Filippov et al.(2018).¹

1. . K. Filippov, M. Hruby and P. Stepanek, in *Temperature-Responsive Polymers*, John Wiley & Sons Ltd, Chichester, UK, 2018, pp. 175–196.

APPENDIX 2. HYDRODYNAMIC DIAMETERS AND PDI FOR P(AA-*n*BA) COPOLYMERS AT DIFFERENT pH

SELF-ASSEMBLY ANALYSIS BY DLS IN BUFFER SOLUTIONS

Table A2.1. Characterization data of the nano-objects formed by the self-assembly of different types of copolymers directly dispersed in different pH buffers using DLS.

Sample ^[a]		pH					
		10	8	7	6	5	4
B10K	D_h (nm) ^[b]	80.0	102.5	87.0	95.1	precipitated	precipitated
	PDI ^[c]	0.25	0.26	0.23	0.24	-	-
B20K	D_h (nm) ^[b]	291.2	279.7	268.8	279.2	precipitated	precipitated
	PDI ^[c]	0.29	0.28	0.34	0.26	-	-
D10K	D_h (nm) ^[b]	22.9	23.5	26.5	30.9	35.4	198.0
	PDI ^[c]	0.26	0.14	0.09	0.06	0.15	0.12
D20K	D_h (nm) ^[b]	30.7	37.3	42.7	46.9	46.9	191.4
	PDI ^[c]	0.04	0.03	0.03	0.02	0.01	0.22
T10K	D_h (nm) ^[b]	16.1	16.4	15.1	15.7	18.3	240.5
	PDI ^[c]	0.19	0.19	0.12	0.13	0.04	0.18
T20K	D_h (nm) ^[b]	24.9	24.5	22.7	20.9	25.3	166.7
	PDI ^[c]	0.16	0.17	0.19	0.12	0.04	0.22
G10K	D_h (nm) ^[b]	11.1	15.2	16.4	20.3	123.4	163.0
	PDI ^[c]	0.13	0.20	0.12	0.05	0.47	0.09
G20K	D_h (nm) ^[b]	26.5	38.9	67.2	137.1	108.1	201.9
	PDI ^[c]	0.35	0.21	0.22	0.26	0.22	0.25

a) All the samples represent the targeted structures after acidolysis of the tBA units in the polymer chain. b) Z-average hydrodynamic diameter of the nanoparticles. c) Polydispersity index of the nanoparticles.

SELF-ASSEMBLY ANALYSIS BY DLS BY POTENTIOMETRIC TITRATION

Table A2.2. Characterization data of the titration study for B10K by DLS.

Decreasing pH with HCl solution			Increasing pH with NaOH solution		
pH	D_h (nm) ^a	PDI ^b	pH	D_h (nm) ^a	PDI ^b
13.13	78.4	0.25	6.06	94.0	0.27
12.01	78.6	0.24	7.04	89.8	0.27
10.96	78.4	0.24	8.03	88.9	0.26
9.78	78.0	0.24	9.16	88.0	0.26
8.96	78.4	0.25	9.99	87.3	0.25
7.87	77.7	0.24	11.01	87.0	0.27
7.11	77.3	0.24	12.02	87.2	0.27
6.08	76.8	0.24			

a) Z-average hydrodynamic diameter of the nanoparticles. b) Polydispersity index of the nanoparticles.

Table A2.3. Characterization data of the titration study for B20K by DLS.

Decreasing pH with HCl solution			Increasing pH with NaOH solution		
pH	D_h (nm) ^a	PDI ^b	pH	D_h (nm) ^a	PDI ^b
13.31	229.6	0.25	6.02	283.9	0.26
12.01	226.4	0.25	7.06	284.1	0.29
10.07	227.4	0.23	8.08	277.1	0.27
9.05	225.9	0.24	9.06	272.6	0.26
8.06	226.9	0.25	10.00	270.2	0.26
7.07	226.7	0.25	11.01	272.5	0.28
6.05	224	0.24	12.02	265.7	0.25
			13.10	264.8	0.25

a) Z-average hydrodynamic diameter of the nanoparticles. b) Polydispersity index of the nanoparticles.

Table A2.4. Characterization data of the titration study for D10K using DLS.

Decreasing pH with HCl solution			Increasing pH with NaOH solution		
pH	D_h (nm) ^a	PDI ^b	pH	D_h (nm) ^a	PDI ^b
13.13	20.6	0.25	4.67	132.1	0.19
10.98	19.6	0.21	5.07	92.8	0.21
9.95	21.2	0.25	5.51	37.0	0.23
8.88	20.6	0.22	6.07	33.6	0.24
8.02	20.5	0.21	7.06	22.2	0.21
7.07	22.8	0.18	8.43	21.2	0.22
6.07	28.1	0.14	9.55	20.0	0.21
5.50	29.7	0.09	11.03	20.2	0.21
5.06	43.2	0.18	12.79	20.0	0.28
4.53	59.9	0.18			
4.20	86.8	0.16			

a) Z-average hydrodynamic diameter of the nanoparticles. b) Polydispersity index of the nanoparticles.

Table A2.5. Characterization data of the titration study for D20K using DLS.

Decreasing pH with HCl solution			Increasing pH with NaOH solution		
pH	D_h (nm) ^a	PDI ^b	pH	D_h (nm) ^a	PDI ^b
12.76	25.9	0.06	4.05	40.3	0.06
10.83	28.1	0.07	5.03	42.0	0.04
9.80	27.5	0.06	6.01	38.8	0.08
8.94	27.6	0.05	7.00	31.1	0.07
8.07	27.6	0.04	8.03	30.1	0.08
7.02	28.9	0.06	9.00	30.6	0.11
6.04	35.1	0.08	10.00	28.3	0.07
5.10	38.2	0.08	11.00	28.7	0.08
4.00	37.1	0.05	12.14	28.2	0.04
3.67	38.5	0.09			

a) Z-average hydrodynamic diameter of the nanoparticles. b) Polydispersity index of the nanoparticles.

Table A2.6. Characterization data of the titration study for T10K using DLS.

Decreasing pH with HCl solution			Increasing pH with NaOH solution		
pH	D_h (nm) ^a	PDI ^b	pH	D_h (nm) ^a	PDI ^b
12.77	17.8	0.26	4.02	128.5	0.28
12.06	17.3	0.25	5.04	16.3	0.12
11.06	16.5	0.22	6.01	14.5	0.15
9.99	15.3	0.15	7.07	16.6	0.21
8.89	16.4	0.20	8.00	20.9	0.37
8.07	17.8	0.28	9.27	16.3	0.20
7.07	16.1	0.20	10.02	16.9	0.25
6.04	14.7	0.16	11.02	17.5	0.27
4.92	15.2	0.09	12.01	16.7	0.22
4.30	20.9	0.08			
4.07	54.1	0.29			
3.54	178.2	0.23			

a) Z-average hydrodynamic diameter of the nanoparticles. b) Polydispersity index of the nanoparticles.

Table A2.7. Characterization data of the titration study for T20K using DLS.

Decreasing pH with HCl solution			Increasing pH with NaOH solution		
pH	D_h (nm) ^a	PDI ^b	pH	D_h (nm) ^a	PDI ^b
12.67	26.9	0.19	3.00	72.0	0.17
12.02	26.3	0.14	3.54	74.6	0.16
10.93	25.9	0.14	4.00	67.1	0.15
9.85	25.8	0.14	4.51	25.9	0.10
8.99	25.9	0.15	5.00	21.6	0.10
8.05	26.8	0.20	5.53	19.7	0.14
7.07	25.8	0.18	6.00	20.4	0.21
6.04	20.9	0.18	7.06	23.9	0.19
5.50	19.5	0.15	8.01	23.8	0.16
5.01	19.5	0.12	9.01	24.9	0.22
4.54	22.2	0.11	10.05	23.9	0.18
4.05	37.1	0.27	11.01	24.0	0.18
3.45	52.4	0.35	12.01	24.7	0.21
2.96	69.8	0.17			

a) Z-average hydrodynamic diameter of the nanoparticles. b) Polydispersity index of the nanoparticles.

Table A2.8. Characterization data of the titration study for G10K using DLS.

Decreasing pH with HCl solution			Increasing pH with NaOH solution		
pH	D_h (nm) ^a	PDI ^b	pH	D_h (nm) ^a	PDI ^b
13.39	11.3	0.29	3.55	187	0.07
12.07	13.4	0.40	4.01	188.4	0.07
10.65	13.1	0.38	5.00	112.4	0.25
8.36	11.9	0.29	5.49	22.7	0.11
8.04	13.3	0.35	6.06	17.4	0.12
7.02	12.9	0.21	7.02	16.9	0.34
6.02	16.6	0.21	8.08	13.0	0.30
5.11	25.5	0.15	9.00	13.2	0.37
4.45	80.0	0.46	10.05	13.8	0.43
4.04	93.4	0.30	11.03	12.1	0.31
3.45	171.6	0.08	12.00	13.3	0.42

a) Z-average hydrodynamic diameter of the nanoparticles. b) Polydispersity index of the nanoparticles.

Table A2.9. Characterization data of the titration study for G20K using DLS.

Decreasing pH with HCl solution			Increasing pH with NaOH solution		
pH	D_h (nm) ^a	PDI ^b	pH	D_h (nm) ^a	PDI ^b
12.71	24.0	0.39	5.33	114.1	0.26
12.02	23.7	0.37	6.03	79.3	0.27
10.92	25.4	0.37	7.01	47.6	0.28
10.05	29.0	0.39	8.04	33.6	0.29
9.05	27.7	0.35	9.00	28.5	0.36
8.02	30.1	0.34	10.00	28.7	0.40
7.05	35.1	0.30	11.02	24.3	0.34
6.06	68.0	0.32	12.02	23.9	0.37
5.18	94.1	0.29			

a) Z-average hydrodynamic diameter of the nanoparticles. b) Polydispersity index of the nanoparticles.

APPENDIX 3. P(DMA–NIPAM) COPOLYMERS SCATTERING DATA FROM DLS AND SANS

HYDRODYNAMIC DIAMETERS AND PDI FROM 25 TO 70 °C OBTAINED BY DLS

Table A3.1. Hydrodynamic diameter (Z-average diameter) and PDI from 25 to 70 °C for P(DMA–NIPAM) statistical copolymers S10K and S20K.

S10K			S20K	
<i>T</i> (°C)	<i>D_h</i> (nm)	<i>PDI</i>	<i>D_h</i> (nm)	<i>PDI</i>
25	30.4	0.34	22.5	0.20
30	25.9	0.38	23.0	0.21
35	28.6	0.36	22.9	0.20
40	26.8	0.38	23.1	0.19
45	26.9	0.33	23.3	0.17
50	25.5	0.33	23.8	0.15
55	25.8	0.31	25.6	0.13
60	386.0	0.16	490.8	0.94
65	precipitated		precipitated	

Table A3.2. Hydrodynamic diameter (Z-average diameter) and PDI from 25 to 70 °C for P(DMA–NIPAM) block copolymers B10K and B20K.

B10K			B20K	
<i>T</i> (°C)	<i>D_h^a</i> (nm)	<i>PDI</i>	<i>D_h^a</i> (nm)	<i>PDI</i>
25	17.2	0.12	22.4	0.19
30	17.6	0.14	22.7	0.19
35	17.6	0.10	23.5	0.16
40	18.7	0.13	26.0	0.12
45	19.6	0.10	29.5	0.07
50	21.0	0.06	29.9	0.05
55	22.0	0.04	30.0	0.05
60	22.5	0.04	30.1	0.04
65	23.0	0.04	30.1	0.04
70	23.5	0.04	30.2	0.04

Table A3.3. Hydrodynamic diameter (Z-average diameter) and PDI from 25 to 70 °C for P(DMA-NIPAM) asymmetric diblock copolymers D10K and D20K. Data obtained from DLS.

<i>T</i> (°C)	D10K		D20K	
	<i>D_h^a</i> (nm)	<i>PDI</i>	<i>D_h^a</i> (nm)	<i>PDI</i>
25	17.2	0.17	22.0	0.19
30	17.0	0.14	22.0	0.18
35	17.1	0.14	22.3	0.19
40	17.1	0.12	23.0	0.19
45	17.3	0.11	23.9	0.18
50	17.6	0.10	25.6	0.13
55	18.3	0.10	28.3	0.08
60	19.3	0.08	30.0	0.05
65	20.7	0.07	30.8	0.05
70	21.9	0.06	31.6	0.04

Table A3.4. Hydrodynamic diameter (Z-average diameter) and PDI from 25 to 70 °C for P(DMA-NIPAM) asymmetric triblock copolymers T10K and T20K. Data obtained from DLS.

<i>T</i> (°C)	T10K		T20K	
	<i>D_h</i> (nm)	<i>PDI</i>	<i>D_h</i> (nm)	<i>PDI</i>
25	18.8	0.19	24.6	0.22
30	18.8	0.16	24.7	0.21
35	19.3	0.17	25.4	0.19
40	19.5	0.15	26.9	0.16
45	19.9	0.13	29.3	0.12
50	20.2	0.12	31.6	0.08
55	20.8	0.10	32.6	0.06
60	21.8	0.07	32.7	0.05
65	22.7	0.06	32.7	0.05
70	23.5	0.05	33.3	0.05

Table A3.5. Hydrodynamic diameter (Z-average diameter) and PDI from 25 to 70 °C for P(DMA–NIPAM) gradient copolymers G10K, G20K and G30K. Data obtained from DLS.

<i>T</i> (°C)	G10K		G20K		G30K	
	<i>D_h</i> (nm)	<i>PDI</i>	<i>D_h</i> (nm)	<i>PDI</i>	<i>D_h</i> (nm)	<i>PDI</i>
25	19.4	0.20	41.8	0.49	47.5	0.40
30	19.8	0.20	40.5	0.48	49.0	0.38
35	20.2	0.20	42.8	0.37	55.4	0.37
40	20.7	0.18	46.1	0.25	85.6	0.11
45	21.7	0.16	50.3	0.12	85.3	0.08
50	24.2	0.10	49.5	0.09	83.8	0.07
55	25.9	0.08	49.0	0.07	81.2	0.05
60	27.2	0.05	48.2	0.06	78.8	0.05
65	28.4	0.04	48.0	0.05	77.3	0.05
70	31.4	0.05	48.1	0.05	76.3	0.03

PARAMETERS OBTAINED FROM THE ANALYSIS AND FITTING OF SANS CURVES

Molar mass of the aggregates is calculated with the following equation:

$$M_w = \frac{I(0) * N_A * d^2}{c * \Delta SLD^2 * 1 \times 10^{29}} \quad \text{Equation A3.1}$$

Aggregate concentration is calculated with the following equation:

$$n_{density} = \frac{c * N_A}{N_{agg} * M_{polymer}} \quad \text{Equation A3.2}$$

The following tables contain the parameters that were obtained from the fitting of SANS curves.

Table A3.6. Resulting parameters from the Guinier region and forward scattering of SANS curves of P(DMA–NIPAM) block copolymers B10K and B20K ($M_n = 10 \text{ kg mol}^{-1}$ and 20 kg mol^{-1}) at 25, 35, 45, 55 and 65 °C

T (°C)		25	35	45	55	65
B10K	M_w^a (kg mol ⁻¹)	68.2	95.7	207	383	497
	N_{agg}^b	7	10	21	40	51
	$n_{density}^c$ (cm ⁻³)	88.3 E15	63 E15	29.1 E15	15.7 E15	12.1 E15
	R_g^d (Å)	56	56	64	74	80
	α^e	1.70	1.50	0.93	0.84	0.82
T (°C)		25	35	45	55	65
B20K	M_w^a (kg mol ⁻¹)	73	130.2	544	642.4	691.3
	N_{agg}^b	3	6	23	27	29
	$n_{density}^c$ (cm ⁻³)	82.4 E15	46.3 E15	11.1 E15	9.37 E15	8.71 E15
	R_g^d (Å)	74	79	96	96	97
	α^e	1.54	1.46	1.00	1.00	0.90

a) Obtained from Equation 1, b) N_{agg} = molar mass of the aggregate/molar mass of the polymer, c) obtained from Equation 2, d) obtained from the fit of the Guinier region with the software SasView (4.2.2), e) obtained from the fitting of the porod region to a power law where $I \propto q^{-\alpha}$.

Table A3.7. Resulting parameters from the Guinier region and forward scattering of SANS curves of P(DMA–NIPAM) asymmetric diblock copolymers D10K and D20K ($M_n = 10 \text{ kg mol}^{-1}$ and 20 kg mol^{-1}) at 25, 35, 45, 55 and 65 °C.

T (°C)		25	35	45	55	65
D10K	M_w^a (kg mol ⁻¹)	63.6	80.3	111	186.2	327.4
	N_{agg}^b	7	9	12	20	35
	$n_{density}^c$ (cm ⁻³)	93 E15	73.7 E15	53.4 E15	31.8 E15	18.1 E15
	R_g^d (Å)	51	53	53	59	70
	α^e	1.3	1.2	1.1	0.85	0.80
T (°C)		25	35	45	55	65
D20K	M_w^a (kg mol ⁻¹)	67.3	86.7	169.0	533.0	760.0
	N_{agg}^b	4	5	9	28	40
	$n_{density}^c$ (cm ⁻³)	89.5 E15	69.5 E15	35.6 E15	11.3 E15	7.92 E15
	R_g^d (Å)	75	77	78	96	103
	α^e	1.5	1.5	1.3	1	0.93

a) Obtained from Equation 1, b) N_{agg} = molar mass of the aggregate/molar mass of the polymer, c) obtained from Equation 2, d) obtained from the fit of the Guinier region with the software SasView (4.2.2), e) obtained from the fitting of the porod region to a power law where $I \propto q^{-\alpha}$.

Table A3.8. Resulting parameters from the Guinier region and forward scattering of SANS curves of P(DMA–NIPAM) asymmetric triblock copolymers T10K and T20K ($M_n = 10 \text{ kg mol}^{-1}$ and 20 kg mol^{-1}) at 25, 35, 45, 55 and 65 °C.

T (°C)		25	35	45	55	65
T10K	M_w^a (kg mol ⁻¹)	65.6	88.4	135	228.3	373
	N_{agg}^b	5	7	11	18	29
	$n_{density}^c$ (cm ⁻³)	91.7 E15	68.1 E15	44.6 E15	26.4 E15	16.2 E15
	R_g^d (Å)	58	58	60	66	74
	α^e	1.45	1.4	1.2	1	0.93
T (°C)		25	35	45	55	65
T20K	M_w^a (kg mol ⁻¹)	73.0	110.3	333.0	625.0	909.4
	N_{agg}^b	3	4	13	24	35
	$n_{density}^c$ (cm ⁻³)	82.5 E15	54.6 E15	18.1 E15	9.63 E15	6.62 E15
	R_g^d (Å)	84	84	97	105	112
	α^e	1.5	1.5	1.3	1.1	1.0

a) Obtained from Equation 1, b) N_{agg} = molar mass of the aggregate/molar mass of the polymer, c) obtained from Equation 2, d) obtained from the fit of the Guinier region with the software SasView (4.2.2), e) obtained from the fitting of the porod region to a power law where $I \propto q^{-\alpha}$.

Table A3.9. Resulting parameters from the Guinier region and forward scattering of SANS curves of P(DMA–NIPAM) gradient copolymers G10K, G20K and G30K ($M_n = 10 \text{ kg mol}^{-1}$, 20 kg mol^{-1} and 30 kg mol^{-1}) at 25, 35, 45, 55 and 65 °C.

T (°C)		25	35	45	55	65
G10K	M_w^a (kg mol ⁻¹)	64.5	85.3	193	443.5	922
	N_{agg}^b	5	6	14	31	65
	$n_{density}^c$ (cm ⁻³)	93.4 E15	70.6 E15	31.2 E15	13.6 E15	6.53 E15
	R_g^d (Å)	66.5	65	70	88.4	110
	α^e	1.53	1.5	1.3	1.1	1.0
T (°C)		25	35	45	55	65
G20K	M_w^a (kg mol ⁻¹)	70.6	121	804	1230	1690
	N_{agg}^b	3	5	36	55	75
	$n_{density}^c$ (cm ⁻³)	85.3 E15	49.8 E15	7.5 E15	5 E15	3.57 E15
	R_g^d (Å)	87	86	125	131	142
	α^e	1.5	1.5	1.2	1.1	1.0
T (°C)		25	35	45	55	65
G30K	M_w^a (kg mol ⁻¹)	67.9	366.2	1746.0	2536	3102
	N_{agg}^b	2	11	54	78	96
	$n_{density}^c$ (cm ⁻³)	88.7 E15	16.44 E15	3.45 E15	2.38 E15	1.94 E15
	R_g^d (Å)	117.8	141.9	184.6	197.2	196.0
	α^e	1.34	1.3	1.1	1.0	0.97

a) Obtained from Equation 1, b) N_{agg} = molar mass of the aggregate/molar mass of the polymer, c) obtained from Equation 2, d) obtained from the fit of the Guinier region with the software SasView (4.2.2), e) obtained from the fitting of the porod region to a power law where $I \propto q^{-\alpha}$.

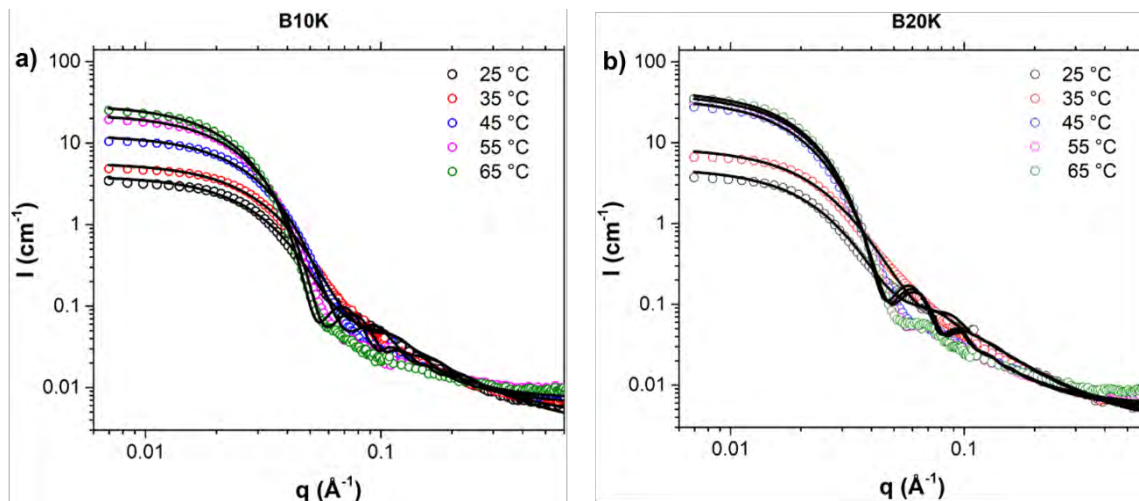


Figure A3.1. Small angle neutron scattering curves of a) B10K and b) B20K at different temperatures, with the fit curves (black lines).

Table A3.10. Parameters obtained from the fit of SANS curves for block copolymers B10K and B20K.

	T (°C)	25	35	45	55	65
B10K	N_{agg}^a *	7	10	21	40	51
	$n_{density}^c$ (cm ⁻³)*	88.3 E15	63 E15	29.1 E15	15.7 E15	12.1 E15
	Vol. core ^c (Å ³)	9453	9707	11380	11974	12404
	Vol. corona ^c (Å ³)	7827	7547	6521	5300	5185
	V_{core}/V_{corona}^d	1.21	1.29	1.75	2.26	2.39
	R core ^c (Å)	54.3	52.6	62.6	75.7	81.6
	R_g^c (Å)	20.5	21.4	22.3	21.1	20.7
B20K	T (°C)	25	35	45	55	65
	N_{agg}^a *	3	6	23	27	29
	$n_{density}^c$ (cm ⁻³)*	82.4 E15	46.3 E15	11.1 E15	9.37 E15	8.71 E15
	Vol. core ^c (Å ³)	29438	24083	31771	32301	33773
	Vol. corona ^c (Å ³)	16893	17366	13089	12050	10973
	V_{core}/V_{corona}^d	1.74	1.39	2.43	2.68	3.08
	R core ^c (Å)	78.3	69	95.5	97	99.5
R_g^c (Å)	29.8	33.1	34.6	31.4	29.6	

a) N_{agg} = molar mass of the aggregate/molar mass of the polymer, b) obtained from Equation 2, c) obtained from the fit of the SANS curve, d) Vol. core/Vol. corona. *(N_{agg} and n density were fixed while the rest of the parameters were varied by the software SasView)

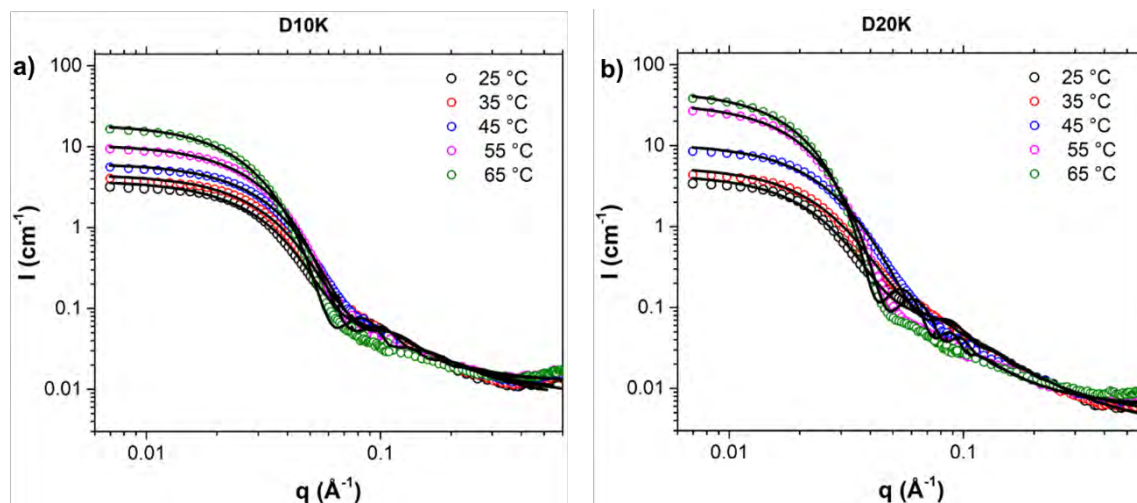


Figure A3.2. Small angle neutron scattering curves of a) D10K and b) D20K at different temperatures, with the fit curves (black lines).

Table A3.11. Parameters obtained from the fit of SANS curves for asymmetric diblock copolymers D10K and D20K.

	T (°C)	25	35	45	55	65
D10K	N_{agg}^a (fix)*	6	8	11	19	33
	$n_{density}^c$ (cm ⁻³)*	93 E15	73.7 E15	53.4 E15	31.8 E15	18.1 E15
	Vol. core ^c (Å ³)	11080	9886	10398	10982	11781
	Vol. corona ^c (Å ³)	8125	7810	7237	6377	5993
	V_{core}/V_{corona}^d	1.36	1.27	1.44	1.72	1.97
	R core ^c (Å)	54.7	51	51.7	58.5	69.4
	R_g^c (Å)	20	20	19.2	20.4	21.9
	T (°C)	25	35	45	55	65
D20K	N_{agg}^a (fix)*	4	5	9	28	40
	$n_{density}^c$ (cm ⁻³)*	89.5 E15	69.5 E15	35.6 E15	11.3 E15	7.92 E15
	Vol. core ^c (Å ³)	18656	18080	21082	25215	26556
	Vol. corona ^c (Å ³)	13233	14191	13575	10284	8817
	V_{core}/V_{corona}^d	1.41	1.27	1.55	2.45	3.01
	R core ^c (Å)	75.6	67.3	68	95.3	106
	R_g^c (Å)	28.6	30	31	31	27.6

a) N_{agg} = molar mass of the aggregate/molar mass of the polymer, b) obtained from Equation 2, c) obtained from the fit of the SANS curve, d) Vol. core/Vol. corona. *(N_{agg} and $n_{density}$ were fixed while the rest of the parameters were varied by the software SasView)

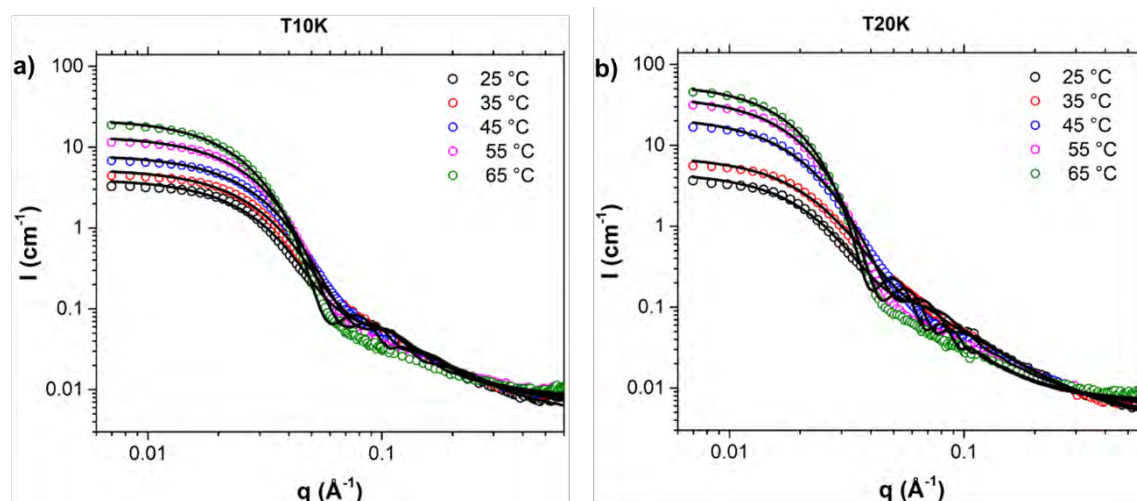


Figure A3.3. Small angle neutron scattering curves of a) T10K and b) T20K at different temperatures, with the fit curves (black lines).

Table A3.12. Parameters obtained from the fit of SANS curves for asymmetric triblock copolymers T10K and T20K.

	T (°C)	25	35	45	55	65
T10K	N_{agg}^a (fix)*	6	8	12	20	32
	$n_{density}^c$ (cm ⁻³)*	91.7 E15	68.1 E15	44.6 E15	26.4 E15	16.2 E15
	Vol. core ^c (Å ³)	10668	10588	11564	12951	13843
	Vol. corona ^c (Å ³)	9391	9447	8609	7695	7159
	V_{core}/V_{corona}^d	1.14	1.12	1.34	1.68	1.93
	R core ^c (Å)	57.2	54.6	56.7	65	74
	R_g^c (Å)	22.5	23	23	23	23
	T (°C)	25	35	45	55	65
T20K	N_{agg}^a (fix)*	2	4	11	21	31
	$n_{density}^c$ (cm ⁻³)*	82.5 E15	54.6 E15	18.1 E15	9.63 E15	6.62 E15
	Vol. core ^c (Å ³)	43805	29973	36683	41564	43670
	Vol. corona ^c (Å ³)	24402	22837	22108	15037	11748
	V_{core}/V_{corona}^d	1.80	1.31	1.66	2.76	3.72
	R core ^c (Å)	87	76	89	105	116
	R_g^c (Å)	35.6	37.6	41.5	37	30

a) N_{agg} = molar mass of the aggregate/molar mass of the polymer, b) obtained from Equation 2, c) obtained from the fit of the SANS curve, d) Vol. core/Vol. corona. *(N_{agg} and $n_{density}$ were fixed while the rest of the parameters were varied by the software SasView)

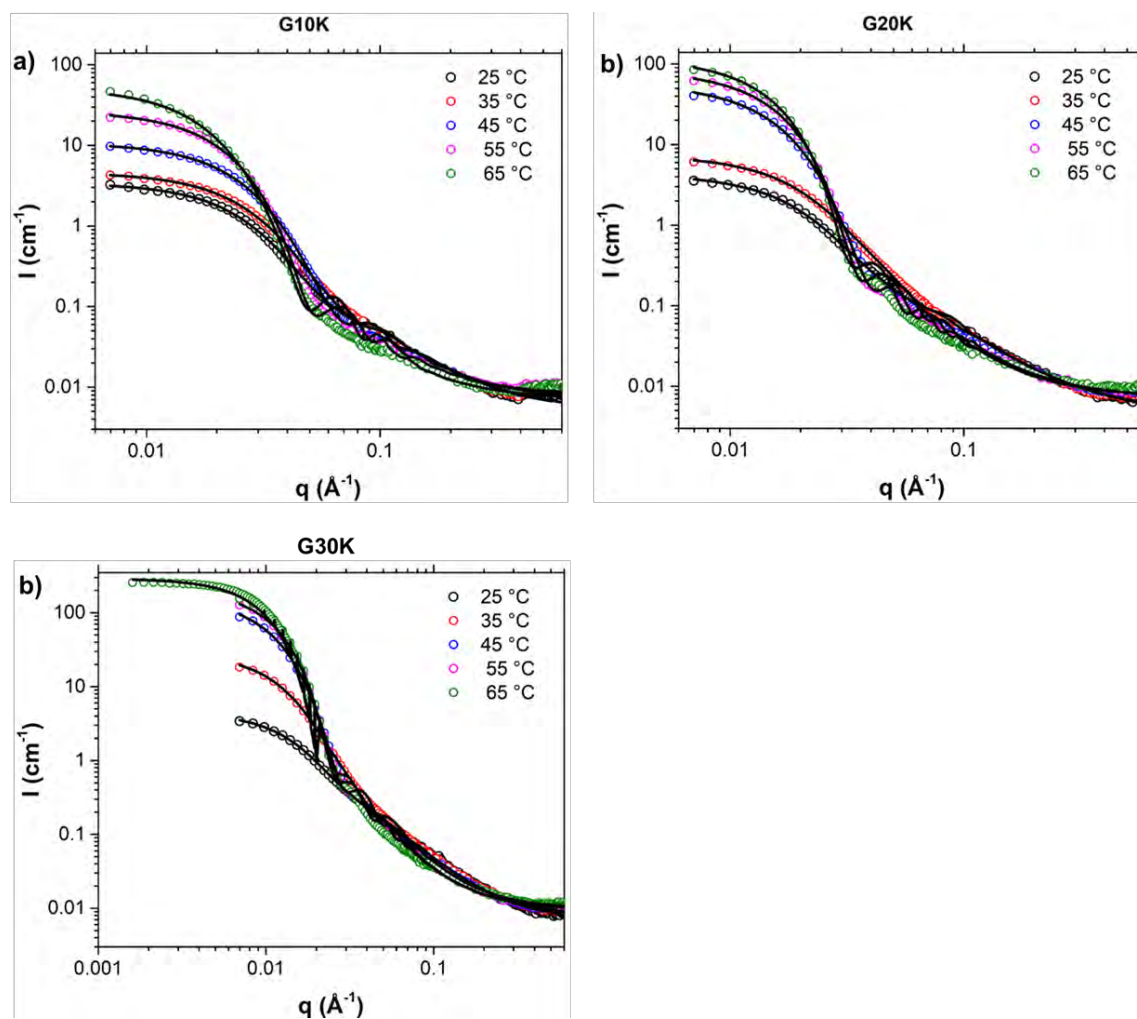


Figure A3.4. Small angle neutron scattering curves of a) G10K, b) G20K and c) G30K at different temperatures, with the fit curves (black lines).

Table A3.13. Parameters obtained from the fit of SANS curves for gradient copolymers G10K, G20K and G30K.

	T (°C)	25	35	45	55	65
G10K	N_{agg}^a (fix)*	5	6	14	31	65
	$n_{density}^c$ (cm ⁻³)*	93.4 E15	70.6 E15	31.2 E15	13.6 E15	6.53 E15
	Vol. core ^c (Å ³)	11030	13121	14033	17216	14376
	Vol. corona ^c (Å ³)	10991	11346	10033	8871	10881
	V_{core}/V_{corona}^d	1.00	1.16	1.40	1.94	1.32
	R core ^c (Å)	58	56	65	85.8	94
	R_g^c (Å)	27.2	27.4	27.8	28.4	40.6
	T (°C)	25	35	45	55	65
G20K	N_{agg}^a (fix)*	3	5	36	55	75
	$n_{density}^c$ (cm ⁻³)*	85.3 E15	49.8 E15	7.5 E15	5 E15	3.57 E15
	Vol. core ^c (Å ³)	21482	21609	27092	30363	32677
	Vol. corona ^c (Å ³)	21775	22859	17543	13162	12129
	V_{core}/V_{corona}^d	0.99	0.95	1.54	2.31	2.69
	R core ^c (Å)	76.4	68.3	114	127.6	140.2
	R_g^c (Å)	40	41.3	44	35.5	33
	T (°C)	25	35	45	55	65
G30K	N_{agg}^a (fix)*	2	11	54	78	96
	$n_{density}^c$ (cm ⁻³)*	88.7 E15	16.44 E15	3.45 E15	2.38 E15	1.94 E15
	Vol. core ^c (Å ³)	30401	30090	42854	49547	50004
	Vol. corona ^c (Å ³)	34889	40311	31556	21773	21958
	V_{core}/V_{corona}^d	0.87	0.75	1.36	2.28	2.28
	R core ^c (Å)	103.2	108.08	164.5	186.4	191.63
	R_g^c (Å)	57.1	69.1	73.2	51.5	44.9

a) N_{agg} = molar mass of the aggregate/molar mass of the polymer, b) obtained from Equation 2, c) obtained from the fit of the SANS curve, d) Vol. core/Vol. corona. *(N_{agg} and n density were fixed while the rest of the parameters were varied by the software SasView)

ABSTRACT

Block copolymers are made from polymer chains of different chemical composition that are covalently joined via their respective end groups. On the other hand, there are statistical copolymers whose monomers are randomly copolymerized together. Between these structures exist asymmetric copolymers, which are defined as a distribution of monomers within the chain which is neither completely segregated as for a block copolymer nor statistically distributed in a manner that is independent of the position along the chain as in the case of statistical copolymers. Based on the latter, the properties of asymmetric copolymers are expected to combine characteristics of block and statistical structures. In this investigation, acrylic acid–(*n*-butyl acrylate) (AA–*n*-BA) copolymers and dimethylacrylamide–*N*-isopropylacrylamide (DMA–NIPAM) copolymers, with targeted molecular weights of 10 kg mol⁻¹ and 20 kg mol⁻¹, were obtained by RAFT polymerization using forced and stepwise synthesis. Both copolymer systems are stimuli-responsive polymers: macromolecules which undergo phase transitions when they experience subtle changes in the environmental conditions. P(AA–*n*-BA) copolymers are pH-responsive and P(DMA–NIPAM) copolymers are thermosensitive.

The composition of the copolymers was always the same (50% AA or 50% NIPAM), but the distribution of the monomer units within the chain was different. Block, statistical, gradient, asymmetric diblock and triblock structures were obtained with the aim to compare their physical and self-assembly properties. The macromolecular characteristics of copolymers were obtained by nuclear magnetic resonance spectroscopy (¹H NMR) and size exclusion chromatography (SEC).

P(AA–*n*BA) copolymers in solution at different pH were studied by dynamic light scattering (DLS), cryogenic transmission electron microscopy (cryo-TEM) and small angle neutron scattering (SANS) and it was possible to demonstrate the changes in size and self-assembly behavior as a function of pH of the copolymers solutions. The results showed that the P(AA–*n*BA) asymmetric copolymers form aggregates of different morphology depending on the pH, for example vesicles at pH 4 or micelles and worms at pH 5. On the other hand, the morphology of block copolymers with the same composition, is not influenced by changes in pH.

P(DMA-NIPAM) copolymers in solutions were analyzed by DLS, SANS and ¹H NMR as a function of temperature. The evolution of hydrodynamic size as a function of temperature could be followed by DLS and the temperature-induced micellization was analyzed by SANS whereas by ¹H NMR, the temperature-induced collapse and resulting loss of mobility of the polymer chains could be followed at a molecular level. Interesting

results were obtained, since low molar mass block copolymers ($M_n = 10 \text{ kg mol}^{-1}$) displayed similar behavior to the corresponding to high molar mass gradient copolymer ($M_n = 20 \text{ kg mol}^{-1}$). This phenomenon was observed by SANS and ^1H NMR, and it was attributed to the short length scale of the block copolymer, in which the chain is short enough that a significant fraction of the NIPAM units in the block copolymer are strongly affected by the DMA of the adjoining block, leading to a gradual change in the effective composition of the polymer as a function of chain length.

RÉSUMÉ

Les monomères d'un copolymère statistique sont aléatoirement mélangés, tandis que ceux d'un copolymère à bloc sont nettement séparés en sections de compositions différentes. Entre ces deux structures modèles existent des copolymères asymétriques, qui sont définis comme une distribution de monomères au sein de la chaîne qui n'est ni complètement ségréguée comme pour un copolymère à bloc ni statistiquement distribuée de manière indépendante de la position au long de la chaîne comme dans le cas des copolymères statistiques. Ainsi, les propriétés des copolymères asymétriques devraient combiner les caractéristiques des structures à bloc et statistiques. Dans cette étude, des copolymères d'acide acrylique–(acrylate de n-butyle) (AA–*n*-BA) et diméthylacrylamide–*N*-isopropylacrylamide (DMA–NIPAM), avec des masses molaires ciblées de 10 kg mol⁻¹ et 20 kg mol⁻¹, ont été obtenus par polymérisation RAFT en utilisant une synthèse forcée et par étapes. Les deux systèmes de copolymères sont des polymères sensibles aux stimuli : des macromolécules qui subissent des transitions de phase lorsqu'elles subissent de subtils changements des conditions environnementales. Les copolymères P(AA–*n*-BA) réagissent au pH et les copolymères P(DMA–NIPAM) sont thermosensibles.

Lors de cette étude, la composition des copolymères a été fixée (50% AA ou 50% NIPAM), mais la distribution des unités de monomères au sein de la chaîne varie. En effet, des structures à blocs, statistiques, à gradient, asymétriques dibloc et tribloc ont été obtenues dans le but de comparer leurs propriétés physiques et d'auto-assemblage. Les caractéristiques macromoléculaires des copolymères ont été obtenues par spectroscopie de résonance magnétique nucléaire (¹H RMN) et chromatographie d'exclusion stérique (SEC).

Les copolymères P(AA–*n*-BA) en solution à différents pH ont été étudiés par diffusion dynamique de la lumière (DLS), microscopie électronique à transmission cryogénique (cryo-TEM) et diffusion de neutrons aux petits angles (SANS) et il a été possible de démontrer les changements de taille et de comportement d'auto-assemblage en fonction du pH des différentes solutions de copolymères. Les résultats ont montré que les copolymères asymétriques P(AA–*n*-BA) forment des agrégats de morphologie différente selon le pH, par exemple des vésicules à pH 4 ou des micelles et des micelles vermiculaires à pH 5. D'autre part, la morphologie des copolymères à bloc de même composition, n'est pas influencée par les changements de pH.

Les copolymères de P(DMA–NIPAM) ont été analysés en solution par DLS, SANS et ¹H RMN en fonction de la température. L'évolution de la taille hydrodynamique en fonction

de la température a pu être suivie par DLS. La micellisation induite par le changement de température a été analysée par SANS. Enfin, l'effondrement de la structure induit par la température et la perte de mobilité résultante des chaînes polymères ont été suivis à un niveau moléculaire par ^1H RMN. Des résultats intéressants ont été obtenus, car les copolymères à bloc de faible masse molaire ($M_n = 10 \text{ kg mol}^{-1}$) présentent un comportement similaire au copolymère à gradient de masse molaire plus élevé ($M_n = 20 \text{ kg mol}^{-1}$). Ce phénomène a été observé par SANS et ^1H RMN, et il a été attribué à la faible longueur du copolymère à bloc : une fraction significative des unités NIPAM dans le copolymère à bloc peuvent être en contact avec le DMA du bloc adjacent, conduisant à un changement progressif de la composition effective du polymère en fonction de la longueur de la chaîne.